

# Water-borne poly(meth)acrylates obtained from functional and renewable monomers

Citation for published version (APA):

Stouten, J. (2023). *Water-borne poly(meth)acrylates obtained from functional and renewable monomers*. [Doctoral Thesis, Maastricht University]. Maastricht University. <https://doi.org/10.26481/dis.20230620js>

## Document status and date:

Published: 01/01/2023

## DOI:

[10.26481/dis.20230620js](https://doi.org/10.26481/dis.20230620js)

## Document Version:

Publisher's PDF, also known as Version of record

## Please check the document version of this publication:

- A submitted manuscript is the version of the article upon submission and before peer-review. There can be important differences between the submitted version and the official published version of record. People interested in the research are advised to contact the author for the final version of the publication, or visit the DOI to the publisher's website.
- The final author version and the galley proof are versions of the publication after peer review.
- The final published version features the final layout of the paper including the volume, issue and page numbers.

[Link to publication](#)

## General rights

Copyright and moral rights for the publications made accessible in the public portal are retained by the authors and/or other copyright owners and it is a condition of accessing publications that users recognise and abide by the legal requirements associated with these rights.

- Users may download and print one copy of any publication from the public portal for the purpose of private study or research.
- You may not further distribute the material or use it for any profit-making activity or commercial gain
- You may freely distribute the URL identifying the publication in the public portal.

If the publication is distributed under the terms of Article 25fa of the Dutch Copyright Act, indicated by the "Taverne" license above, please follow below link for the End User Agreement:

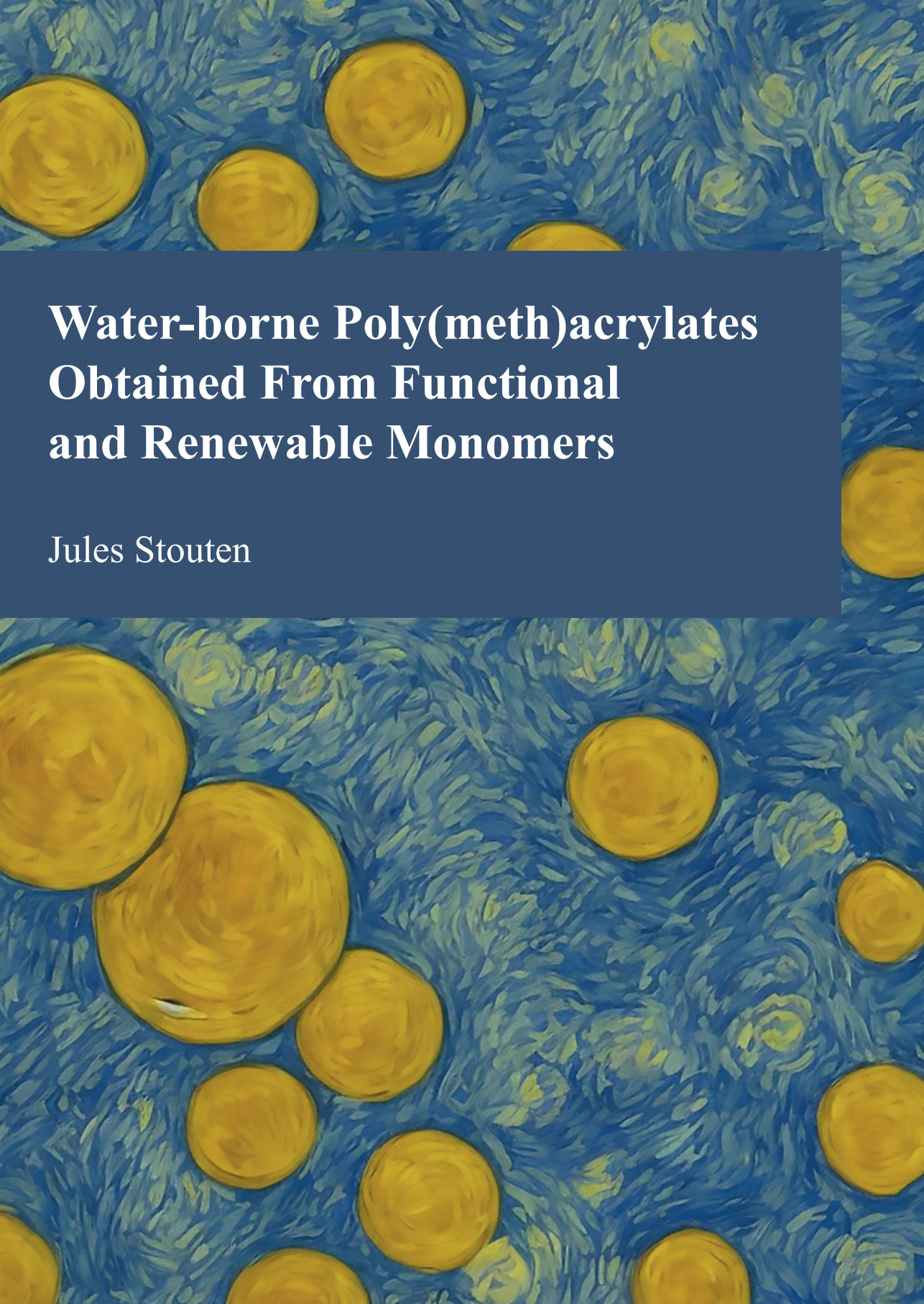
[www.umlib.nl/taverne-license](http://www.umlib.nl/taverne-license)

## Take down policy

If you believe that this document breaches copyright please contact us at:

[repository@maastrichtuniversity.nl](mailto:repository@maastrichtuniversity.nl)

providing details and we will investigate your claim.



# **Water-borne Poly(meth)acrylates Obtained From Functional and Renewable Monomers**

Jules Stouten





# Water-borne Poly(meth)acrylates Obtained From Functional and Renewable Monomers

by

Jules Stouten

Water-borne Poly(meth)acrylates Obtained From Functional and Renewable Monomers

Jules Stouten

Maastricht University, 2023

ISBN: 978-94-6469-338-6

© 2023, Jules Stouten

Cover design generated using DreamStudio

Printed by [www.proefschriftmaken.nl](http://www.proefschriftmaken.nl)



# Water-borne Poly(meth)acrylates Obtained From Functional and Renewable Monomers

DISSERTATION

to obtain the degree of Doctor at Maastricht University,  
on the authority of the Rector Magnificus, Prof. dr. Pamela Habibović  
in accordance with the decision of the Board of Deans,  
to be defended in public  
on Tuesday 20<sup>th</sup> of June 2023, at 16:00h

by

Jules Stouten

**Supervisors:**

Dr. Katrien Bernaerts

Prof. Dr. Andrij Pich

**Assessment Committee:**

Prof. Dr. Romano Orrù (Chair)

Prof. Dr. Guillaume Delaittre *University of Wuppertal*

Prof. Dr. Maarten Honing

Dr. Bart Noordover *Allnex Bergen op Zoom, NL*

This work was carried out in the framework of INTERREG-Program Deutschland-Nederland, which is co-financed by the European Union, the MWIDE NRW, the Ministerie van Economische Zaken en Klimaat and the provinces of Limburg, Gelderland, Noord-Brabant and Overijssel







# Table of contents

<b>Prologue</b> .....	<b>13</b>
<b>Chapter 1 Introduction</b> .....	<b>17</b>
Aim and scope of this thesis .....	21
Outline .....	24
References .....	26
<b>Chapter 2 UV curable Biobased Polyacrylates based on a Multifunctional Monomer derived from Furfural</b> .....	<b>31</b>
Abstract.....	31
Introduction .....	32
Experimental section .....	34
Results and discussion .....	40
Conclusions .....	55
References .....	56
Appendix A.....	60
<b>Chapter 3 Micellar Drug Delivery Vehicles formed from Amphiphilic Block Copolymers Bearing Photo-Cross-linkable Cyclopentenone Side Groups</b> .....	<b>69</b>
Abstract.....	69
Introduction .....	70
Experimental section .....	72
Results and discussion .....	78
Conclusions .....	91
References .....	92
Appendix B.....	96
<b>Chapter 4 Development of Biobased Polyacrylate Latexes based on 4CPA Synthesized by RAFT Polymerization Induced Self-Assembly</b> .....	<b>111</b>
Abstract.....	111
Introduction .....	112
Experimental section .....	114
Results and discussion .....	117
Conclusions .....	129
References .....	130

Appendix C.....	132
<b>Chapter 5 Biobased and Functional Latexes Synthesized by Polymerization Induced Self-Assembly for UV Curable Films.....</b>	<b>137</b>
Abstract.....	137
Introduction .....	138
Experimental section .....	140
Results and discussion .....	150
Conclusions .....	165
References .....	167
Appendix D.....	170
<b>Chapter 6 Synthesis and Characterization of Water-borne Vanillin Polymethacrylates Containing Dynamic Imine Cross-links.....</b>	<b>181</b>
Abstract.....	181
Introduction .....	182
Experimental section .....	183
Results and discussion .....	190
Conclusions .....	200
References .....	201
Appendix E.....	203
<b>Thesis conclusions.....</b>	<b>209</b>
<b>Impact.....</b>	<b>213</b>
References .....	215
<b>Samenvatting.....</b>	<b>217</b>
<b>Acknowledgments.....</b>	<b>221</b>
<b>Curriculum Vitae.....</b>	<b>223</b>







“Mit warheit mag ichs sagen / das so oft ich die schöne Ordnung / wie eins aus dem  
anderen folget und abgenommen wirdt / mit meinem Gedanken auff einmahl durchlauffe /  
so ists / alls hett ich ein göttlichen / nit mit bedeutenden buchstaben / sondern mit  
wesentlichen dingen in die Welt selbsten geschribenen Spruch gelesen / dessen inhalts:  
Mensch streckh deine Vernunfft hieher / diese Dinge zu begreifen.”

“Ik mag werkelijk zeggen dat telkens ik in gedachten die prachtige orde aanschouw, hoe elk  
ding uit een ander volgt en zelf ook opgevolgd wordt, het is alsof ik een goddelijke tekst  
gelezen heb, die niet met letters maar met wezenlijke dingen in de wereld zelf geschreven is  
en die zegt: mens, laat uw verstand zich tot hier uitstrekken zodat gij deze dingen begrijpen  
zult.”

Johannes Kepler, *Prognosticum Auff das Jahr nach Christi unsers Heylandes geburt 1604*,  
10 december 1603



## Prologue

While life may often seem chaotic, all events in the universe follow the laws of nature, which scientists are continuously attempting to discover and formulate. While at times, the possibilities for technological advancement might seem endless, scientists are continuously uncovering the fundamental boundaries set by the universe itself. One of such developments was the formulation of the laws of thermodynamics. The second law of thermodynamics dictates that entropy, or the amount of disorder in an isolated system must always increase with time. For example, everyone knows that building a house of cards is quite difficult, while bringing it to a (collapsed) disordered state requires very little effort. Conversely, the motions of the cards and the surrounding air molecules will never align and spontaneously bring the house of cards back together. This concept also applies to the combustion of gasoline in your car, the combustion gases will not return to a liquid and fill your tank overnight.<sup>1</sup> Other examples are the incomplete conversion of heat energy to mechanical energy in the steam engine (Carnot cycle),<sup>2</sup> or the evaporation of water. In fact, there are countless situations in life where disorder is much more likely to occur than order. Yet, I, the author of this thesis am able to place letters in a well-defined order to form words, which on its own form structured sentences, and above that a coherent story. Even more so, the human body is composed of an incredibly complex ordered structure of atoms, molecules, and cells, all working together to stay alive and produce thoughts, ideas, and physical actions. This apparent contradiction between disorder and order has fascinated people for ages.

While the second law of thermodynamics indeed holds for the whole universe, which is becoming more disordered as time passes, localized systems can decrease in entropy. This only holds when somewhere else the entropy is increased to bring the net balance to positive. Life is the most incredible example of localized order in the universe. In practice, this means that a living animal must continuously export entropy by consuming ordered molecules such as sugars, fats, and proteins, and converting those into body heat and more disordered CO<sub>2</sub> and H<sub>2</sub>O molecules.<sup>3</sup>

Next to life, we also find more simplistic non-living examples of localized order in the universe. For example, snowflakes that can grow into beautiful and repetitive patterns. The process that governs this; crystallization, is an important topic for any scientist studying physics, chemistry, geology, or materials science. Crystallization produces heat, resulting in an increased disorder of the surrounding molecules that increase in temperature, ‘allowing’ the crystallizing molecules to arrange into ordered crystals. Another example is the formation of ordered micelles in water from amphiphilic molecules consisting of a hydrophobic segment (dislikes water) and a hydrophilic segment (likes water). This segmental division will cause the molecules to self-assemble spontaneously into structures where the hydrophobic segments are encapsulated away from the aqueous surrounding, and the hydrophilic segments are dissolved in the water.<sup>4</sup>

As a final example, I would like to mention the thermodynamics of polymerization. Like all chemical reactions, thermodynamics govern the spontaneity and extent of the reaction. In

the case of polymer synthesis, we aim to bring (some) order into a chaotic mixture of small monomers by arranging them into long chains. The polymerization process is almost always accompanied with a decrease in entropy. An exception is the polymerization of sulfur.<sup>5</sup> Therefore, the decreasing entropy is compensated by increasing the disorder elsewhere. For example, this can happen by the exclusion of a condensate in a polycondensation reaction. In the case of radical polymerization, the entropy is increased by the formation of heat due to the release of bond energy. The formation of heat by radical polymerization of vinyl monomers such as styrene or methyl methacrylate occurs by the formation of more stable C-C single bonds from C=C double bonds.<sup>6</sup>

Scientists have been using the features of polymerization for the production of self-organizing systems, by carefully tuning the structures of these compounds to produce surfactants (soaps, detergents etc.), water-borne plastics, and nanomedicine delivery vehicles to name a few. The complexity and potential of such self-organizing systems is immense and will likely occupy scientists for many years to come. In this thesis, I will discuss the topics of radical polymerization, and self-assembly in aqueous medium. While the topic of thermodynamics of polymerization is not directly investigated in this thesis, it is part of the fundamental understandings that make up the foundations of any research in the field of chemistry.



1



---

# Chapter 1 Introduction

---

## *Water-borne polyacrylates*

One of the first chemical reactions invented by mankind was the production of soap, mentioned first by the Sumerians around 2800 BC.<sup>7</sup> The recipe is similar to the one we use today, and contains oil, water, and wood ash (containing potassium carbonate, or potash), which was later changed to potassium hydroxide. In this reaction, the oil, consisting of triglycerides is hydrolyzed and the produced potassium salts of the fatty acids function as a soap by attracting oily substances while being stabilized in the aqueous environment by the water-soluble salt ends. This process is very useful for the cleaning of surfaces such as the skin, fabrics, and wool from grease. However, the act of carrying greasy substances in water can also be extended to many other compounds that are not water-soluble. For example, today we use soaps in the process of compartmentalization of hydrophobic monomers for the production of water-borne polymers consisting of nanosized particles.

The topic of water-borne polymer synthesis became relevant since the development of synthetic latexes to replace natural rubbers during the first half of the 20<sup>th</sup> century.<sup>8</sup> Initially, the focus was on producing synthetic styrene butadiene rubbers. However, the methodology can be employed for the production of a large range of polymers, including acrylates. In the production of polyacrylate latexes, acrylic monomers such as methyl methacrylate, acrylic acid, and butyl acrylate are polymerized by free radical polymerization (FRP). The mentioned monomers serve a specific role in the final copolymer composition. They typically can be classified into ‘soft monomers’, ‘hard monomers’, and ‘functional monomers’. ‘Soft’ and ‘hard’ implicate the decreasing and increasing effect of the monomer on the glass transition temperature ( $T_g$ ) of the respective copolymer (Figure 1.1). Functional monomers can be employed in order to improve or introduce a variety of properties. For example, colloidal stability and adhesion to certain substrates can be enhanced by the incorporation of methacrylic acid in the monomer feed.<sup>9-10</sup> Alternatively, hydroxyethylmethacrylate can be incorporated as a site for post-polymerization modification or cross-linking on the hydroxyl groups (Figure 1.1).<sup>11</sup> The conventional acrylic monomers are currently derived from finite fossil resources, the use of which is recently under increased strain.<sup>12</sup> Therefore, one of the main motivators for this work is the exploration of novel biobased monomers for water based latex synthesis. To do that, it is important to understand the emulsion polymerization process and the role of the monomers within the system.

In short, the emulsion polymerization is carried out by mixing a soap, acrylic monomers, water, and a water-soluble initiator under mechanical agitation.<sup>8</sup> The soap, from now on called surfactant, will orient on the monomer droplets to stabilize the emulsion, and excess surfactant will self-assemble into micelles. In the presence of a heat activated radical initiator, initiation and propagation of monomers that migrate from the monomer droplets through the water phase will form short oligoradicals. The oligoradicals can migrate into the micelles and

nucleate to form a particle. After nucleation, more monomers are attracted from the droplets to the micelles where further propagation and growth of the polymer particles occurs. When all monomer is consumed, a colloid consisting of polymer particles stabilized by surfactant in water is obtained.<sup>8</sup>

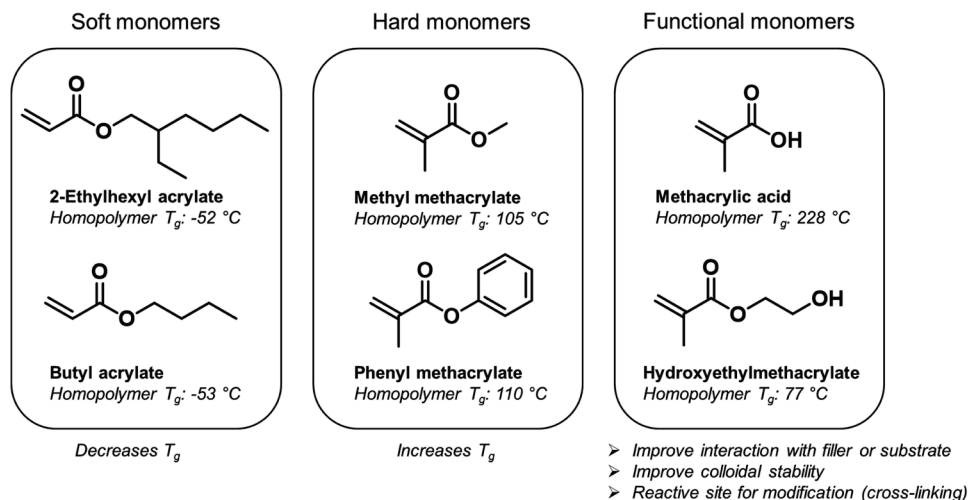


Figure 1.1. Some examples of conventional fossil based acrylic monomers and their functionality in the polymer latex.

More recently, industry and academia are increasing the effort in the continuous development of water-borne polymer systems due to the adverse environmental and health effects connected to the release of Volatile Organic Components (VOC) of solvent borne coatings.<sup>13</sup> Even though the carrier consists mostly of water, typical water-borne coatings also require some amount of VOC (usually below 10% by weight) in their formulation.<sup>13</sup> This requirement for VOC is related to the mechanism of film formation.<sup>14</sup> Since the water-borne emulsion consists of nano-sized thermoplastic particles stabilized by a surfactant, film formation is achieved by coalescence of the particles to form a homogenous layer. Coalescence requires diffusion of the chains into neighboring particles. This process is closely related to the  $T_g$  of the polymers, and this is where the main contradiction arises in water-borne coating systems; A low  $T_g$  is required to allow for movement and diffusion of the polymer chains, while a high  $T_g$  is required for good physical and mechanical properties of the final film. Film formation can be facilitated by incorporating VOC's that persist in the polymer particles to soften the resin and allow coalescence. After film formation, the VOC's evaporate in the environment causing the hardening of the film.

Besides reduction in the use of VOC's, the use of water as a reaction medium during polyacrylate synthesis can bring other benefits. For example, radical polymerization results in fast reaction rates, and high molecular weights, but, as explained before, is also exothermic. Under certain conditions, the heat of polymerization can auto-accelerate the rate

of polymerization causing a dangerous increase in the viscosity and temperature in the reactor.<sup>15</sup> The aqueous medium in an emulsion polymerization is therefore of excellent aid to effectively promote heat transfer and avoid runaway of the reaction. Other advantages that are linked to the use of water instead of solvents are that it is cheap, abundant, safe, green, and the system exhibits a low viscosity independent from molecular weight.<sup>16</sup> These advantages are essential for products that we require in our everyday lives. Some examples of applications for water-borne polyacrylates are coatings, paints, and adhesives.<sup>17</sup> In this thesis, we use the advantages of water-borne radical polymerization for the production of novel materials with reduced environmental and health impacts.

### *Controlled radical polymerization*

Decades of research and development on the process of radical and emulsion polymerization followed through the second half of the 20<sup>th</sup> century until the revolutionary discovery of controlled radical polymerization (CRP). CRP opened the door to the production of well-defined polymer structures with a controllable molecular weight, something that was impossible using free radical polymerization.<sup>18</sup> The most prevalent examples of CRP techniques today are Nitroxide-Mediated Polymerization (NMP)<sup>19</sup>, Atom Transfer Radical Polymerization (ATRP)<sup>20</sup>, and Reversible-Addition Fragmentation chain-Transfer (RAFT).<sup>21</sup> In FRP, the formation of macromolecules is governed by initiation, propagation, and termination events. Between initiation and termination, the polymer chain can grow uncontrollably long, a process that leads to broad dispersities. After termination, a macromolecule containing a dead chain end is obtained, meaning that it can no longer undergo further propagation reactions. In the case of CRP, polymer chains are obtained that contain a dormant chain end that can be reactivated in the reaction with a free radical, meaning that block copolymers structures can be obtained with a secondary addition of monomer and initiator (Figure 1.2).

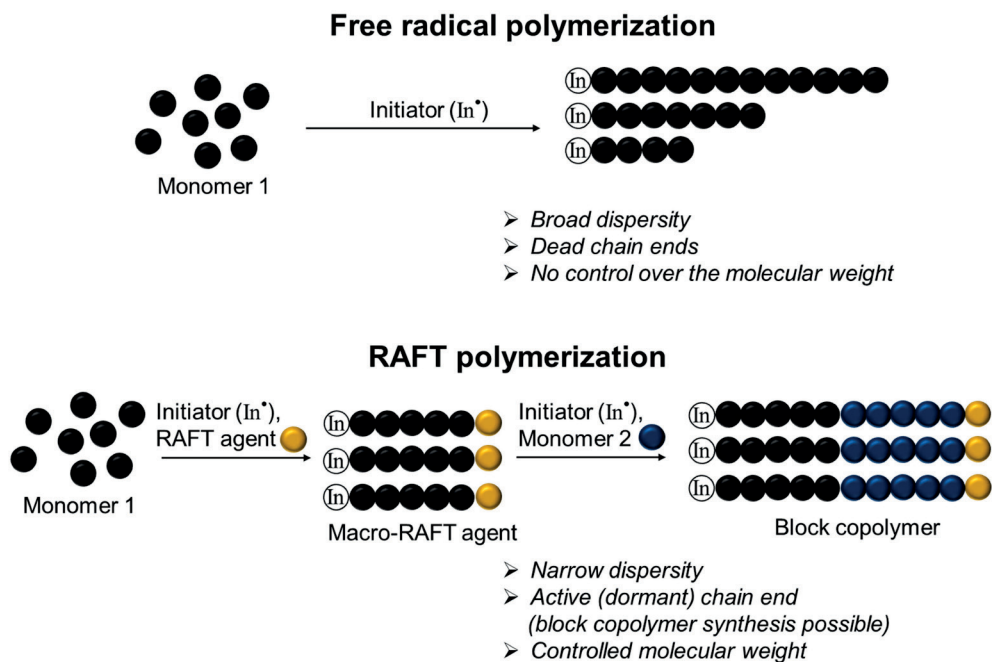


Figure 1.2. Schematic overview and characteristics of free radical polymerization and Reversible-Addition Fragmentation chain-Transfer (RAFT) polymerization.

One of the most prevalent CRP techniques at the moment is RAFT. RAFT is a Reversible Deactivation Radical Polymerization (RDRP) and is carried out in the presence of a chain transfer agent, or RAFT agent. Similar to FRP, a radical initiator is used for the formation of radicals in the system. The initiator is able to propagate with the monomers in the mixture, but quickly reacts with the RAFT agent, entering the dormant state. Alternating between the active and the dormant state is maintained by reaction of the RAFT agent end groups. With a sufficiently high deactivation rate, extensive propagation during the active state is limited causing all chains to grow at the same rate. While the amount of radicals produced by the initiator also causes an equal amount of chains with dead ends to form, the ratio of RAFT agent to monomer largely determines the degree of polymerization (DP). If the amount of initiator is kept relatively low, the contribution of the initiator to the molecular weight can be neglected. The aspects considering RAFT polymerization have been reviewed previously.<sup>21-23</sup>

RAFT polymerization yields polymers with controlled molecular weight, narrow dispersity, and a RAFT agent end group. Therefore, RAFT polymers can be employed in a subsequent polymerization functioning as a macro-RAFT agent to yield block copolymers.<sup>24-25</sup> This method has been an effective tool in the preparation of amphiphilic block copolymers consisting of acrylic, methacrylic, and styrenic monomers.<sup>26</sup> Since the molecular weight, and

thus block length can be facilely controlled and a large variety of monomer structures are available, a plethora of amphiphilic block copolymers can be synthesized. For example, the block lengths can be changed in order to tune the lipophilic-to-hydrophilic balance (LHB).<sup>27</sup> LHB is a tool to predict the surfactant properties of a given amphiphilic macromolecule. Alternatively, copolymerization within the blocks can be employed to tune the hydrophilicity or hydrophobicity of the individual blocks.<sup>28</sup> Finally, functional groups can be built along the polymer backbone, that can undergo post-polymerization modification reactions. In this way, the resulting self-assembled amphiphilic block copolymer can be further functionalized by attaching or detaching of molecules<sup>29</sup>, or cross-linking induced by external stimuli such as UV light.<sup>30</sup>

### *Polymerization induced self-assembly*

Self-assembled micelles consisting of amphiphilic block copolymers can also be synthesized *in-situ*, meaning during the reaction they already persist in the aqueous environment, instead of isolating the macromolecule before introduction into water. This process, called polymerization induced self-assembly (PISA) can be performed in order to obtain well-defined micellar objects having tunable morphologies.<sup>31-32</sup> Alternatively, the method can be employed in order to obtain surfactant-free latexes with high solid content.<sup>33</sup> RAFT is an excellent tool to perform the PISA process, while maintaining CRP conditions. The process was first reported by Ferguson et al.<sup>34</sup> and involves the use of a water-soluble macro-RAFT agent, typically based on poly(acrylic acid) or poly(ethylene glycol). Before the discovery of PISA, the introduction of RAFT conditions in emulsion polymerization led to several problems including loss of colloidal stability and molecular weight control.<sup>34</sup>

Similar to free radical emulsion polymerization, initiation of migrating hydrophobic monomers in a RAFT PISA occurs in the aqueous phase. The water-soluble macro-RAFT agent will function as a chain transfer agent for the growing macromolecule, resulting in a short block copolymer. The moment the hydrophobic segment reaches a certain critical DP, the macromolecule will spontaneously self-assemble by removing the hydrophobic segment from the aqueous environment due to the unfavorable interactions with the surrounding water molecules. The formed micelles contain the growing chain ends in the hydrophobic core. Monomers will rapidly diffuse from the monomer droplets to the growing micelles due to the large disparity in monomer concentration. Polymerization will continue in the micellar cores until all monomers are consumed. The macro-RAFT agent, which is covalently attached to the latex particles, extends in the aqueous phase and acts as a stabilizer. The RAFT PISA process is the main route in obtaining biobased water-borne polyacrylates in this thesis.

### **Aim and scope of this thesis**

With the growing global demand for biobased alternatives for fossil-based acrylic monomers, the investigation towards novel biobased monomers is required to widen the scope of available structures. In the effort to replace fossil-based monomers, biobased drop-in alternatives might not be available for each monomer, or at the desired quantities. Therefore,

novel structures derived from renewable resources are of interest as well. However, the use of new structures will be accompanied by differences in handling, reactivity, and properties of the resulting polymers in contrast to the conventional monomers. This thesis will investigate the synthesis and polymerization of two novel and multifunctional biobased monomers and exploit their additional functionality. The aim is to use this monomer functionality for post-polymerization reactions to produce cross-linked polymer materials such as films and coatings.

Cross-linking of the films formed from soft thermoplastic acrylic latexes overcomes some fundamental problems related to the film formation mechanism by coalescence of aqueous dispersed latex particles. Instead of the use of VOC's, hardening of the film is achieved by cross-linking. Cross-linking has many desirable effects, improving the mechanical properties, solvent resistance, barrier properties, and blocking resistance of the final film.<sup>35</sup> Therefore, besides the synthesis of water-borne polyacrylates, we also aim to investigate the properties of the materials that are formed thereof. Some practical applications where UV cross-linking of polymers can bring added value are investigated, such as barrier films<sup>36</sup>, and micellar drug-delivery vehicles.<sup>37</sup>

In this work, two main modes of cross-linking are investigated. The chemical reactions that result in the cross-linking are [2 + 2] photocyclodimerization in the presence of UV light, and imine formation between an aldehyde and amine (Figure 1.3). The common strategy that is followed throughout this thesis is the use of RAFT controlled radical polymerization of acrylate and methacrylate monomers for the incorporation of functional side groups along the polymer backbone. The requirements of such multifunctional monomers is that they contain a (meth)acrylate group, and another functionality to enable post-polymerization cross-linking reactions. The first functional monomer used in this thesis is 4-oxocyclopentenyl acrylate (4CPA). This monomer is obtained by esterification between acryloyl chloride and 4-hydroxycyclopentenone (4HCP).<sup>38</sup> 4HCP in turn, is obtained by the Piancatelli rearrangement of furfuryl alcohol, which is a biobased platform molecule.<sup>39-40</sup> The second functional monomer is 2-(methacryloyloxy)ethyl vanillin (MEV), which is obtained from vanillin. Vanillin is one of the main biobased building blocks that is derived from lignin. Currently, about 15% of the total amount of vanillin is produced from lignin.<sup>41</sup>

Besides the biobased functional monomers, also several biobased comonomers are used in this thesis that function as hard or soft monomers to tune the  $T_g$  of the final copolymer, and overall reduce the degree of cross-linking by diluting the amount of functionality on the polymer backbone. The comonomers that are included in this thesis are 2-octyl acrylate, a byproduct of castor oil production, isobornyl acrylate obtained from terpenes, and tetrahydrofurfuryl alcohol derived from C5 sugars (Figure 1.3).<sup>42-43</sup> These acrylic monomers can typically be considered as partially biobased, since the acrylic acid group, which is attached via esterification to the biobased alcohol, is currently not industrially derived from renewable resources.<sup>44</sup> Despite that, continuous developments are ongoing towards the biobased synthesis of acrylic acid that is feasible on an industrial scale.<sup>45-46</sup>

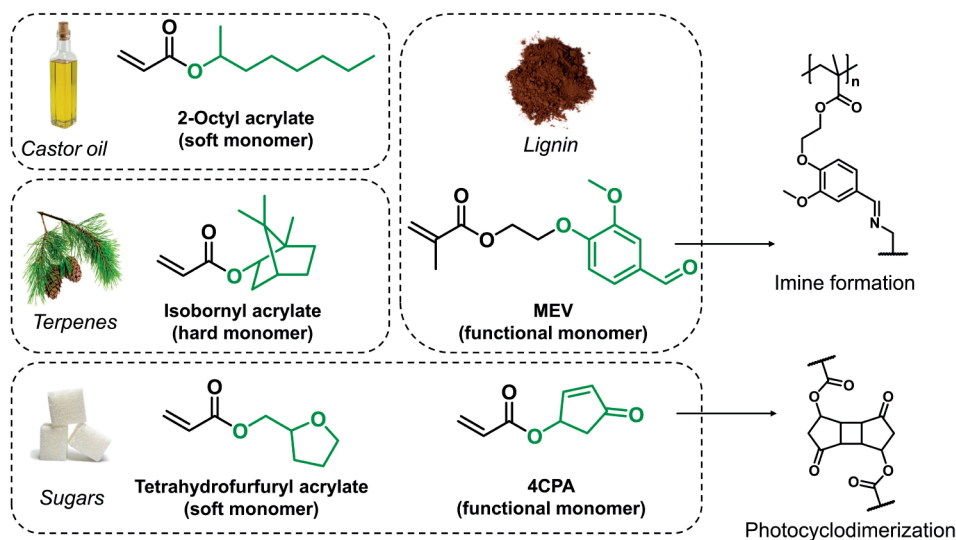


Figure 1.3. Overview of the biobased monomers used in this research and their functionality in the latex.

The cross-linking mechanisms employed in this thesis have certain advantages over other methods that can involve, for example, an initiator, or the addition of a cross-linker permanently linking polymer chains into a network.<sup>47</sup> The self-cross-linking of the polymer chains as a result of the photocyclodimerization of 4CPA is a facile and straightforward strategy, that allows more operational freedom since the film formation and cross-linking step are separated. Since no external reagents such as cross-linkers, sensitizers, or initiators are required, non cross-linked latexes and films can be safely stored or shipped. Furthermore, the degree of cross-linking, which affects the physical properties, can be easily tuned by controlling the amount of UV irradiation on the film. Another application where self-cross-linking of polymer chains under UV light is of benefit, is in the stabilization of micellar aggregates to prevent premature disintegration in dilute conditions, enabling certain biomedical applications.<sup>48</sup> Similar to films and coatings, the self-assembly of the block copolymers and subsequent cross-linking of the formed morphologies can be separated, avoiding the problems related to incorporation or leeching of cross-linkers.

The use of imine bonds as cross-links adds an additional feature to the cross-linked materials. Following the work on dynamers,<sup>49</sup> the principle of covalent bond exchange was recently transferred to cross-linked polymers having dynamic cross-links called covalent adaptable networks (CAN's). A class of CAN's, to which also imine cross-linked polymers belong, are vitrimers.<sup>50</sup> A vitrimer contains covalent bonds that can exchange under external stimuli such as temperature, maintaining a constant amount of cross-links within the system. The exchange between cross-links allow for macroscale deformation, showing a certain amount of plasticity driven by heat. Whereas classical thermosets show an inherently elastic response under stress due to the permanent cross-links and cannot be reprocessed, vitrimers can be

mechanically recycled under the conditions that allow for motion of the polymer chains (typically above the  $T_g$ ), and where bond exchange is rapid enough to allow flow (typically referred to as the topology freezing transition temperature  $T_v$ ). The topic of CAN's has been excellently reviewed recently in multiple cases.<sup>51-53</sup>

## Outline

The development of biobased and functional water-borne polyacrylates is divided in several chapters. The general structure of the thesis is shown in Figure 1.4.

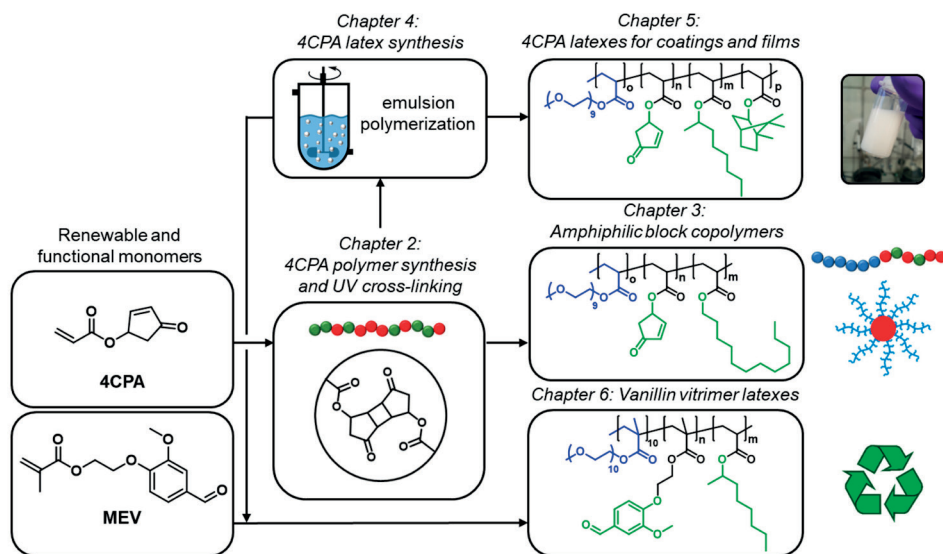


Figure 1.4. Schematic overview and structure of the thesis.

The investigation towards 4CPA polymers forms the major backbone of this thesis. A thorough and fundamental investigation towards the (co)polymerization and cross-linking of 4CPA polyacrylates is presented in **Chapter 2**. The polymerization kinetics, and the thermal and chemical properties of the resulting (co)polymers are characterized. The UV cross-linking that occurs as a result of the proposed [2 + 2] photocycloaddition between the cyclopentenone side groups is demonstrated using both polymers and model molecules. This chapter forms the foundation upon which following chapters are based.

One way to introduce hydrophobic polymers into water is by attaching a hydrophilic segment at one end, and allowing the resulting amphiphilic block copolymer to orient itself into micelles. This strategy herein employed using 4CPA as a part of the hydrophobic segment is described in **Chapter 3**. While the block copolymerization and self-assembly process can teach us the behavior of 4CPA based polyacrylates dispersed in water, the micelles were also proposed to be used as a nanosized hydrophobic drug delivery vehicle.

The development of 4CPA latexes produced via polymerization induced self-assembly (PISA) is discussed in **Chapter 4**. At a small scale, screening is performed of the optimal



reaction conditions and comonomer type and composition to obtain stable latexes containing a high fraction of solids. Furthermore, the effect of the reaction conditions on the latex particle size, gel content, and monomer conversion is investigated.

Using the knowledge from Chapter 4, the most promising recipes were scaled up for further characterization of the latex and the resulting UV cross-linked films. **Chapter 5** largely deals with the development of cross-linked films from 4CPA latexes containing different ratios of biobased comonomers as presented in Figure 1.3. The topics that are investigated are film formation, UV curing, evaluation of the mechanical properties, application as films on a substrate and evaluation of the surface properties, and addition of cellulose nanocrystals as a filler to produce mechanically reinforced composites.

The strategy for the production of 4CPA latexes via PISA in Chapter 4 was also employed for the production of latexes based on MEV. The unique combination of water-borne polyacrylate synthesis and cross-linking via imine formation to obtain vitrimers is presented in **Chapter 6**. The characterization, cross-linking, rheological and thermal properties, and recycling of the latex vitrimers is demonstrated in this chapter. The results are compared to a similar polymer obtained from solution, showing that the contribution of the hydrophilic stabilizing segment can bring a rather strong influence on the final material properties.

### References

1. Peters, A., *Concise chemical thermodynamics*. CRC Press: **2010**.
2. Carnot, S., Reflections on the motive power of fire, and on machines fitted to develop that power. *Paris: Bachelier* **1824**.
3. Schrodinger, E., *What is life? With mind and matter and autobiographical sketches*. Cambridge university press: **2012**.
4. Riess, G., Micellization of block copolymers. *Progress in Polymer Science* **2003**, 28 (7), 1107-1170.
5. Ivin, K., Thermodynamics of addition polymerization. *Journal of Polymer Science Part A: Polymer Chemistry* **2000**, 38 (12), 2137-2146.
6. Sawada, H., Thermodynamics of Polymerization. I. *Journal of Macromolecular Science, Part C* **1969**, 3 (2), 313-338.
7. Lowe, D. B., *The chemistry book: from gunpowder to graphene, 250 milestones in the history of chemistry*. Sterling: **2016**.
8. Lovell, P. A.; Schork, F. J., Fundamentals of emulsion polymerization. *Biomacromolecules* **2020**, 21 (11), 4396-4441.
9. Koh, A. Y.; Mange, S.; Bothe, M.; Leyrer, R. J.; Gilbert, R. G., The influence of copolymerization with methacrylic acid on poly (butyl acrylate) film properties. *Polymer* **2006**, 47 (4), 1159-1165.
10. Ceska, G., The effect of carboxylic monomers on surfactant-free emulsion copolymerization. *Journal of Applied Polymer Science* **1974**, 18 (2), 427-437.
11. Zhang, C. Y.; Zhu, Z. W.; Gong, S. L., Synthesis of stable high hydroxyl content self-emulsifying waterborne polyacrylate emulsion. *Journal of Applied Polymer Science* **2017**, 134 (21).
12. Aguirre, M.; Hamzehlou, S.; González, E.; Leiza, J. R., Renewable feedstocks in emulsion polymerization: Coating and adhesive applications. In *Advances in Chemical Engineering*, Elsevier: **2020**; Vol. 56, pp 139-186.
13. Stockwell, C. E.; Coggon, M. M.; Gkatzelis, G. I.; Ortega, J.; McDonald, B. C.; Peischl, J.; Aikin, K.; Gilman, J. B.; Trainer, M.; Warneke, C., Volatile organic compound emissions from solvent- and water-borne coatings—compositional differences and tracer compound identifications. *Atmospheric Chemistry and Physics* **2021**, 21 (8), 6005-6022.
14. Winnik, M. A., Latex film formation. *Current Opinion in Colloid & Interface Science* **1997**, 2 (2), 192-199.
15. O'Neil, G. A.; Torkelson, J. M., Recent advances in the understanding of the gel effect in free-radical polymerization. *Trends in Polymer Science* **1997**, 11 (5), 349-355.
16. Schwalm, R., *UV coatings: basics, recent developments and new applications*. Elsevier: **2006**.
17. Bao, Y.; Ma, J.; Zhang, X.; Shi, C., Recent advances in the modification of polyacrylate latexes. *Journal of Materials Science* **2015**, 50 (21), 6839-6863.
18. Matyjaszewski, K.; Spanswick, J., Controlled/living radical polymerization. *Materials Today* **2005**, 8 (3), 26-33.
19. Hawker, C. J.; Bosman, A. W.; Harth, E., New polymer synthesis by nitroxide mediated living radical polymerizations. *Chemical Reviews* **2001**, 101 (12), 3661-3688.
20. Matyjaszewski, K.; Xia, J., Atom transfer radical polymerization. *Chemical Reviews* **2001**, 101 (9), 2921-2990.
21. Moad, G.; Rizzardo, E.; Thang, S. H., Living radical polymerization by the RAFT process. *Australian Journal of Chemistry* **2005**, 58 (6), 379-410.

22. Perrier, S., 50th Anniversary Perspective: RAFT Polymerization, A User Guide. *Macromolecules* **2017**, *50* (19), 7433-7447.
23. Moad, G.; Rizzardo, E.; Thang, S. H., Living radical polymerization by the RAFT process—a third update. *Australian Journal of Chemistry* **2012**, *65* (8), 985-1076.
24. Chaduc, I.; Zhang, W.; Rieger, J.; Lansalot, M.; d'Agosto, F.; Charleux, B., Amphiphilic Block Copolymers from a Direct and One-pot RAFT Synthesis in Water. *Macromolecular Rapid Communications* **2011**, *32* (16), 1270-1276.
25. Keddie, D. J., A guide to the synthesis of block copolymers using reversible-addition fragmentation chain transfer (RAFT) polymerization. *Chemical Society Reviews* **2014**, *43* (2), 496-505.
26. York, A. W.; Kirkland, S. E.; McCormick, C. L., Advances in the synthesis of amphiphilic block copolymers via RAFT polymerization: stimuli-responsive drug and gene delivery. *Advanced Drug Delivery Reviews* **2008**, *60* (9), 1018-1036.
27. Griffin, W. C., Classification of surface-active agents by "HLB". *Journal of the Society of Cosmetic Chemists* **1949**, *1*, 311-326.
28. Figg, C. A.; Carmean, R. N.; Bentz, K. C.; Mukherjee, S.; Savin, D. A.; Sumerlin, B. S., Tuning hydrophobicity to program block copolymer assemblies from the inside out. *Macromolecules* **2017**, *50* (3), 935-943.
29. Talelli, M.; Iman, M.; Varkouhi, A. K.; Rijcken, C. J.; Schiffflers, R. M.; Etrych, T.; Ulbrich, K.; van Nostrum, C. F.; Lammers, T.; Storm, G., Core-crosslinked polymeric micelles with controlled release of covalently entrapped doxorubicin. *Biomaterials* **2010**, *31* (30), 7797-7804.
30. Shi, Y.; Cardoso, R. M.; Van Nostrum, C. F.; Hennink, W. E., Anthracene functionalized thermosensitive and UV-crosslinkable polymeric micelles. *Polymer Chemistry* **2015**, *6* (11), 2048-2053.
31. d'Agosto, F.; Rieger, J.; Lansalot, M., RAFT-Mediated Polymerization-Induced Self-Assembly. *Angewandte Chemie International Edition* **2020**, *59* (22), 8368-8392.
32. Canning, S. L.; Smith, G. N.; Armes, S. P., A critical appraisal of RAFT-mediated polymerization-induced self-assembly. *Macromolecules* **2016**, *49* (6), 1985-2001.
33. Lesage de la Haye, J.; Martin-Fabiani, I.; Schulz, M.; Keddie, J. L.; D'agosto, F.; Lansalot, M., Hydrophilic MacroRAFT-mediated emulsion polymerization: Synthesis of latexes for cross-linked and surfactant-free films. *Macromolecules* **2017**, *50* (23), 9315-9328.
34. Ferguson, C. J.; Hughes, R. J.; Nguyen, D.; Pham, B. T.; Gilbert, R. G.; Serelis, A. K.; Such, C. H.; Hawket, B. S., Ab initio emulsion polymerization by RAFT-controlled self-assembly. *Macromolecules* **2005**, *38* (6), 2191-2204.
35. Winnik, M. A., Interdiffusion and crosslinking in thermoset latex films. *Journal of Coatings Technology* **2002**, *74* (925), 49-63.
36. Lai, C.-L.; Chen, J.-T.; Fu, Y.-J.; Liu, W.-R.; Zhong, Y.-R.; Huang, S.-H.; Hung, W.-S.; Lue, S. J.; Hu, C.-C.; Lee, K.-R., Bio-inspired cross-linking with borate for enhancing gas-barrier properties of poly (vinyl alcohol)/graphene oxide composite films. *Carbon* **2015**, *82*, 513-522.
37. van Nostrum, C. F., Covalently cross-linked amphiphilic block copolymer micelles. *Soft Matter* **2011**, *7* (7), 3246-3259.
38. Stouten, J.; Vanpoucke, D. E.; Van Assche, G.; Bernaerts, K. V., UV-Curable Biobased Polyacrylates Based on a Multifunctional Monomer Derived from Furfural. *Macromolecules* **2020**, *53* (4), 1388-1404.
39. Piancatelli, G.; Scettri, A.; Barbadoro, S., A useful preparation of 4-substituted 5-hydroxy-3-oxocyclopentene. *Tetrahedron Letters* **1976**, *17* (39), 3555-3558.
40. Ulbrich, K.; Kreitmeier, P.; Reiser, O., Microwave-or microreactor-assisted conversion of furfuryl alcohols into 4-hydroxy-2-cyclopentenones. *Synlett* **2010**, *2010* (13), 2037-2040.

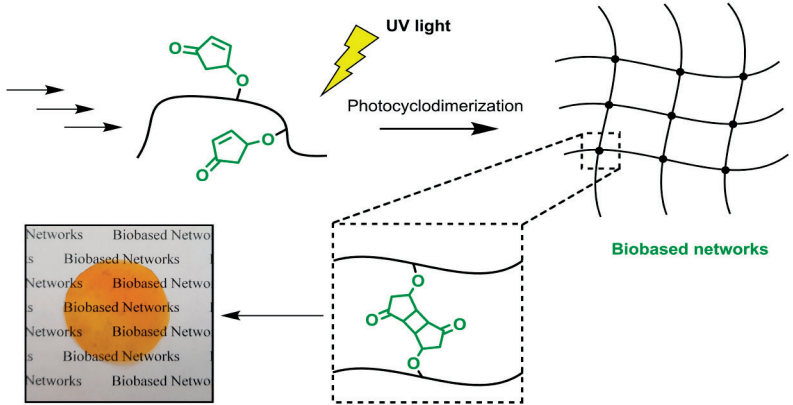
41. Fache, M.; Boutevin, B.; Caillol, S., Vanillin production from lignin and its use as a renewable chemical. *ACS Sustainable Chemistry & Engineering* **2016**, *4* (1), 35-46.
42. Veith, C.; Diot-Néant, F.; Miller, S. A.; Allais, F., Synthesis and polymerization of bio-based acrylates: A review. *Polymer Chemistry* **2020**, *11* (47), 7452-7470.
43. Lebedevaite, M.; Talacka, V.; Ostrauskaite, J., High biorenewable content acrylate photocurable resins for DLP 3D printing. *Journal of Applied Polymer Science* **2021**, *138* (16), 50233.
44. Lin, M. M., Selective oxidation of propane to acrylic acid with molecular oxygen. *Applied Catalysis A: General* **2001**, *207* (1-2), 1-16.
45. Hermens, J. G.; Jensma, A.; Feringa, B. L., Highly Efficient Biobased Synthesis of Acrylic Acid. *Angewandte Chemie* **2022**, *134* (4), e202112618.
46. Sun, D.; Yamada, Y.; Sato, S.; Ueda, W., Glycerol as a potential renewable raw material for acrylic acid production. *Green Chemistry* **2017**, *19* (14), 3186-3213.
47. Huang, M.; Liu, Y.; Klier, J.; Schiffman, J. D., High-Performance, UV-Curable Cross-Linked Films via Grafting of Hydroxyethyl Methacrylate Methylene Malonate. *Industrial & Engineering Chemistry Research* **2020**, *59* (10), 4542-4548.
48. Talelli, M.; Barz, M.; Rijcken, C. J.; Kiessling, F.; Hennink, W. E.; Lammers, T., Core-crosslinked polymeric micelles: Principles, preparation, biomedical applications and clinical translation. *Nano Today* **2015**, *10* (1), 93-117.
49. Skene, W. G.; Lehn, J.-M. P., Dynamers: polyacylhydrazone reversible covalent polymers, component exchange, and constitutional diversity. *Proceedings of the National Academy of Sciences* **2004**, *101* (22), 8270-8275.
50. Montarnal, D.; Capelot, M.; Tournilhac, F.; Leibler, L., Silica-like malleable materials from permanent organic networks. *Science* **2011**, *334* (6058), 965-968.
51. Denissen, W.; Winne, J. M.; Du Prez, F. E., Vitrimers: permanent organic networks with glass-like fluidity. *Chemical Science* **2016**, *7* (1), 30-38.
52. Guerre, M.; Taplan, C.; Winne, J. M.; Du Prez, F. E., Vitrimers: directing chemical reactivity to control material properties. *Chemical Science* **2020**, *11* (19), 4855-4870.
53. Podgórski, M.; Fairbanks, B. D.; Kirkpatrick, B. E.; McBride, M.; Martinez, A.; Dobson, A.; Bongiardina, N. J.; Bowman, C. N., Toward stimuli-responsive dynamic thermosets through continuous development and improvements in covalent adaptable networks (CANs). *Advanced Materials* **2020**, *32* (20), 1906876.



# 2



**Biomass**



---

# Chapter 2 UV curable Biobased Polyacrylates based on a Multifunctional Monomer derived from Furfural

---

This chapter is based on the following publication:

Stouten, J., Vanpoucke, D. E., Van Assche, G., & Bernaerts, K. V. (2020). UV-Curable Biobased Polyacrylates Based on a Multifunctional Monomer Derived from Furfural. *Macromolecules*, 53(4), 1388-1404.

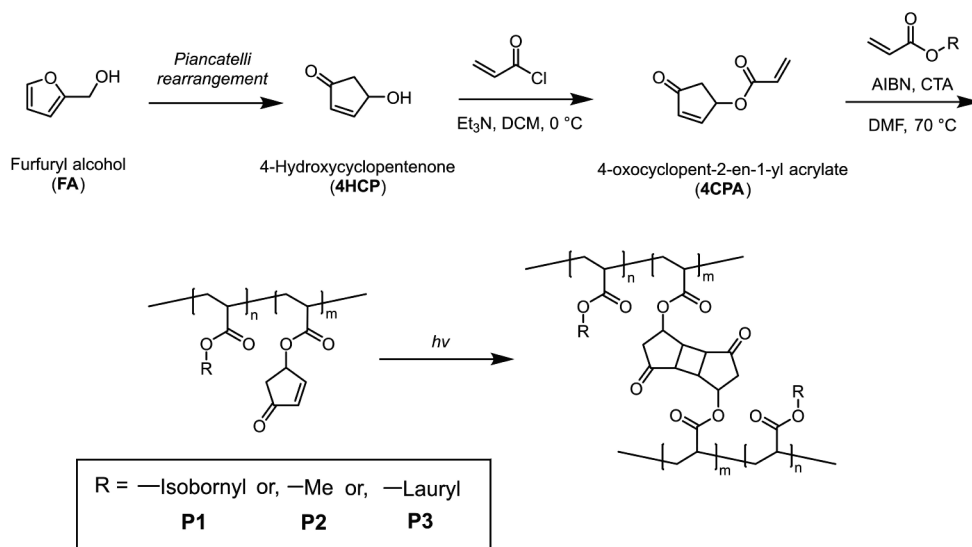
## Abstract

The controlled polymerization of a new biobased monomer, 4-oxocyclopent-2-en-1-yl acrylate, was established via reversible addition-fragmentation chain-transfer (co)polymerization to yield polymers bearing pendent cyclopentenone units. 4CPA contains two reactive functionalities, namely a vinyl group and an internal double bond, and is an unsymmetrical monomer. Therefore, competition between the internal double bond and the vinyl group eventually leads to gel formation. With RAFT polymerization, when aiming for a degree of polymerization of 100, maximum 4CPA conversions of the vinyl group between 19% and 45% were obtained without gel formation or extensive broadening of the dispersity. When the same conditions were applied in the copolymerization of 4CPA with lauryl acrylate, methyl acrylate, and isobornyl acrylate, 4CPA conversions of the vinyl group between 63% and 95% were reached. The additional functionality of 4CPA in copolymers was demonstrated by model studies with 4-oxocyclopent-2-en-1-yl acetate (**1**), which readily dimerized under UV light via [2 + 2] photocyclodimerization. Through characterization with NMR spectroscopy and EI-MS, a mixture of head-to-head and head-to-tail dimers of (**1**) were identified. Using the dimerization mechanism, solvent-cast LA and MA copolymers containing 30 mol% 4CPA were cross-linked under UV light to obtain freestanding films. The cross-linked films were characterized by DSC, DMA, FTIR, gel content, and swelling experiments. This is the first case where 4CPA is described as a monomer for functional biobased polymers that can undergo additional UV curing via photodimerization.

## Introduction

The conversion of plant-derived chemicals into useful materials has recently become more prominent due to the trend towards sustainability and renewability. In this context, extensive research has been devoted to new and renewable chemicals derived from biomass. The conversion of C5 and C6 sugars into platform molecules serves as a major route towards fine chemicals, fuels, and polymers.<sup>1-2</sup> One of those platform molecules is furfural, which can be converted to furfuryl alcohol.<sup>3</sup> Although direct conversion into furanoic monomers for aromatic polymers has been subject to extensive investigation,<sup>4</sup> further conversion of furfuryl alcohol into 4-hydroxycyclopentenone (4HCP) via the Piancatelli rearrangement is also possible (Scheme 2.1).<sup>5</sup>

4HCP is a versatile molecule with a high functional group density, which allows extensive chemical modification. It has been subjected to a variety of different chemistries including [2 + 2] photocycloaddition<sup>6-12</sup>, Diels-Alder<sup>13-15</sup>, 1,4-addition<sup>16-21</sup>, [3 + 2] cycloaddition<sup>22-23</sup>, and the synthesis of esters from the alcohol group of 4HCP.<sup>24</sup> It is recognized as a platform for complex natural products which mainly include prostaglandins.<sup>8</sup> Nonetheless, it has never been regarded as a potential monomer in functional polymers until now.



Scheme 2.1. Procedure for the synthesis of 4-oxocyclopentenyl acrylate (4CPA), and subsequently RAFT copolymerization and photo-cross-linking. CTA = chain transfer agent, R =  $-\text{CH}_3$  for methyl acrylate, R = -isobornyl for isobornyl acrylate and R =  $-(\text{CH}_2)_{11}\text{CH}_3$  for lauryl acrylate.

The secondary alcohol of 4HCP allows for acrylation with acryloyl chloride yielding 4-oxocyclopent-2-en-1-yl acrylate (4CPA). Upon polymerization of the acrylate, the pendent cyclopentenone unit can potentially provide useful functionality for postpolymerization modification, transformation into other functionalities, or cross-linking (Scheme 2.1). For



example, by making use of the  $\alpha,\beta$  unsaturated ketone group of 4CPA, UV light can induce the coupling of pendent cyclopentenone units via a photodimerization reaction. Schiess and Suter have previously investigated the photocyclodimerization of 4-oxocyclopent-2-en-1-yl acetate (**1**), the acetate of 4HCP.<sup>25</sup> However, the aim of the investigation was to obtain the elimination products of the dimer. They found that with UV-light exposure of the pure compound, dimerization was in competition with homolytic cleavage of the acetoxy group. This was confirmed by performing the dimerization in ether, which yielded the solvent adduct of (**1**). In the molten state, after 27 h irradiation with UV light, the head-to-tail (HT) dimer could be isolated with a yield of 9.5%. The deacetylated head-to-head (HH) and HT dimers were obtained with a 32% and 26% yield, respectively.<sup>25</sup> The ability of (**1**) to dimerize under UV light suggests that 4CPA based polymers can be employed for photocuring applications. This serves as a potential route to biobased networks for film and coating applications.

In many cases, UV curable polymers undergo network formation via a free radical mechanism. These systems make up the majority of the radiation curing market<sup>26</sup>, and usually require a photoinitiator, cross-linker, and reactive diluent depending on the method that is applied. Cross-linking via photodimerization of functional monomers proceeds readily with or without the addition of a photosensitizer and thus does not require any additional, often toxic additives such as initiators or cross-linkers to achieve network formation. Several functional groups that can undergo photocycloadditions have been incorporated in polymers, some of which include coumarin<sup>27-30</sup>, cinnamic acid<sup>31-32</sup>, conjugated furanes<sup>33</sup>, or anthracene<sup>34-37</sup> groups.

Direct free radical polymerization of the functional monomer 4CPA, gives rise to additional difficulties induced by the double bond in the ring. For example, selectivity between functional groups is crucial in obtaining good control over the molecular weight. This was shown for the polymerization of divinyl monomers.<sup>38-40</sup> If the difference in reactivity of the vinyl groups is not large enough, participation of the pendent vinyl groups can cause cyclization, branching or cross-linking reactions. One major strategy to reduce side reactions from the pendent vinyl group is to decrease the amount of the divinyl monomer via copolymerization with a monofunctional monomer. For the (co)polymerization of 4CPA, controlled radical polymerization (CRP) is applied. This way, molecular weight is limited to sufficiently short chains, so gel formation of the 4CPA (co)polymers is prevented. Reversible addition-fragmentation chain transfer (RAFT) polymerization is one of the major CRP techniques and provides a high tolerance to functional groups in the synthesis of well-defined polymers.<sup>41</sup>

4HCP is a versatile building block in organic chemistry, which makes it a promising monomer for functional polymers. In this chapter, 4CPA is proposed as a new biobased functional monomer, which can, after being incorporated in the polymer chain, undergo photocyclodimerization reactions to generate networks. Because of the functionality of 4CPA, a selective CRP technique should be established for the preparation of well-defined polymers. Therefore, the synthesis of 4CPA based homo- and copolymers with various

biobased comonomers via RAFT polymerization is explored. The biobased comonomers that were used in this research can all be obtained by esterification of a biobased alcohol with acrylic acid (Scheme 2.1). The resulting monomers can be considered partially or potentially biobased, depending on the alcohol used. In addition, acrylic acid can be considered potentially biobased<sup>42</sup> but currently, most acrylic acid is produced via the oxidation of propylene.<sup>43</sup> The monomers used in this research are methyl acrylate, isobornyl acrylate and lauryl acrylate. Additionally, 4-oxocyclopent-2-en-1-yl acetate was used as a model compound to obtain information on the 4CPA reactivity and dimerization in UV light. The latter reaction was confirmed experimentally by NMR spectroscopy and EI-MS. Furthermore, cross-linking and film formation under UV light of the 4CPA copolymers was followed by characterization with FTIR spectroscopy, dynamic mechanical analysis (DMA), dynamic scanning calorimetry (DSC), gel content and swelling studies.

## Experimental section

### Materials

Azobisisobutyronitrile (AIBN, Sigma-Aldrich) was recrystallized from methanol prior to use. Isobornyl acrylate (IBOA; technical, Sigma-Aldrich) and lauryl acrylate (LA; >98%, TCI) were passed over a basic alumina column prior to use to remove the stabilizer. Methyl acrylate (MA; 99%, Sigma-Aldrich) was distilled prior to use. Pyridine, dichloromethane (DCM), and triethylamine were distilled over calcium hydride (CaH<sub>2</sub>) prior to use. Cyanomethyl dodecyl trithiocarbonate (CDT) was synthesized according to a procedure mentioned in the literature.<sup>44</sup> 2-(Dodecylthiocarbonothioylthio)-2-methylpropionic acid (DDMAT; 98%, Sigma-Aldrich), trioxane (≥99%, Sigma-Aldrich), biphenyl (>99%, Sigma-Aldrich), acetophenone (AP; 99%, Sigma-Aldrich), sodium sulfate (≥99%, Sigma-Aldrich), acetic anhydride (≥99%, Sigma-Aldrich), *trans*-2-[3-(4-*tert*-butylphenyl)-2-methyl-2-propenylidene]-malononitrile (DCTB; Sigma-Aldrich, >98%), potassium trifluoroacetate (KTFA; Sigma Aldrich, 98%), acryloyl chloride (96%, Alfa Aesar), furfuryl alcohol (≥98%, Fischer Scientific), hydrogen chloride (HCl; 37% solution in H<sub>2</sub>O, Acros Organics), sodium bicarbonate (>99%, Acros organics), sodium chloride (≥99.8%, Roth), *tert*-butyl methylether (TBME; 99.9%), acetic acid (AcOH; 99.7%), and CDCl<sub>3</sub> (99.8%, Cambridge Isotope Laboratories) were used as received. All other solvents were obtained from Biosolve and were used as received.

### Characterization

#### *Differential scanning calorimetry (DSC)*

DSC (TA instruments, Qseries, DSC Q2000) with a heating rate of 10 °C/min was used to obtain information on the phase transition temperatures. Before DSC measurements, the samples were dried for 24 h at 50-80 °C in vacuum before measurement under nitrogen atmosphere. The polymers were subjected to two heating and cooling cycles, the second was used for determination of the phase transition points. The inflection point was used for reporting of the *T<sub>g</sub>*.

*Gel permeation chromatography (GPC)*

GPC was performed at 30 °C using a Waters GPC equipped with a Waters 2414 refractive index detector. Tetrahydrofuran (THF) was used as the eluent at a flow rate of 1 mL/min. Three linear columns (Styragel HR1, Styragel HR4 and Styragel HR5) including a Styragel Guard column were used. Molecular masses are given relative to polystyrene standards. The polymers were dissolved in THF with a concentration of 3 mg/mL and filtered over a 0.2 µm PTFE syringe filter.

*Nuclear magnetic resonance (NMR) spectroscopy*

<sup>1</sup>H NMR (300 MHz) and <sup>13</sup>C NMR (75 MHz) spectra were recorded on a Bruker Avance III HD Nanobay 300 MHz apparatus at 298K in CDCl<sub>3</sub>. For <sup>1</sup>H NMR measurements 16 scans were used and for <sup>13</sup>C NMR measurements 1024 scans. NMR spectroscopy was used for structural characterization. <sup>1</sup>H NMR spectroscopy was used for the determination of monomer conversion in the homopolymerization of 4CPA, and the disappearance of the vinyl protons was followed over time relative to trioxane, which was added as an internal standard to the reaction mixture.

*Gas chromatography with flame ionization detector (GC-FID)*

GC-FID measurements were performed on a Shimadzu GC-2010 equipped with a Supelco SPB-1 capillary column (30 m × 0.25 mm × 0.25 µm film thickness). GC-FID was used to follow the disappearance of the individual monomers in the copolymerizations relative to biphenyl as the internal standard. The temperature program was as follows: an initial temperature of 80 °C was maintained for 3 min, and then increased to 140 °C with a heating rate of 10 °C/min. This temperature was maintained for 1 min, and further increased to 300 °C with a heating rate of 20 °C/min and was maintained at 300 °C for 5 min (the total run time of 23 min).

*Fourier-transform infrared (FTIR) spectroscopy*

FTIR spectra were recorded on a Shimadzu (MIRacle 10) spectrometer. Samples were measured by applying a sample on the ATR crystal and the spectra were recorded between 400 cm<sup>-1</sup> and 4000 cm<sup>-1</sup>, with a resolution of 4 cm<sup>-1</sup> and with 64 accumulations per spectrum.

*Dynamic mechanical analysis (DMA)*

DMA was performed in a TA Instruments DMA Q800 to determine the viscoelastic behavior of the polymer networks. Rectangular samples of 0.13-0.40 mm thick, and 5.65-10 mm wide, were measured in tension mode at a frequency of 1 Hz, oscillation strain of 0.05-0.1%, and using a heating rate of 2 °C/min. The transition temperatures were determined at the intersection of the tangents of the storage modulus. The samples were dried beforehand for 24 h at 50 °C in vacuum.

### *Electron impact mass spectrometry (EI-MS)*

EI-MS of the model dimer compound was recorded on a Shimadzu QP2010 ultra mass spectrometer using direct MS injection. The sample was heated to 350 °C with a heating rate of 20 °C/min.

### *Matrix-assisted laser desorption/ionization time-of-flight mass spectrometry (MALDI-ToF-MS)*

MALDI-ToF-MS spectra were recorded on a Bruker UltrafleXtreme spectrometer with a 355 nm Nd:Yag laser (2 kHz repetition pulse/Smartbeam-II<sup>TM</sup>) and a grounded steel plate. DCTB was used as the matrix (20 mg/mL in THF), and KTFA was used a cationization agent (10 mg/mL in THF). The polymers were dissolved in THF (10 mg/mL). Solutions of matrix, salt and polymer were mixed in volume ratios of 200:10:30, respectively. All mass spectra were recorded in the reflector mode. Poly(ethylene glycol) standards with  $M_n$  of 5000, 10 000 and 15 000 g/mol were used for calibration. mMass was used to compare theoretical isotope distributions with experimental isotope distributions. Contour plots were generated using COCONUT version 1.5.<sup>45</sup>

### *Melting point*

Melting points were determined using a Mettler Toledo MP90 melting point system. A heating rate of 10 °C/min was used.

### **Swelling experiments**

The swelling ratio of the cross-linked polymers was determined by immersing an accurately weighed sample of approximately 50 mg into 5 mL of chloroform for 24 h at room temperature. The swollen solids were weighed, and then filtered and dried for 24 h at 50 °C in vacuum. All swelling experiments were performed in triplicate.

The soluble fraction and swelling ratio were calculated accordingly:

$$\text{Soluble fraction} = (m_{\text{initial}} - m_{\text{dry}})/m_{\text{initial}}$$

$$\text{Swelling ratio} = (m_{\text{swollen}} - m_{\text{initial}})/m_{\text{initial}}$$

### **4-Hydroxycyclopent-2-en-1-one (4HCP) synthesized in flow<sup>46</sup>**

A solution of furfuryl alcohol (25.0 g, 255 mmol) in water (500 mL) was adjusted with AcOH to pH = 4 and heated in a flow reactor consisting of a stainless steel coil of 6 meters with back-pressure regulator at 240 °C (flow pump 5 mL/min of solution and 0.3 mL of toluene per minute). After completion, the mixture was extracted with TBME (3 × 30 mL) and the water layer was concentrated under reduced pressure. The crude yield was not determined. The reaction was scaled up to 10 L reaction volume. The crude product (150 g material from several batches) was purified by vacuum distillation using a Vigreux column of 30 cm (heating bath 130 °C, pressure: 0.001 mbar, distillation temperature: 90 °C) yielding the title compound as an almost colorless oil, which was stored in a freezer at -20 °C.

Yield: 50 g.  $^1\text{H}$  NMR spectroscopy (300 MHz,  $\text{CDCl}_3$ ):  $\delta$  (ppm) = 2.19-2.82 (m, 2H,  $\text{CH}_2$ ); 2.98 (s, 1H, OH); 5.02 (m, 1H, CH-OH); 6.20 (d, 1H, CH-C=O); 7.57 (dd, 1H, CH-C-O).  $^{13}\text{C}$  NMR spectroscopy (75 MHz,  $\text{CDCl}_3$ ):  $\delta$  (ppm) = 44.4 ( $\text{CH}_2$ ); 70.5 (CH-OH); 135.1 (CH-C=O); 163.7 (CH-C-O); 207.2 (C=O).  $^1\text{H}$  NMR and  $^{13}\text{C}$  NMR spectra are shown in Figure A1.

### Synthesis of 4-oxocyclopent-2-en-1-yl acrylate (4CPA)

4-Hydroxycyclopent-2-en-1-one (85.8 g, 0.875 mol, 1 eq.) was dissolved in DCM (860 mL) and cooled with an ice-water bath to 0 °C. Triethylamine (106 g, 145 mL, 1.05 mol, 1.20 eq.) was added followed by the slow addition of acryloyl chloride (87.1 g, 78.2 mL, 0.962 mol, 1.10 eq.). The temperature was kept below 18 °C during the addition. After the addition was completed, stirring was continued for 5.5 h at a temperature between 16 °C and 18 °C. TBME (1200 mL) was added. The solids were removed by filtration over a thin layer of silica gel and washed with TBME (800 mL). The yellow filtrate was concentrated under reduced pressure at 35 °C and redissolved in DCM. The organic layer was washed with dilute HCl,  $\text{NaHCO}_3$ , water, and finally brine (twice). The organic layer was dried over  $\text{Na}_2\text{SO}_4$ , filtered and concentrated under reduced pressure. The crude material was purified by vacuum distillation (bath temperature 100 °C, pressure  $10^{-3}$  mbar, bp: 60 °C). 4CPA was isolated as a slightly yellow oil. Yield: 111.6 g (84%).  $^1\text{H}$  NMR spectroscopy (300 MHz,  $\text{CDCl}_3$ ):  $\delta$  (ppm) = 2.31-2.91 (m, 2H,  $\text{CH}_2\text{-C=O}$ ); 5.89 (dd, 1H,  $\text{CH}_2\text{=CH}$ ), 5.91-5.96 (m, 1H, CH-O); 6.05-6.18 (m, 1H, CH=CH $_2$ ); 6.34 (dd, 1H, CH-C=O); 6.44 (dd, 1H,  $\text{CH}_2\text{=CH}$ ); 7.59 (dd, 1H, CH-C-O).  $^{13}\text{C}$  NMR spectroscopy (75 MHz,  $\text{CDCl}_3$ ):  $\delta$  (ppm) = 40.1 ( $\text{CH}_2\text{-C=O}$ ); 72.2 (C-O); 127.8 (CH=CH $_2$ ); 132.1 (CH $_2\text{=CH}$ ); 137.2 (CH-C=O); 159.0 (CH-C-O); 165.6 (C=O<sub>acrylate</sub>); 204.9 (C=O<sub>cyclopentenone</sub>).  $^1\text{H}$  NMR and  $^{13}\text{C}$  NMR spectra are shown in Figure A2.

### Synthesis of 4-oxocyclopent-2-en-1-yl methacrylate (4CPMA)

4-Hydroxycyclopent-2-en-1-one (5.0 g, 50.97 mmol, 1 eq.), DMAP (32 mg, 0.26 mmol, 0.005 eq.), triethylamine (10.24 mL, 73.91 mmol, 1.45 eq.), and dichloromethane (170 mL) were brought in a nitrogen-filled Schlenk flask equipped with magnetic stir bar. The flask was placed in an ice bath and while stirring, methacryloyl chloride (5.43 mL, 56.07 mmol, 1.1 eq.) was added dropwise over the course of 30 min. The mixture was allowed warm to room temperature and was left stirring overnight. Cold water was added and the organic layer was separated. The organic layer was washed with dilute HCl,  $\text{NaHCO}_3$ , and then brine. The solvent was evaporated and a light yellow oil was obtained with a yield of 4.2 g (50%).  $^1\text{H}$  NMR and  $^{13}\text{C}$  NMR spectra are shown in Figure A3.

**Model compound 4-oxocyclopent-2-en-1-yl acetate (1)**

(1) was synthesized according to a procedure previously reported in literature<sup>47</sup> (Figure 2.1).

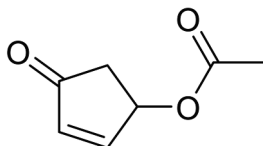


Figure 2.1. Chemical structure of 4-oxocyclopent-2-en-1-yl acetate (1).

In summary, the synthesis was as follows. A 100 mL two-neck round bottom flask was charged with 4HCP (5.0 g, 51 mmol, 1 eq.). The flask was evacuated and flushed with nitrogen. DCM (50 mL) was added and the mixture was cooled to 0 °C using an ice bath. pyridine (7.9 g, 100 mmol, 2 eq.) was added to the cold solution while stirring with a magnetic stirrer. To the mixture, acetic anhydride (7.8 g, 76.5 mmol, 1.5 eq.) was added dropwise while maintaining the temperature at 0 °C. After the complete addition of the acetic anhydride, the reaction mixture was allowed to warm to room temperature, and was stirred for 15 h. The reaction was quenched by adding cold, dilute HCl. The organic layer was washed with dilute HCl, followed by water, NaHCO<sub>3</sub> and finally with brine. The organic layer was dried over Na<sub>2</sub>SO<sub>4</sub> and the solvent was evaporated under vacuum. The residue was purified by vacuum distillation (bp: 60 °C at 10<sup>-3</sup> mbar). (1) was obtained as a light-yellow oil which crystallized upon cooling. Yield: 4.39 g (62%). Melting point: 35 °C. <sup>1</sup>H NMR spectroscopy (300 MHz, CDCl<sub>3</sub>): δ (ppm) = 2.08 (s, 3H, CH<sub>3</sub>); 2.25-2.87 (m, 2H, CH<sub>2</sub>); 5.84 (m, 1H, CH-O); 6.32 (dd, 1H, CH-C=O); 7.56 (dd, 1H, CH-CH-O). <sup>13</sup>C NMR spectroscopy (75 MHz, CDCl<sub>3</sub>): δ (ppm) = 21.0 (CH<sub>3</sub>); 41.1 (CH<sub>2</sub>); 72.0 (CH-O); 137.1 (CH-C=O); 159.1 (CH-CH-O); 170.5 (C=O<sub>acetate</sub>); 205.0 (C=O<sub>cyclopentenone</sub>). <sup>1</sup>H NMR and <sup>13</sup>C NMR spectra are shown in Figure A4.

**Photodimerization of (1)**

A solution of (1) (386 mg, 2.76 mmol) was prepared in acetone (5 mL). The mixture was irradiated using a 400 W metal halide, UVA lamp in a Dymax ECE 2000 UV chamber under a nitrogen flow. Inside the chamber, the solution reached a maximum temperature of approximately 40 °C. The disappearance of (1) was followed by gas chromatography. After 230 min, irradiation was stopped and excess acetone was evaporated under reduced pressure. The viscous liquid was extracted with diethyl ether, from which white crystals precipitated at -20 °C. Yield: 71.3 mg (18.4%). Melting point: 81 °C. <sup>1</sup>H NMR spectroscopy (300 MHz, CDCl<sub>3</sub>): δ (ppm) = 2.00 (s, 3H, CH<sub>3</sub>); 2.11 (s, 3H, CH<sub>3</sub>); 2.43-3.16 (m, 8H, CH<sub>2</sub>, CH<sub>cyclobutane</sub>); 5.32 (d, 1H, CH-O); 5.43 (q, 1H, CH-O). <sup>13</sup>C NMR spectroscopy (75MHz, CDCl<sub>3</sub>): δ (ppm) = 20.9 (CH<sub>3</sub>); 21.1 (CH<sub>3</sub>); 40.4 (CH); 41.9 (CH<sub>2</sub>); 42.6 (CH<sub>2</sub>); 42.9 (CH); 43.8 (CH); 45.9 (CH); 70.0 (CH-O); 75.1 (CH-O); 170.0 (C=O<sub>acetate</sub>); 170.2 (C=O<sub>acetate</sub>); 212.7 (C=O<sub>ring</sub>); 213.5 (C=O<sub>ring</sub>). MS for C<sub>14</sub>H<sub>16</sub>O<sub>6</sub>: m/z = 280 g/mol (calculated: 280.09 g/mol).

### Homopolymerization of 4CPA

In a typical experiment, 4CPA was polymerized using CDT as the RAFT agent (Table 2.1, entry 3). 4CPA (500 mg, 3.29 mmol, 500 eq.), AIBN (1.1 mg, 0.0066 mmol, 1 eq.), CDT (10.4 mg, 0.033 mmol, 5 eq.), dimethylformamide (DMF) (2 mL), and trioxane (5 wt% relative to monomer) were added to a 5 mL Schlenk flask equipped with magnetic stir bar. The mixture was degassed by at least three consecutive freeze-pump-thaw cycles. The flask was immersed in a thermostated oil bath at 70 °C. During the reaction, samples were taken at several time intervals for  $^1\text{H}$  NMR spectroscopy to check the monomer conversion. After 5 h, the polymerization was stopped by cooling to room temperature and diluting with THF. The polymer was precipitated twice in a 20-fold excess of methanol, and dried at 70 °C under vacuum for 24 h.

### Copolymerization of 4CPA with biobased comonomers

All copolymerizations were performed under the same conditions; a 40 wt% monomer concentration in the solvent was maintained for all monomers. In the following experiment poly(4CPA-*co*-LA) with 30 mol% 4CPA incorporation (P3-3/7 in Table 2.2) was prepared. 4CPA (4.0 g, 26.3 mmol, 150 eq.), LA (14.8 g, 61.4 mmol, 350 eq.), AIBN (29 mg, 0.175 mmol, 1 eq.), CDT (278 mg, 0.877 mmol, 5 eq.), DMF (29.8 mL), and biphenyl (5 wt% relative to monomers) were added to a 100 mL Schlenk flask equipped with a magnetic stir bar. The solution was degassed by at least three consecutive freeze-pump-thaw cycles. The flask was then immersed in a thermostated oil bath at 70 °C. Samples were taken at several time intervals for GPC to check the molecular weight development and for GC-FID analysis to track the individual monomer conversions. After 6 h, the reaction was stopped by cooling the mixture to room temperature and diluting with THF. The overall monomer conversion at this point was 71.8%. The polymer was precipitated twice in 800 mL methanol, and dried at 60 °C under vacuum. A yellow viscous polymer was obtained. Yield: 12.75 g (68.0%).

### Photo-cross-linking

Polymer films were prepared by dissolving 300 mg of a copolymer (P2-3/7 or P3-3/7 in Table 2.2) in 3 mL of chloroform, with or without the addition of acetophenone photosensitizer. The solutions were cast on quartz glass slides (50 × 70 mm) and the solvent was allowed to evaporate for at least one hour. The film was placed in a Dymax ECE 2000 UV chamber under a nitrogen flow and irradiated using a 400 W metal halide, UVA lamp. The distance of the sample to the lamp was 18 cm. The film was irradiated for 30 min on each side.

## Results and discussion

### Reactivity study towards internal double bond of 4CPA

The 4CPA polymerizability was studied using the model compound 4-oxocyclopent-2-en-1-yl acetate (**1**). As mentioned in the introduction section, the internal double bond in 4CPA can participate during the polymerization of the acrylate, eventually leading to gelation of the polymer. To evaluate the reactivity of the internal double bond in the cyclopentenone unit, model compound (**1**) was subjected to RAFT polymerization conditions as described for the homopolymerization of 4CPA in the experimental section. No conversion of (**1**) could be observed in GC-FID and  $^1\text{H}$  NMR spectroscopy analysis after 6 h at 70 °C. The inability of homopolymerization of (**1**) can be attributed to steric effects. It is known that 1,2-disubstituted alkenes are challenging to homopolymerize, however copolymerization can proceed quite readily.<sup>48</sup> This result suggests that cyclization, branching, or cross-linking reactions by coupling of the pendent cyclopentenone units in the given polymerization conditions of 4CPA are unlikely to take place. Nevertheless, participation in the radical polymerization of the enone unit by propagation in the presence of acrylates is not ruled out.

To further investigate the reactivity of (**1**), the model compound was copolymerized with 4CPA using CDT as the chain transfer agent in DMF at 70 °C, with  $[\text{AIBN}]_0/[\text{CDT}]_0/[\text{4CPA}]_0/[(\mathbf{1})]_0 = 0.2:1:50:50$ . Samples were taken at several time intervals for MALDI-ToF-MS analysis. In Figure A5 the MALDI-ToF-MS spectrum, of a sample obtained after 50 min and 14% 4CPA conversion is shown. The conversion was kept low in order to avoid gel formation or extensive branching of the polymer and reduce effects of changing monomer composition. In the MALDI-ToF-MS spectrum, several polymeric distributions can be observed, with the main distribution belonging to the 4CPA homopolymer (Figure A5b). Interestingly, the largest distribution did not contain RAFT agent end groups but instead possessed hydrogen or double bond end groups resulting from termination and transfer processes. Most of the other smaller distributions could be assigned as copolymers of 4CPA and (**1**) containing one or two units of (**1**). Due to a large amount of different distributions observed in MALDI-ToF-MS of copolymers, full characterization of the polymer can be challenging. This is made more convenient by converting the one-dimensional spectra into two-dimensional contour plots. The contour plot of the copolymerization of 4CPA and (**1**) is shown in Figure 2.2, and gives an indication of the copolymer composition based on the position and shape of the distribution. In this case, the distribution is located close to the x-axis, which indicates the amount of 4CPA units incorporated in the chain. The tendency towards incorporation of 4CPA and (**1**) into the polymer chains is strongly in favor of 4CPA, which is mainly attributed to the differences in stability of the formed radical, and steric influences of the side groups of the reactive double bonds. Since some chains did contain incorporation of (**1**) at low conversion, gelation in the homopolymerization of 4CPA is expected to occur at high conversions and/or degree of polymerization (DP), since only a few linkages between polymer chains are enough to cause gel formation in the material.



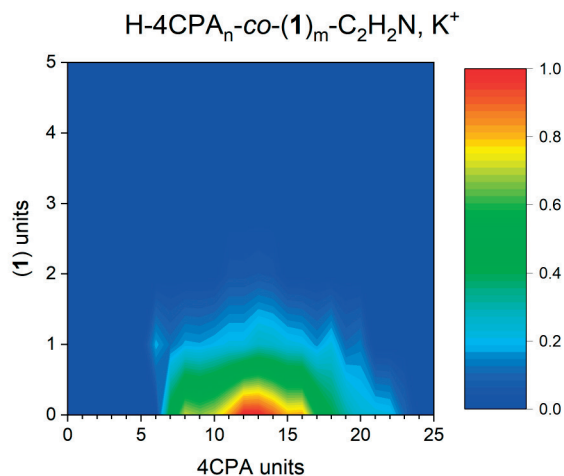


Figure 2.2. MALDI-ToF-MS contour plot of the copolymer  $\text{H-4CPA}_n\text{-co-(1)}_m\text{-C}_2\text{H}_2\text{N, K}^+$  formed after 50 min during the RAFT copolymerization of 4CPA and (1) in a 50:50 ratio.

### Homopolymerization of 4CPA and 4CPMA

In the homopolymerization of 4CPA, several reaction conditions were varied to observe the effect on the molecular weight and conversion. Experiments were performed at 70 °C, using AIBN as the thermal initiator, and two different RAFT agents were investigated: DDMAT and CDT. The results are summarized in Table 2.1. During the polymerization, aliquots were withdrawn from the solution at several time intervals. Samples were analyzed by  $^1\text{H}$  NMR spectroscopy and GPC to determine the conversion and molecular weight, respectively. Monomer conversion was determined by comparing the acrylate protons at 5.93, 6.10, and 6.34 ppm (Figure A2a) with the signal from trioxane at 5.14 ppm, which was added as an internal standard.

Table 2.1. RAFT homopolymerization of 4CPA.

Entry	CTA	[I]/[CTA]/[M]	Time (min)	Solvent	4CPA conc. (wt%)	Monomer conv. <sup>c</sup> (%)	$M_{n,th}^d$ (kg/mol)	$M_{n,GPC}^a$ (kg/mol)	$\bar{D}^a$
1		0.2/1/20	2760	Toluene	20	— <sup>c</sup>	— <sup>c</sup>	— <sup>c</sup>	— <sup>c</sup>
2		0.2/1/20	330	DMF	20	71.8	2.5	3.9	1.18
3	CDT	0.2/1/100	305	DMF	20	45.2	7.2	6.6	1.25
4		0.2/1/100	90	DMF	60	51.2	— <sup>b</sup>	— <sup>b</sup>	— <sup>b</sup>
5		0.2/1/20	60	None	Bulk	89.7	3.7	8.6	7.96
6		0.2/1/100	360	DMF	20	19.0	3.3	4.4	1.08
7	DDMAT	0.2/1/100	140	DMF	60	29.6	4.9	6.0	1.13
8		0.2/1/20	150	None	Bulk	57.2	2.1	4.4	1.12

<sup>a</sup> Determined by THF GPC against polystyrene standards, the results are of the final polymer after precipitation in methanol; <sup>b</sup> Polymer formed a gel at higher conversions; <sup>c</sup> Polymer precipitated in the reaction solvent; <sup>d</sup> Calculated as follows:  $M_{n,th} = MW_{CTA} + (DP_{n,th} \times \% \text{ conversion}_{4CPA} \times 152.1)$ ; <sup>e</sup> Determined by <sup>1</sup>H NMR spectroscopy by comparing the acrylate vinyl resonances with trioxane as the internal standard.

The free radical polymerization of alkyl acrylates typically leads to extensive branching and gel formation, even at low monomer conversions due to inter- and intramolecular (i.e. backbiting) chain transfer reactions to polymer.<sup>49</sup> However, it has been shown that radicals exhibit an enhanced selectivity in the presence of a reversible deactivation process (i.e. RAFT polymerization) and transfer to polymer reactions are suppressed. This is related to the time of radical deactivation, which is typically shorter than the time of backbiting for a RAFT agent with sufficiently high chain transfer constant.<sup>50</sup> Indeed, initial studies towards the free radical polymerization of the 4CPA yielded an insoluble gel quickly after the reaction temperature was reached. Therefore, RAFT polymerization was employed for the synthesis of poly(4CPA) homopolymers without gel formation. With the selection of a suitable chain transfer agent, RAFT is a convenient technique for the controlled polymerization of alkyl acrylates.

Initially, toluene was selected as the solvent (Table 2.1, entry 1); however, the polymer was not soluble and precipitated during the reaction. Therefore, the solvent was changed to DMF, which was a suitable solvent for the homopolymerization of 4CPA. With  $[AIBN]_0/[CDT]_0/[4CPA]_0 = 0.2/1/20$  in DMF at 20 wt% monomer concentration (Table 2.1, entry 2), a monomer conversion of 71.8% was reached while the dispersity was only 1.18. This promising result indicates that competition of the internal double bond is limited, even at a reasonable high conversion. However, the targeted DP of this experiment is only 20. In an attempt to increase the DP with  $[AIBN]_0/[CDT]_0/[4CPA]_0 = 0.2/1/100$  (Table 2.1, entry 3) a lower monomer conversion was obtained, but the molecular weight was increased from 3.9 to 6.6 kg/mol while the dispersity remained low at 1.25. Improving the conversion by increasing the monomer concentration from 20 to 60 and 100% (Table 2.1, entry 3, 4 and 5),

resulted in gel formation above 50% conversion when a DP of 100 was targeted. Given the low rate coefficients for intermolecular chain transfer reactions (which cause gel formation in acrylates) relative to intramolecular chain transfer reactions,<sup>51</sup> gel formation at elevated conversion is unlikely caused by chain transfer to polymer processes, but mainly due to contribution of the pendent cyclopentenone unit of 4CPA. Secondary reactions involving the cyclopentenone unit can take place because a resonance stabilized radical can be formed on the ring due to the presence of the enone group. In our case, the low conversions that were obtained for some of the reactions could also be explained by termination and transfer reactions, which were observed in the copolymerization of 4CPA with (1) using MALDI-ToF-MS (Figure A4).

Under the same conditions as the experiment in Table 2.1, entry 3, the RAFT agent was changed to DDMAT, which resulted in a decrease in the monomer conversion from 45 to 19% (entry 6). Similarly, when the reaction was performed at higher concentrations (entry 4 vs. 7) or in bulk (entry 5 vs. 8), a lower monomer conversion was reached with DDMAT compared to CDT, which could however prevent gel formation. In Figure 2.3, the kinetics of the polymerization with both RAFT agents is shown. A faster initial reaction rate is observed for CDT compared to DDMAT. Since both RAFT agents have the same trithiocarbonate Z-group, the difference lies in the RAFT pre-equilibrium and re-initiation stage. In this case, CDT with the cyanoalkyl R-group appears to be a more efficient chain transfer agent in contrast to DDMAT.<sup>52</sup>

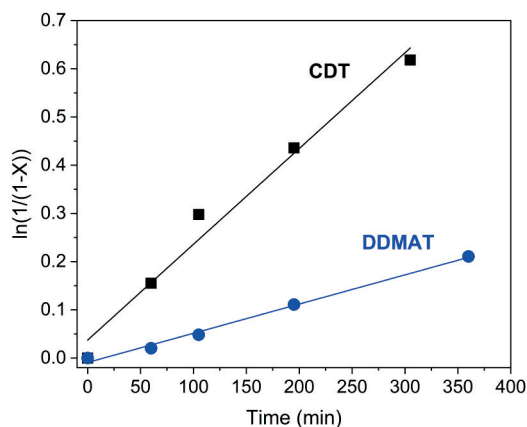


Figure 2.3. First order plot of the homopolymerization of 4CPA with two RAFT agents CDT (▪) and DDMAT (•), Table 1, Entries 5 and 8, respectively.

<sup>1</sup>H NMR and <sup>13</sup>C NMR spectroscopy were used to confirm the structure of poly(4CPA). In general, the proposed structure corresponds well with the spectra. The characteristic main chain (-CH<sub>2</sub>-CH-) signals at 1.5-2.5 ppm are clearly observed in the <sup>1</sup>H NMR spectrum (Figure 2.4a). Based on the resonances at 6.36 and 7.60 ppm, which possess the same integral as the (-O-CH-) protons in the cyclopentenone group, the internal double bond remains

nearly intact during the polymerization, at least within the error margin of the NMR measurement. The double bond content of the polymer (Table 2.1, entry 3) was calculated with  $^1\text{H}$  NMR spectroscopy by comparing the resonances at 6.36 and 7.60 ppm, with the main chain resonances between 1.40 and 2.12 ppm. At a conversion of 45.2%, 94% of the secondary double bonds were maintained in the polymer. The RAFT agent end group could also be observed, with the resonances of the methylene groups of the dodecyl chain at 1.27 and 3.38 ppm, and the methyl group at 0.89 ppm. The presence of the trithiocarbonate end group in the purified polymer indicates that RAFT conditions are maintained during the polymerizations. Also in the  $^{13}\text{C}$  NMR spectrum (Figure 2.4b) of poly(4CPA) the resonances corresponding to the internal double bond in the ring are present at 137.6 and 158.4 ppm. The peaks corresponding to the (CH) group in the main chain and the methylene carbon of the pendent cyclopentenone group overlap at 40.84 ppm. However, DEPT analysis revealed the presence of both the secondary and tertiary substituted carbons (Figures A6 and A7).

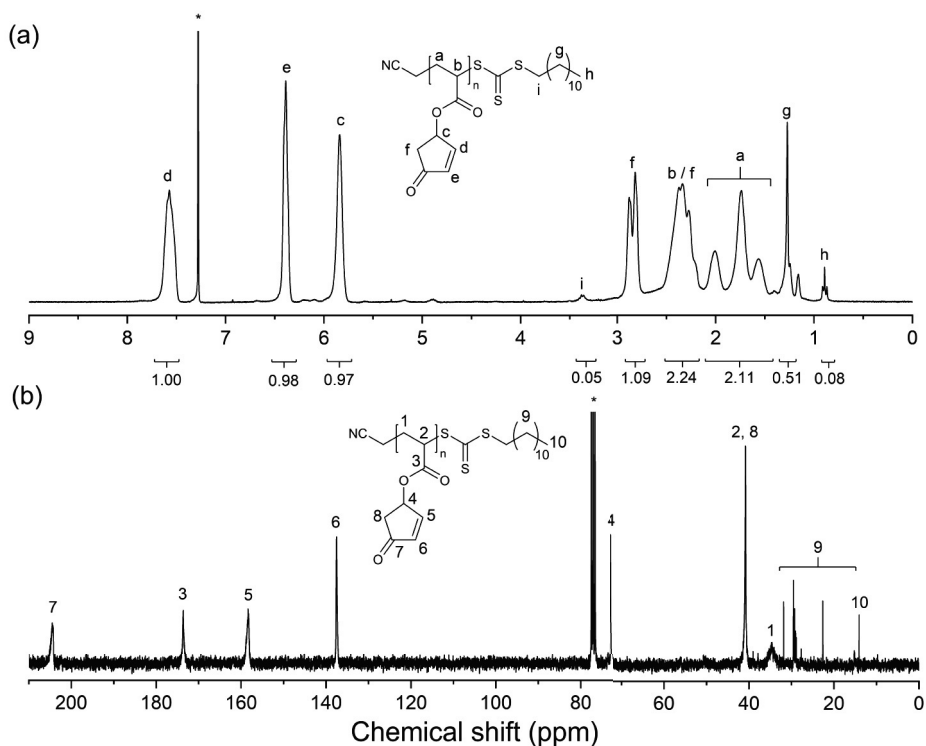


Figure 2.4. (a)  $^1\text{H}$  NMR and (b)  $^{13}\text{C}$  NMR spectra in  $\text{CDCl}_3$  of poly(4CPA) (Table 2.1, entry 3) synthesized by RAFT polymerization using CDT as the RAFT agent. \* = solvent signal.

As a comparison to the acrylate ester of 4HCP, the methacrylate ester was also synthesized. The polymerization was performed analogous to the procedure from Table 2.1, entry 3, but instead 4-Cyano-4-(phenylcarbonothioylthio)pentanoic acid was used as a RAFT agent, which is more suitable for methacrylate polymerization. Compared to the acrylate, slightly higher conversion was reached without cross-linking. This is also reflected in the molecular

weight of the homopolymer, which is significantly higher (Figure 2.5a). However, this also goes at the expense of control over the reaction: higher dispersities and a higher molecular weight shoulder are observed. As expected, the  $T_g$  of the homopolymer is also significantly increased due to the lower conformational freedom of the polymethacrylate backbone. The  $T_g$  of the 4CPA poly acrylate was 62 °C, whereas the methacrylate had a  $T_g$  of 139 °C (Figure 2.5b). Since, in the future latex applications with accompanying low  $T_g$  polymers are targeted, the acrylate was further investigated in copolymerization.

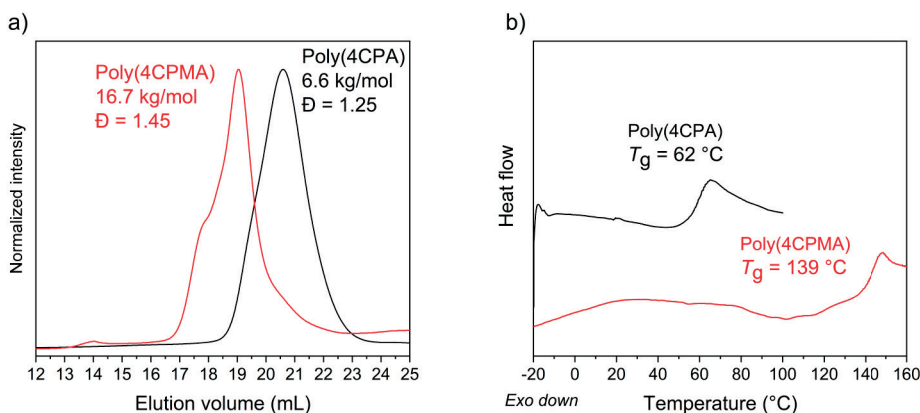


Figure 2.5. a) Overlay of the GPC traces of poly(4CPMA) (red) and poly(4CPA) (black). b) Overlay of the DSC curves of poly(4CPMA) and poly(4CPA).

### Copolymerization of 4CPA with IBOA, MA, and LA

To reduce secondary reactions of the pendent cyclopentenone units in the RAFT polymerization of 4CPA and increase acrylate monomer conversion, copolymerization with several biobased comonomers was investigated. The comonomers that were used are isobornyl acrylate (IBOA), methyl acrylate (MA), and lauryl acrylate (LA). Copolymerization was performed with a 40 wt% monomer concentration in DMF at 70 °C with  $[AIBN]_0/[CDT]_0/[M_1]_0/[M_2]_0 = 0.2/1/50/50$ . The results are summarized in Table 2.2.

Table 2.2. RAFT copolymerization of 4CPA with comonomers IBOA, MA, and LA.

Entry	Co-monomer	$f_{4CPA}$	$F_{4CPA}^c$	Conv. 4CPA (%)	Conv. comonomer (%)	$M_{n,th}^c$ (kg/mol)	$M_{n,GPC}^a$ (kg/mol)	$\bar{D}^a$	$T_g$ (°C)	$T_m$ (°C)
P1-6/4	IBOA	0.60	0.62	64	56	10.8	13.1	7.46	80	
P1-5/5		0.50	0.51	69	61	11.9	12.8	2.21	87	
P1-4/6		0.40	0.42	67	59	11.8	9.6	1.34	89	
P1-3/7		0.30	0.32	71	63	12.7	11.0	1.27	88	
P1-2/8		0.20	0.20	78	71	14.5	11.8	1.33	92	
P1-1/9		0.10	0.09	71	64	13.4	8.3	1.26	96	
P2-5/5	MA	0.50	0.54	81	80	9.9	19.2	7.94	55	
P2-4/6		0.40	0.42	81	76	9.2	13.2	2.57	46	
P2-3/7		0.30	0.30	86	82	9.2	12.4	1.44	36	
P2-2/8		0.20	0.26	90	86	9.0	13.8	1.78	35	
P2-1/9		0.10	0.11	95	91	8.8	9.2	1.19	17	
P3-6/4	LA	0.60	0.62	67	59	12.1	14.7	5.85	21	
P3-5/5		0.50	0.51	65	57	12.1	12.6	1.17	12	
P3-4/6		0.40	0.39	73	67	14.1	14.0	1.30	-2	
P3-3/7		0.30	0.29	63	57	12.8	11.2	1.25	$\bar{d}$	$\bar{d}$
P3-2/8		0.20	0.19	71	67	15.4	13.8	1.30	$\bar{b}$	-3

<sup>a</sup> Determined by THF GPC against polystyrene standards, the results are of the final polymer after precipitation in methanol; <sup>b</sup> Not observed; <sup>c</sup> Determined with <sup>1</sup>H NMR spectroscopy; <sup>d</sup> Glass transition and melting peak overlap in the DSC; <sup>e</sup> Calculated from:  $M_{n,th} = 317.58 + (DP_{n,th,4CPA} \times conv_{4CPA} / 100 \times 152.1) + (DP_{n,th,comonomer} \times conv_{comonomer} / 100 \times MW_{comonomer})$ .

None of the copolymerizations resulted in insoluble networks, even at high conversions, which is an improvement compared to the homopolymerizations. Using MA as the comonomer and  $[4CPA]_0/[MA]_0 = 1/9$ , the conversion of 4CPA reached 95% while maintaining a narrow dispersity of 1.19 (Table 2.2, entry P2-1/9). When the 4CPA to MA feed ratio was increased, the control over the molecular weight was lost due to participation of the pendent cyclopentenone units, which in turn leads to branching and increase in the dispersity. At  $[4CPA]_0/[MA]_0 = 3/7$ , a sudden increase in molecular weight and dispersity occurred at 60% monomer conversion (Figure 2.6a). The non-linearity of the molecular weight with the conversion suggests that controlled conditions are not upheld during the polymerization. This is also represented in the GPC traces over time, which show the evolution of additional distributions in a later stage of the polymerization (Figure 2.6c). These do not appear as evidently for the copolymerizations with LA and IBOA, though a slight increase in dispersity occurs. Also, higher DP's were reached with MA which contribute to the generally higher dispersity for poly(4CPA-*co*-MA). In the case of IBOA and LA, a higher 4CPA incorporation was allowed without loss of molecular weight control. Only when  $[4CPA]_0/[LA]_0$  and  $[4CPA]_0/[IBOA]_0 = 6/4$  the molecular weight did not increase linearly with monomer conversion and high dispersities of the final copolymers were observed (Figure 2.6b). The evolution of a second distribution in the GPC traces indicates the onset of cross-linking reactions (Figure 2.6d). The steric hindrance of borneol and dodecanol esters

of IBOA and LA, respectively, are believed to reduce participation of the pendent cyclopentenone units in the polymerization as opposed to the less bulky MA.

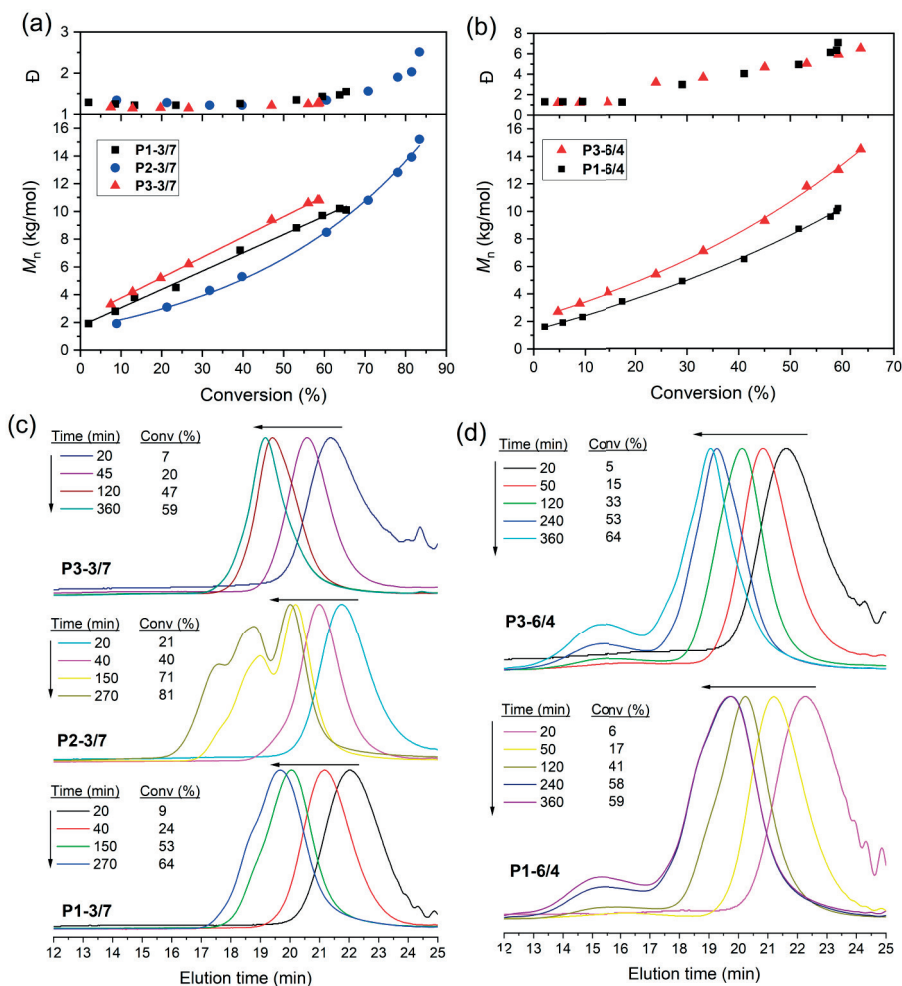


Figure 2.6. Molecular weight evolution over the total monomer conversion of the copolymers (a) P1-3/7, P2-3/7, P3-3/7; (b) P3-6/4, P1-6/4, and (c) and (d) are the GPC traces over time of the same reactions. P1 = poly(4CPA-co-IBOA), P2 = poly(4CPA-co-MA) and P3 = poly(4CPA-co-LA).

In all copolymerizations, 4CPA was the fastest reacting monomer relative to MA, IBOA or LA (Figure 2.7b-d). However, when the 4CPA feed fraction was lowered; a higher overall monomer reactivity was obtained. The initial monomer reactivity is shown in the semi-logarithmic kinetic plot obtained for the copolymerization of 4CPA with MA (Figure 2.7a). The change in the steepness of the curve upon increasing the comonomer content was observed for all the comonomers tested. This is another indication that chain termination and

transfer events are more prevalent in the presence of 4CPA but do not affect the rate of 4CPA consumption relative to the comonomer.

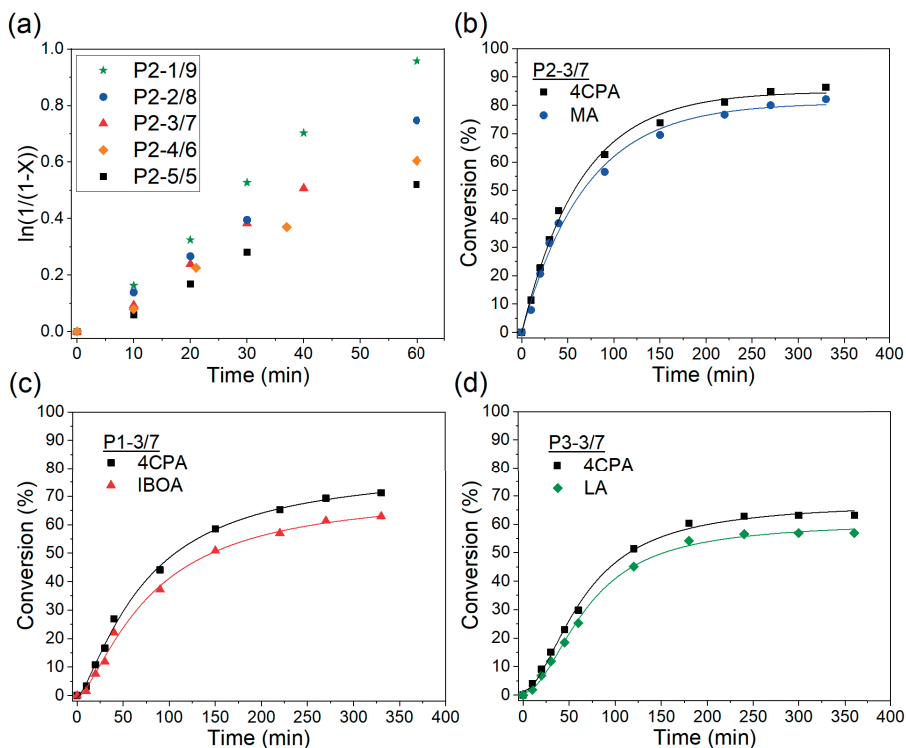


Figure 2.7. (a) First-order kinetic plots of the copolymerization of 4CPA with MA with different feed fractions of 4CPA, calculated from the overall conversion; conversion plots of the copolymerization of 4CPA with feed fraction 0.3 together with (b) MA; (c) IBOA; and (d) LA.

The thermal behavior of the synthesized copolymers was analyzed by DSC to monitor the effect of the amount of the comonomer on the glass transition temperature. The homopolymer of 4CPA has a glass transition temperature of 62 °C (Figure 2.5b), which is reduced to 55 °C upon copolymerization with one monomer equivalent MA (Figure A8). Further incorporation of MA in the copolymer resulted in a significant decrease in the glass transition temperature from 55 °C at 54% MA to 17 °C at 91% MA incorporation. Alternatively, when 4CPA was copolymerized with IBOA a gradual increase in the glass transition temperature was observed for samples containing a higher fraction of the rigid IBOA. Poly(4CPA-*co*-IBOA) containing 51% IBOA had a  $T_g$  of 80 °C, whereas 91% IBOA incorporation resulted in a  $T_g$  of 96 °C. Similar to copolymerization with MA, LA also had a reducing effect on the  $T_g$ . Side chain crystallinity was observed for poly(4CPA-*co*-LA) with LA fractions of 0.71 and 0.81; the latter has a melting point of -3 °C. Crystallinity of homopolymers<sup>53</sup> and copolymers<sup>54</sup> from (meth)acrylates containing long pendent n-alkyl chains is known for these types of polymers.



In general, the  $T_g$  of a polymer is a physical process for amorphous polymers, affecting chain mobility, which is important for film formation and post-polymerization reactions. In this case, UV curing by the reaction of the pendent cyclopentenone units is the targeted cross-linking reaction. At temperatures above the  $T_g$ , the increased mobility of the polymer chains favors the cross-linking reactions, resulting in a higher cross-linking degree.<sup>27</sup> Furthermore, steric hindrance from bulky comonomers can influence the reactivity of side groups as well.<sup>55</sup> Therefore, careful selection of the copolymer composition is required to achieve facile cross-linking.

In Figure 2.8, an overlay of the  $^1\text{H}$  NMR spectra of the copolymers P1-3/7, P2-3/7 and P3-3/7 (Table 2.2) is shown. The peak signals correspond well with the proposed structures.  $^1\text{H}$  NMR spectroscopy was also used to calculate the monomer ratio in the copolymer. This was performed by comparing the resonances of the (CH-O) protons of the monomers, which appear at 3.67, 4.02, 4.64, and 5.84 ppm for MA, LA, IBOA, and 4CPA, respectively. In general, the comonomer ratios in the final copolymer corresponded well with the monomer feed ratios even at incomplete conversion (Table 2.2). Unfortunately, the presence of the RAFT agent end group could only be assigned to copolymers containing MA, since the resonances originating from the methyl groups of LA and IBOA overlap with those from the RAFT end group.

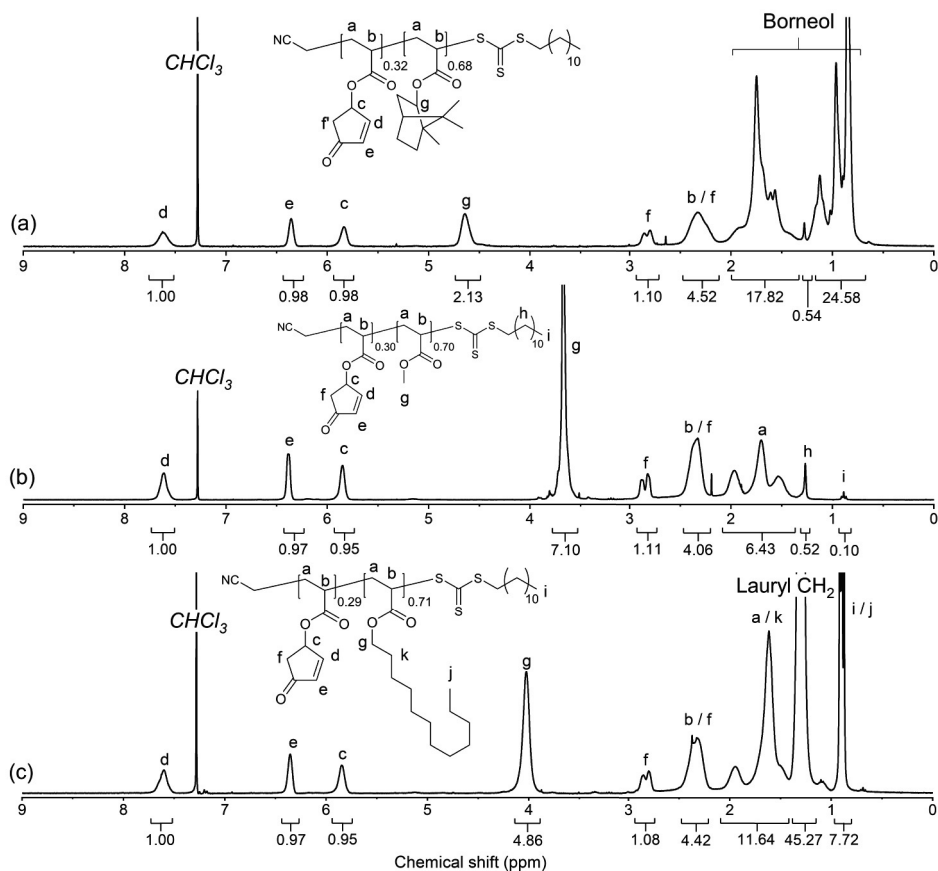
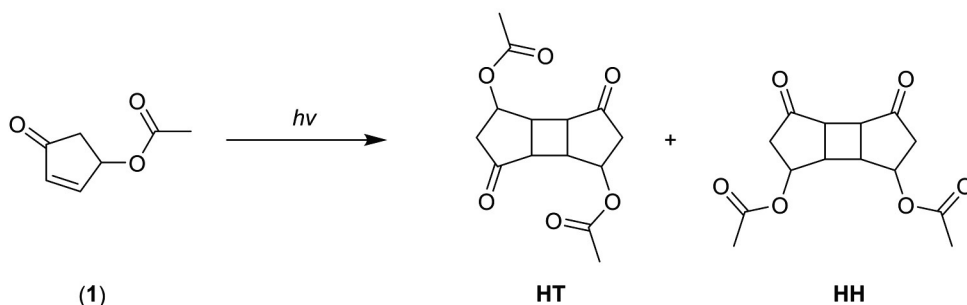


Figure 2.8.  $^1\text{H}$  NMR spectra of copolymers (a) poly(4CPA-co-IBOA) P1-3/7, (b) poly(4CPA-co-MA) P2-3/7, and (c) poly(4CPA-co-LA) P3-3/7 (300 MHz,  $\text{CDCl}_3$ ).

### Photodimerization of (1)

In literature, the photodimerization of cyclopentenone is well established<sup>56-59</sup> but apart from one study in 1978<sup>25</sup>, nothing was reported for 4-hydroxycyclopentenone's. To demonstrate the photodimerization of 4CPA and polymers derived thereof in a model reaction, compound (1) was irradiated with UV light in acetone. This yielded a mixture of the two possible adducts head-to-tail (HT) and head-to-head (HH) (Scheme 2.2). The ratio between adducts HT and HH was found to be 53:47 by comparing the resonances corresponding to the CH-O protons which appear at 5.32 and 5.43 ppm in the  $^1\text{H}$  NMR spectrum (Figure 2.9a). In studies toward the photocyclodimerization of cyclopentenone it was shown that the concentration, and solvent polarity have a moderate influence on the HT and HH ratio, with HH adducts becoming more important at higher concentrations and in more polar solvents.<sup>57</sup> The  $^1\text{H}$  NMR spectrum assignment in Figure 2.9a is supported by HSQC analysis (Figure A9), which show coupling with the cyclobutane and methylene carbons. It must be noted, that some additional peak splitting in the experimental spectrum can be expected since the dimer mixture consists

not only of conformers, but also stereoisomers. Indeed, small signals are observed in the  $^{13}\text{C}$  NMR spectrum close to the main signals, and additional (minor) splitting of the methyl groups in the  $^1\text{H}$  NMR spectrum is also observed.



Scheme 2.2. Photocyclodimerization of (1) in acetone yielding the head-to-tail (HT) and head-to-head (HH) dimers.

The proposed structure also corresponds well with the  $^{13}\text{C}$  NMR spectrum (Figure 2.9b). Together with DEPT-135 analysis (Figure A10), which distinguishes the methylene protons from the cyclobutane protons between 38 and 48 ppm, and HSQC (Figure A9), which shows coupling between  $\text{C}_{\text{H-O}}$  carbons and the attached protons, all the spectral lines in the  $^{13}\text{C}$  NMR spectrum could be assigned.

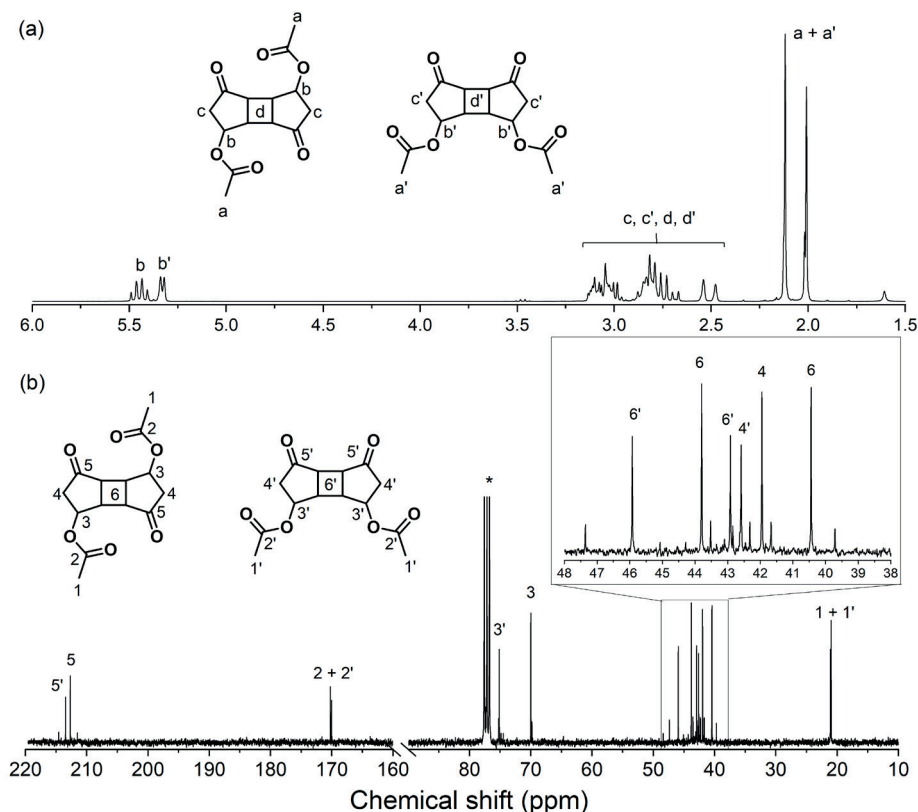


Figure 2.9. (a) <sup>1</sup>H NMR and (b) <sup>13</sup>C NMR spectrum of the HT and HH dimer of (1) in CDCl<sub>3</sub>.

Further characterization of the obtained dimers using direct injection MS confirmed the observations made in NMR spectroscopy, a mass of 280 g/mol was found, which corresponds to the dimer mass (Figure A11). Additional fragmentation masses of 220 and 160 g/mol were observed, which likely belong to the elimination products (one or two molecules of acetic acid removed).

### Photo-cross-linking

With these promising results, we continued with the photo-cross-linking of 4CPA copolymers to produce freestanding films (Figure 2.10a). Poly(4CPA-*co*-LA) P3-3/7 and poly(4CPA-*co*-MA) P2-3/7 were prepared on a larger scale for UV curing experiments. Unfortunately, the cured film of polymer P1-3/7 turned out to be too brittle to produce freestanding films. The polymers were cured for 30 min on both sides in a UV chamber under nitrogen flow. In the chamber, the temperature of the film reached a maximum of 90 °C after 60 min irradiation, which is well above the *T*<sub>g</sub> of P2-3/7 and P3-3/7. Curing of freestanding polymer films proceeded without the addition of a photoinitiator or cross-linker. Therefore, since α,β-unsaturated ketones have been shown to readily dimerize under UV light, cross-linking occurs via a photodimerization between the pendent cyclopentenone units. The

addition of acetophenone (AP) as a photosensitizer improved the cross-linking slightly. Several weight ratios of copolymer and AP were investigated.

To test the degree of cross-linking of the produced films, swelling studies were performed; the obtained gel content values are summarized in Figure 2.10b. The films showed a high swelling ratio in chloroform, which is a good solvent for the copolymers (Figure A12). In general, the films exhibited a high cross-linking degree. For poly(4CPA-*co*-LA) P3-3/7, the gel content ranged between 82 and 90% depending on the AP concentration. Upon the addition of 1 wt% of AP, the gel content increased from 82 to 89.5%. Increasing the AP concentration to 10 wt% did not result in a significant change in the gel content after 60 min curing. It was therefore decided to continue with the formulation containing 1 wt% AP for further characterization. Polymer poly(4CPA-*co*-MA) P2-3/7 was only cross-linked using 1 wt% AP, which resulted in a gel content of 97%. The reason for the lower gel content in P3-3/7 compared to P2-3/7 could be the steric hindrance of the bulkier lauryl acrylate units. As a control, the homopolymer of lauryl acrylate was prepared according to the same procedure for the copolymerizations, except DMF was replaced by toluene as the solvent. Irradiation of a layer of the homopolymer for a total of 60 min did not result in any cross-linking. The polymer dissolved completely when it was introduced in chloroform. This confirms that the introduction of 4CPA in the polymer chain results in cross-linking under UV light.

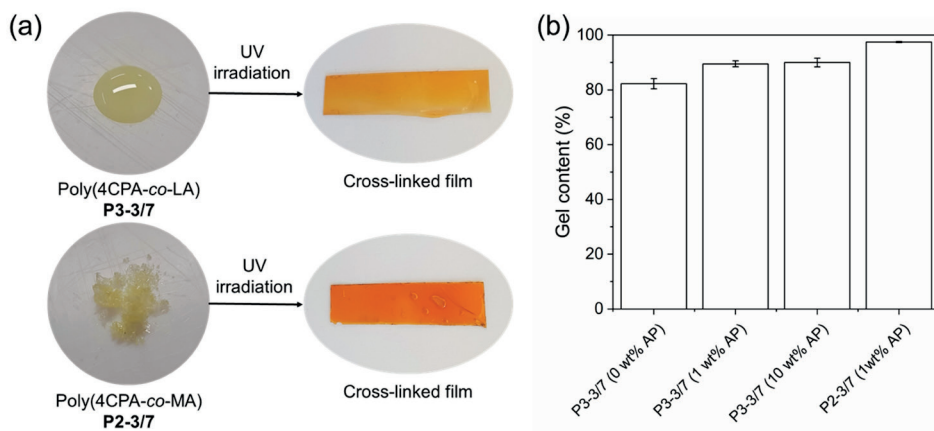


Figure 2.10. (a) Preparation of the UV cross-linked films of poly(4CPA-*co*-LA) and poly(4CPA-*co*-MA) (b) Gel content for the copolymer formulations in  $\text{CHCl}_3$  prepared with various amounts of AP as a photosensitizer. P2 = poly(4CPA-*co*-MA) and P3 = poly(4CPA-*co*-LA).

FTIR was used to characterize the change in functional groups as result of the cross-linking (Figure 2.11). For both poly(4CPA-*co*-MA) P2-3/7 and poly(4CPA-*co*-LA) P3-3/7 the characteristic band corresponding to the internal double bond in the ring disappeared. The disappearance of the C=C stretch signal at  $1593 \text{ cm}^{-1}$  is only observed a weak signal due to

the low functional group concentration and low sensitivity of FTIR towards detection of C=C bonds.

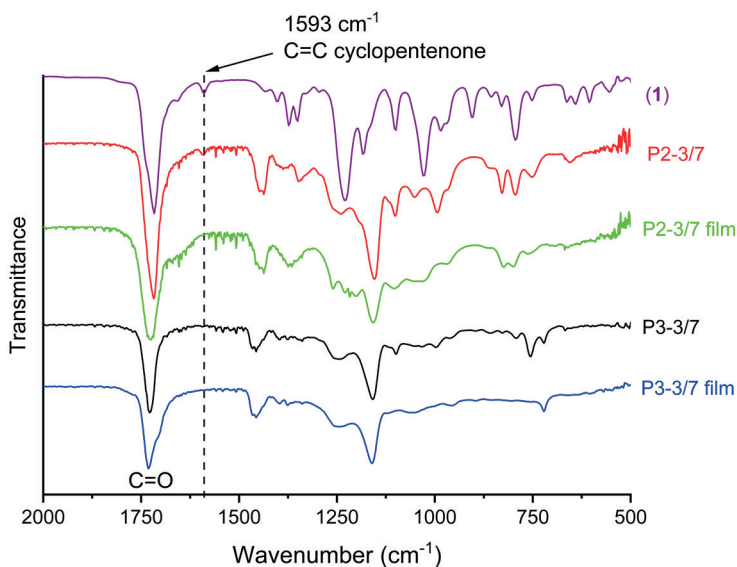


Figure 2.11. FTIR spectrum of the 4CPA copolymers before and after cross-linking under UV light, in purple: (1), red: poly(4CPA-*co*-MA) P2-3/7, green: cross-linked film of P2-3/7, black: poly(4CPA-*co*-LA) P3-3/7, blue: cross-linked film of P3-3/7.

The cross-linked films were characterized by DMA and DSC to observe the changes in physical properties as a result of photo-cross-linking. The DSC of the cross-linked film of poly(4CPA-*co*-MA) P2-3/7 clearly showed an increase in  $T_g$  of about 18 °C compared to the non cross-linked polymer (Figure 2.12a). The observed  $T_g$  of 47 °C corresponds well with what is observed in DMA, where the intersection of the tangent lines of the storage modulus lies at 45 °C (Figure A13a). The maximum of the  $\tan \delta$  appears at a considerably higher temperature of 90 °C. A broad transition is observed in the DMA spectrum as indicated by the broad  $\tan \delta$  peak, which may be explained by incomplete cross-linking or dangling chain ends. In the case of the LA copolymer P3-3/7, two endothermic events overlap in both the polymer and the cross-linked film. In the DSC traces (Figure 2.12b), a melting peak is observed between -30 °C and 10 °C, which arises from the side chain crystallinity. As mentioned before, this only occurs in copolymers containing a high LA fraction. The melt peak is likely superimposed on a glass transition, indicated by the difference in baseline levels before and after the transition. A similar event is observed in DMA, where a large decrease at approximately -3 °C (Figure A13b) follows a small decrease in the loss modulus at approximately -30 °C. The intersection of the tangents of the storage modulus lies at -3 °C, which corresponds to the melting temperature of the side chain crystals formed in homo- and copolymers of LA as indicated in Table 2.2. Therefore, it is suspected that the first transition corresponds to the glass transition and the second to the melting of the side chain crystals.<sup>53-</sup>

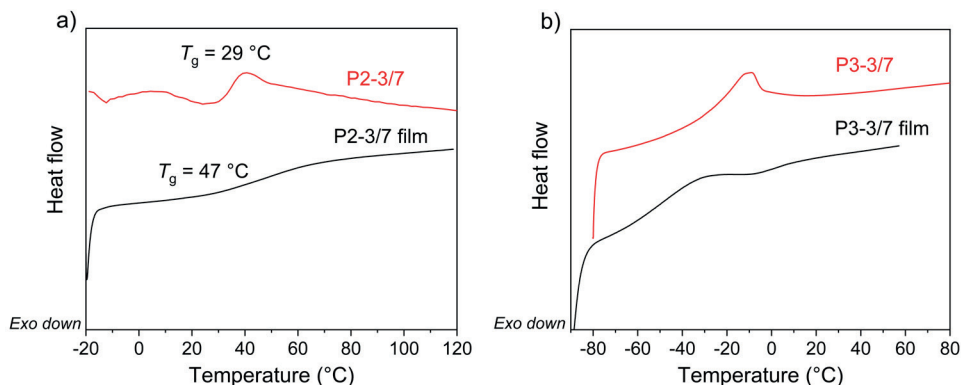


Figure 2.12. DSC traces of the polymers (red) and cross-linked films (black) of (a) poly(4CPA-co-MA) P2-3/7 and (b) poly(4CPA-co-LA) P3-3/7.

## Conclusions

In this work, the polymerization of a novel biobased acrylate monomer, which contains a cyclopentenone group, is presented. The pendent units can undergo [2 + 2] photocyclodimerization to produce cross-linked networks. We have demonstrated the controlled (co)polymerization of 4CPA without gel formation via the cyclopentenone unit, resulting in polymers with narrow dispersity. To obtain polymers with a higher targeted DP (e.g. 100), copolymerization with a comonomer under RAFT conditions is required. The type and amount of comonomer did affect the control during polymerization. Comonomers with a large side group provide more steric hindrance around the pendent double bonds in the ring and thus allow a larger incorporation of 4CPA while maintaining control over the molecular weight.

With the help of model studies, dimerization via [2 + 2] photocycloaddition was demonstrated for model compound 4-oxocyclopent-2-en-1-yl acetate. Using 2D NMR spectroscopy the spectral lines of the dimerization product of 4-oxocyclopent-2-en-1-yl acetate in  $^1\text{H}$  and  $^{13}\text{C}$  NMR spectra were identified. In a similar fashion, the intermolecular photodimerization reaction of 4CPA was successfully applied in copolymers resulting in coupling of polymer chains to produce networks. Irradiation of solvent casted poly(4CPA-co-LA) and poly(4CPA-co-MA) with UV light, resulted in cross-linked freestanding films, which possessed a high gel content.

## References

1. Climent, M. J.; Corma, A.; Iborra, S., Conversion of biomass platform molecules into fuel additives and liquid hydrocarbon fuels. *Green Chemistry* **2014**, *16* (2), 516-547.
2. Gallezot, P., Process options for converting renewable feedstocks to bioproducts. *Green Chemistry* **2007**, *9* (4), 295-302.
3. Mariscal, R.; Maireles-Torres, P.; Ojeda, M.; Sádaba, I.; Granados, M. L., Furfural: a renewable and versatile platform molecule for the synthesis of chemicals and fuels. *Energy & environmental science* **2016**, *9* (4), 1144-1189.
4. Decostanzi, M.; Auvergne, R.; Boutevin, B.; Caillol, S., Biobased phenol and furan derivative coupling for the synthesis of functional monomers. *Green chemistry* **2019**, *21* (4), 724-747.
5. Piancatelli, G.; Scettri, A.; Barbadoro, S., A useful preparation of 4-substituted 5-hydroxy-3-oxocyclopentene. *Tetrahedron Letters* **1976**, *17* (39), 3555-3558.
6. Le Liepvre, M.; Ollivier, J.; Aitken, D. J., Synthesis of Functionalized Bicyclo [3.2. 0] heptanes—a Study of the [2+ 2] Photocycloaddition Reactions of 4-Hydroxycyclopent-2-enone Derivatives. *European Journal of Organic Chemistry* **2009**, *2009* (34), 5953-5962.
7. Stensen, W.; Svendsen, J. S.; Hofer, O.; Sydnes, L. K., Photochemical [2+ 2] Cycloadditions. III. Addition of 4-Substituted 2-Cyclopentenones to Allene; Configuration Determination by Lanthanide-Induced Shift Studies. *Acta Chemica Scandinavica* **1988**, *42*, 259-268.
8. Schrader, T. O.; Snapper, M. L., Stereodivergent synthesis of all 15-F2 isoprostanes. *Journal of the American Chemical Society* **2002**, *124* (37), 10998-11000.
9. Shizuka, M.; Snapper, M. L., Selective synthesis of ent-15-epi-F2t-isoprostane and a deuterated derivative. *Synthesis* **2007**, *2007* (15), 2397-2403.
10. De Gregori, A.; Jommi, G.; Sisti, M.; Gariboldi, P.; Merati, F., Studies directed towards the total synthesis of dicyclopenta [a, d] cyclooctane terpenoids. *Tetrahedron* **1988**, *44* (9), 2549-2568.
11. Farcet, J. B.; Himmelbauer, M.; Mulzer, J., Photochemical and thermal [2+ 2] cycloaddition to generate the bicyclo [3.2. 0] heptane core of bielschowskysin. *European Journal of Organic Chemistry* **2013**, *2013* (20), 4379-4398.
12. Nettekoven, M.; Püllmann, B.; Martin, R. E.; Wechsler, D., Evaluation of a flow-photochemistry platform for the synthesis of compact modules. *Tetrahedron Letters* **2012**, *53* (11), 1363-1366.
13. Jacobo, S. H.; Chang, C.-T.; Lee, G.-J.; Lawson, J. A.; Powell, W. S.; Pratico, D.; FitzGerald, G. A.; Rokach, J., Total synthesis of 8, 12-iso-iPF3 $\alpha$ -VI, an EPA-derived isoprostane: stereoselective introduction of the fifth asymmetric center. *The Journal of organic chemistry* **2006**, *71* (4), 1370-1379.
14. Jeroncic, L. O.; Cabal, M. P.; Danishefsky, S. J.; Shulte, G. M., On the diastereofacial selectivity of Lewis acid-catalyzed carbon-carbon bond forming reactions of conjugated cyclic enones bearing electron-withdrawing substituents at the gamma.-position. *The Journal of Organic Chemistry* **1991**, *56* (1), 387-395.
15. Dols, P. P. M.; Klunder, A. J.; Zwanenburg, B., 4-Hydroxycyclopent-2-en-1-one and derivatives as chiral synthetic equivalents of cyclopentadienone in asymmetric Diels-Alder reactions. *Tetrahedron* **1994**, *50* (28), 8515-8538.
16. Morita, Y.; Suzuki, M.; Noyori, R., An organozinc aid in alkylation and acylation of lithium enolates. *The Journal of Organic Chemistry* **1989**, *54* (8), 1785-1787.
17. Suzuki, M.; Morita, Y.; Koyano, H.; Koga, M.; Noyori, R., Three-component coupling synthesis of prostaglandins. A simplified, general procedure. *Tetrahedron* **1990**, *46* (13-14), 4809-4822.

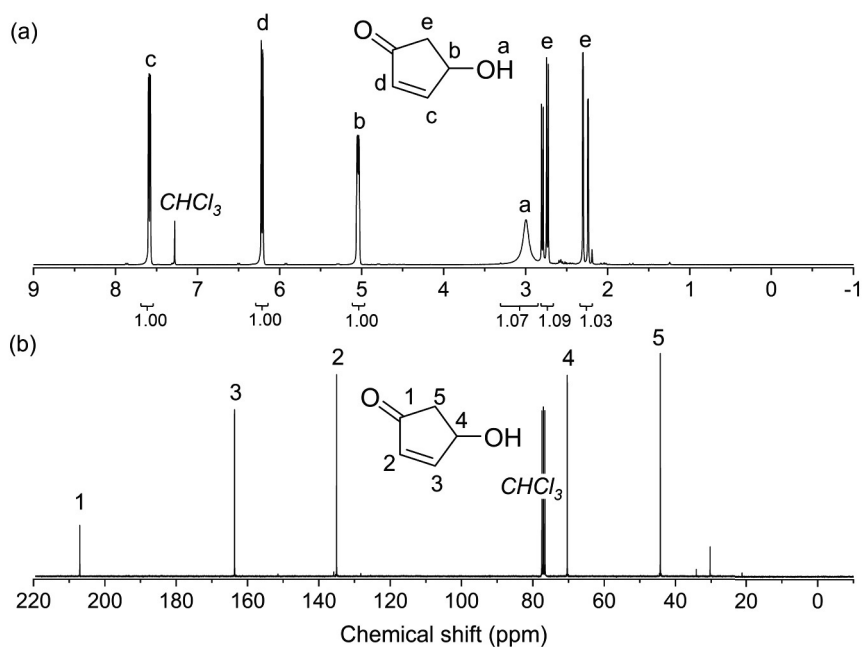
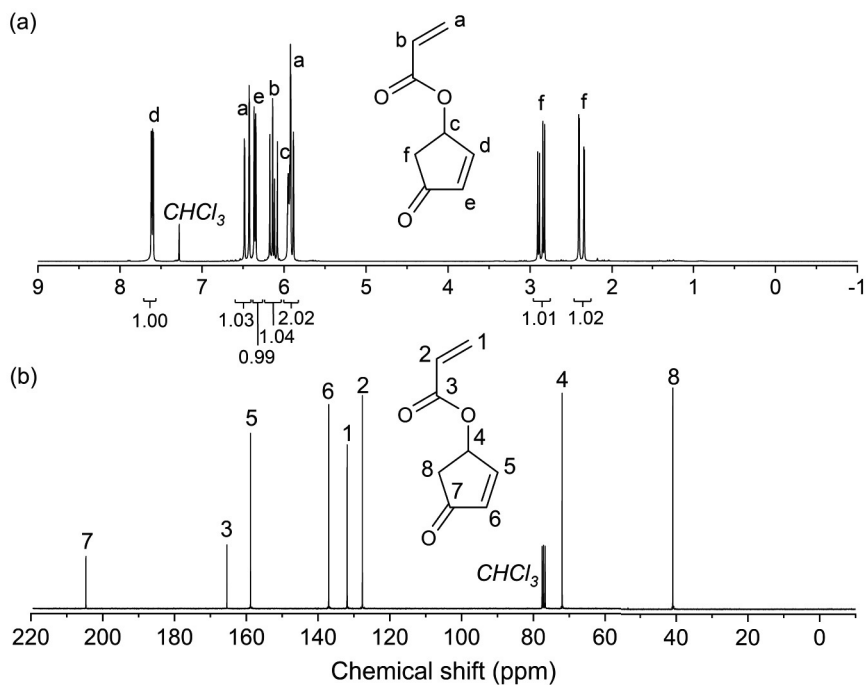


18. Lipshutz, B. H.; Wood, M. R.; Tirado, R., Michael additions of functionalized organozinc reagents mediated by catalytic quantities of copper (I). *Journal of the American Chemical Society* **1995**, *117* (22), 6126-6127.
19. Fürstner, A.; Grela, K.; Mathes, C.; Lehmann, C. W., Novel and flexible entries into prostaglandins and analogues based on ring closing alkyne metathesis or alkyne cross metathesis. *Journal of the American Chemical Society* **2000**, *122* (48), 11799-11805.
20. Ichikawa, M.; Takahashi, M.; Aoyagi, S.; Kibayashi, C., Total synthesis of (-)-incarvilline,(+)-incarvine C, and (-)-incarvillateine. *Journal Of The American Chemical Society* **2004**, *126* (50), 16553-16558.
21. O'Byrne, A.; Murray, C.; Keegan, D.; Palacio, C.; Evans, P.; Morgan, B. S., The thio-adduct facilitated, enzymatic kinetic resolution of 4-hydroxycyclopentenone and 4-hydroxycyclohexenone. *Organic & biomolecular chemistry* **2010**, *8* (3), 539-545.
22. Basra, S. K.; Drew, M. G.; Mann, J.; Kane, P. D., A novel approach to bis-isoxazolines using a latent form of cyclopentadienone. *Journal of the Chemical Society, Perkin Transactions 1* **2000**, (21), 3592-3598.
23. Adembri, G.; Paoli, M. L.; Rossi, P.; Sega, A., Synthesis of enantiopure bis-isoxazolines from (4R)-(+)-4-acetoxycyclopent-2-enone. *Tetrahedron: Asymmetry* **2001**, *12* (4), 619-623.
24. Mitscher, L.; Clark III, G.; Hudson, P., Terrein, an optically active prostaglandin synthon of fungal origin. II. Chemical conversion to 4 (R)-acetoxo-2-cyclopentenone. *Tetrahedron Letters* **1978**, *19* (29), 2553-2556.
25. Schiess, P.; Suter, C., Photochemische Bildung zweier [2+ 2]-Dimeren von Cyclopentadienon aus 5-Acetoxy-3-oxocyclopenten. *Synthesis* **1978**, *1978* (07), 543-543.
26. Davidson, R., *Radiation curing*. iSmithers Rapra Publishing: 2001; Vol. 12.
27. Huyck, R. H.; Trenor, S. R.; Love, B. J.; Long, T. E., Photodimerization of coumarin functionalized poly (alkyl acrylate) and poly (alkyl methacrylate) random copolymers: Influence of copolymer composition on photocrosslinking. *Journal of Macromolecular Science, Part A: Pure and Applied Chemistry* **2007**, *45* (1), 9-15.
28. Imai, Y.; Naka, K.; Chujo, Y., Reversible formation of interpenetrating polymer network structure in organic-inorganic polymer hybrids. *Polymer journal* **1998**, *30* (12), 990.
29. Trenor, S. R.; Long, T. E.; Love, B. J., Development of a light-deactivatable PSA via photodimerization. *The Journal of Adhesion* **2005**, *81* (2), 213-229.
30. Delzenne, G.; Laridon, U. In *Photosensitive polymers-synthesis and properties of coumarin-modified polymers*, Industrie Chimique Belge-Belgische Chemische Industrie, 1966; p 158.
31. Minsk, L.; Smith, J.; Van Deusen, W.; Wright, J., Photosensitive polymers. I. Cinnamate esters of poly (vinyl alcohol) and cellulose. *Journal of Applied Polymer Science* **1959**, *2* (6), 302-307.
32. Robertson, E.; Van Deusen, W.; Minsk, L., Photosensitive polymers. II. Sensitization of poly (vinyl cinnamate). *Journal of Applied Polymer Science* **1959**, *2* (6), 308-311.
33. Lasseguette, E.; Gandini, A.; Belgacem, M. N.; Timpe, H.-J., Synthesis, characterization and photocrosslinking of copolymers of furan and aliphatic hydroxyethylesters prepared by transesterification. *Polymer* **2005**, *46* (15), 5476-5483.
34. Xu, J.-F.; Chen, Y.-Z.; Wu, L.-Z.; Tung, C.-H.; Yang, Q.-Z., Dynamic covalent bond based on reversible photo [4+ 4] cycloaddition of anthracene for construction of double-dynamic polymers. *Organic letters* **2013**, *15* (24), 6148-6151.
35. Radl, S. V.; Roth, M.; Gassner, M.; Wolfberger, A.; Lang, A.; Hirschmann, B.; Trimmel, G.; Kern, W.; Griesser, T., Photo-induced crosslinking and thermal de-crosslinking in polynorbornenes bearing pendant anthracene groups. *European polymer journal* **2014**, *52*, 98-104.

36. Zheng, Y.; Micic, M.; Mello, S. V.; Mabrouki, M.; Andreopoulos, F. M.; Konka, V.; Pham, S. M.; Leblanc, R. M., PEG-based hydrogel synthesis via the photodimerization of anthracene groups. *Macromolecules* **2002**, *35* (13), 5228-5234.
37. Coursan, M.; Desvergne, J. P.; Deffieux, A., Reversible photodimerisation of  $\omega$ -anthrylpolystyrenes. *Macromolecular Chemistry and Physics* **1996**, *197* (5), 1599-1608.
38. Akiyama, M.; Yoshida, K.; Mori, H., Controlled synthesis of vinyl-functionalized homopolymers and block copolymers by RAFT polymerization of vinyl methacrylate. *Polymer* **2014**, *55* (3), 813-823.
39. Ma, J.; Cheng, C.; Sun, G.; Wooley, K. L., Well-defined polymers bearing pendent alkene functionalities via selective RAFT polymerization. *Macromolecules* **2008**, *41* (23), 9080-9089.
40. Lin, Y.; Liu, X.; Li, X.; Zhan, J.; Li, Y., Reversible addition-fragmentation chain transfer mediated radical polymerization of asymmetrical divinyl monomers targeting hyperbranched vinyl polymers. *Journal of Polymer Science Part A: Polymer Chemistry* **2007**, *45* (1), 26-40.
41. Chiefari, J.; Chong, Y.; Ercole, F.; Krstina, J.; Jeffery, J.; Le, T. P.; Mayadunne, R. T.; Meijs, G. F.; Moad, C. L.; Moad, G., Living free-radical polymerization by reversible addition-fragmentation chain transfer: the RAFT process. *Macromolecules* **1998**, *31* (16), 5559-5562.
42. Beerthuis, R.; Rothenberg, G.; Shiju, N. R., Catalytic routes towards acrylic acid, adipic acid and  $\epsilon$ -caprolactam starting from biorenewables. *Green Chemistry* **2015**, *17* (3), 1341-1361.
43. Wittcoff, H. A.; Reuben, B. G.; Plotkin, J. S., *Industrial organic chemicals*. John Wiley & Sons: 2012.
44. Gupta, J.; Keddie, D. J.; Wan, C.; Haddleton, D. M.; McNally, T., Functionalisation of MWCNTs with poly (lauryl acrylate) polymerised by Cu (0)-mediated and RAFT methods. *Polymer Chemistry* **2016**, *7* (23), 3884-3896.
45. Engler, M. S.; Crotty, S.; Barthel, M. J.; Pietsch, C.; Knop, K.; Schubert, U. S.; Böcker, S., COCONUT-An Efficient Tool for Estimating Copolymer Compositions from Mass Spectra. *Analytical chemistry* **2015**, *87* (10), 5223-5231.
46. Ulbrich, K.; Kreitmeier, P.; Reiser, O., Microwave-or microreactor-assisted conversion of furfuryl alcohols into 4-hydroxy-2-cyclopentenones. *Synlett* **2010**, *2010* (13), 2037-2040.
47. Ghorpade, S. R.; Bastawade, K. B.; Gokhale, D. V.; Shinde, P. D.; Mahajan, V. A.; Kalkote, U. R.; Ravindranathan, T., Enzymatic kinetic resolution studies of racemic 4-hydroxycyclopent-2-en-1-one using Lipozyme IM®. *Tetrahedron: Asymmetry* **1999**, *10* (21), 4115-4122.
48. Heuts, J. P. A., Theory of Radical Reactions. In *Handbook of radical polymerization*, Matyjaszewski, K., Davis, T. P., Ed. John Wiley & Sons, Inc.: New York, 2002; pp 1-76.
49. Ballard, N.; Asua, J. M., Radical polymerization of acrylic monomers: An overview. *Progress in Polymer Science* **2018**, *79*, 40-60.
50. Ballard, N.; Rusconi, S.; Akhmatskaya, E.; Sokolovski, D.; de la Cal, J. C.; Asua, J. M., Impact of competitive processes on controlled radical polymerization. *Macromolecules* **2014**, *47* (19), 6580-6590.
51. Ballard, N.; Hamzehlou, S.; Asua, J. M., Intermolecular transfer to polymer in the radical polymerization of n-butyl acrylate. *Macromolecules* **2016**, *49* (15), 5418-5426.
52. Keddie, D. J.; Moad, G.; Rizzardo, E.; Thang, S. H., RAFT agent design and synthesis. *Macromolecules* **2012**, *45* (13), 5321-5342.
53. Jordan Jr, E. F.; Feldeisen, D. W.; Wrigley, A., Side-chain crystallinity. I. Heats of fusion and melting transitions on selected homopolymers having long side chains. *Journal of Polymer Science Part A-1: Polymer Chemistry* **1971**, *9* (7), 1835-1851.

54. Jordan Jr, E. F.; Artymyshyn, B.; Speca, A.; Wrigley, A., Side-chain crystallinity. II. Heats of fusion and melting transitions on selected copolymers incorporating n-octadecyl acrylate or vinyl stearate. *Journal of Polymer Science Part A-1: Polymer Chemistry* **1971**, *9* (11), 3349-3365.
55. Dong, W.; Li, H.; Chen, M.; Ni, Z.; Zhao, J.; Yang, H.; Gijsman, P., Biodegradable bio-based polyesters with controllable photo-crosslinkability, thermal and hydrolytic stability. *Journal of Polymer Research* **2011**, *18* (6), 1239-1247.
56. Eaton, P. E., On the Mechanism of the Photodimerization of Cyclopentenone. *Journal of the American Chemical Society* **1962**, *84* (12), 2454-2455.
57. Ruhlen, J. L.; Leermakers, P. A., On the Photodimerization of Cyclopentenone. *Journal of the American Chemical Society* **1966**, *88* (23), 5671-5672.
58. Ruhlen, J. L.; Leermakers, P. A., Photochemistry of cyclopentenone in various media. *Journal of the American Chemical Society* **1967**, *89* (19), 4944-4948.
59. Wagner, P. J.; Bucheck, D. J., Inefficiency and reversibility in the photodimerization of 2-cyclopentenone. *Canadian Journal of Chemistry* **1969**, *47* (4), 713-714.

## Appendix A

Figure A1. (a) <sup>1</sup>H NMR and (b) <sup>13</sup>C NMR spectrum of 4HCP in CDCl<sub>3</sub>.Figure A2. (a) <sup>1</sup>H NMR and (b) <sup>13</sup>C NMR spectrum of 4CPA in CDCl<sub>3</sub>.

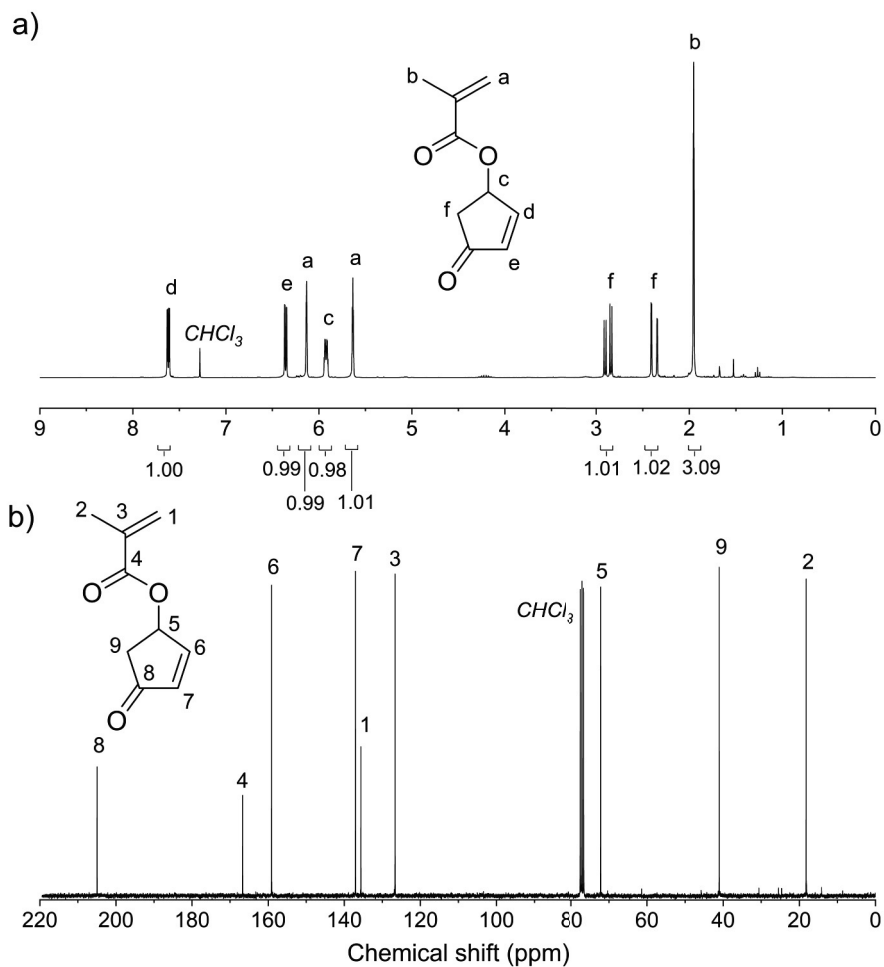


Figure A3. a)  $^1\text{H}$  NMR and b)  $^{13}\text{C}$  NMR spectrum of 4CPMA in  $\text{CDCl}_3$ .

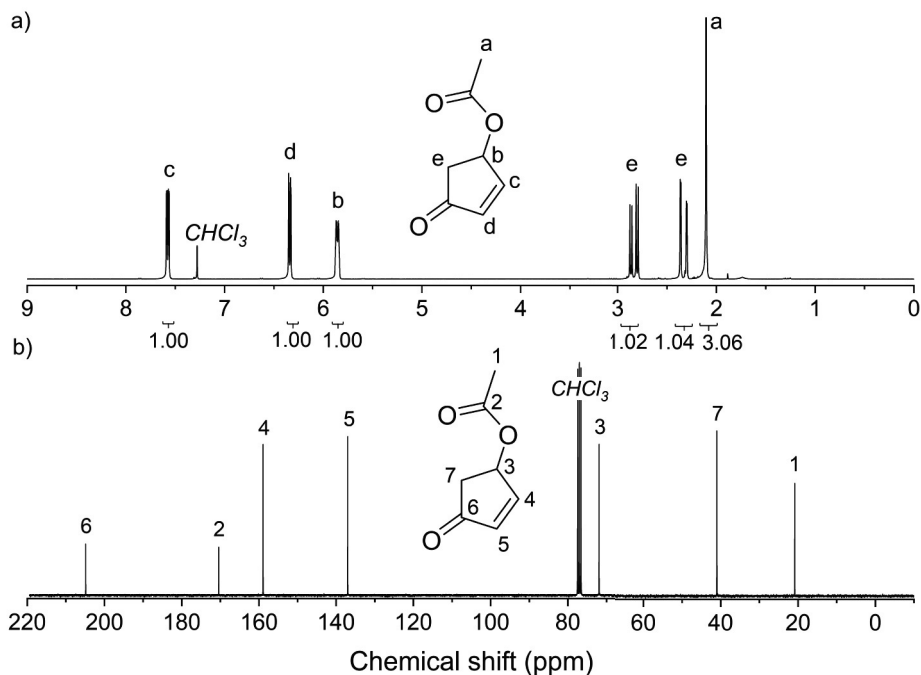


Figure A4. (a)  $^1\text{H}$  NMR and (b)  $^{13}\text{C}$  NMR spectrum of 4-oxocyclopent-2-en-1-yl acetate (**1**) in  $\text{CDCl}_3$ .

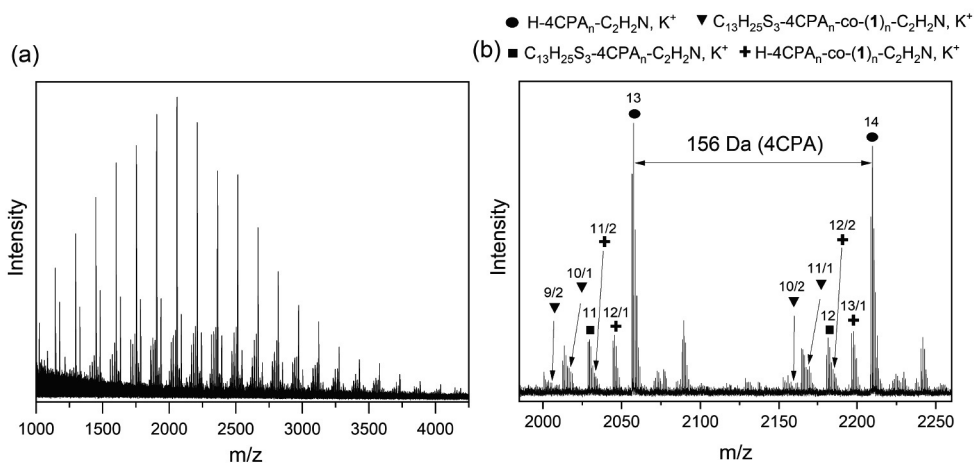
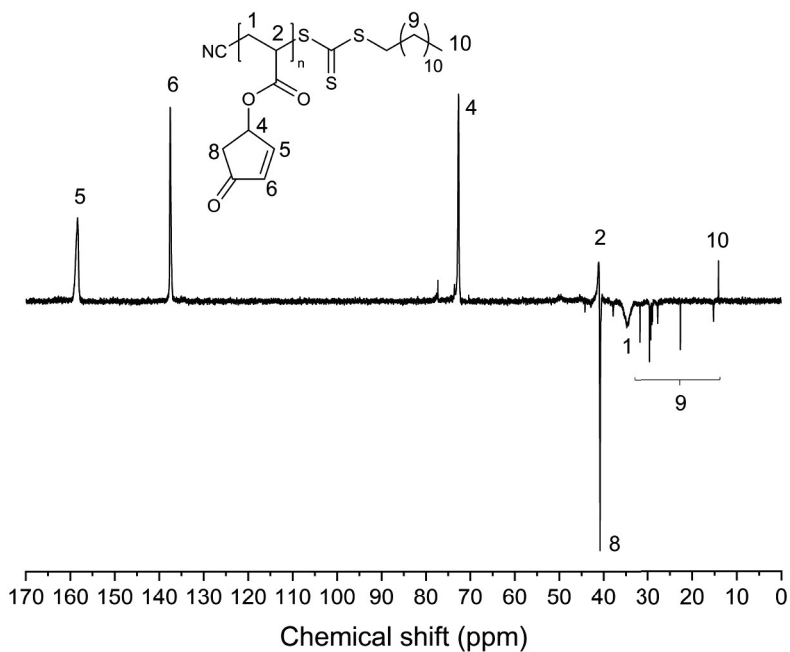
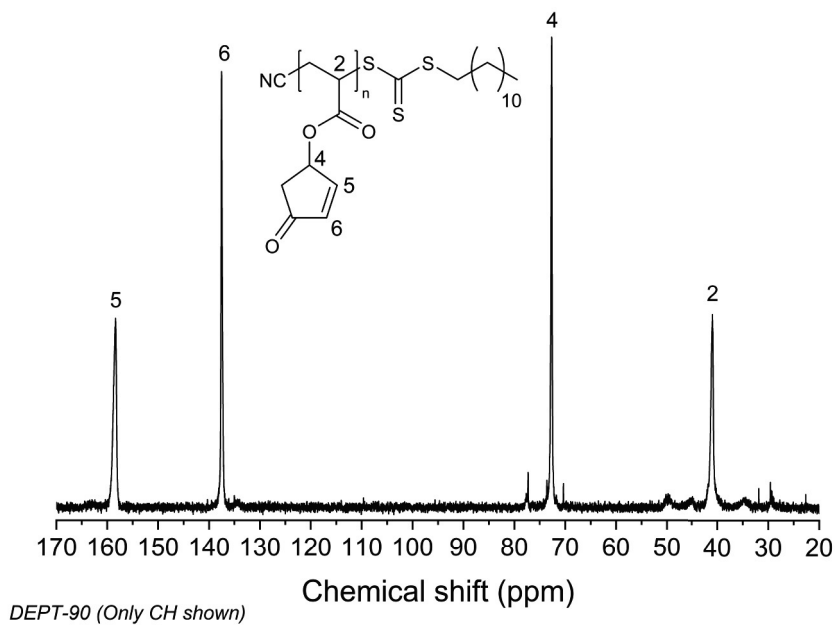


Figure A5. (a) MALDI-ToF-MS spectrum of the copolymer formed after 50 minutes during the RAFT polymerization of 4CPA and (**1**) in a 50:50 ratio, (b) zoom-in of (a).


 Figure A6. DEPT-135 of poly(4CPA) in  $CDCl_3$ .

 Figure A7. DEPT-90 of poly(4CPA) in  $CDCl_3$ .

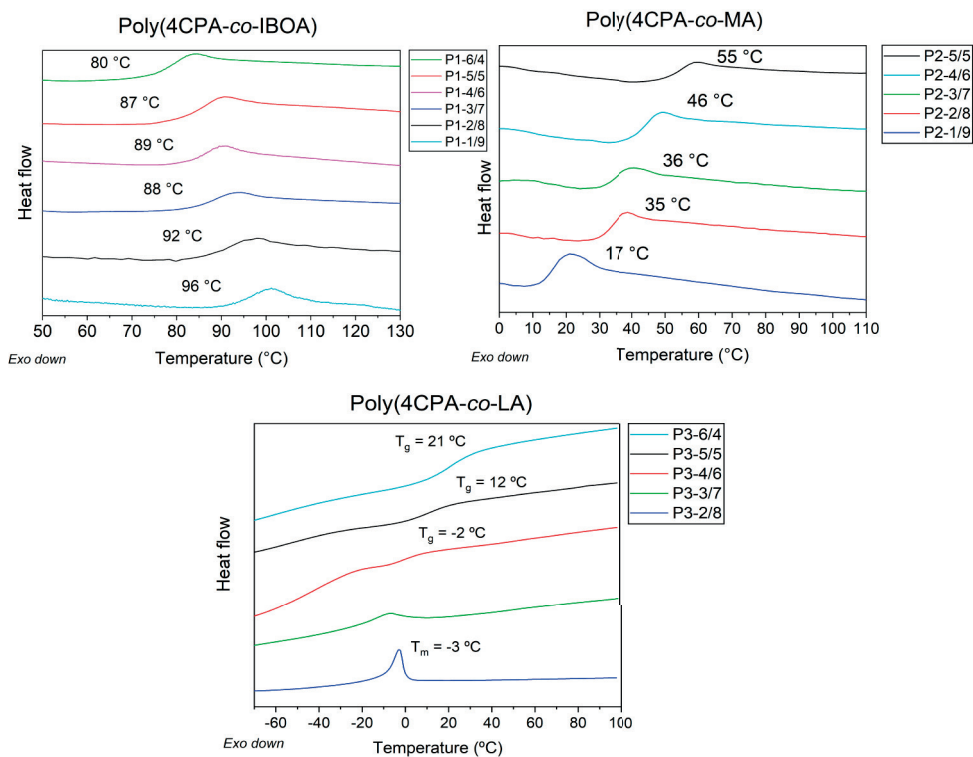


Figure A8. DSC traces of copolymers poly(4CPA-co-IBOA) (P1), poly(4CPA-co-MA) (P2) and poly(4CPA-co-LA) (P3).



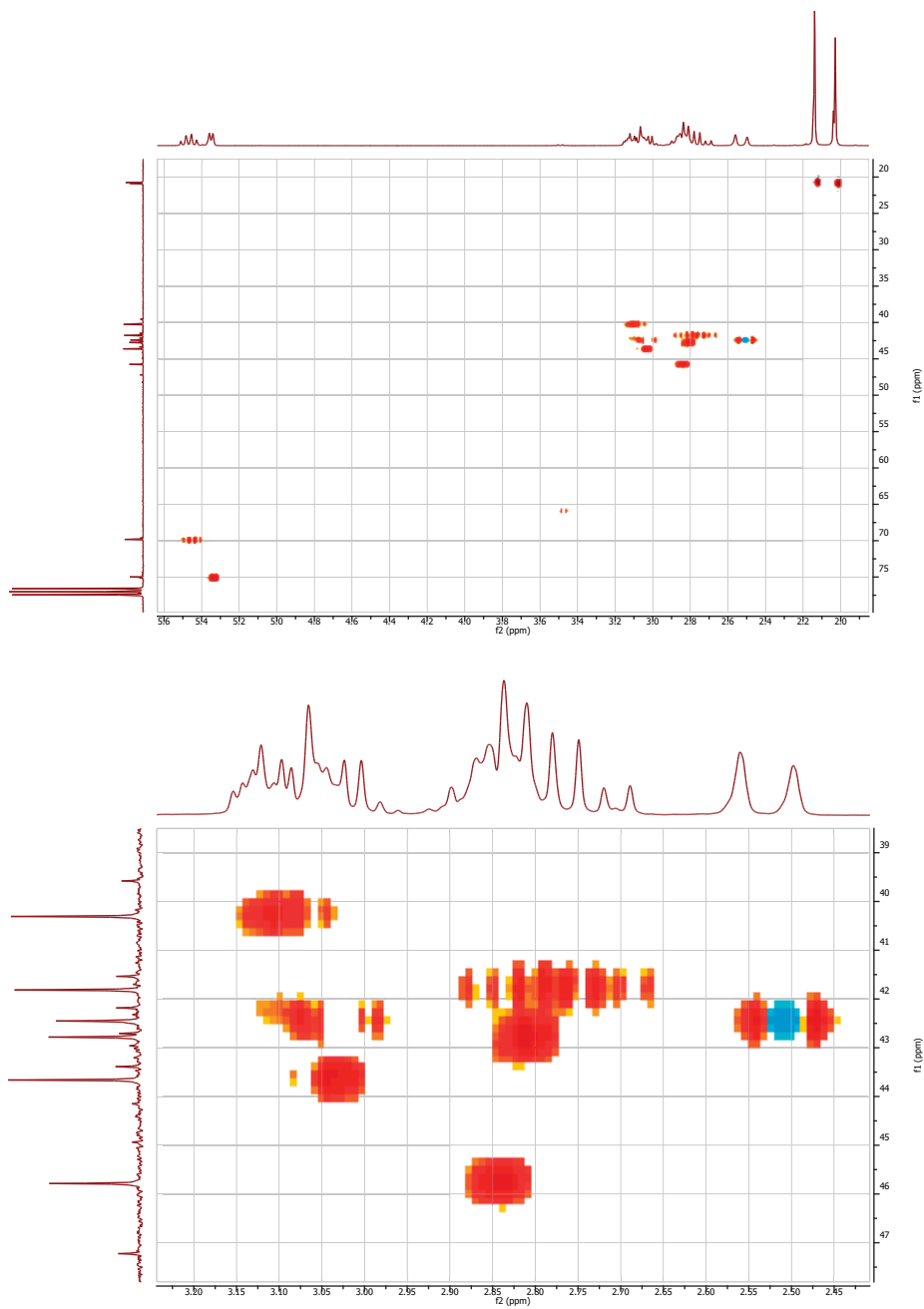
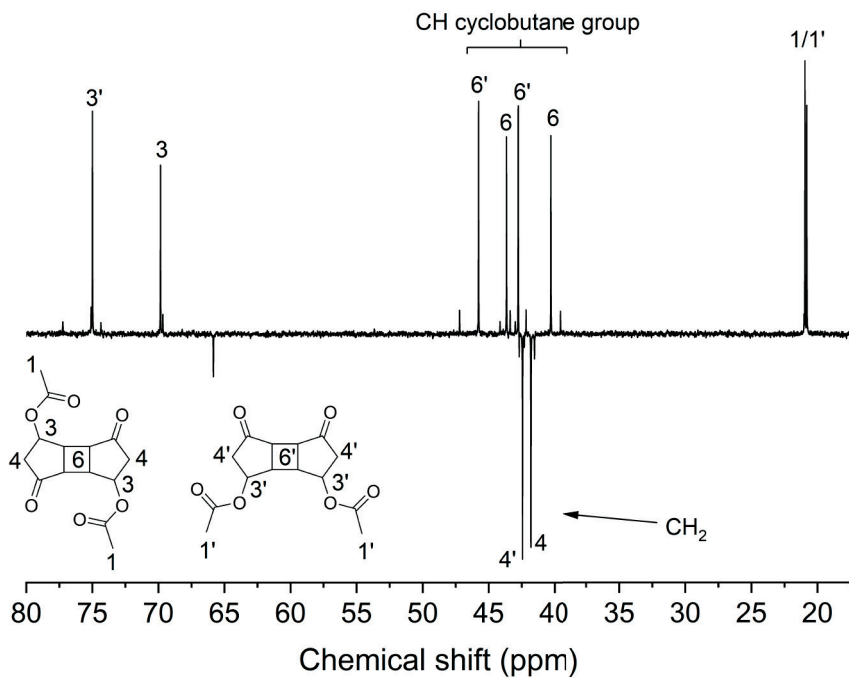


Figure A9. HSQC of the dimers of (1).



DEPT-135 ( $\text{CH}_2 = \text{negative}$ ,  $\text{CH}$  and  $\text{CH}_3 = \text{positive}$ )

Figure A10. DEPT-135 of the model dimers of (1) in  $\text{CDCl}_3$ .

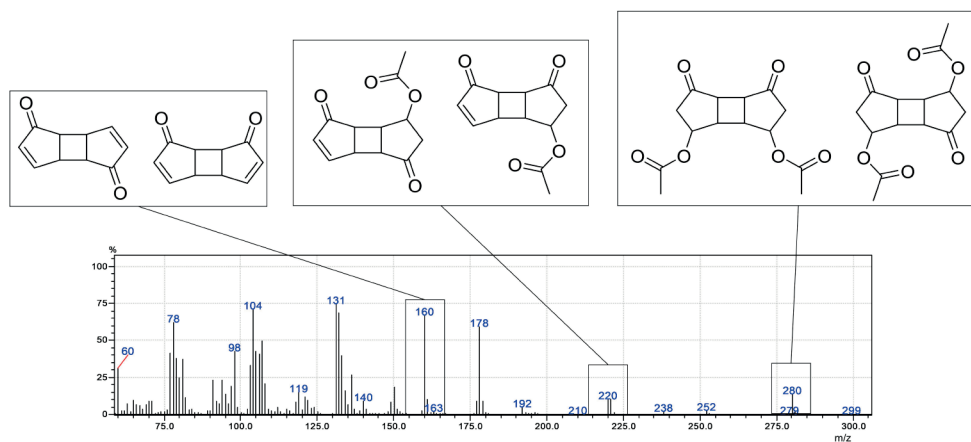


Figure A11. MS spectrum of model dimer of (1) including the proposed chemical structures of target compound (1) and elimination products.

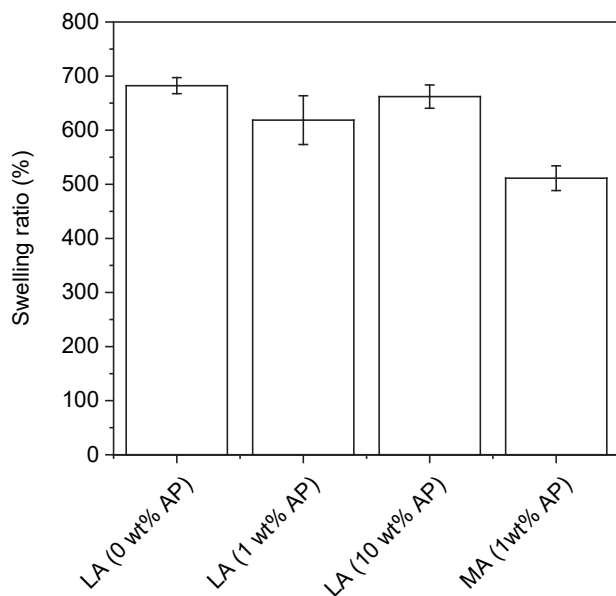


Figure A12. Swelling ratio in CHCl<sub>3</sub> of the prepared cross-linked films of poly(4CPA-*co*-LA) P3-3/7 containing various contents of acetophenone, and poly(4CPA-*co*-MA) P2-3/7 containing 1 wt% acetophenone.

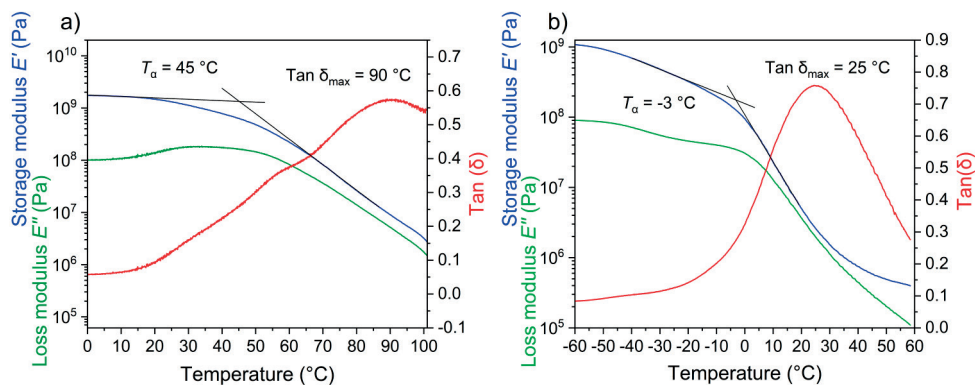
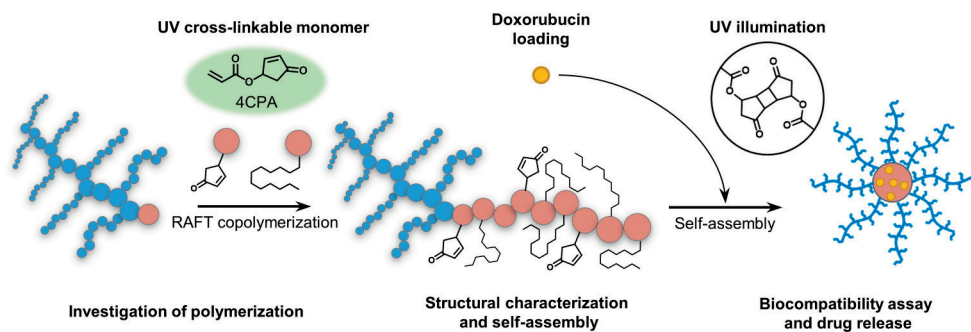


Figure A13. DMA traces of the cross-linked films of (a) poly(4CPA-*co*-MA) P2-3/7 and (b) poly(4CPA-*co*-LA) P3-3/7.

# 3



---

# Chapter 3 Micellar Drug Delivery Vehicles formed from Amphiphilic Block Copolymers Bearing Photo-Cross-linkable Cyclopentenone Side Groups

---

This chapter is based on the following publication:

Stouten, J., Sijstermans, N., Babilotte, J., Pich, A., Moroni, L., & Bernaerts, K. V. (2022). Micellar drug delivery vehicles formed from amphiphilic block copolymers bearing photo-cross-linkable cyclopentenone side groups. *Polymer Chemistry*, 13(33), 4832-4847.

## Abstract

Amphiphilic block copolymers are of specific interest in the field of nanomedicine, and are used to encapsulate hydrophobic drugs for targeted drug delivery. To improve micellar stability in highly diluted conditions, cross-linkable functional groups can be incorporated in the polymer backbone to covalently link the block copolymers and create nanogels. In this work, we propose the use of a poly(oligo(ethylene glycol) methyl ether acrylate) macro-RAFT agent for the controlled polymerization of 4-oxocyclopentenyl acrylate and lauryl acrylate to obtain amphiphilic block copolymers. The cyclopentenone side groups belonging to the 4CPA monomer are able to dimerize under illumination with UV light, resulting in core cross-linked assemblies. A series of block copolymers containing different hydrophilic and hydrophobic block lengths were synthesized. The block copolymers were able to self-assemble after direct dissolution in water to form micellar structures. However, more defined, smaller, and spherical micelles of between 29 and 161 nm were obtained by producing them via a solvent exchange method. The micellar cores were cross-linked using UV irradiation and remained stable in organic solvent. The unmodified micelles dissociated and formed smaller assemblies upon introduction in organic solvent. The drug loading capacity was firstly investigated using the model drug probes pyrene and Nile red. The most promising block copolymer was loaded with doxorubicin with a loading content of 23.8%. In vitro release studies showed a delayed DOX release from the UV cross-linked micelles. Furthermore, the release was accelerated at lower pH. Cell viability essays of the DOX loaded micelles confirmed the relevance of the synthesized block copolymers as drug delivery vehicles by showing high cytotoxicity towards breast adenocarcinoma cells. The same non-loaded micelles showed low cytotoxicity at the targeted concentrations towards mouse fibroblast cells.

### Introduction

Amphiphilic block copolymers have been widely investigated in the field of nanotechnology and biomedical engineering.<sup>1</sup> Upon introduction in aqueous medium, the incompatible hydrophobic blocks causes the macromolecule to self-assemble into organized structures to reduce the overall free energy. Compared to small surfactant molecules, amphiphilic block copolymers have a low critical aggregation concentration (CAC), and improved micellar stability.<sup>2</sup> Therefore, they can serve as drug delivery vehicles for hydrophobic drugs by encapsulating the drug and allowing transportation through the body.<sup>3</sup>

Since micelle formation is a reversible process, a commonly faced problem is the premature disintegration, or instability of the micellar structures.<sup>4</sup> Strong dilution or introduction in a different solvent brings the block copolymers in a state where they are more likely to exist as unimers and not in organized micellar structures. One way to tune the stability is to change hydrophilic and hydrophobic block lengths. Typically, a decrease in the CAC can be expected as a result of increasing molecular weight and hydrophobic-to-hydrophilic block length ratio.<sup>2,5</sup> This in turn, can also affect other properties of the resulting micellar structures such as size, shape, and drug loading capacity.<sup>6</sup> Furthermore, for block copolymers with relatively long hydrophobic chains, reaching the thermodynamic equilibrium of micelle formation occurs on a much longer timescale compared to small molecule surfactants. Therefore, the size and shape of the micelles can be highly dependent on the method used for preparation.<sup>3</sup> Another way to stop the reversible micelle formation process is covalent cross-linking between the block copolymer chains to freeze the self-assembled state and improve micellar stabilization.<sup>7</sup>

Core cross-linking of the polymeric micelles retains the micelle structure in dilute conditions and in solvents, avoiding dissociation into unimers. Core cross-linking is straightforward and can be achieved through addition of cross-linkers following micelle formation. This raises concerns regarding the transport of the cross-linker to the micelle core. A more facile method is self-cross-linking of functional groups present on the polymer backbone of the associating (or non-soluble) block. In this way, cross-linking can be induced by external stimuli such as UV light and avoids the addition, and removal of potentially hazardous cross-linker residues. Furthermore, cross-linking can be performed at a wide range of micellar concentrations.

Previous studies on UV-cross-linkable block copolymer micelles have reported the use of pendent functionality including cinnamoyl<sup>8-9</sup>, coumarin<sup>10-11</sup>, anthracene<sup>12</sup>, benzophenone<sup>13</sup>, tetrazole,<sup>14</sup> and thymine<sup>15-16</sup> groups.<sup>17</sup> Another monomer that is able to dimerize via [2 + 2] photocyclodimerization under UV light is 4-oxocyclopentenyl acrylate (4CPA) (Figure 3.1b).<sup>18</sup> 4CPA is a promising monomer of interest due to the scalable and biobased synthesis of its precursor 4-hydroxycyclopentenone in flow using water as the main solvent, or under supercritical water conditions.<sup>18-20</sup> Amphiphilic block copolymers based on 4CPA for drug delivery applications have not yet been produced, and are therefore an interesting subject of investigation to expand the scope of photo curable polymers in the field of self-assembly. Furthermore, the afore mentioned studies on the synthesis and self-assembly of UV curable

amphiphilic block-copolymers, did not include a thorough investigation towards the effects of the individual block lengths on the amphiphilic properties, self-assembly process, and drug loading content. Studies towards the loading and release of therapeutic drugs such as doxorubicin (DOX), and the *in vitro* cytotoxicity of polymers bearing UV-cross-linkable groups are also often lacking.

In this work, we aim to explore the use of 4CPA in core cross-linked amphiphilic block copolymers synthesized by RAFT polymerization. RAFT controlled polymerization is an outstanding and facile method for synthesizing well-defined block copolymers, while maintaining control over the individual block length.<sup>21-23</sup> As a hydrophilic block and simultaneously macro-RAFT agent, poly(oligo(ethylene glycol) methyl ether acrylate) (POEGA) was used (Figure 3.1a). Block copolymers containing PEG hydrophilic segments are well established in drug delivery applications. They result in stable drug delivery carriers that are highly biocompatible and resistant to protein adsorption.<sup>5, 24</sup> Similarly to PEG, POEGA synthesized by RAFT polymerization bearing trithiocarbonate end groups, displays good biocompatibility<sup>25-26</sup> Herein, POEGA blocks of various lengths were employed in a RAFT polymerization with a mixture of lauryl acrylate (LA) and 4CPA in a 70:30 mol% ratio to function as the hydrophobic block. The biobased LA was chosen because its hydrophobic character promotes micellar formation by means of hydrophobic interactions to form well-defined micellar aggregates.<sup>27</sup> Decoration of the hydrophobic block with long alkyl chains has been reported to lead to low CAC values.<sup>28</sup> Encapsulation with the model probes pyrene and nile red will resolve the most promising block copolymer structure resulting in micelles with a small size and capable of high drug encapsulation. Furthermore, the cytotoxicity of these UV-cross-linkable micelles will be evaluated before and after loading with DOX indicating the potential for application as drug delivery vehicles. DOX is a hydrophobic therapeutic drug used to treat different types of cancer, including breast cancer.<sup>29</sup>

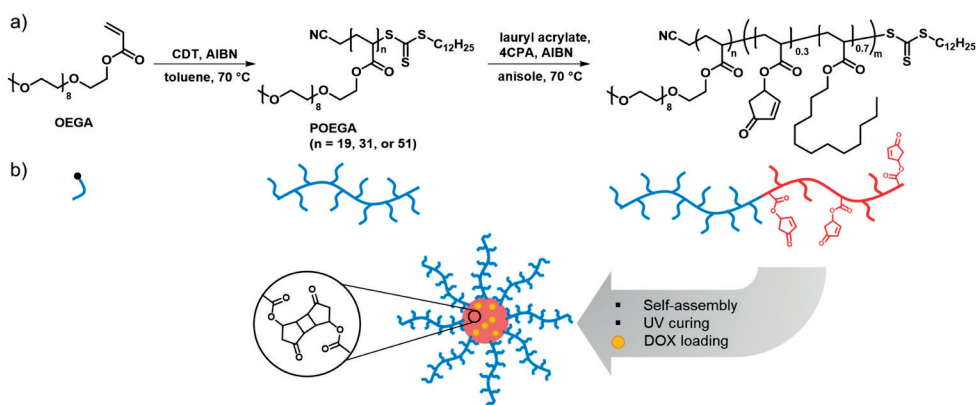


Figure 3.1. a) Synthesis of the POEGA macro-RAFT agent and 4CPA based block copolymers, b) a schematic representation of the self-assembled and UV cured micelles.

## Experimental section

### Materials

Azobisisobutyronitrile (AIBN, Sigma-Aldrich) was recrystallized from methanol prior to use. Oligo(ethylene glycol) methyl ether acrylate (OEGA, average  $M_n$  of 480 g/mol, Sigma-Aldrich), and lauryl acrylate (LA, >98.0%, TCI) were passed over an alumina column to remove the inhibitor and stored at -20 °C. 4-Oxocyclopent-2-ene-1-yl acrylate (4CPA) was synthesized according to a procedure mentioned in the literature and stored at -20 °C.<sup>18</sup> Cyanomethyl dodecyl trithiocarbonate (CDT) was synthesized according to a procedure reported previously and stored at 4 °C.<sup>30</sup> Trans-2-[3-(4-tert-butylphenyl)-2-methyl-2-propenylidene]malononitrile (DCTB, ≥96%, Sigma-Aldrich), Triethylamine (TEA, ≥99%, Sigma-Aldrich), sodium trifluoroacetate (KTFA, 98%, Sigma-Aldrich), 1,3,5-trioxane (≥99%, Sigma-Aldrich), naphthalene (99.5%, Sigma-Aldrich), pyrene (>99%, Alfa-Aesar), Nile red (TCI), doxorubicin hydrochloride (DOX-HCl, >95.0%, TCI), D<sub>2</sub>O (99.8 atom % D, Acros organics), and CDCl<sub>3</sub> (99.8 atom % D, Cambridge Isotope Laboratories) were used as received. All other solvents were obtained from Biosolve and were used as received. Regenerated cellulose dialysis membranes with a molecular weight cut-off of 1 kDa were purchased from Fisher Scientific.

### Synthesis of Poly(oligo(ethylene glycol) methyl ether acrylate) (POEGA) macro-RAFT agent

Three POEGA macro-RAFT agents with different block lengths were synthesized; these are summarized in Table 3.1. The syntheses were all performed in the same way except the ratios between monomer and RAFT agent were varied to aim for different block lengths. In an exemplary synthesis, a 100 mL Schlenk flask equipped with magnetic stirrer was charged with oligo(ethylene glycol) methyl ether acrylate (OEGA) (15.0 g, 31.25 mmol, 220 eq.), CDT (451 mg, 1.42 mmol, 10 eq.), AIBN (23.3 mg, 0.142 mmol, 1 eq.), trioxane (130 mg, as internal standard), and toluene (42 mL, monomer concentration was 30 wt%). The mixture was degassed by sparging with nitrogen for at least 30 minutes. The flask was sealed with a nitrogen-filled balloon and the polymerization was started by placing the flask in a 70 °C oil bath. The monomer conversion was followed by <sup>1</sup>H NMR spectroscopy by comparing the acrylate resonances with the trioxane resonances at 5.20 ppm. The reaction was stopped after 5 hours. The polymer was precipitated three times in hexane and dried in a vacuum oven at 40 °C overnight. The <sup>1</sup>H NMR spectrum of the final polymer in CDCl<sub>3</sub> is shown in Figure B1. The degree of polymerization was calculated by comparing the RAFT agent end-group resonance at 0.86 ppm with the POEGA resonance at 4.14 ppm. Yield: 14.9 g of a yellow viscous liquid (95%).

### Synthesis of block copolymers

Using the three POEGA macro-RAFT agents, a series of nine block copolymers were synthesized with different hydrophobic block lengths. The molar feed ratio of 4CPA:LA was kept at 3:7. In an exemplary synthesis (POEGA<sub>19</sub>-HB<sub>16</sub>), a 25 mL Schlenk flask equipped



with magnetic stirrer was charged with 4CPA (500 mg, 3.29 mmol, 6 eq.), LA (1844 mg, 7.67 mmol, 14 eq.), AIBN (18 mg, 0.11 mmol, 0.2 eq.), POEGA<sub>19</sub> macro-RAFT agent (5096 mg, 0.54 mmol, 1 eq.), naphthalene (60 mg, as GC-FID internal standard), and anisole (3.51 mL, monomer concentration was 40 wt%). The mixture was degassed by at least three consecutive freeze-pump-thaw cycles. After the last cycle, the flask was filled with nitrogen, and the mixture thoroughly homogenized. The flask was sealed with a nitrogen-filled balloon and the polymerization was started by placing the flask in a 70 °C oil bath. The reaction was continued until the monomer conversion plateaued according to GC-FID analysis. After the reaction was finished, the flask was cooled to room temperature and the polymer purified by dialysis against methanol in a regenerated cellulose dialysis membrane with a molecular weight cutoff of 1 kDa. The polymer was dried overnight in a vacuum oven at 40 °C and then stored at 4 °C. Yield: 3.89 g of a yellow viscous liquid (52%).

The monomer ratios in the purified polymer were determined by comparing the resonances of 4CPA, OEGA and LA at 7.58, 3.65, and 0.88 ppm, respectively. After correction for the molecular weight, the hydrophilic-to-lipophilic balance (HLB) values were calculated according to the Griffin equation:<sup>31</sup>

$$HLB = \frac{W_H}{(W_H+W_L)} \times 20$$

Where  $W_H$  corresponds to the weight fraction of the hydrophilic block (OEGA) and  $W_L$  corresponds to the weight fraction of the lipophilic block (4CPA and LA).

### Determination of the reactivity ratios

The monomer reactivity ratios between 4CPA and LA were determined using the Jaacks method.<sup>32</sup> Two polymerizations were carried out, each with an excess (95:5) of one of the monomers, 4CPA or LA. In an exemplary synthesis, a 5 mL Schlenk flask equipped with magnetic stirrer was filled with 4CPA (200 mg, 1.315 mmol, 500 eq.), LA (15.8 mg, 0.0658 mmol, 25 eq.), POEGA<sub>19</sub> (319 mg, 0.0343 mmol, 13 eq.), AIBN (2.6 mg, 0.0158 mmol, 6 eq.), anisole (0.327 mL), and naphthalene (10 mg, as internal standard). The mixture was degassed by sparging with nitrogen for at least 30 minutes. The flask was sealed with a nitrogen-filled balloon and the polymerization was started by placing the flask in a 70 °C oil bath. The monomer conversion was followed by GC-FID, by observing the disappearance of the monomer peaks relative to the internal standard peak. The reactivity ratios were determined from the resulting Jaacks plots.

### Preparation of micelles and UV cross-linking

#### *Solvent exchange method*

Block-copolymer micelles were prepared by a solvent exchange method.<sup>33</sup> This method was performed by dissolving the block-copolymer in an organic solvent and inducing micelle formation by slowly adding water. The procedure was as follows: a 250 mL round-bottom flask equipped with magnetic stirrer was charged with 20 mg of block-copolymer and 10 mL

THF. The solution was then stirred for 20 minutes to homogenize the system. 90 mL water was added dropwise over the course of three hours with an addition rate of about 0.5 mL/min to induce micelle formation. The final block-copolymer concentration was 0.2 mg/mL in a solvent ratio H<sub>2</sub>O:THF of 90:10. To remove the remaining THF, the mixture was then dialyzed against H<sub>2</sub>O in regenerated cellulose dialysis membranes with a molecular weight cut-off of 1kDa for 24 hours. To cross-link the micelles, the colloidal solution was irradiated for 30 minutes using a 400 W metal halide, UVA lamp in a Dymax ECE 2000 UV chamber under a nitrogen flow. The distance of the lamp to the samples was 20 cm. The emitted wavelength of the lamp was in the range of UVA radiation between 350 and 450 nm.

### *Nanoprecipitation method*

The block copolymer (20 mg) was dissolved in 10 mL THF. The solution was added dropwise to 90 mL water while stirring. The addition of the block copolymer solution was completed within 10 minutes, and the mixture was left stirring for 1 hour to homogenize the system. The mixture was dialyzed against H<sub>2</sub>O in regenerated cellulose dialysis membranes with a molecular weight cut-off of 1kDa for 24 hours. The particle size was measured on DLS to compare the nanoprecipitation method with the solvent exchange method.

### **Micelle loading with hydrophobic probes and doxorubicin**

Loading of the micelles using the probes Nile red and pyrene was performed as follows. In a 25 mL round-bottom flask equipped with magnetic stir bar were dissolved 6 mg block copolymer and 6 mg Nile red or pyrene in 1 mL THF. The solution was thoroughly homogenized for 30 minutes and then 9 mL deionized water was added drop-wise over the course of about 1 hour. The solids were filtered over 2-3 μm filtration paper. Prior to characterization with UV-Vis, 2 mL of the Nile red loaded micelles was lyophilized and the remaining solids were dissolved in 2 mL methanol. For the pyrene loaded micelles, 200 μL of the colloidal solution was diluted in 3800 μL methanol.

To produce the DOX loaded micelles, 40 mg DOX-HCl was dissolved in 10 mL DMSO and to that 30 μL TEA was added to produce the hydrophobic form of DOX. The mixture was stirred for 1 hour and then 100 mg of the block copolymer POEGA<sub>19</sub>-HB<sub>50</sub> was added. After thorough homogenization, 90 mL water was added dropwise over the course of 1 hour. The precipitated DOX was filtered over a 2-3 μm paper filter and the loaded micelles were dialyzed against water (using regenerated cellulose dialysis membranes with a molecular weight cut-off of 1 kDa) to remove the DMSO.

The concentration of loaded compound was determined, after correcting for the dilutions, with UV-Vis spectroscopy by comparing the measured absorptions to a calibration curve. The drug loading content (DLC) and Encapsulation Efficiency (EE) were calculated as follows:

$$DLC = \frac{\text{Weight of encapsulated model drug}}{(\text{Weight of encapsulated model drug} + \text{weight of block copolymer})} \times 100\%$$

$$EE = \frac{\text{Weight of encapsulated model drug}}{\text{Weight of model drug in feed}} \times 100\%$$

## Characterization

### *Nuclear magnetic resonance (NMR) spectroscopy*

Structural characterization and OEGA monomer conversion determination was performed using  $^1\text{H}$  NMR spectroscopy.  $^1\text{H}$  NMR (300 MHz) spectra were recorded on a Bruker Avance III HD Nanobay 300 MHz apparatus at 298K and with 16 scans. The polymers were dissolved in  $\text{CDCl}_3$  or  $\text{D}_2\text{O}$ . OEGA conversion was determined by following the disappearance of OEGA acrylate group resonances relative to trioxane as the internal standard, which was added at the beginning of the polymerization.

Diffusion-Ordered NMR (DOSY) spectra were recorded on a Bruker Avance III HD 700 MHz spectrometer at 298K. The polymers were dissolved in  $\text{CDCl}_3$ . Delays of big delta and little delta were set to 50 ms and 5 ms, respectively. 8 scans were averaged for each collected FID and diffusion profiles were sampled over 32 gradient power levels selected linearly between 2% and 98% of the maximum spectrometer gradient strength. Recorded pseudo 2D diffusion data were processed in DOSY2d mode, and diffusion coefficients  $D$  ( $\text{m}^2/\text{s}$ ) were fitted using (mono)exponential fitting of spectral proton resonance lines in intensity mode.

### *Gas chromatography with flame ionization detection (GC-FID)*

GC-FID measurements were performed on a Shimadzu GC-2010 equipped with a Supelco SPB-1 capillary column ( $30 \text{ m} \times 0.25 \text{ mm} \times 0.25 \mu\text{m}$  film thickness). GC-FID was used to follow the disappearance of the individual monomers in the copolymerizations relative to naphthalene as the internal standard, which was added at the beginning of the polymerization. The temperature program was as follows: an initial temperature of  $80 \text{ }^\circ\text{C}$  was maintained for 3 min and then increased to  $140 \text{ }^\circ\text{C}$  with a heating rate of  $10 \text{ }^\circ\text{C}/\text{min}$ . This temperature was maintained for 1 min and further increased to  $300 \text{ }^\circ\text{C}$  with a heating rate of  $20 \text{ }^\circ\text{C}/\text{min}$  and was maintained at  $300 \text{ }^\circ\text{C}$  for 5 min (the total run time of 23 min).

### *Gel permeation chromatography (GPC)*

GPC was used to determine the molar mass and the dispersity. Approximately 5 mg of polymer was dissolved in 1.5 mL of dimethylformamide containing 6 g/L AcOH and 0.035 mol/L LiCl. The solution was filtered over a  $0.2 \mu\text{m}$  PTFE syringe filter. The polymer solutions were then measured on a Waters GPC at  $40 \text{ }^\circ\text{C}$ . DMF containing 6 g/L AcOH and 0.035 mol/L LiCl was used as the eluent. Three columns (Styragel HR4, Styragel HR2, and Styragel HR0.5) including a guard column were used. For the calibration curve, poly(methyl methacrylate) standards with a molar mass ranging from 800 to 2 200 000 g/mol were used.

### *Differential scanning calorimetry (DSC)*

The isolated unmodified and cross-linked micelles were measured on a Netzsch DSC 214 Polyma instrument. Prior to measurement, the samples were dried at 40 °C in a vacuum oven. The samples were heated in 2 cycles under nitrogen atmosphere from -40 °C to 100 °C with a rate of 10 °C/min. The second cycle was used for determination of the phase transition points. The inflection point was used for reporting of the  $T_g$ .

### *UV-Vis spectroscopy*

UV-Vis measurements were performed on a Shimadzu UV-3600 UV-Vis-NIR spectrophotometer using quartz cuvettes. The spectra were recorded from 800 to 200 nm with a slit width of 1 nm. Changes in absorptions of the pyrene and Nile red solutions in methanol were recorded at 334 and 552 nm, respectively. The presence of DOX in water was recorded at 482 nm.

### *Dynamic light scattering (DLS)*

The size distribution of the block copolymer assemblies was determined using DLS. The aqueous colloidal solutions prepared via the solvent exchange method were measured directly without dilution. The block copolymers that were directly dissolved in water were measured at the same concentration of the micelles prepared via the solvent exchange method, which was 0.2 mg/mL. The samples were measured on a Malvern Instruments Zetasizer Nano ZS DLS instrument at 25 °C and a fixed angle of 173°.

### *Cryogenic transmission electron microscopy (Cryo-TEM)*

The block copolymer assemblies were visualized by Cryo-TEM. The block copolymer assemblies were concentrated to a concentration of 5 mg/mL. A thin aqueous film was formed by applying a 5  $\mu$ l droplet of the suspension to a bare specimen grid. Glow-discharged holey carbon grids were used. After the application of the suspension, the grid was blotted against filter paper, leaving a thin sample film spanning the grid holes. These films were vitrified by plunging the grid into ethane, which was kept at its melting point by liquid nitrogen, using a Vitrobot (Thermo Fisher Scientific Company, Eindhoven, Netherlands) and keeping the sample before freezing at 95% humidity. The vitreous sample films were transferred to a Tecnai Arctica cryo-electron microscope (Thermo Fisher Scientific, Eindhoven, Netherlands). Images were taken at 200 kV with a field emission gun using a Falcon III direct electron detector.

### *Matrix-assisted laser desorption/ionization time-of-flight mass spectroscopy (MALDI-ToF-MS)*

MALDI-ToF-MS spectra were recorded on a Bruker UltrafleXtreme spectrometer with a 355 nm Nd:Yag laser (2 kHz repetition pulse/Smartbeam-II) and a grounded steel plate. DCTB was used as the matrix (20 mg/mL in THF), and KTFA was used as a cationization agent (10 mg/mL in THF). The polymers were dissolved in THF (10 mg/mL). Solutions of the matrix,

salt, and polymer were mixed in volume ratios of 200:10:30, respectively. All mass spectra were recorded in the linear mode. Poly(ethylene glycol) standards with an  $M_n$  of 5000, 10 000, and 15 000 g/mol were used for calibration. mMass was used to process the data.

#### *Surface tension*

The surface tension was determined by the pendant drop method using an Attension Theta optical tensiometer. Block copolymer solutions with known concentration were prepared in milli-Q water. The surface tension was calculated by the OneAttension analysis software from the shape of the drop (5  $\mu$ L) using the Young-Laplace equation. The concentration range that was evaluated was between  $5 \times 10^{-5}$  and  $8 \times 10^{-2}$  mM. The critical aggregation concentration (CAC) was calculated at the intersection of the tangent lines of the linear region and the plateau.

#### *Gel content*

Gel content measurements were performed on the cross-linked and unmodified micelles. Excess H<sub>2</sub>O of both micellar solutions was evaporated in a rotary evaporator to a final micelle concentration of about 1.5 mg/mL. A paper filter was accurately weighed ( $W_1$ ) and the micelle solution was added dropwise, and was allowed to dry overnight ( $W_2$ ). The filter was then extracted in a Soxhlet setup using THF for 24 hours, and dried overnight ( $W_3$ ) in a 40 °C vacuum oven. The gel content measurements were performed in triplicate. The gel content was calculated as follows:

$$\text{Gel content} = \frac{(W_3 - W_1)}{(W_2 - W_1)} \times 100\%$$

#### *In vitro release of DOX*

The *in vitro* release of DOX from the unmodified and cross-linked micelles was performed in a PBS buffer with a pH of 7.4, and a sodium acetate buffer with a pH of 5.0. For the release experiment, 5 mL of the DOX loaded micelles was transferred to a dialysis bag with a molecular weight cut-off of 1 kDa. The dialysis bag was the submersed in 100 mL of the buffer and the mixture was gently stirred at 100 rpm. After several time intervals, 2 mL of the dialysis liquid was taken and replaced with 2 mL of the fresh buffer. The samples were analyzed using UV-Vis to determine the DOX concentration.

#### *In vitro cytotoxicity assay*

The cytotoxicity was evaluated by measuring cell metabolic activity by a PrestoBlue® assay, which is a good indicator of cell viability. Two types of cells were used, L929 fibroblast cell line from mouse for the evaluation of the non-loaded micelles and MDA-MB-231 human cell line of breast adenocarcinoma for the evaluation of the DOX loaded micelles. The cells were obtained from ATCC. For both cell type the culture medium used was Dulbecco's Modified Eagle's Medium (DMEM, ThermoFisher) with glutamax supplemented with 1% penicillin-streptomycin and 10% fetal bovine serum (FBS).

L929 cells were seeded at  $5 \times 10^3$  cell/cm<sup>2</sup> in 48-well plates for the pre-loading evaluation. Cells were cultured in cell culture medium during 48 h to reach subconfluence (80%). Prior to the complementation of the medium, the micelles were concentrated using evaporation to 20 mg/mL and then diluted in the cell medium to the appropriate concentration. The media was complemented with unmodified micelles, cross-linked micelles, or POEGA macro-RAFT agent. For each condition, 3 concentrations were tested: 2, 0.2, and 0.02 mg/mL. MDA-MB-231 cells were seeded at  $2.5 \times 10^4$  cells/cm<sup>2</sup> in 48-well plates for the post-loading evaluation. Cells were cultured in the cell culture medium for 48 h to reach subconfluence (80%). Then the media was complemented with either unmodified micelles, or cross-linked micelles or free DOX. For all conditions 3 concentrations of DOX were tested: 0.1, 1, and 10  $\mu$ g/mL. Untreated cell control was always included as a reference (100% cell viability).

After 72 h, the cells were incubated 30 min with PrestoBlue® solution diluted in the culture medium (1:9 v/v). Then supernatants were collected to measure the fluorescence (Excitation 560 nm / Emission 590 nm) using a CLARIOstar plate reader.

## Results and discussion

Block copolymers consisting of POEGA as the hydrophilic block and a copolymer of 4CPA and LA as the hydrophobic block were synthesized with different POEGA and hydrophobic block lengths. For the hydrophilic block, POEGA macro-RAFT agents with a degree of polymerization of 19, 31, and 51 were used (Table 3.1). An overlay of the GPC traces is shown in Figure B2. The POEGA macro-RAFT agents were employed in a solvent polymerization to attach the hydrophobic block consisting of 30 mol% 4CPA and 70 mol% LA. Three different hydrophobic block lengths were synthesized with a targeted degree of polymerization (DP) of 20, 40, and 60, resulting in nine unique block copolymers (Table 3.2). Corrected for the molecular weight, these compositions result in block copolymers with a relatively large hydrophilic weight fraction and corresponding high HLB value. Block copolymer micelles containing large and dense hydrophilic shells such as provided by the nonionic POEGA possess higher stability and improved stealth properties.<sup>24, 34-35</sup>

Table 3.1. Characteristics of the synthesized POEGA macro-RAFT agents.

Polymer	Molar feed ratio			OEGA Conv. (%)	DP <sub>NMR</sub>	M <sub>n, NMR</sub> (kg/mol)	DP <sub>th</sub>	M <sub>n, th</sub> (kg/mol)	M <sub>n, GPC</sub> (kg/mol)	Đ
	OEGA	RAFT	AIBN							
POEGA <sub>19</sub>	22	1	0.1	85	22	10.9	19	9.3	10.4	1.16
POEGA <sub>31</sub>	40	1	0.1	77	35	17.1	31	15.2	15.1	1.21
POEGA <sub>51</sub>	70	1	0.1	73	71	34.4	51	24.3	19.7	1.28

## Block copolymer synthesis

Table 3.2. Characteristics of the synthesized amphiphilic block copolymers.

Polymer	Molar feed ratio <sup>a</sup>	Conv. 4CPA (%)	Conv. LA (%)	$M_{n, th}^b$ (kg/mol)	$M_{n, NMR}^c$ (kg/mol)	Molar ratio <sup>1</sup> H NMR <sup>c</sup>	HLB value
	4CPA : LA : AIBN						
POEGA <sub>19</sub> -HB <sub>16</sub>	6 : 14 : 0.2	81	83	12.8	16.5	17 : 42 : 41	12.2
POEGA <sub>19</sub> -HB <sub>37</sub>	12 : 28 : 0.2	92	91	17.1	24.2	23 : 53 : 24	8.3
POEGA <sub>19</sub> -HB <sub>50</sub>	18 : 42 : 0.4	86	83	20.0	29.8	22 : 58 : 20	7.1
POEGA <sub>31</sub> -HB <sub>17</sub>	6 : 14 : 0.2	86	87	18.9	22.5	10 : 35 : 55	14.5
POEGA <sub>31</sub> -HB <sub>38</sub>	12 : 28 : 0.4	93	95	23.3	29.3	16 : 49 : 35	10.8
POEGA <sub>31</sub> -HB <sub>49</sub>	18 : 42 : 0.4	82	82	25.7	31.4	18 : 48 : 34	10.7
POEGA <sub>51</sub> -HB <sub>15</sub>	6 : 14 : 0.2	76	78	27.6	40.0	6 : 23 : 71	16.8
POEGA <sub>51</sub> -HB <sub>32</sub>	12 : 28 : 0.2	79	81	31.2	45.2	11 : 33 : 56	14.7
POEGA <sub>51</sub> -HB <sub>47</sub>	18 : 42 : 0.4	74	81	34.5	50.2	12 : 39 : 49	13.5

<sup>a</sup> Keeping the molar feed ratio of the macro-RAFT agent at 1. <sup>b</sup> Calculated as follows:  $M_{n, th} = \text{target DP}_{4CPA} \times \text{conv}_{4CPA} \times 152.05 + \text{target DP}_{LA} \times \text{conv}_{LA} \times 240.39 + MW_{th, POEGA \text{ macro-RAFT}}$ . <sup>c</sup> Calculated as follows for block copolymers synthesized with POEGA<sub>19</sub>:  $DP_{NMR, 4CPA} = I_{4CPA, 7.59 \text{ ppm}} / (I_{OEGA15, 3.38 \text{ ppm}} / 66)$ ,  $DP_{NMR, LA} = (I_{LA, 0.88 \text{ ppm}} / 3) / (I_{OEGA15, 3.38 \text{ ppm}} / 66)$ ,  $M_{n, NMR} = DP_{4CPA} \times 152.05 + DP_{LA} \times 240.39 + MW_{NMR, POEGA19 \text{ macro-RAFT}}$ . For block copolymers synthesized with POEGA<sub>31</sub> and POEGA<sub>51</sub> the integral of the OEGA resonance at 3.38 ppm was divided by 105 and 213, respectively.

Copolymerization of 4CPA with LA in the presence of the POEGA macro-RAFT agents proceeded without cross-linking that could occur as a result of side reactions on the pendent cyclopentenone units. Previous investigation of the solvent (co)polymerization of 4CPA under RAFT control, showed that by targeting a sufficiently low DP and 4CPA-to-comonomer ratio, cross-linking can indeed be avoided.<sup>18</sup> In the <sup>1</sup>H NMR spectrum of POEGA<sub>19</sub>-HB<sub>37</sub>, the resonances corresponding to the 4CPA double bond are well visible, indicating the preservation of the cyclopentenone group on the polymer backbone (Figure 3.4a). According to the <sup>1</sup>H NMR spectra of the purified block copolymers, the monomer molar ratios match with the corresponding feed ratios, taking the differences in monomer conversion into account. The molar contribution of OEGA in the final structures increases as expected with increasing POEGA block length, leading to a set of amphiphilic block copolymers with HLB values between 7.1 and 16.8. In Table 3.2, the monomer composition and HLB values of all synthesized block copolymers is presented.

In the copolymerization with LA, 4CPA displays a very similar reactivity as shown in Figure 3.1a. A similar behavior is observed in the copolymerization plot drawn from the reactivity ratios (Figure 3.1b and Figure B3a, b). 4CPA has a slightly higher tendency to polymerize relative to LA, but the copolymerization is close to statistical, resulting in an almost random distribution of cyclopentenone units on the hydrophobic backbone. Statistical

copolymerization is generally expected for n-alkyl acrylates,<sup>36</sup> and in this case indicates that the cyclopentenone double bond in 4CPA does not drastically influence the reactivity ratios.

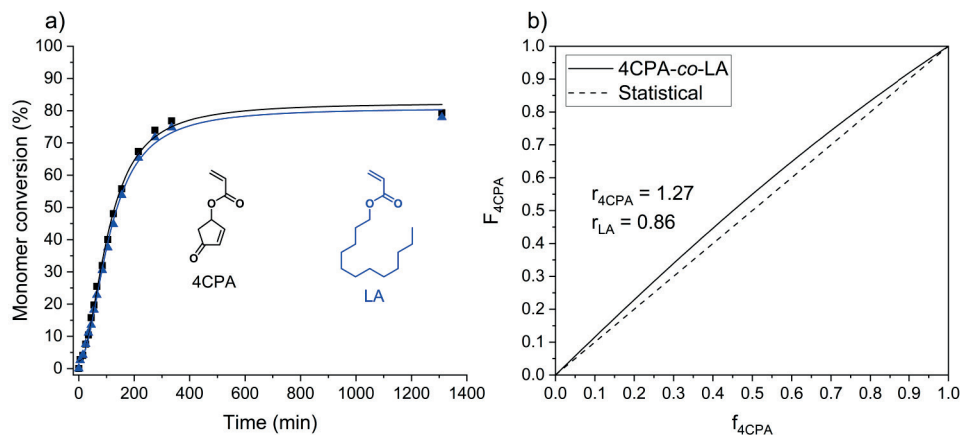


Figure 3.2. a) Monomer conversion as a function of time for the copolymerization of 4CPA (black squares) with LA (blue triangles) using macro-RAFT agent POEGA<sub>19</sub> (POEGA<sub>19</sub>-HB<sub>37</sub>). b) Copolymerization plot of 4CPA and LA.

The characterization of the block copolymers using GPC yielded inconsistent values for  $M_n$ . The obtained molecular weights were lower for the block copolymers in comparison to the macro-RAFT agent (Table B1). Characterization of block copolymers via GPC, especially when the chemical or physical characteristics of the blocks differ significantly, can lead to misleading results.<sup>37</sup> The block copolymers presented here exhibit a stark difference in terms of hydrophobicity and functional groups between the hydrophilic and hydrophobic block. The observation of a decrease in molecular weight of the block copolymers in comparison to the macro-RAFT agent was observed before and is related to changes in block and column interaction, contraction, or collapse of the polymer coil.<sup>37-38</sup> Block copolymerization involving the chain extension of the POEGA macro-RAFT agents was instead characterized via MALDI-ToF-MS (Figure B4a-d). For the block copolymers, shoulders towards higher molecular weight are observed in overlay with the corresponding macro-RAFT agent. Since the MALDI-ToF-MS technique is more sensitive towards low molecular weight compounds, the curves are not representative of the actual polymer composition. Therefore, the formation of block copolymers instead of two separate homopolymers, was confirmed by diffusion ordered spectroscopy (DOSY). By comparing the DOSY spectrum of block copolymer POEGA<sub>19</sub>-HB<sub>51</sub> with its corresponding macro-RAFT agent POEGA<sub>19</sub>, a decreased diffusion coefficient value for the block copolymer is observed (Figure B5 and B6). Both the hydrophobic and hydrophilic signal exhibit the same value for D suggesting the presence of one species with constant molar mass. Similarly, the longer macro-RAFT agent POEGA<sub>31</sub>, shows a lower value for D compared to POEGA<sub>19</sub>, reflecting the higher molecular weight of a single species (Figure B7).



## Surface-active properties

Solutions of the POEGA macro-RAFT agents and the amphiphilic block copolymers in water significantly lowered the surface tension (Figure 3.3). The observed moderate values for the surface tension are in line with what can be expected for POEGA based polymeric surfactants.<sup>39-40</sup> The block copolymer surface tension at the critical aggregation concentration (CAC) ( $\gamma_{CAC}$ ) ranged between 57 and 59 mN m<sup>-1</sup>. For the POEGA macro-RAFT agents the  $\gamma_{CAC}$  was slightly lower at 58, 57, and 55 mN m<sup>-1</sup> for POEGA<sub>51</sub>, POEGA<sub>31</sub>, and POEGA<sub>19</sub>, respectively. Surprisingly a large effect of the length of the hydrophilic block was observed, but not for the hydrophobic block (Table B2). The CAC decreases with increasing hydrophilic block length, irrespective of the hydrophobic block length. Therefore, the CAC decrease is more likely an effect of the molecular weight increase. The lack of trend in the observed CAC values with the hydrophobic block length is opposite of the expected trend, but has been reported before with block copolymers containing complex or grafted structures.<sup>40-42</sup>

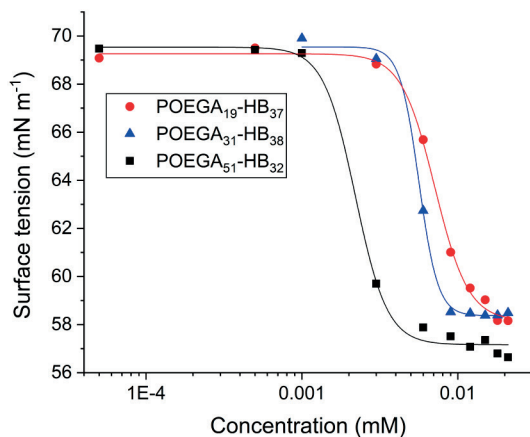


Figure 3.3. Surface tension as a function of the block copolymer concentration, investigating the effect of POEGA hydrophilic block length. The calculations related to determination of the molar concentration herein are performed using the theoretical molecular weight as presented in Table 3.2.

## Self-assembly of block copolymers

The self-assembly behavior in water of the 4CPA block copolymers was firstly demonstrated by measuring the <sup>1</sup>H NMR spectrum of the block copolymer, in this case POEGA<sub>19</sub>-HB<sub>37</sub> separately in CDCl<sub>3</sub> and D<sub>2</sub>O (Figure 3.4). In CDCl<sub>3</sub>, the resonances corresponding to both the hydrophilic block and the hydrophobic block are well resolved. Upon dissolution in D<sub>2</sub>O, only the resonances corresponding to the hydrophilic POEGA block are visible (Figure 3.4b). The resonances belonging to 4CPA at 7.59, 6.35, 5.83, and 2.78 ppm and LA at 4.01, 1.27,

and 0.89 ppm were not visible in the spectrum. This is consistent with the self-assembly of the block copolymer into a core-shell structure with a collapsed hydrophobic core shielded by the POEGA hydrophilic shell.

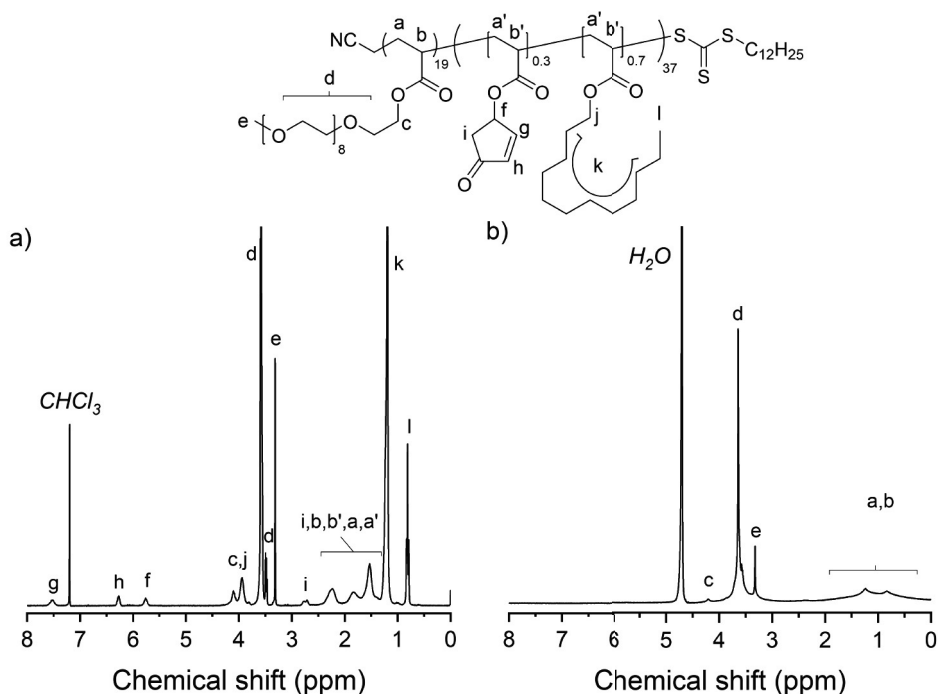


Figure 3.4.  $^1\text{H}$  NMR spectrum of block copolymer POEGA<sub>19</sub>-HB<sub>37</sub> in a)  $\text{CDCl}_3$  and b)  $\text{D}_2\text{O}$ .

Further investigation towards the self-assembly of 4CPA block copolymers was performed by DLS. Direct dissolution of the block copolymers resulted in visibly slightly turbid mixtures for the block copolymers POEGA<sub>19</sub>-HB<sub>37</sub> and POEGA<sub>19</sub>-HB<sub>50</sub> due to their low HLB value (<10). This is also reflected in the DLS spectra, showing typically large sizes and in some cases a second, larger size distribution, which indicate the presence of aggregates (Table B3). Overall, direct dissolution of the block copolymers in water resulted in a wide range of sizes of between 29 and 257 nm. In some cases, a larger micellar population was also observed. From the perspective of certain nanotechnology applications, these sizes are rather large. In the field of nanomedicine the utilization of smaller sub-100 nm micelles is favored for the blood circulation and tissue penetration.<sup>24</sup> Improved performance of encapsulated drugs is observed when micelles of sub-50 nm are used due to the improved tumor tissue penetration and accumulation as a result of the enhanced permeability and retention (EPR) effect.<sup>43-45</sup> Furthermore, a smaller size is believed to improve the stealth properties of drug delivery vehicles, which is related to the curvature of vehicle surface.<sup>24</sup> Therefore, in order to attempt to reduce the size, the solvent exchange method of micelle formation was explored. Herein, the block copolymers were dissolved in an organic solvent

that is a good solvent for both blocks, in this case THF. Then water is slowly added dropwise to induce micelle formation in a controlled and reproducible fashion. Remaining THF is then removed by dialysis against water. The resulting assembly dispersions were all optically clear. As a result of the solvent exchange method, in almost all cases the size was greatly reduced to sub-50 nm level (Figure 3.5). The exceptions are the block copolymers with the smallest hydrophobic block length, which resulted in micelles with a size between 88 and 161 nm. Indeed, the graph shows that the hydrophobic block length strongly influences the resulting size of the micelle. The formation of micelles with a size between 29 and 40 nm is achieved for the block copolymers with intermediate hydrophobic block length. In static light scattering analysis of similar amphiphilic PEG-*block*-poly alkyl acrylate micelles with comparable molecular weight and micelle size an aggregation number of between 111 and 133 was found.<sup>46-47</sup> Based on the structural similarity, and comparable molecular weight and size of these POEGA block copolymer micelles, a similar aggregation number can be expected for the assemblies described here. For block copolymer POEGA<sub>31</sub>-HB<sub>49</sub>, micelles were also prepared via the nanoprecipitation method for comparative purposes. In this method, the block copolymer dissolved in a good solvent, in this case THF, is added dropwise to a stirring container of water, following an inverse methodology in comparison to the solvent exchange method. The resulting micelles showed a similar particle size distribution in DLS compared to the micelles obtained via the solvent exchange method. Particles obtained via the nanoprecipitation method were slightly smaller in size but exhibited a slightly larger dispersity (Figure B8).

The obtained micelles from block copolymer POEGA<sub>19</sub>-HB<sub>50</sub> were stable after storage for 4 months. No visual coagulation or sedimentation was observed and according to DLS, the sizes remained the same (Figure B9).

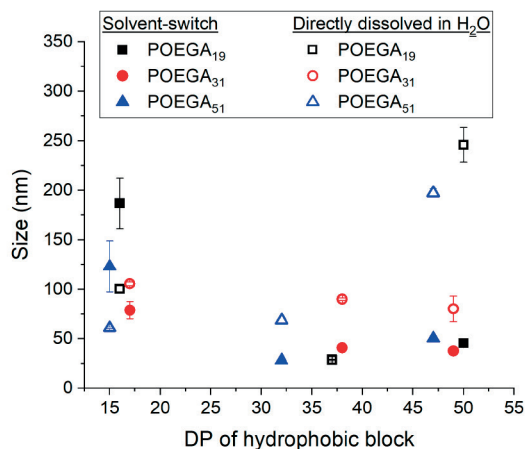


Figure 3.5. Effect of the DP of the hydrophobic block for block copolymers with POEGA<sub>19</sub>, POEGA<sub>31</sub>, and POEGA<sub>51</sub> on the size measured in DLS. The sizes corresponding to two different methods of micelle formation are depicted. The solid symbols represent the solvent exchange method and the open symbols direct dissolution in H<sub>2</sub>O.

### UV induced cross-linking of block copolymer micelles

Micellar structures of block copolymers bearing pendent cyclopentenone units as a part of the hydrophobic core were cross-linked using UV light. Previous research has demonstrated the UV-induced [2 + 2] photocyclodimerization of cyclopentenone side groups on a polyacrylate backbone.<sup>18</sup> Core cross-linking was demonstrated on the block copolymer with the longest hydrophobic segment POEGA<sub>19</sub>-HB<sub>50</sub>. After self-assembly via the solvent exchange method, a DLS spectrum was measured to determine the initial size of the micelles, which was 36 nm (Figure 3.6). A portion of the micelles was then dialyzed against THF. Replacing the aqueous medium with THF caused the micelles to dissociate and form smaller micelles of about 9 nm in diameter. Despite the solubility of the individual blocks in THF<sup>18</sup>, self-assembly could still occur due to the strong difference in hydrophobicity between the blocks, possibly resulting in an inverse micelle.<sup>48</sup> The formation of 9 nm particles in THF was confirmed separately by directly dissolving the block copolymer in THF. The same size distribution was found in DLS (Figure 3.6b). The other portion of block copolymer micelles was irradiated in a UV chamber for 30 minutes. Similarly, a DLS spectrum was measured before and after dialysis against THF. In this case, the size remained the same, indicating that the micelles stayed intact due to the covalent cross-linking as a result of cyclopentenone dimerization. Another indication of the significance of cross-linking is the gel content measurement of the UV irradiated micelles. Soxhlet extraction in THF revealed a gel content of  $92 \pm 3\%$ , while the unmodified micelles were completely soluble in THF. DSC spectra of the dried micelles were recorded before and after UV cross-linking (Figure B10). The unmodified micelles show a melting point of  $-12.4\text{ }^{\circ}\text{C}$  belonging to the side chain crystals of the LA unit.<sup>18, 49</sup> The melting peak of the cross-linked micelles is decreased to  $-17.1\text{ }^{\circ}\text{C}$  and with a significantly lower melting enthalpy, caused by the disruption of crystal formation as a result of cross-linking.

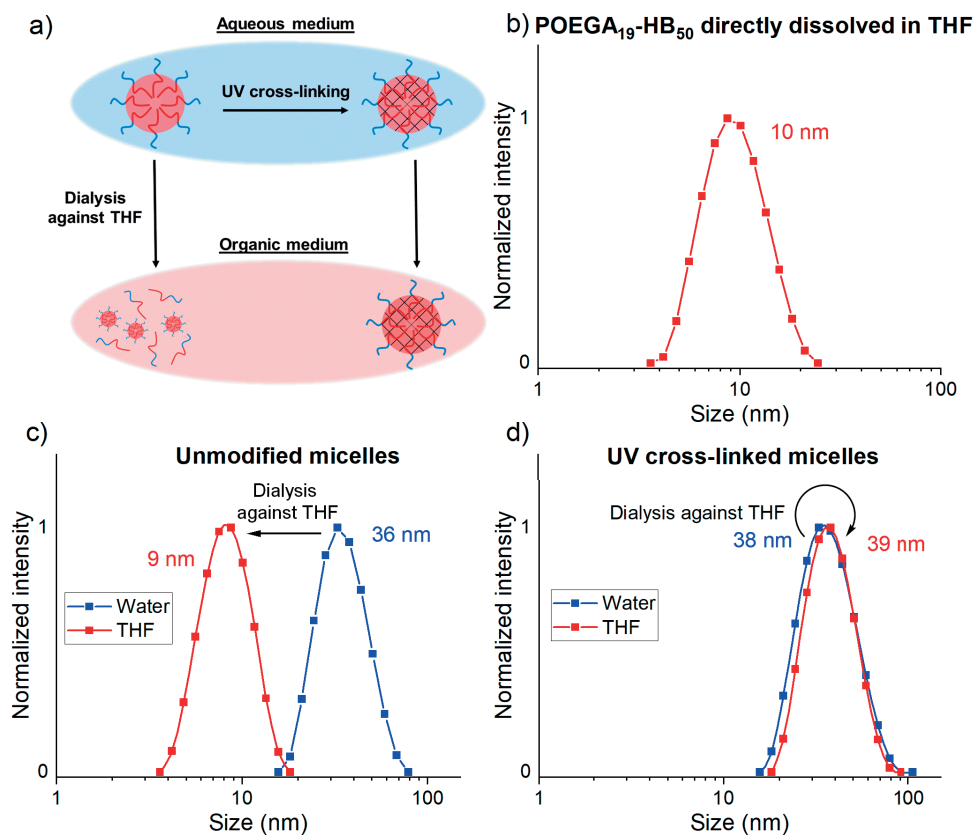


Figure 3.6. DLS results of the UV cross-linked and unmodified micelles obtained from POEGA<sub>19</sub>-HB<sub>50</sub> in water and THF. a) Schematic representation of the micelles in THF, which dissociate and form smaller micelles, but the cross-linked micelles retain their size. b) DLS curve of POEGA<sub>19</sub>-HB<sub>50</sub> directly dissolved in THF. c) Unmodified micelles of POEGA<sub>19</sub>-HB<sub>50</sub> before and after dialysis against THF. d) Cross-linked micelles of POEGA<sub>19</sub>-HB<sub>50</sub> before and after dialysis against THF. The size distributions are normalized on the y-axis.

Unmodified and UV cross-linked block copolymer micellar assemblies from POEGA<sub>19</sub>-HB<sub>37</sub> were subjected to further characterization via cryo-TEM (Figure 3.7b-c). As a result of changes in chemical structure and HLB value, various assembly morphologies could in theory be obtained. Generally, spherical micellar assemblies can be expected when the hydrophilic block is larger than the hydrophobic block, which is the case here.<sup>50-51</sup> In general, the sizes observed in cryo-TEM (Figure 3.7b-d) corresponded well with those obtained from DLS (Figure 3.7a). One of the benefits of core-cross-linking of block copolymer assemblies via external stimuli is that generally the size and shape is well maintained. Indeed, UV cross-linking did not affect the size or shape of the micelles in any way according to DLS and cryo-TEM (Figure 3.7a-c). A size for the cross-linked micelles of 28 nm and 29 ± 8 nm (n = 193) is measured with the DLS and cryo-TEM, respectively. Interestingly, a very different

morphology is obtained when the block copolymer is directly dissolved in water (Figure 3.7d). As suggested by DLS, and confirmed by cryo-TEM, the primary size of the micelles is very small, about 29 nm. However, the assemblies have an oblong shape instead of spherical, and tend to aggregate into larger structures. According to cryo-TEM, the length average diameter is  $34 \pm 6$  nm ( $n = 187$ ) and the width average diameter is  $24 \pm 3$  nm. Aggregation is also observed in the DLS, which shows the presence of larger micellar structures of 167 nm.

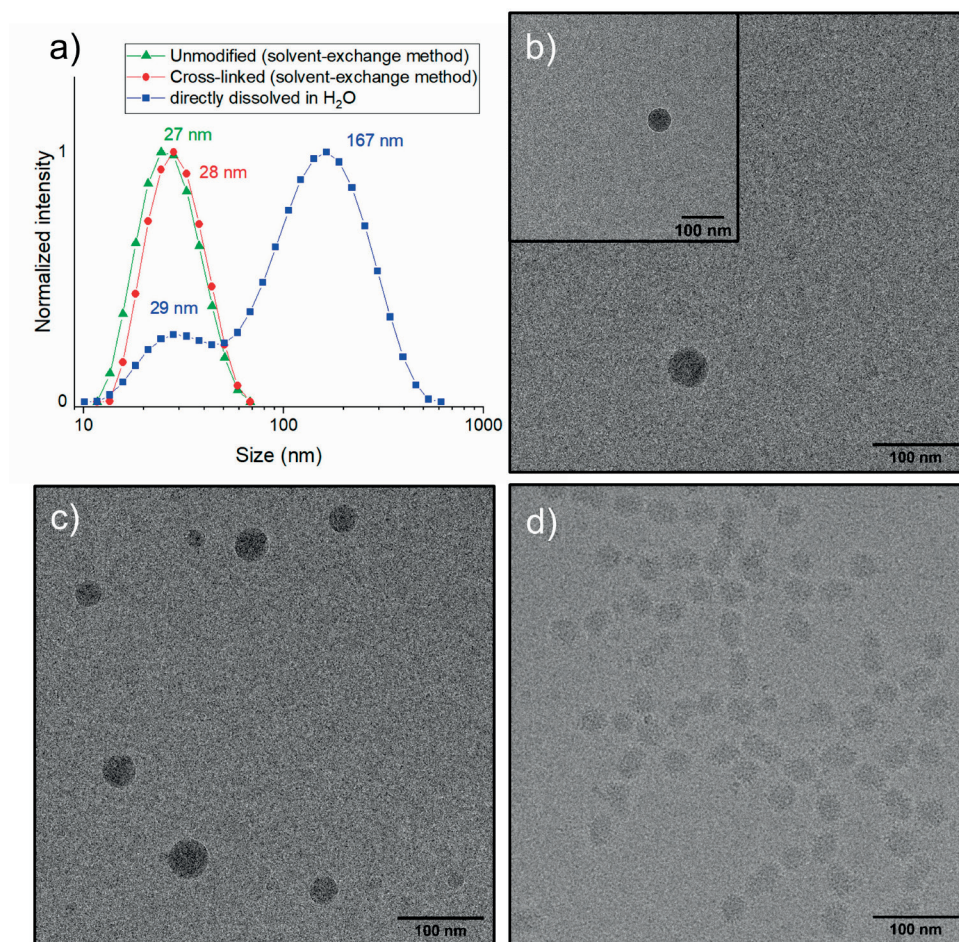


Figure 3.7. Characterization of the size and shape of assemblies from block copolymer POEGA<sub>19</sub>-HB<sub>37</sub>. a) DLS size distributions of POEGA<sub>19</sub>-HB<sub>37</sub> directly dispersed in water, and prepared via the solvent exchange method (unmodified and cross-linked). The size distributions are normalized on the y-axis. Cryo-TEM images of POEGA<sub>19</sub>-HB<sub>37</sub> block copolymer assemblies b) unmodified (average diameter  $40 \pm 14$  nm,  $n = 15$ ), c) cross-linked (average diameter =  $29 \pm 8$  nm,  $n = 193$ ), and d) directly dissolved in water (length average diameter =  $34 \pm 6$  nm,  $n = 187$ , width average diameter =  $24 \pm 3$  nm,  $n = 187$ ). Errors reported are standard deviations.



### Model drug loading of block copolymers

Another benefit of the solvent exchange method is that it can be effectively combined with hydrophobic drug encapsulation to obtain block copolymer encapsulated drugs. The hydrophobic drug is simply added to the solution of block copolymer in THF, which is followed by drop-wise addition of water to induce micelle formation. In this work, the drug loading content (DLC) of all the block copolymers presented in Table 3.2 was investigated using two model probes, pyrene and nile red on unmodified micelles. Both compounds are incompatible with the aqueous environment and are commonly used to probe micellar loading efficiency.<sup>52-54</sup> The solvent exchange method results in optically clear liquids for the pyrene loaded micelles, and in the case of nile red encapsulated micelles, the liquid turned red (Figure B11). In Figure 3.8a, b, the DLC is presented as a function of the DP of the hydrophobic block for the three different POEGA macro-RAFT agents. For pyrene encapsulation, a clear trend is observed. With the increase in the hydrophobic block length, the DLC increased from 0.9 to 1.8% for POEGA<sub>51</sub>, from 1.8 to 2.7% for POEGA<sub>31</sub>, and from 2.5 to 3.8% for POEGA<sub>19</sub> (Figure 3.8). This shows the importance of the hydrophobic block length in block copolymer design, and suggests that pyrene persists in the hydrophobic micellar cores. The DLC's observed in this model study are rather low, but in accordance with loading values obtained for some long-chain poly alkyl acrylate amphiphilic block copolymers with various hydrophobic compounds.<sup>55-57</sup> Nonetheless, the loading capacity is strongly influenced by the encapsulation method.<sup>58</sup> In a control experiment where no block copolymer was added during the solvent exchange method, no appreciable amount of pyrene or nile red was detected by UV-Vis (Figure B12). The model drug loaded micelles corresponding to all the block copolymers were colloiddally stable. No pyrene or nile red precipitation was observed during storage over several weeks.

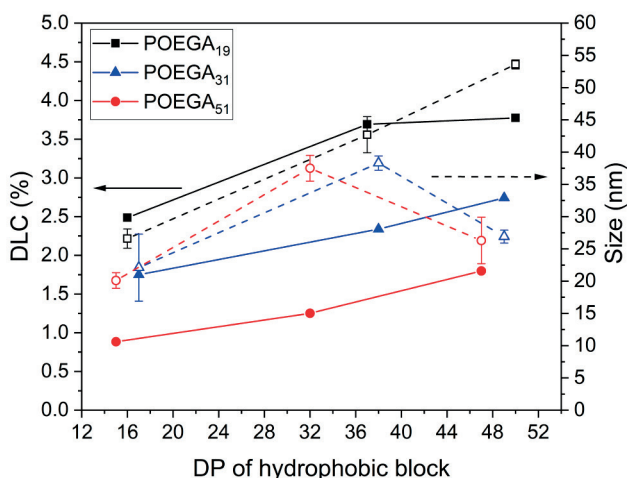


Figure 3.8. Investigation of the DLC and size of the pyrene loaded micelles using DLS as a function of the DP of hydrophobic block.

In contrast to the pyrene encapsulation, no clear effect of the block length was observed for the DLC of Nile red loaded micelles (Figure B13). The DLC for the block copolymer micelles ranged between 1.1 and 2.3%. A possible explanation for the absence of effect of the block lengths on Nile red encapsulation is that Nile red can also persist in the hydrophilic PEG layer, possibly due to the presence of polar groups, that are not present in the structure of pyrene.<sup>53</sup>

The size and shape of polymeric micelles is influenced by the formulation parameters involved in preparing the drug loaded micelles.<sup>2</sup> One of them is the concentration of polymer and drugs including possible interactions between them.<sup>59</sup> Addition of a drug during the self-assembly can result in both smaller or larger micelles.<sup>60-61</sup> Therefore, the size of micelles after dye encapsulation was assessed using DLS (Figure 3.8). In general, the pyrene-loaded micelles (21 to 54 nm) exhibited a very similar size as the unmodified micelles (29 to 50 nm). The three exceptions are the block copolymers with the smallest hydrophobic block length. The size of pyrene loaded block copolymers micelles POEGA<sub>19</sub>-HB<sub>16</sub>, POEGA<sub>31</sub>-HB<sub>17</sub>, and POEGA<sub>51</sub>-HB<sub>15</sub> were reduced drastically compared to the unmodified micelles. The initial size of between 88 and 161 nm was reduced to between 21 and 30 nm. The presence of pyrene and the interactions with the hydrophobic block can influence the micellar formation process, favoring smaller micelles.

Another interesting observation is the drastic increase in size for some of the Nile red loaded micelles (Figure B13). This was observed for the block copolymers with a relatively large POEGA fraction. These are POEGA<sub>19</sub>-HB<sub>16</sub>, POEGA<sub>31</sub>-HB<sub>17</sub>, POEGA<sub>51</sub>-HB<sub>15</sub>, and POEGA<sub>51</sub>-HB<sub>32</sub> and consist of 41, 55, 71, and 56 mol% POEGA, respectively (Table 3.2). Like pyrene, the presence of Nile red during the solvent exchange procedure could have affected the micelle formation, possibly by aggregation or fusion into larger micelles. Another possibility is the increase of the hydrophobic part of the micelle, by addition of the Nile red, affecting the self-assembly process.<sup>62</sup>

### **Doxorubicin loading and *in vitro* release**

POEGA<sub>19</sub>-HB<sub>50</sub>, which showed the highest pyrene loading content, was used for the DOX loading in both the unmodified and UV cross-linked form. Similar to the pyrene loading, DOX was loaded by the solvent exchange method by dissolving the DOX together with the block copolymer in an organic solvent and inducing micelle formation by slow addition of water. Compared to pyrene, the DOX was loaded in significantly higher amounts. The drug loading content for the unmodified micelles was 23.8%, and the corresponding encapsulation efficiency was also high at 78.3%. Similarly, the UV cross-linked micelles were also loaded with DOX, which was performed after the UV curing step to avoid degradation of DOX by UV light. DOX loading of the cross-linked micelles resulted in a DLC of 3.4%. The absence of the self-assembly process accompanying the DOX loading for unmodified micelles could explain the reduced loading efficiency for the UV cross-linked micelles. The photograph in Figure B14 of the DOX loaded micelles displays the transparent and red colored solutions, indicating successful DOX encapsulation. The average size of the DOX loaded micelles was



determined by DLS was 156 nm for the unmodified micelles and 84 nm for the cross-linked micelles.

The *in vitro* release of DOX from the micelles was tested at a pH of 7.4 and 5.0 (Figure 3.9). The DOX release is fast initially and the release rate decreases after about 24 hours, after which only a slow increase in the cumulative DOX release is observed. For both the unmodified and cross-linked micelles, the DOX release was significantly faster at a pH of 5.0 in contrast to 7.4. While initially the release rate of the unmodified and cross-linked micelles is similar, a significant difference in the DOX release was observed after 72 hours. For the unmodified micelles, 50 % of DOX was released at a pH of 5.0. The cross-linked micelles showed a significantly lower release of 31% after 72 hours. Possible incorporation of comonomers improving the interaction of DOX with the micellar vehicle via  $\pi$ - $\pi$  interactions or reversible covalent bonds could further delay the initial fast DOX release rate.<sup>63</sup> The release profile is characterized by a fast, partial release in the first 8 hours, followed by a very slow release over time. In case of the experiment performed at a pH of 7.4 the release appears to have halted almost completely after the first several hours of release. At a lower pH of 5, a slow release is continued in the days thereafter. An initial release burst could have been caused by the release of a fraction of DOX weakly associated to the POEGA shells of the micelles. The following release of DOX from the micellar cores is much slower, especially in neutral pH, where DOX is very sparsely soluble.

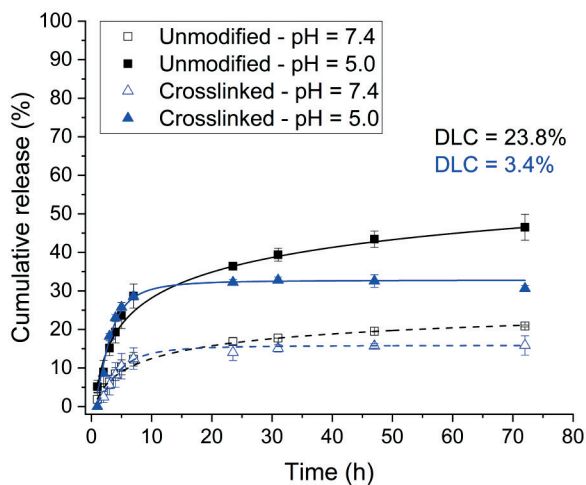


Figure 3.9. Cumulative DOX release in medium of pH = 7.4 and pH = 5.0 from block copolymer micelles of POEGA<sub>19</sub>-HB<sub>50</sub>.

### Cell viability

Cytotoxicity of the POEGA<sub>19</sub>-HB<sub>50</sub> unmodified and UV cross-linked micelles was tested with healthy L929 mouse fibroblast cells. Both micelles were compared to the POEGA<sub>19</sub> macro-RAFT agent, which showed low cytotoxicity (Figure 10a).<sup>26</sup> The cells showed higher

viability with low concentrations of micelles, similar to the POEGA macro-RAFT agent. However, at an elevated concentration of 2 mg/mL, low to zero cell viability was observed for the micelles, whereas POEGA showed cell viability of around 50%. The cells morphology, round instead of elongated, support the previous observation on the cytotoxic effect (Figure B15). At concentrations above 0.2 mg/mL, the cross-linked micelles showed a higher cytotoxicity compared to the unmodified micelles. This could possibly be caused by the evolution of small molecules as a result of the UV irradiation due to homolytic cleavage or hydrolysis reactions of the ester groups.

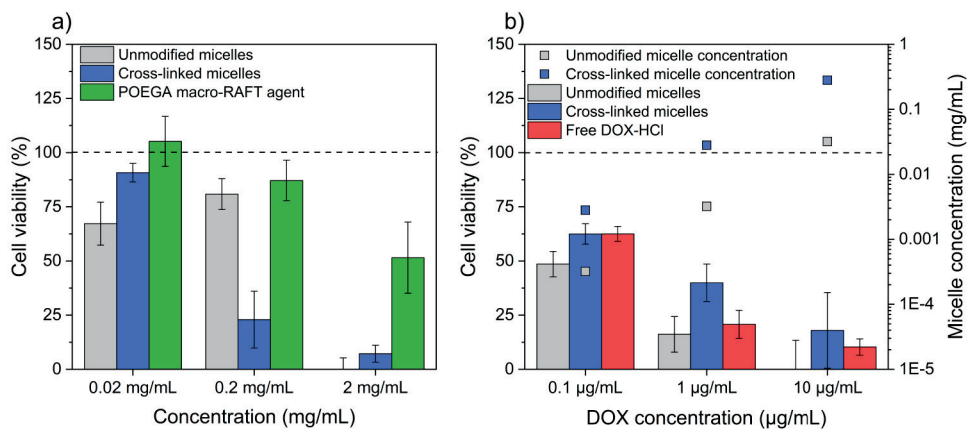


Figure 3.10. a) Cell viability of L929 cells in the presence of various concentrations of unmodified and cross-linked micelles, and POEGA macro-RAFT agent after 72 hours exposure. b) Cell viability of MDA-MB-231 cells in the presence of various concentrations of DOX loaded unmodified and cross-linked micelles, and free DOX-HCl after 72 hours exposure.

The same micelles from POEGA<sub>19</sub>-HB<sub>50</sub> loaded with DOX, were tested on MDA-MB-231 breast adenocarcinoma cells at a DOX concentration of 0.1, 1, and 10 µg/mL. The cell viability was compared with free DOX-HCl. In the graph in Figure 10b, the cell viability as a function of the DOX concentration is shown. The DOX loaded micelles clearly had an impact on cell viability, a decrease of cell viability was observed demonstrating a cytotoxic effect. This effect is also illustrated by cell morphology (Figure B16), many round cells were observed. Plus, at high concentrations, many dead cells were noticed (Figure B16). The cell viability also decreases with increasing DOX concentration. The cell viability is reduced to below 20% in all cases at a DOX concentration of 10 µg/mL after 72 hours, indicating the cytotoxic effect of DOX on the MDA-MB-231 cells. Interestingly, higher cell viability was observed with the cross-linked micelles, at all instances compared to the free DOX-HCl and unmodified micelles. This result indicates a delayed exposure of the DOX to the cells, as suggested by the previous results (Figure 9). Furthermore, the DOX loaded micelles showed cytotoxicity towards MDA-MB-231 cells at a concentration of micelles that is not cytotoxic

towards the L929 cells (i.e. below 0.2 mg/mL). Optimizations in DOX loading and block copolymer design could improve the cytotoxic effect of DOX against breast adenocarcinoma cells.

## Conclusions

In this work, we successfully synthesized UV cross-linkable amphiphilic block copolymers containing cyclopentenone side groups on the hydrophobic backbone. Utilizing RAFT controlled copolymerization with POEGA as the hydrophilic block, 4CPA and LA readily copolymerized to form the hydrophobic block. In this way, a series of block copolymers exhibiting various block lengths and ratios were synthesized and further investigated. According to  $^1\text{H}$  NMR spectroscopy, the cyclopentenone double bond remained intact during polymerization, which is required for the possibility of dimerization under UV-light to obtain core cross-linked micelles.

Self-assembly of block copolymers in water was demonstrated by  $^1\text{H}$  NMR spectroscopy, DLS, and cryo-TEM. Preparation of the assemblies via a solvent exchange method yielded smaller and more defined spherical micelles compared to direct dissolution in  $\text{H}_2\text{O}$ . As shown for block copolymer POEGA<sub>19</sub>-HB<sub>37</sub>, it formed oblong micelles as part of a larger aggregated structure. The size of the micelles prepared by the solvent exchange method was also strongly influenced by changes in hydrophobic block length. Especially medium to long hydrophobic blocks led to sub 50-nm micelles. The hydrophilic block length also influenced the surface tension properties of the block copolymers. All macro-RAFT agents and block copolymers significantly reduced the surface tension above the CAC.

The synthesized block copolymers were successfully loaded with model drugs. In here, the solvent exchange method was easily combined with model drug loading, by simply dissolving the model drug together with the block copolymer prior to water addition. This was demonstrated using the probes pyrene and Nile red. The best loading capacities were obtained for pyrene with block copolymer containing the relatively largest hydrophobic blocks, suggesting that pyrene persists in the micellar cores. Compared to unmodified micelles, the size of pyrene-loaded micelles remained similar (<50 nm), or was drastically reduced in some cases. The small size is a requirement for potential use as drug delivery devices in nanomedicine applications. The results from the micellar probe experiments were used to load the micelles with the cancer therapeutic drug, doxorubicin at a high drug loading content of 23.8%. The micelles showed a partial pH dependent release of the DOX, indicating the efficacy in therapeutic applications where inclusion in the acidic environment of the intracellular organelles via endocytosis is the mode of micellar uptake. L929 cells showed a good cell viability in presence of the micelles, proving the low cytotoxicity of the developed drug vehicles. The micelles are effective vehicles for the hydrophobic DOX as indicated by *in vitro* cell viability tests with breast carcinoma MDA-MB-231 cell line.

## References

1. Cabral, H.; Miyata, K.; Osada, K.; Kataoka, K., Block copolymer micelles in nanomedicine applications. *Chemical Reviews* **2018**, *118* (14), 6844-6892.
2. Lu, Y.; Zhang, E.; Yang, J.; Cao, Z., Strategies to improve micelle stability for drug delivery. *Nano Research* **2018**, *11* (10), 4985-4998.
3. Xu, W.; Ling, P.; Zhang, T., Polymeric micelles, a promising drug delivery system to enhance bioavailability of poorly water-soluble drugs. *Journal of Drug Delivery* **2013**, *2013*.
4. Read, E. S.; Armes, S. P., Recent advances in shell cross-linked micelles. *Chemical Communications* **2007**, (29), 3021-3035.
5. Gaucher, G.; Dufresne, M.-H.; Sant, V. P.; Kang, N.; Maysinger, D.; Leroux, J.-C., Block copolymer micelles: preparation, characterization and application in drug delivery. *Journal of Controlled Release* **2005**, *109* (1-3), 169-188.
6. Chen, C.; Yu, C. H.; Cheng, Y. C.; Peter, H.; Cheung, M. K., Biodegradable nanoparticles of amphiphilic triblock copolymers based on poly (3-hydroxybutyrate) and poly (ethylene glycol) as drug carriers. *Biomaterials* **2006**, *27* (27), 4804-4814.
7. O'Reilly, R. K.; Hawker, C. J.; Wooley, K. L., Cross-linked block copolymer micelles: functional nanostructures of great potential and versatility. *Chemical Society Reviews* **2006**, *35* (11), 1068-1083.
8. Yusa, S.-i.; Sugahara, M.; Endo, T.; Morishima, Y., Preparation and characterization of a pH-responsive nanogel based on a photo-cross-linked micelle formed from block copolymers with controlled structure. *Langmuir* **2009**, *25* (9), 5258-5265.
9. Sandholzer, M.; Bichler, S.; Stelzer, F.; Slugovc, C., UV-induced crosslinking of ring opening metathesis block copolymer micelles. *Journal of Polymer Science Part A: Polymer Chemistry* **2008**, *46* (7), 2402-2413.
10. Jiang, J.; Qi, B.; Lepage, M.; Zhao, Y., Polymer micelles stabilization on demand through reversible photo-cross-linking. *Macromolecules* **2007**, *40* (4), 790-792.
11. He, J.; Zhao, Y., Light-responsive polymer micelles, nano-and microgels based on the reversible photodimerization of coumarin. *Dyes and Pigments* **2011**, *89* (3), 278-283.
12. Shi, Y.; Cardoso, R. M.; Van Nostrum, C. F.; Hennink, W. E., Anthracene functionalized thermosensitive and UV-crosslinkable polymeric micelles. *Polymer Chemistry* **2015**, *6* (11), 2048-2053.
13. Chen, Y.; Tavakley, A. E.; Mathiason, T. M.; Taton, T. A., Photocrosslinked poly (vinylbenzophenone)-core micelles via mild Friedel-Crafts benzylation of polystyrene amphiphiles. *Journal of Polymer Science Part A: Polymer Chemistry* **2006**, *44* (8), 2604-2614.
14. Nardi, M.; Scherer, T.; Yang, L.; Kübel, C.; Barner-Kowollik, C.; Blasco, E., Stabilizing self-assembled nano-objects using light-driven tetrazole chemistry. *Polymer Chemistry* **2021**, *12* (11), 1627-1634.
15. Kaur, G.; Chang, S. L.; Bell, T. D.; Hearn, M. T.; Saito, K., Bioinspired core-crosslinked micelles from thymine-functionalized amphiphilic block copolymers: Hydrogen bonding and photo-crosslinking study. *Journal of Polymer Science Part A: Polymer Chemistry* **2011**, *49* (19), 4121-4128.
16. Barbarini, A. L.; Estenez, D. A.; Martino, D. M., Crosslinkable micelles from diblock amphiphilic copolymers based on vinylbenzyl thymine and vinylbenzyl triethylammonium chloride. *Journal of Applied Polymer Science* **2015**, *132* (19).
17. Pasparakis, G.; Vamvakaki, M., Multiresponsive polymers: nano-sized assemblies, stimuli-sensitive gels and smart surfaces. *Polymer Chemistry* **2011**, *2* (6), 1234-1248.

18. Stouten, J.; Vanpoucke, D. E.; Van Assche, G.; Bernaerts, K. V., UV-Curable Biobased Polyacrylates Based on a Multifunctional Monomer Derived from Furfural. *Macromolecules* **2020**, *53* (4), 1388-1404.
19. Ulbrich, K.; Kreitmeier, P.; Reiser, O., Microwave-or microreactor-assisted conversion of furfuryl alcohols into 4-hydroxy-2-cyclopentenones. *Synlett* **2010**, *2010* (13), 2037-2040.
20. Arcile, G.; Ouazzani, J.; Betzer, J.-F., Efficient Piancatelli rearrangement on a large scale using the Zippertex technology under subcritical water conditions. *Reaction Chemistry & Engineering* **2022**.
21. Keddie, D. J., A guide to the synthesis of block copolymers using reversible-addition fragmentation chain transfer (RAFT) polymerization. *Chemical Society Reviews* **2014**, *43* (2), 496-505.
22. Parkatzidis, K.; Wang, H. S.; Truong, N. P.; Anastasaki, A., Recent developments and future challenges in controlled radical polymerization: a 2020 update. *Chem* **2020**, *6* (7), 1575-1588.
23. Corrigan, N.; Jung, K.; Moad, G.; Hawker, C. J.; Matyjaszewski, K.; Boyer, C., Reversible-deactivation radical polymerization (Controlled/living radical polymerization): From discovery to materials design and applications. *Progress in Polymer Science* **2020**, *111*, 101311.
24. Vonarbourg, A.; Passirani, C.; Saulnier, P.; Benoit, J.-P., Parameters influencing the stealthiness of colloidal drug delivery systems. *Biomaterials* **2006**, *27* (24), 4356-4373.
25. Lutz, J. F., Polymerization of oligo (ethylene glycol)(meth) acrylates: Toward new generations of smart biocompatible materials. *Journal of Polymer Science Part A: Polymer Chemistry* **2008**, *46* (11), 3459-3470.
26. Pissuwan, D.; Boyer, C.; Gunasekaran, K.; Davis, T. P.; Bulmus, V., In vitro cytotoxicity of RAFT polymers. *Biomacromolecules* **2010**, *11* (2), 412-420.
27. Azeri, Ö.; Schönfeld, D.; Noirez, L.; Gradzielski, M., Structural control in micelles of alkyl acrylate-acrylate copolymers via alkyl chain length and block length. *Colloid and Polymer Science* **2020**, *298*, 829-840.
28. Li, F.; Danquah, M.; Mahato, R. I., Synthesis and characterization of amphiphilic lipopolymers for micellar drug delivery. *Biomacromolecules* **2010**, *11* (10), 2610-2620.
29. Tacar, O.; Sriamornsak, P.; Dass, C. R., Doxorubicin: an update on anticancer molecular action, toxicity and novel drug delivery systems. *Journal of Pharmacy and Pharmacology* **2013**, *65* (2), 157-170.
30. Gupta, J.; Keddie, D. J.; Wan, C.; Haddleton, D. M.; McNally, T., Functionalisation of MWCNTs with poly (lauryl acrylate) polymerised by Cu (0)-mediated and RAFT methods. *Polymer Chemistry* **2016**, *7* (23), 3884-3896.
31. Griffin, W. C., Classification of surface-active agents by "HLB". *Journal of the Society of Cosmetic Chemists* **1949**, *1*, 311-326.
32. Jaacks, V., A novel method of determination of reactivity ratios in binary and ternary copolymerizations. *Die Makromolekulare Chemie: Macromolecular Chemistry and Physics* **1972**, *161* (1), 161-172.
33. Mai, Y.; Eisenberg, A., Self-assembly of block copolymers. *Chemical Society Reviews* **2012**, *41* (18), 5969-5985.
34. Zhou, J.; Yao, H.; Ma, J., Recent advances in RAFT-mediated surfactant-free emulsion polymerization. *Polymer Chemistry* **2018**, *9* (19), 2532-2561.
35. Vittaz, M.; Bazile, D.; Spenlehauer, G.; Verrecchia, T.; Veillard, M.; Puisieux, F.; Labarre, D., Effect of PEO surface density on long-circulating PLA-PEO nanoparticles which are very low complement activators. *Biomaterials* **1996**, *17* (16), 1575-1581.

36. O'Leary, K.; Paul, D., Copolymers of poly (n-alkyl acrylates): synthesis, characterization, and monomer reactivity ratios. *Polymer* **2004**, *45* (19), 6575-6585.
37. Philipps, K.; Junkers, T.; Michels, J. J., The block copolymer shuffle in size exclusion chromatography: the intrinsic problem with using elugrams to determine chain extension success. *Polymer Chemistry* **2021**, *12* (17), 2522-2531.
38. Guzik, A.; Raffa, P., Direct synthesis via RAFT of amphiphilic diblock polyelectrolytes facilitated by the use of a polymerizable ionic liquid as a monomer. *Polymer Chemistry* **2021**, *12* (38), 5505-5517.
39. Raffa, P.; Broekhuis, A. A.; Picchioni, F., Amphiphilic copolymers based on PEG-acrylate as surface active water viscosifiers: Towards new potential systems for enhanced oil recovery. *Journal of Applied Polymer Science* **2016**, *133* (42).
40. Raffa, P.; Wever, D. A. Z.; Picchioni, F.; Broekhuis, A. A., Polymeric surfactants: synthesis, properties, and links to applications. *Chemical Reviews* **2015**, *115* (16), 8504-8563.
41. Lee, J.-H.; Jung, S.-W.; Kim, I.-S.; Jeong, Y.-I.; Kim, Y.-H.; Kim, S.-H., Polymeric nanoparticle composed of fatty acids and poly (ethylene glycol) as a drug carrier. *International Journal of Pharmaceutics* **2003**, *251* (1-2), 23-32.
42. Peng, D.; Zhang, X.; Feng, C.; Lu, G.; Zhang, S.; Huang, X., Synthesis and characterization of amphiphilic graft copolymers with hydrophilic poly (acrylic acid) backbone and hydrophobic poly (methyl methacrylate) side chains. *Polymer* **2007**, *48* (18), 5250-5258.
43. Cabral, H.; Kataoka, K., Progress of drug-loaded polymeric micelles into clinical studies. *Journal of Controlled Release* **2014**, *190*, 465-476.
44. Cabral, H.; Matsumoto, Y.; Mizuno, K.; Chen, Q.; Murakami, M.; Kimura, M.; Terada, Y.; Kano, M.; Miyazono, K.; Uesaka, M., Accumulation of sub-100 nm polymeric micelles in poorly permeable tumours depends on size. *Nature Nanotechnology* **2011**, *6* (12), 815-823.
45. Tang, L.; Yang, X.; Yin, Q.; Cai, K.; Wang, H.; Chaudhury, I.; Yao, C.; Zhou, Q.; Kwon, M.; Hartman, J. A., Investigating the optimal size of anticancer nanomedicine. *Proceedings of the National Academy of Sciences* **2014**, *111* (43), 15344-15349.
46. Chroni, A.; Mavromoustakos, T.; Pispas, S., Nano-Assemblies from Amphiphilic PnBA-b-POEGA Copolymers as Drug Nanocarriers. *Polymers* **2021**, *13* (7), 1164.
47. Piogé, S.; Fontaine, L.; Gaillard, C. d.; Nicol, E.; Pascual, S., Self-assembling properties of well-defined poly (ethylene oxide)-b-poly (ethyl acrylate) diblock copolymers. *Macromolecules* **2009**, *42* (12), 4262-4272.
48. Garnier, S.; Laschewsky, A., Non-ionic amphiphilic block copolymers by RAFT-polymerization and their self-organization. *Colloid and Polymer Science* **2006**, *284* (11), 1243-1254.
49. Jordan Jr, E. F.; Artymyshyn, B.; Specca, A.; Wrigley, A., Side-chain crystallinity. II. Heats of fusion and melting transitions on selected copolymers incorporating n-octadecyl acrylate or vinyl stearate. *Journal of Polymer Science Part A-1: Polymer Chemistry* **1971**, *9* (11), 3349-3365.
50. Zhang, L.; Eisenberg, A., Multiple morphologies of "crew-cut" aggregates of polystyrene-b-poly (acrylic acid) block copolymers. *Science* **1995**, *268* (5218), 1728-1731.
51. d'Agosto, F.; Rieger, J.; Lansalot, M., RAFT-Mediated Polymerization-Induced Self-Assembly. *Angewandte Chemie International Edition* **2020**, *59* (22), 8368-8392.
52. Karanikolopoulos, N.; Choinopoulos, I.; Pitsikalis, M., Poly {dl-lactide-b-[oligo (ethylene glycol) methyl ether (meth) acrylate]} block copolymers. Synthesis, characterization, micellization behavior in aqueous solutions and encapsulation of model hydrophobic compounds. *Journal of Polymer Science* **2020**, *58* (11), 1582-1600.
53. Kurniasih, I. N.; Liang, H.; Mohr, P. C.; Khot, G.; Rabe, J. r. P.; Mohr, A., Nile red dye in aqueous surfactant and micellar solution. *Langmuir* **2015**, *31* (9), 2639-2648.

54. Trappmann, B.; Ludwig, K.; Radowski, M. R.; Shukla, A.; Mohr, A.; Rehage, H.; Böttcher, C.; Haag, R., A new family of nonionic dendritic amphiphiles displaying unexpected packing parameters in micellar assemblies. *Journal of the American Chemical Society* **2010**, *132* (32), 11119-11124.
55. Arshad, M.; Pradhan, R. A.; Ullah, A., Synthesis of lipid-based amphiphilic block copolymer and its evaluation as nano drug carrier. *Materials Science and Engineering: C* **2017**, *76*, 217-223.
56. Sarkar, P.; Ghosh, S.; Saha, R.; Sarkar, K., RAFT polymerization mediated core-shell supramolecular assembly of PEGMA-co-stearic acid block co-polymer for efficient anticancer drug delivery. *RSC Advances* **2021**, *11* (28), 16913-16923.
57. Laskar, P.; Saha, B.; Ghosh, S. K.; Dey, J., PEG based random copolymer micelles as drug carriers: the effect of hydrophobe content on drug solubilization and cytotoxicity. *RSC Advances* **2015**, *5* (21), 16265-16276.
58. Sant, V. P.; Smith, D.; Leroux, J.-C., Enhancement of oral bioavailability of poorly water-soluble drugs by poly (ethylene glycol)-block-poly (alkyl acrylate-co-methacrylic acid) self-assemblies. *Journal of Controlled Release* **2005**, *104* (2), 289-300.
59. Cheng, J.; Teply, B. A.; Sherifi, I.; Sung, J.; Luther, G.; Gu, F. X.; Levy-Nissenbaum, E.; Radovic-Moreno, A. F.; Langer, R.; Farokhzad, O. C., Formulation of functionalized PLGA-PEG nanoparticles for in vivo targeted drug delivery. *Biomaterials* **2007**, *28* (5), 869-876.
60. Astete, C. E.; Sabliov, C. M., Synthesis and characterization of PLGA nanoparticles. *Journal of Biomaterials Science, Polymer Edition* **2006**, *17* (3), 247-289.
61. Konan, Y. N.; Cerny, R.; Favet, J.; Berton, M.; Gurny, R.; Allémann, E., Preparation and characterization of sterile sub-200 nm meso-tetra (4-hydroxyphenyl) porphyrin-loaded nanoparticles for photodynamic therapy. *European Journal of Pharmaceutics and Biopharmaceutics* **2003**, *55* (1), 115-124.
62. Parkatzidis, K.; Truong, N. P.; Rolland, M.; Lutz-Bueno, V.; Pilkington, E. H.; Mezzenga, R.; Anastasaki, A., Transformer-Induced Metamorphosis of Polymeric Nanoparticle Shape at Room Temperature. *Angewandte Chemie International Edition* **2022**, *61* (8), e202113424.
63. Talelli, M.; Iman, M.; Varkouhi, A. K.; Rijcken, C. J.; Schiffelers, R. M.; Etrych, T.; Ulbrich, K.; van Nostrum, C. F.; Lammers, T.; Storm, G., Core-crosslinked polymeric micelles with controlled release of covalently entrapped doxorubicin. *Biomaterials* **2010**, *31* (30), 7797-7804.

## Appendix B

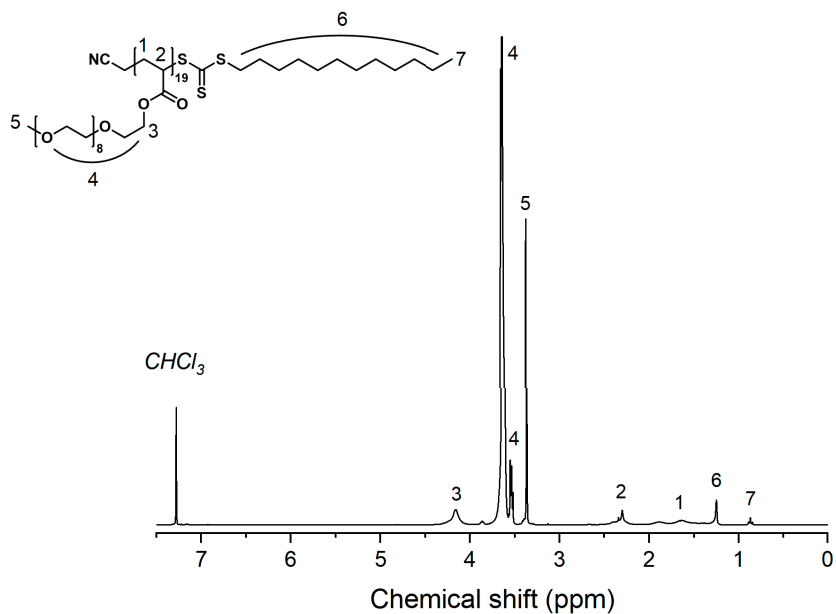
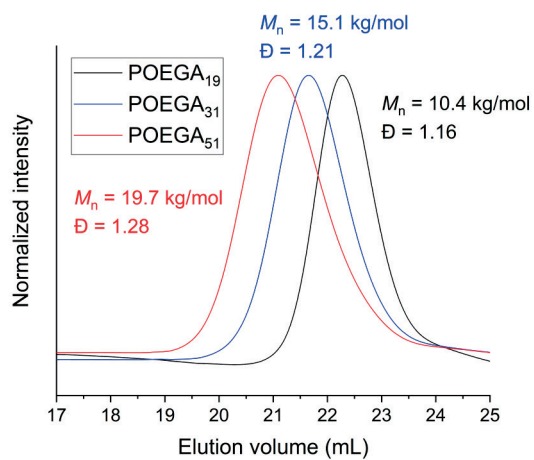
Figure B1. Assigned <sup>1</sup>H NMR spectrum of POEGA<sub>19</sub> macro-RAFT agent in CDCl<sub>3</sub>.

Figure B2. Overlay of the GPC traces of POEGA macro-RAFT agents using DMF containing 6 g/L AcOH and 0.035 mol/L LiCl as the eluent.



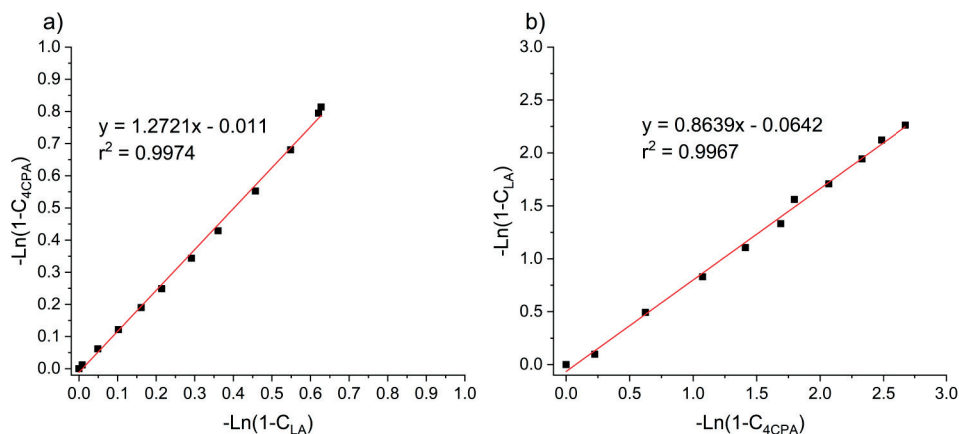


Figure B3. Jaacks plots of the copolymerization of 4CPA with LA. a) Excess 4CPA and b) excess LA.

Table B1. GPC results of the synthesized block copolymers.

Polymer	$M_{n, GPC}$ (g/mol)	$\bar{D}$
POEGA <sub>19</sub>	10.4	1.16
POEGA <sub>19</sub> -HB <sub>16</sub>	5.8	1.61
POEGA <sub>19</sub> -HB <sub>37</sub>	5.6	1.63
POEGA <sub>19</sub> -HB <sub>50</sub>	6.8	1.46
POEGA <sub>31</sub>	15.1	1.21
POEGA <sub>31</sub> -HB <sub>17</sub>	8.5	1.84
POEGA <sub>31</sub> -HB <sub>38</sub>	10.1	2.27
POEGA <sub>31</sub> -HB <sub>49</sub>	9.4	1.59
POEGA <sub>51</sub>	19.7	1.28
POEGA <sub>51</sub> -HB <sub>15</sub>	14.9	1.71
POEGA <sub>51</sub> -HB <sub>32</sub>	10.7	2.07
POEGA <sub>51</sub> -HB <sub>47</sub>	13.8	1.96

The eluent that was used was DMF containing 6 g/L AcOH and 0.035 mol/L LiCl. Molecular weights are given relative to poly(methyl methacrylate) standards.

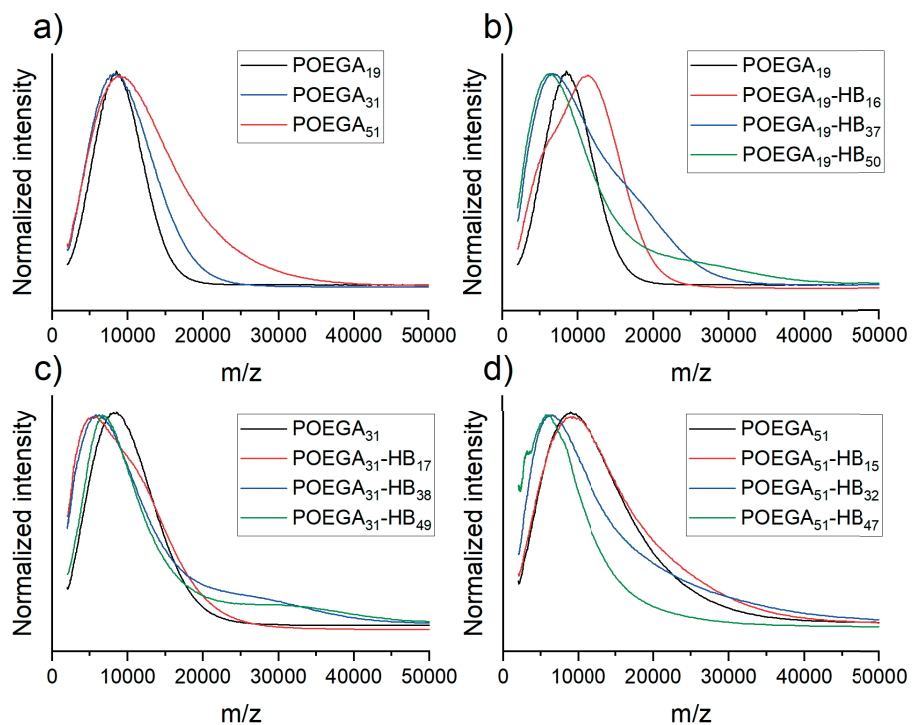


Figure B4. MALDI-ToF-MS spectra of a) POEGA macro-RAFT agents, b) POEGA<sub>19</sub> block copolymers, c) POEGA<sub>31</sub> block copolymers, and d) POEGA<sub>51</sub> block copolymers.

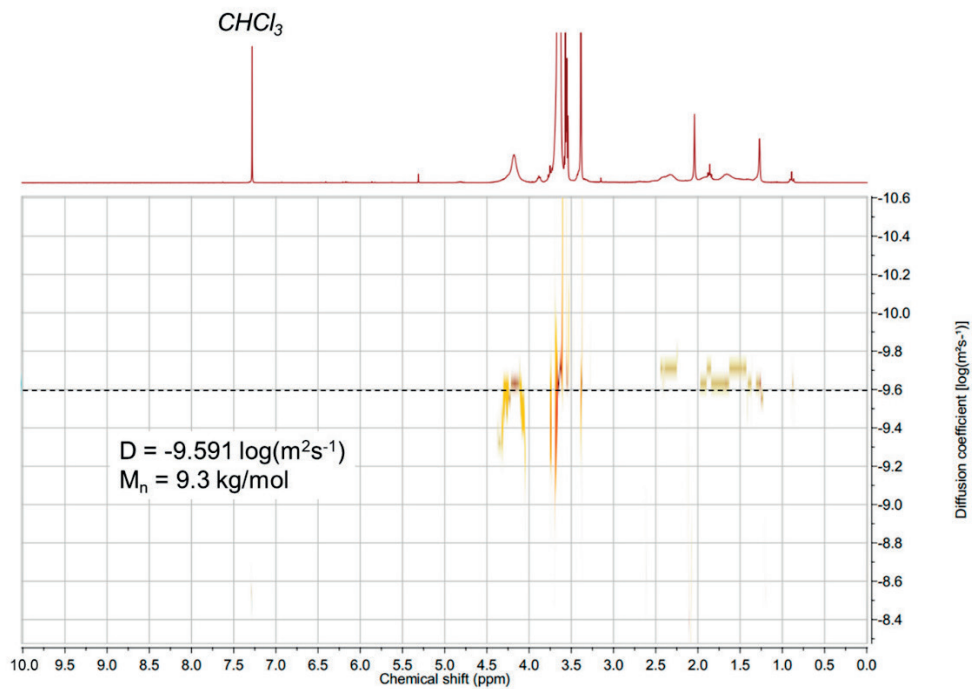
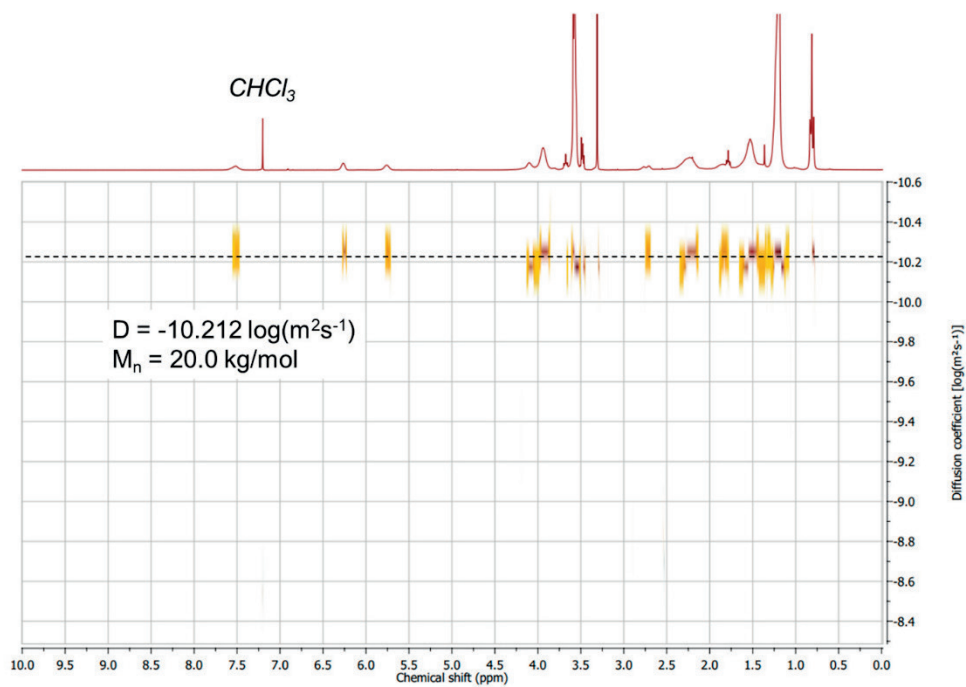


Figure B5. DOSY spectrum of POEGA<sub>19</sub>.

Figure B6. DOSY spectrum of POEGA<sub>19</sub>-HB<sub>50</sub>.

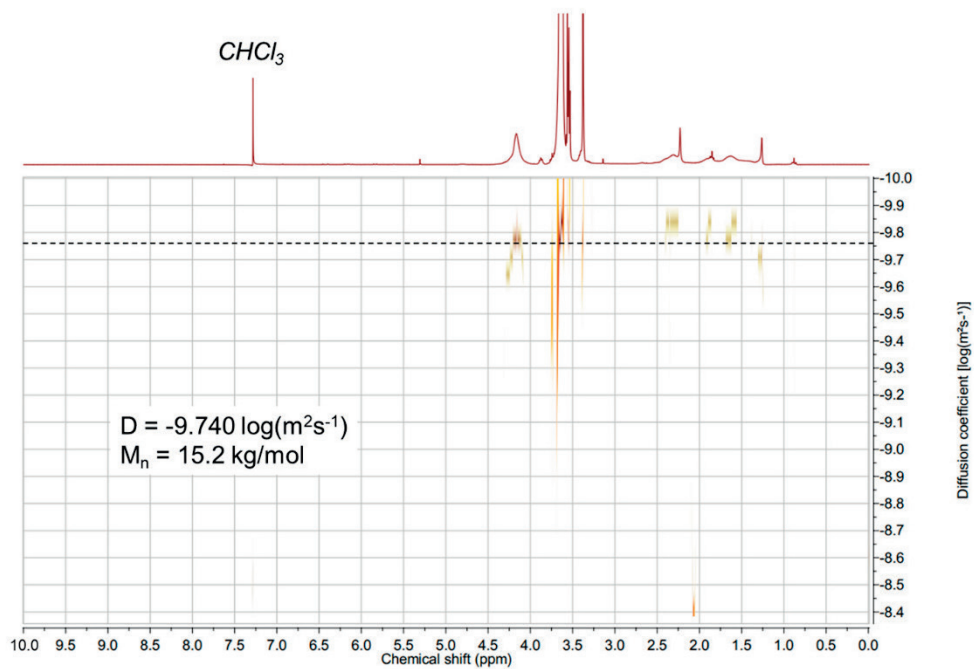


Figure B7. DOSY spectrum of POEGA<sub>31</sub>.

Table B2. Results of the surface tension measurements of POEGA macro-RAFT agents and block copolymers.

Entry	$M_{n,th}$ (kg/mol)	CAC (mM)	CAC (mg/L)
POEGA <sub>19</sub>	9.3	0.0050	47
POEGA <sub>31</sub>	15.2	0.0028	43
POEGA <sub>51</sub>	24.3	0.0017	41
POEGA <sub>19</sub> -HB <sub>16</sub>	12.8	0.0122	156
POEGA <sub>19</sub> -HB <sub>37</sub>	17.1	0.0120	205
POEGA <sub>19</sub> -HB <sub>50</sub>	20.0	0.0393	786
POEGA <sub>31</sub> -HB <sub>17</sub>	18.9	0.0085	161
POEGA <sub>31</sub> -HB <sub>38</sub>	23.3	0.0076	177
POEGA <sub>31</sub> -HB <sub>49</sub>	25.7	0.0082	211
POEGA <sub>51</sub> -HB <sub>15</sub>	27.6	0.0040	110
POEGA <sub>51</sub> -HB <sub>32</sub>	31.2	0.0036	112
POEGA <sub>51</sub> -HB <sub>47</sub>	34.5	0.0039	135

Table B3. DLS results for the prepared block-copolymers directly dissolved in water, and prepared via the solvent-switch method before dialysis (90/10 v/v% H<sub>2</sub>O/THF) and after dialysis (100% H<sub>2</sub>O).

Entry	Directly dissolved in H <sub>2</sub> O			Prepared by solvent exchange method					
	Peak 1 size (nm)	Peak 2 size (nm)	PDI	Before dialysis			After dialysis		
				Peak 1 size (nm)	Peak 2 size (nm)	PDI	Peak 1 size (nm)	Peak 2 size (nm)	PDI
POEGA <sub>19</sub> -HB <sub>16</sub>	99	-	0.368	310	-	0.215	161	-	0.274
POEGA <sub>19</sub> -HB <sub>37</sub>	29	167	0.470	45	-	0.554	27	-	0.181
POEGA <sub>19</sub> -HB <sub>50</sub>	257	-	0.396	63	-	0.193	43	-	0.250
POEGA <sub>31</sub> -HB <sub>17</sub>	104	-	0.294	219	-	0.210	88	-	0.455
POEGA <sub>31</sub> -HB <sub>38</sub>	89	378	0.745	63	-	0.258	40	192	0.341
POEGA <sub>31</sub> -HB <sub>49</sub>	67	813	0.703	47	-	0.189	36	-	0.220
POEGA <sub>51</sub> -HB <sub>15</sub>	61	-	0.226	297	-	0.236	149	-	0.278
POEGA <sub>51</sub> -HB <sub>32</sub>	69	264	0.429	42	260	0.634	29	198	0.506
POEGA <sub>51</sub> -HB <sub>47</sub>	202	-	0.375	66	600	0.309	50	286	0.355

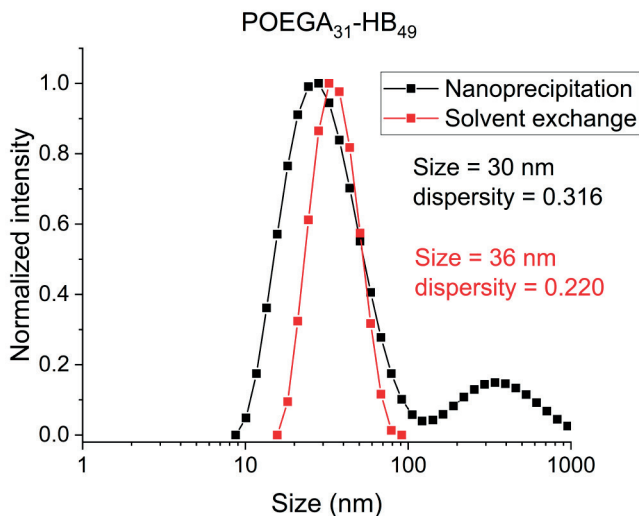


Figure B8. DLS results of POEGA<sub>31</sub>-HB<sub>49</sub> micelles obtained via solvent exchange and nanoprecipitation.

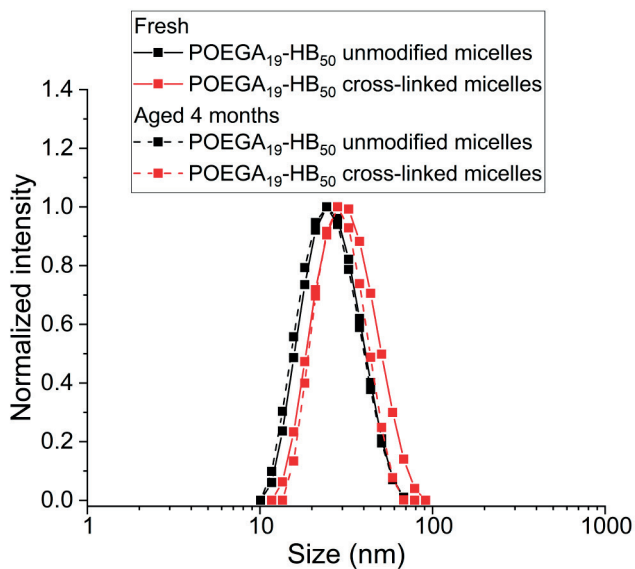


Figure B9. DLS results of unmodified micelles and cross-linked micelles obtained from block copolymer POEGA<sub>19</sub>-HB<sub>50</sub> directly after preparation and after 4 months storage.

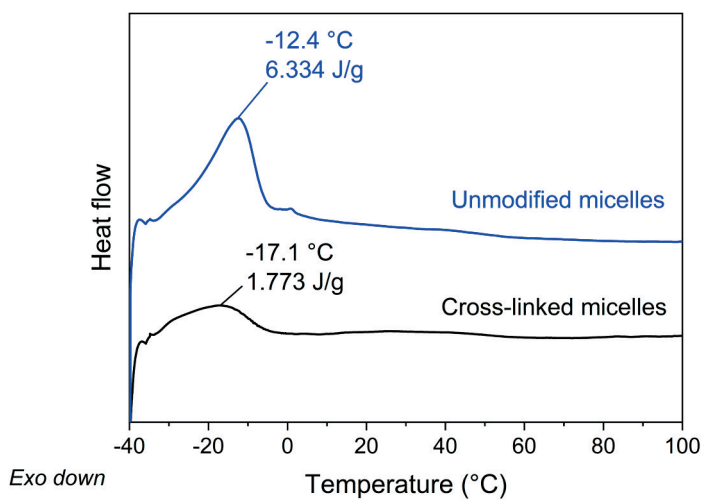


Figure B10. Overlay of the DSC traces of unmodified micelles (blue) and UV cross-linked micelles (black) of POEGA<sub>19</sub>-HB<sub>50</sub>.

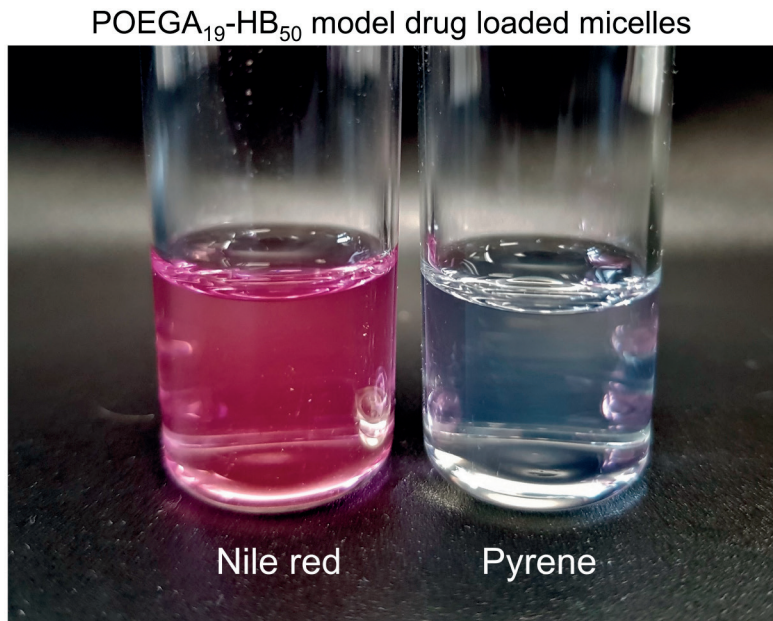


Figure B11. Photograph of Nile red and Pyrene loaded micelles from block copolymer POEGA<sub>19</sub>-HB<sub>50</sub>.



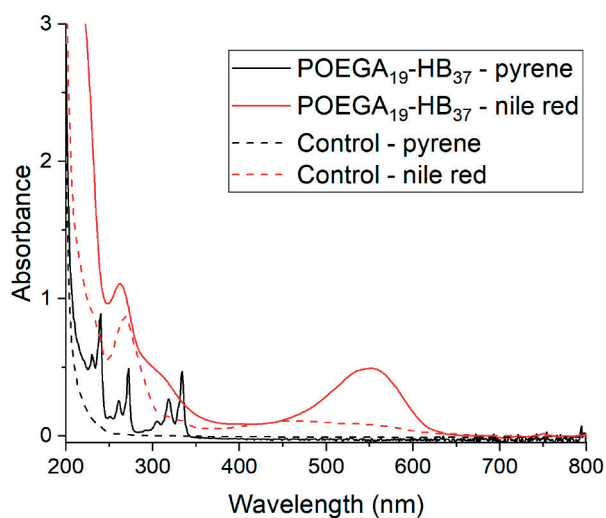


Figure B12. UV-Vis spectrum in methanol of pyrene and Nile red loaded micelles from POEGA<sub>19</sub>-HB<sub>37</sub>, and the control samples without block copolymer.

Table B4. Encapsulation efficiency for pyrene and Nile red.

Block copolymer	EE (pyrene) (%)	EE (Nile red) (%)
POEGA <sub>19</sub> -HB <sub>16</sub>	2.2	2.4
POEGA <sub>19</sub> -HB <sub>37</sub>	3.6	2.2
POEGA <sub>19</sub> -HB <sub>50</sub>	3.7	1.8
POEGA <sub>31</sub> -HB <sub>17</sub>	1.4	1.8
POEGA <sub>31</sub> -HB <sub>38</sub>	2.1	1.1
POEGA <sub>31</sub> -HB <sub>49</sub>	2.5	1.1
POEGA <sub>51</sub> -HB <sub>15</sub>	0.5	1.4
POEGA <sub>51</sub> -HB <sub>32</sub>	0.9	2.1
POEGA <sub>51</sub> -HB <sub>47</sub>	1.5	1.5

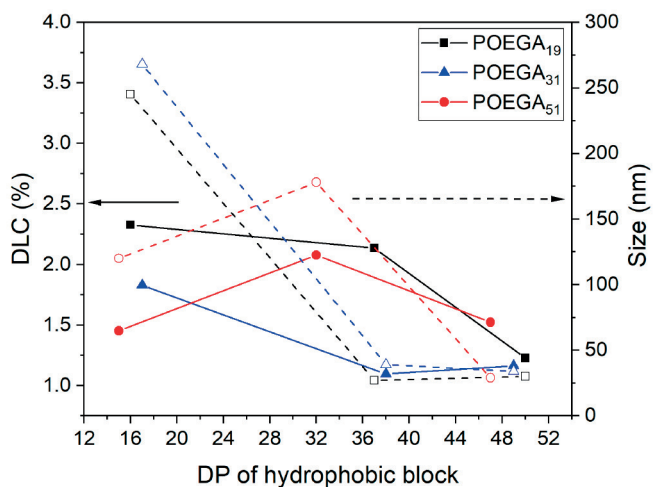


Figure B13. Investigation of the DLC and particle size in DLS of the Nile red loaded block copolymers as a function of the DP of hydrophobic block.

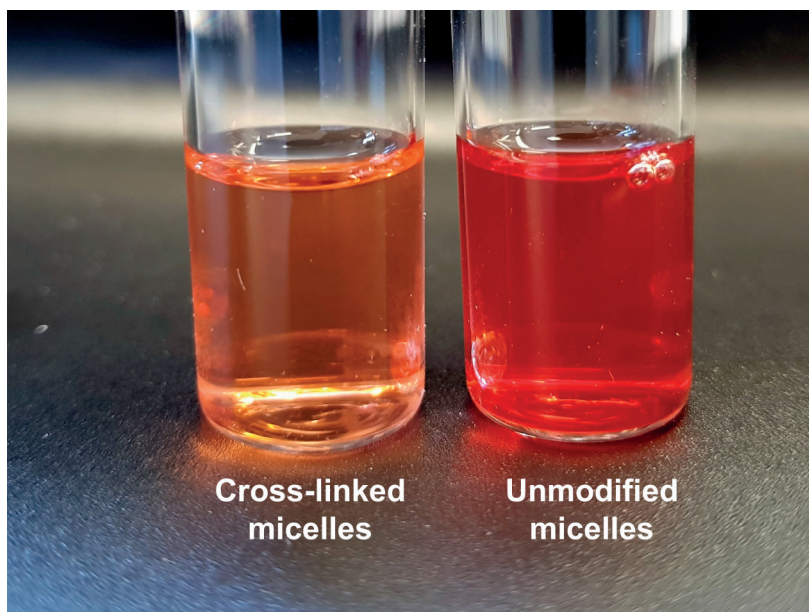


Figure B14. Photograph of the cross-linked and unmodified DOX loaded micelles from block copolymer POEGA<sub>19</sub>-HB<sub>50</sub>.

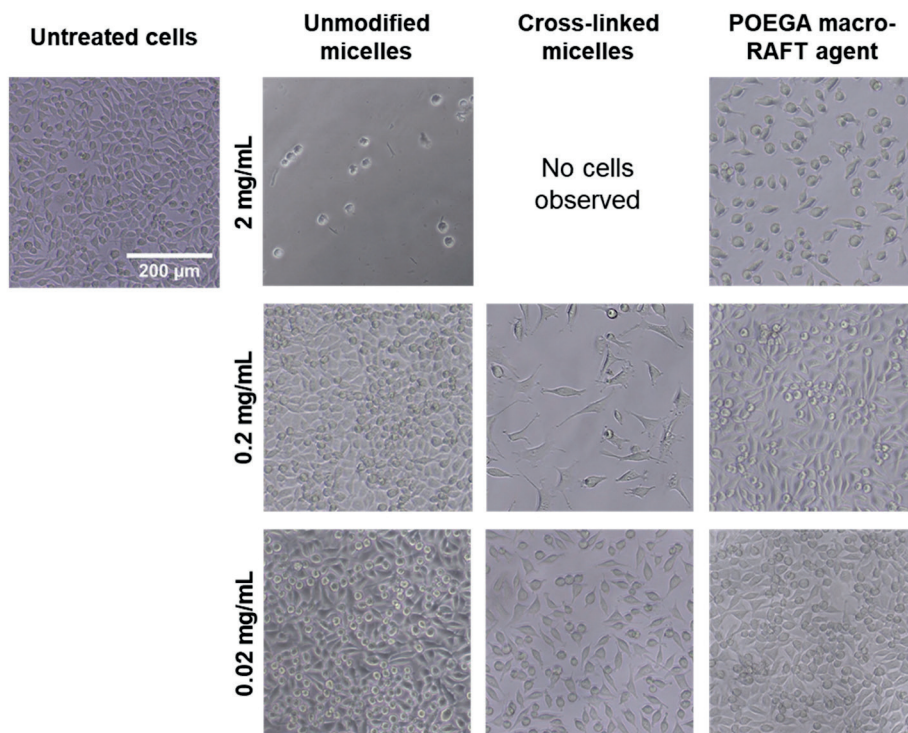


Figure B15. Microscope photographs of the L929 cell line incubated with unmodified micelles, cross-linked micelles and POEGA macro-RAFT agent at several concentrations for 72 hours. No cells observed indicates cell death.

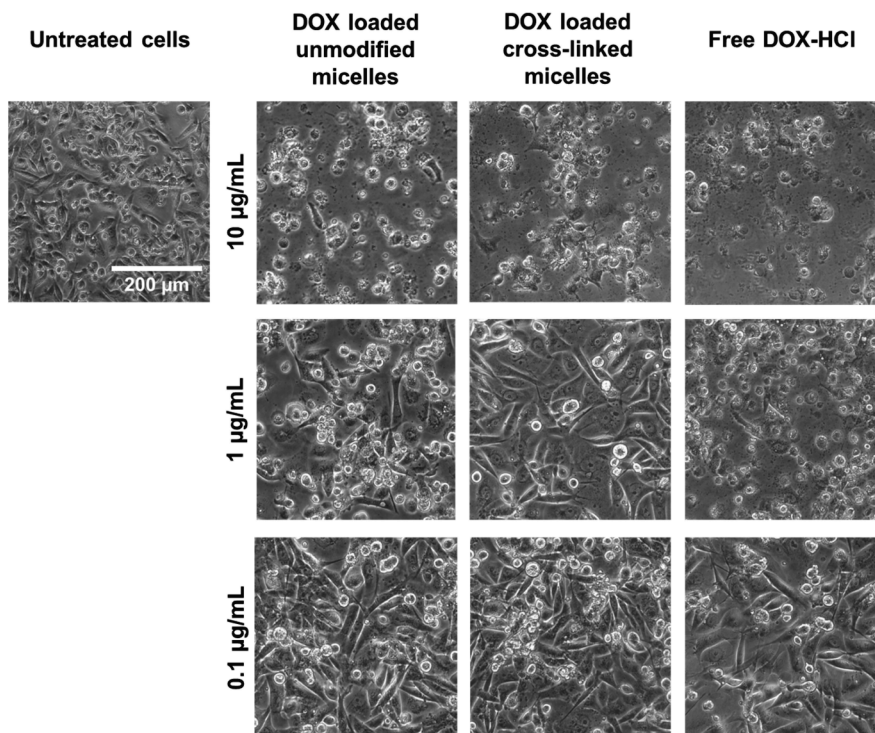
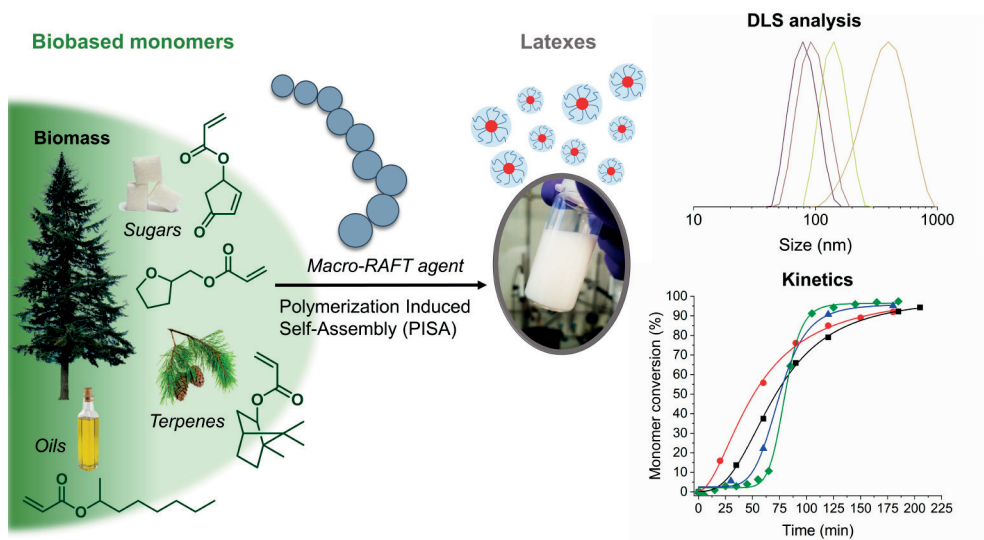


Figure B16. Microscope photographs of the MDA-MB-231 cell line incubated with DOX loaded unmodified micelles, cross-linked micelles and free DOX-HCl at several concentrations for 72 hours.



# 4



---

# Chapter 4 Development of Biobased Polyacrylate Latexes based on 4CPA Synthesized by RAFT Polymerization Induced Self-Assembly

---

## Abstract

The water-borne synthesis of biobased acrylic polymers is interesting due to the increasing strain on the use of solvents, coalescence agents, and fossil based monomers in coating products. Complete removal of coalescence agents from high  $T_g$  latex binders results in poor film formation. An alternative strategy is to implement a cross-linking step of a low  $T_g$  resin to increase the  $T_g$  after film formation, and in that way omit the requirement for a coalescence agent. Cross-linking also significantly improves certain mechanical and physical properties of the resulting films and coatings. In this work, 4-oxocyclopentenyl acrylate is being investigated as a UV curable monomer for the synthesis of biobased and cross-linkable latexes. The latexes were synthesized using a Polymerization Induced Self-Assembly approach under Reversible Addition-Fragmentation chain-Transfer control. Since the latexes are used as a product themselves, important considerations are a sufficiently high solid content (around 40 wt%), small particle size, high monomer conversion, and good colloidal stability. Stable latexes containing up to 25 mol% 4CPA in the monomer composition were produced at a solid content of 40 wt% and having a low particle size of between 98 and 138 nm. As the comonomers, the biobased tetrahydrofurfuryl acrylate, isobornyl acrylate, and 2-octyl acrylate were successfully incorporated in the final latex polymer.

## Introduction

In the past decades, water-based polymer coatings have become more and more attractive in contrast to solvent-based systems due to increasing environmental and personal safety regulations. In water-based systems, the binder (i.e. acrylate latex) is dispersed in the aqueous phase and stabilized by surfactants. Using water as the carrier, the system omits the use of organic solvents. In many cases, some amount of coalescence agent is required to achieve proper film formation and increase in  $T_g$  after drying. By combining the water-based technology with a post film formation curing step, this problem can be relieved. The cross-linking can be achieved by means of external stimuli such as heat or UV to achieve the desired increase in film properties. For example, mechanical and solvent resistance properties are improved compared to regular latex binders due to the presence of a cross-linked network.<sup>1</sup>

With the recent introduction of controlled radical polymerization in heterogeneous media<sup>2</sup>, the polymerization of monomers in a controlled fashion for the production of functional acrylate latexes is becoming more convenient. In the past years, Reversible Addition-Fragmentation chain-Transfer Polymerization Induced Self-Assembly (RAFT PISA) has emerged as a prominent technique to produce self-assembled block copolymer structures with a high solid content.<sup>3-4</sup> The use of RAFT PISA has enabled the synthesis of well-defined and functional polymeric nano-objects<sup>5</sup>, partially due to the high functional group tolerance of RAFT.<sup>6</sup> Typically, the synthesis is performed with a water-soluble macromolecule functionalized with a RAFT agent end group. This is chain extended with one or more hydrophobic monomers to form a second block, which gradually becomes insoluble and at a critical length self-assembles into particles. Therefore, RAFT PISA is an excellent strategy to produce surfactant free latexes where the hydrophilic stabilizer is covalently attached to the latex particles.

The use of RAFT PISA specifically tailored towards the production of latexes is an ongoing interest for researchers.<sup>7-11</sup> Recently, the application of RAFT PISA latexes for coating and film applications has been reported<sup>12-19</sup>, although the available literature on this topic is still limited. A common drawback of the previously developed RAFT PISA latexes is the requirement for a co-solvent during the synthesis to facilitate the self-assembly process and avoid coagulation. This is undesirable when low Volatile Organic Compound (VOC) applications are targeted. Another typical requirement for latex binders in coating applications is the high solid content. A higher solid content improves the overall efficiency in terms of space-time yield, transportation, and during formulation. The particle size is another important property and is correlated with latex stability, viscosity, and film formation.<sup>20-21</sup> Since the latex produced after synthesis is considered as a final product, no further purification techniques are to be employed to remove residual monomer or solvent. Therefore, it is important that the synthesis occurs in water as the medium while achieving (near) complete monomer conversion.

In chapter 2, we have reported the RAFT solution polymerization of a new biobased monomer 4-oxocyclohex-2-en-1-yl acrylate (4CPA) for the synthesis of polyacrylates



capable of undergoing self-cross-linking under UV light via photocyclodimerization.<sup>22</sup> This functionality of 4CPA is intended to be incorporated into water-based polymer systems resulting in latexes capable of undergoing photo-cross-linking as a post film formation curing process. Since the free radical polymerization of 4CPA resulted in densely cross-linked polymers as mentioned in chapter 2, the latexes here will be synthesized by RAFT PISA. RAFT control during emulsion polymerization is desired to limit the molecular weight and suppress side reactions that might cause extensive cross-linking of the particles. The purpose is to develop biobased latexes based on 4CPA that are suitable for film and coating applications. Since coalescence of the latex particles is required during film formation, cross-linking during polymerization should be limited and the 4CPA functionality remain intact for post-polymerization curing reactions.

In this work, we explore the use of 4CPA in latexes synthesized by the RAFT PISA method using a POEGA macro-RAFT agent (Figure 4.1). Copolymerization with butyl acrylate served to evaluate and understand the relationship between the reaction conditions and latex properties such as particle size, monomer conversion, and gel content. Then, copolymerization with biobased monomers isobornyl acrylate, 2-octyl acrylate, and tetrahydrofurfuryl acrylate was investigated. The goal is to develop a synthesis route towards 4CPA latexes with high solid content and small particle size, and understanding the effect of monomer structure and reaction conditions on the latex properties.

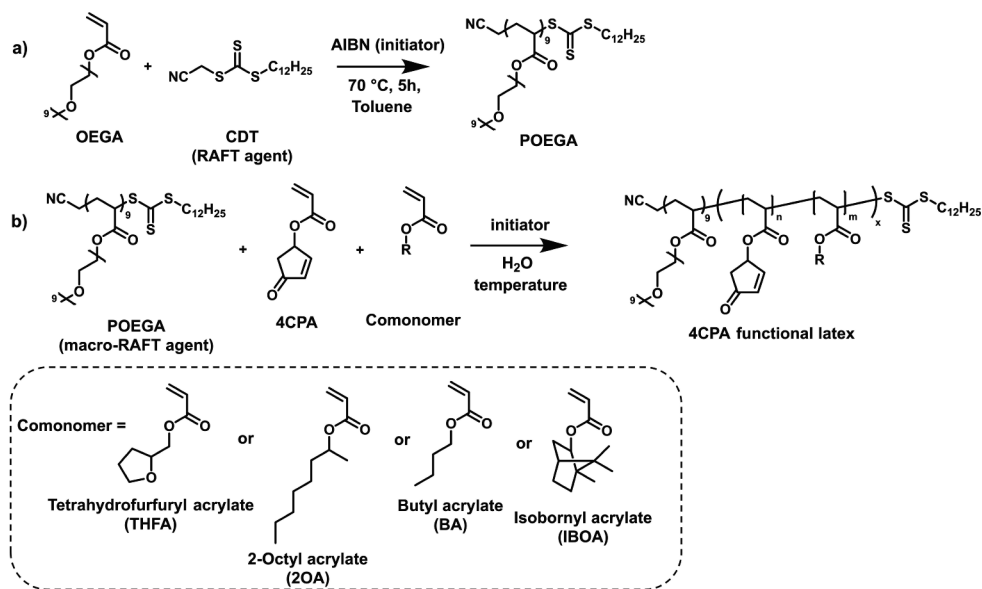


Figure 4.1. a) Reaction scheme for the synthesis of POEGA macro-RAFT agent. b) Reaction scheme for the synthesis of the biobased 4CPA based latexes via RAFT PISA.

## Experimental section

### Materials

4-Oxocyclopent-2-en-1-yl acrylate (4CPA) was synthesized according to a procedure described in chapter 2.<sup>22</sup> Cyanomethyl dodecyl trithiocarbonate (CDT) was synthesized according to a procedure described in the literature.<sup>23</sup> Azobisisobutyronitrile (AIBN) was recrystallized from methanol prior to use. Butyl acrylate (BA,  $\geq 99\%$ , Sigma-Aldrich), isobornyl acrylate (IBOA, technical, Sigma-Aldrich), tetrahydrofurfuryl acrylate (THFA, 98%, abcr), and 2-octyl acrylate (2-OA,  $>98\%$ , abcr) were passed over a basic alumina column and stored in the freezer. Trioxane ( $\geq 99\%$ , Sigma-Aldrich), 4,4'-azobis(4-cyanovaleric acid) (ACVA), 2,2'-Azobis[2-(2-imidazolin-2-yl)propane]dihydrochloride (VA-044,  $>98.0\%$ , TCI), oligo(ethylene glycol) methyl ether acrylate (OEGA, average  $M_n$  of 480 g/mol, Sigma-Aldrich), naphthalene ( $>99\%$ , Alfa-Aesar),  $\text{CDCl}_3$  (99.8%, Cambridge Isotope Laboratories), and sodium bicarbonate ( $\text{NaHCO}_3$ ) were used as received. All solvents were obtained from Biosolve and were used as received.

### Instrumentation

#### *Gel permeation chromatography (GPC)*

GPC was performed at 30 °C using a Waters GPC equipped with a Waters 2414 refractive index detector. THF was used as the eluent at a flow rate of 1 mL/min. Three linear columns were used (Styragel HR1, Styragel HR4 and Styragel HR5) including a Styragel Guard column. Molecular masses are given relative to polystyrene standards. Samples were prepared by dissolving the dried polymer in THF with a concentration of 3 mg/mL and subsequently filtered over a 0.2  $\mu\text{m}$  PTFE syringe filter.

#### *Nuclear magnetic resonance (NMR) spectroscopy*

$^1\text{H}$  NMR (300 MHz) spectra were recorded on a Bruker Avance III HD Nanobay 300 MHz apparatus at 298K in  $\text{CDCl}_3$ . For  $^1\text{H}$  NMR measurements 16 scans were used.  $^1\text{H}$  NMR samples were prepared by drying the latex in a vacuum oven overnight at 50 °C followed by dissolution in  $\text{CDCl}_3$ . Some latex samples were partially soluble in  $\text{CDCl}_3$  as a result of branching or cross-linking. Any remaining solids were filtered prior to the NMR measurement.

#### *Gas chromatography with flame ionization detector (GC-FID)*

GC-FID measurements were performed on a Shimadzu GC-2010 equipped with a Supelco SPB-1 capillary column (30 m  $\times$  0.25 mm  $\times$  0.25  $\mu\text{m}$  film thickness). GC-FID was used to follow the disappearance of the individual monomers in the (co)polymerizations relative to naphthalene as internal standard. The temperature program was as follows: an initial temperature of 80 °C was maintained for 3 min, and then increased to 140 °C with a heating rate of 10 °C/min. This temperature was maintained for 1 min, and further increased to 300 °C with a heating rate of 20 °C/min and was maintained at 300 °C for 5 min (a total run time

of 23 min). Prior to measurement, samples from both solvent and emulsion polymerization were diluted in THF. Several drops of the reaction mixture were dissolved in 1.5 mL THF. If some undissolved residues remained due to (partial) cross-linking of the latex particles, the mixture was filtered over a 0.2  $\mu\text{m}$  PTFE syringe filter.

#### *Dynamic light scattering (DLS)*

The particle size distribution of the latexes was determined using DLS. The aqueous emulsions were diluted with distilled water until they became slightly turbid. The samples were measured on a Malvern Instruments Zetasizer Nano ZS DLS instrument at 25 °C and at a fixed angle of 173°.

#### *Gel content*

Gel content measurements were performed by accurately weighing a paper filter ( $W_1$ ) and applying a few drops of latex, which was allowed to dry overnight to the air at room temperature ( $W_2$ ). The filter was then extracted in a Soxhlet setup using THF for 24 hours, and dried overnight ( $W_3$ ). The gel content was calculated as follows:

$$\text{Gel content} = \frac{(W_3 - W_1)}{(W_2 - W_1)} \times 100\%$$

#### **Determination of the reactivity ratios**

The reactivity ratios of 4CPA with IBOA, THFA, and 2OA were determined via the Jaacks method.<sup>24</sup> To determine the reactivity ratios of one monomer pair, two polymerization reactions were executed with one monomer in large excess relative to the other in each of the reactions. In an exemplary reaction, a 25 mL Schlenk flask equipped with magnetic stirrer was charged with 4CPA (500 mg, 3.29 mmol, 500 eq.), 2OA (30 mg, 0.16 mmol, 25 eq.), AIBN (1 mg, 6.56  $\mu\text{mol}$ , 1 eq.), CDT (21 mg, 0.07 mmol, 10 eq.), dimethyl formamide (0.84 mL), and naphthalene (25 mg, as internal standard). The mixture was homogenized and degassed by sparging with nitrogen for 30 min. The nitrogen purge was stopped and the flask was sealed with a nitrogen-filled balloon. An aliquot for GC-FID analysis was taken and the flask was immersed into a 70 °C oil bath. Over the course of the polymerization, several aliquots were taken for GC-FID analysis to determine the monomer conversion. The reactivity ratios were extracted from the resulting Jaacks plot.

#### **Synthesis of Poly(oligo(ethylene glycol) methyl ether acrylate) (POEGA<sub>9</sub>) macro-RAFT agent**

The POEGA macro-RAFT agent was synthesized with a target degree of polymerization (DP) of 10 (target  $M_n = 5117$  g/mol). The synthesis was as follows; Oligo(ethylene glycol) acrylate (average  $M_n = 480$  g/mol) (17.82 g, 37.13 mmol, 150 eq.), AIBN (40.7 mg, 0.25 mmol, 1 eq.), and CDT (1.18 g, 3.71 mmol, 15 eq.) were added to a 250 mL Schlenk flask equipped with magnetic stirrer. Toluene (82 mL, 20 wt% monomer concentration) and trioxane (200 mg, as internal <sup>1</sup>H NMR standard) were added and the mixture was degassed by sparging with nitrogen for 45 minutes. The flask was placed in a 70 °C oil bath and the

mixture was reacted for 5 hours. Samples were taken regularly for  $^1\text{H}$  NMR to follow the monomer conversion. After the reaction was completed, the polymer was precipitated three times in hexane and dried in a 40 °C vacuum oven overnight. Final monomer conversion was 81%. Yield: 15.03 g (79.1%).  $\text{DP}_{\text{NMR}} = 9$ ,  $M_{\text{n, NMR}} = 4.6$  kg/mol, THF GPC  $M_{\text{n}} = 6.3$  kg/mol,  $\text{Đ} = 1.06$ . The  $^1\text{H}$  NMR spectrum is shown in figure C1 and is in good agreement with the expected polymer structure. The  $^1\text{H}$  NMR molecular weight was obtained by comparing the resonances belonging to the RAFT agent end group at 0.86 ppm and the POEGA polymer at 3.36 ppm. Since the  $^1\text{H}$  NMR molecular weight correlates well to the theoretical molecular weight ( $M_{\text{n, theo}} = 4.2$  kg/mol) and the molecular weight obtained from GPC, it can be concluded that a high end-group fidelity is obtained for this macro-RAFT agent.

### **Synthesis of 4CPA latexes**

4CPA latexes were synthesized by the copolymerization of 4CPA with comonomers in the presence of the POEGA macro-RAFT agent with DP of 9 (POEGA<sub>9</sub>). During the reaction, the conversion of the monomers was actively followed by GC-FID, the reaction was stopped when the monomer conversion plateaued. Two main methods were used for the synthesis of the latexes via RAFT PISA.

The first method uses ACVA as the initiator and is executed at 65 °C. In a typical synthesis (Table 4.2, entry 7) 4CPA (300 mg, 1.97 mmol, 50 eq.), BA (759 mg, 5.92 mmol, 150 eq.), POEGA<sub>9</sub> (181 mg, 0.0395 mmol, 1 eq.), and naphthalene (22 mg, as internal standard) were added to a 25 mL Schlenk flask equipped with a magnetic stir bar. In a separate vial, ACVA (11.1 mg, 0.0395 mmol, 1 eq.) and NaHCO<sub>3</sub> (11 mg) were dissolved in water (9.53 mL). While stirring, the initiator solution was added to the monomers. The total mixture was then degassed by sparging with nitrogen for 30 minutes. In some cases, the mixture was sonicated for 3 minutes using a Branson microtip sonifier probe operated at an amplitude of 30% in order to investigate the effect of an emulsification step prior to the start of the polymerization. The flask was immersed in a 65 °C oil bath while stirring at 600 rpm for 225 min. After completion of the reaction, a turbid white latex was obtained, which was stored at 4 °C.

The second method uses VA-044 as the initiator and is executed at 50 °C. In a typical synthesis (Table 4.5, entry 4) 4CPA (300 mg, 1.97 mmol, 50 eq.), butyl acrylate (405 mg, 3.16 mmol, 80 eq.), IBOA (575 mg, 2.76 mmol, 70 eq.), POEGA<sub>9</sub> (183 mg, 0.039 mmol, 1 eq.), VA-044 (6.4 mg, 0.020 mmol, 0.5 eq.), water (11.5 mL), and naphthalene (40 mg, as internal standard) were added to a 25 mL Schlenk flask equipped with a magnetic stir bar. The mixture was sparged with nitrogen for 30 minutes and the flask was immersed in a 50 °C oil bath while stirring at 600 rpm. After completion of the reaction, a turbid white latex was obtained, which was stored at 4 °C.

## Results and discussion

### RAFT PISA of butyl acrylate using ACVA at 65 °C

Firstly, RAFT PISA was executed using ACVA as the radical initiator at 65 °C, which is a common initiator in emulsion polymerization. A similar temperature was used for the solution polymerization of 4CPA in chapter 2. Before introducing 4CPA to the monomer composition, a polymerization with pure butyl acrylate (BA) was attempted. This experiment served to evaluate if the selected conditions resulted in a controlled and completed polymerization producing a stable latex. The result are summarized in Table 4.1.

Table 4.1. RAFT PISA of BA using ACVA as the initiator at 65 °C.

Entry	I:RAFT:M	Time (min)	Solids (wt%)	BA Conv. (%)	Size (nm)	PDI	$M_{n,th}^a$ (kg/mol)	$M_{n,GPC}$ (kg/mol)	$\bar{D}$
1	1:1:100	80	10	95	110	0.043	16.8	22.1	1.40

<sup>a</sup> Calculated as follows: target  $DP_{BA} \times conversion_{BA} \times 128.17 + 4600$ .

The polymerization with BA proceeded rapid and resulted in a monomer conversion of 95% after 80 minutes. In Figure 4.2a, the BA conversion is plotted as a function of time. The monomer conversion can be facily followed using GC-FID revealing the extent of polymerization. The characteristic S-shaped curve is formed by an initial lag phase, which is followed by a rapid increase in the monomer conversion. This transition marks the formation of self-assembled particles in which polymerization continues through the fast transport of monomer to the particles. It is at this point that also a strong visual change of the reaction mixture takes place, from semi-transparent to completely turbid and milky white with a blue haze. The same phenomenon is observed in the first order conversion plot (Figure 4.2a), which is separated in two linear phases. The first phase marks a slow solution polymerization, while the second phase shows rapid acceleration of the reaction.

Judging from the graph in Figure 4.2b, it is evident that the molecular weight increases linearly with the monomer conversion indicating controlled polymerization conditions. The dispersity initially increases rapidly due to the formation of a bimodal distribution (Figure 4.2c), but then decreases slightly to a final value of 1.40. Figure 4.2c confirms chain extension of the macro-RAFT agent by decrease in intensity of the macro-RAFT agent peak relative to a main distribution, which is shifting to lower elution times with increasing reaction time.

The particle size of the final latex was determined with DLS. The latex consisted of small particles of 110 nm with a narrow particle size distribution. In general, the results indicate that RAFT PISA with a POEGA macro-RAFT agent under the selected reaction conditions is a suitable method for producing low solid content latexes.

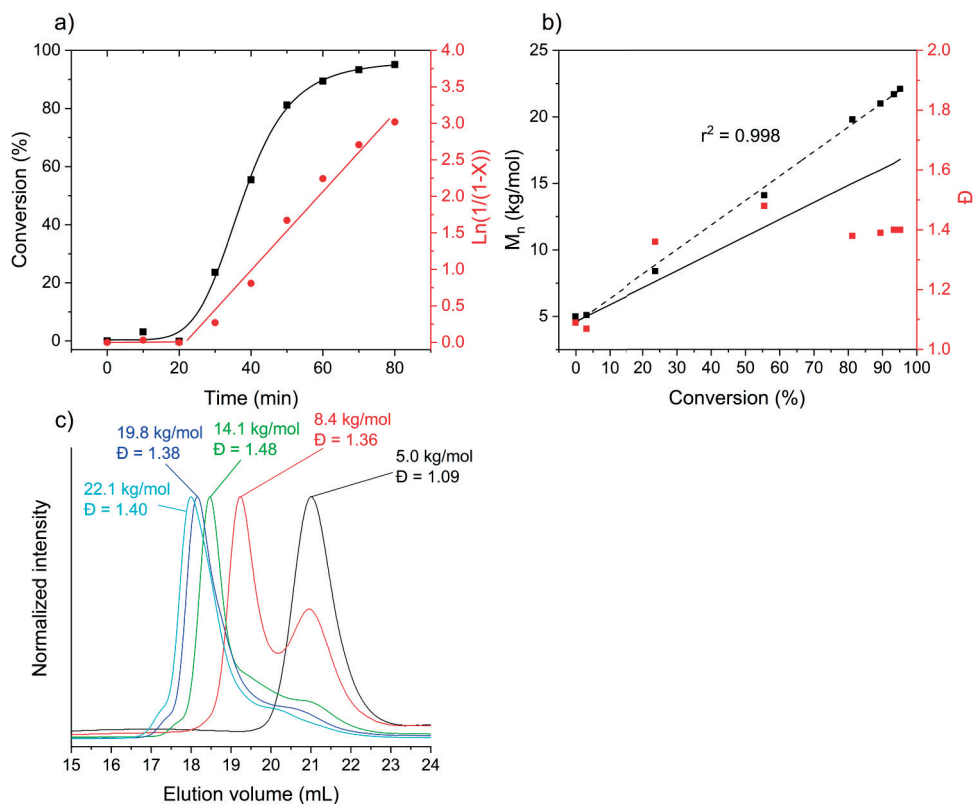


Figure 4.2. a) BA conversion and first order kinetics as a function of time. b)  $M_n$  and dispersity as a function of BA conversion measured by GPC. The solid line indicates the theoretical molecular weight evolution; the dashed line indicates the linear fit of the molecular weight evolution. c) Overlay of the GPC traces after several time intervals over the course of the polymerization.

### Screening of 4CPA and butyl acrylate copolymerization

The next step was the introduction of 4CPA in the monomer feed. The reaction parameters that were changed were the monomer feed composition, I:RAFT:M ratio, addition of surfactant, and solid content. The results are summarized in Table 4.2.

Table 4.2. Results of the RAFT PISA of 4CPA and BA.

Entry	Molar ratio I:RAFT:M	Molar feed ratio 4CPA : BA	Time <sup>c</sup> (min)	Solids <sup>d</sup> (wt%)	Conversion		M <sub>n, th</sub> <sup>e</sup> (kg/mol)	Size (nm)	PDI	Gel (%)
					4CPA (%)	BA (%)				
1	0.5:1:100	0.5 : 0.5	1260	8	28	56	10.3	N/A	N/A	N/A
2	1:1:100	0.5 : 0.5	1260	8	96	99	18.2	957	0.520	N/A
3	1:1:100	0.25 : 0.75	1260	8	90	98	17.4	124	0.010	72
4	1:1:100	0.25 : 0.75	210	10	89	96	17.2	132	0.164	48
5	1:1:100	0.1 : 0.9	240	10	88	95	16.9	102	0.037	28
6	1:1:200	0.25 : 0.75	280	5	70	95	28.2	203	0.061	83
7	1:1:200	0.25 : 0.75	225	10	88	97	29.9	237	0.210	82
8	1:1:200	0.25 : 0.75	255	20	92	95	29.8	534	0.685	– <sup>b</sup>
9	1:1:300	0.25 : 0.75	255	10	49	62	28.0	598	0.456	– <sup>b</sup>
10 <sup>a</sup>	1:1:200	0.25 : 0.75	225	10	91	98	30.3	234	0.250	59
11 <sup>a, f</sup>	1:1:200	0.25 : 0.75	300	10	87	96	29.6	201	0.050	53
12 <sup>a, g</sup>	1:1:200	0.25 : 0.75	216	10	85	98	29.9	188	0.094	48
13 <sup>g</sup>	1:1:200	0.25 : 0.75	285	10	77	93	28.3	168	0.031	46
14 <sup>g</sup>	1:1:200	0.25 : 0.75	220	20	85	87	27.8	N/A	N/A	– <sup>b</sup>

<sup>a</sup> Prior to heating to 65 °C, the mixture was sonicated for 3 min at 30% amplitude using a microtip sonifier probe. <sup>b</sup> Unstable emulsion. <sup>c</sup> Time until the monomer conversion plateaued according to GC. <sup>d</sup> The theoretical value of the solid content is reported and is considered as the weight fraction of monomers in water. <sup>e</sup> The theoretical molecular weight was calculated as follows: target DP<sub>BA</sub> × conversion<sub>BA</sub> × 128.17 + target DP<sub>4CPA</sub> × conversion<sub>4CPA</sub> × 152 + 4600. <sup>f</sup> 0.17 wt% Tween-80 was added at the start of the polymerization. <sup>g</sup> 0.51 wt% Tween-80 was added at the start of the polymerization.

The introduction of 4CPA to the copolymerization with BA to produce functional latexes is not straightforward. In contrast to the RAFT PISA of BA, incorporation of 4CPA resulted in gel formation in all latexes. Intraparticle cross-linking can occur due to participation of the cyclopentenone unit in the radical polymerization.<sup>25</sup> While some intraparticle cross-linking is not bothersome for the desired application of films and coatings, highly cross-linked particles could result in problems during the film formation step where coagulation is required to obtain a mechanically strong film. The results in Figure 4.5a suggest an increase in the gel content of the latex with increasing amount of 4CPA in the monomer feed ( $f_{4CPA}$ ) but the gel content does not exceed 83% in any of the experiments in Table 4.2. The onset of cross-linking is also observed in the GPC results (Figure 4.3). Although a linear relationship between the molecular weight and conversion is observed until about 90% monomer conversion, completion of the polymerization leads to cross-linking nonetheless, which restricts further characterization in GPC. Furthermore, the dispersity increases drastically above 80% monomer conversion indicating the onset of cross-linking.

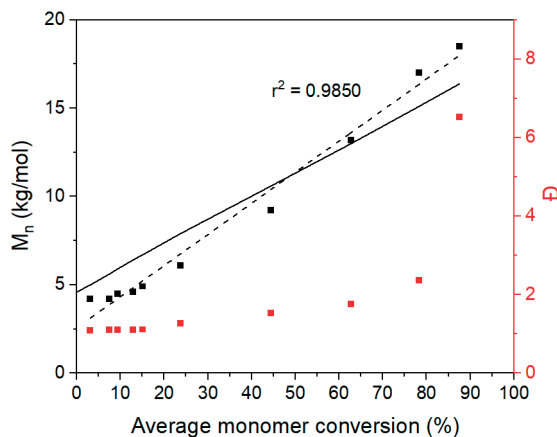


Figure 4.3. GPC results of the RAFT PISA of 4CPA and BA (Table 4.2, entry 4). The molecular weight and dispersity as a function of the monomer conversion. The solid line indicates the theoretical molecular weight evolution; the dashed line indicates the linear fit of the molecular weight evolution.

In the experiments presented in Table 4.2, entry 1 and 2, the effect of initiator concentration on the monomer conversion and particle size is investigated. With the addition of 50 mol% 4CPA in the monomer feed, a relative large amount of initiator is required to achieve full conversion. An I:RAFT:M molar ratio of 0.5:1:200 only resulted in partial monomer conversion after 1260 minutes, whereas full conversion was achieved after doubling the initiator concentration. The resulting latex was unstable and phase separation was observed within several days. The size of the final latex particles was 957 nm, which is presumably too large in the scope of obtaining stable and high solids latexes and resulting in homogenous film formation.

In an attempt to decrease the particle size and improve the colloidal stability, the amount of 4CPA in the monomer feed was lowered. It was found that decreasing the amount of 4CPA from 50 mol% to 10 or 25 mol% had a strong influence on the particle size (Table 4.2, entries 3-5), which ranged between 102 and 132 nm. A series of stable latexes were synthesized with successful incorporation of 4CPA in the polymer structure, having 25 mol% 4CPA in the monomer feed. The  $^1\text{H}$  NMR spectrum of the polymer of Table 4.2, entry 4 is shown in Figure 4.4. The spectrum corresponds well with the proposed structure. Furthermore, the resonances corresponding to the pendent cyclopentenone ring (indicated in Figure 4.4 with resonances 1, 2, 3, and 4) remained mostly intact during the polymerization. In Table 4.3, the values indicating the theoretical and experimental monomer composition from the polymer in Table 4.2, entry 4, are shown. The monomer composition obtained from the  $^1\text{H}$  NMR spectrum corresponds quite well with the theoretical ratio. A slightly lower amount (about 88%) of 4CPA units is observed in  $^1\text{H}$  NMR, indicating that some 4CPA monomers have participated in side reactions. The latex is partially cross-linked, as suggested by the gel content of 48%.



Therefore, only the soluble polymer chains are visible in the NMR spectrum, indicating again the participation of 4CPA in cross-linking reactions. Since the latexes in this chapter and chapter 5 are partially cross-linked, the  $^1\text{H}$  NMR spectrum might not reflect the true composition of the complete polymer.

Table 4.3. Values on the theoretical and experimental monomer composition and amount of intact 4CPA units of the latex from Table 4.2, entry 4.

Polymer from experiment	Theoretical monomer composition in copolymer		Experimental monomer composition in copolymer		Mol% of found 4CPA units
	4CPA	BA	4CPA	BA	
Table 4.2, entry 4	0.24	0.76	0.21	0.79	88

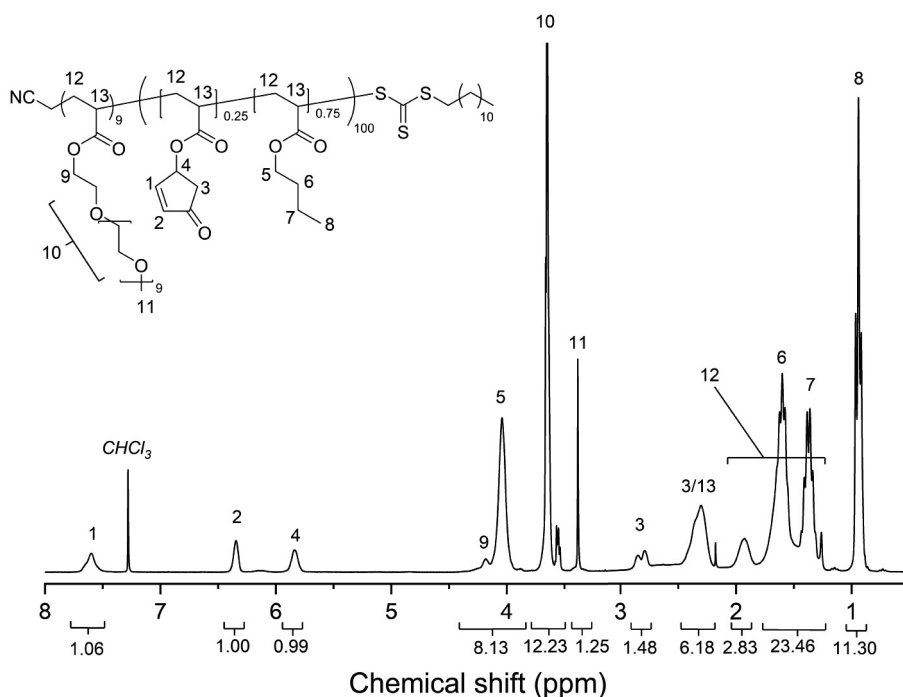


Figure 4.4.  $^1\text{H}$  NMR spectrum of the dried RAFT PISA block copolymer containing 25 mol% 4CPA (Table 4.2, entry 4) measured in  $\text{CDCl}_3$ .

The incorporation of 4CPA also had a pronounced effect on the polymerization kinetics (Figure 4.5b). In the polymerization using only BA in the monomer feed, maximum conversion was reached in 80 minutes, whereas in the reaction with 25 mol% 4CPA in the feed, this took 210 minutes. The induction phase is longer and the inflection point of the curves is shifted to longer times for polymerizations containing 4CPA. In addition, the slope of the curve in the 1<sup>st</sup> order plot, which is an indication of the reaction rate, is lower for the

copolymerization with 4CPA compared to the BA homopolymerization. For one, it is likely that 4CPA influences the conditions for self-assembly of the block copolymer chains, leading to large differences in the first induction phase of the emulsion polymerization. At the critical DP of chain extension, self-assembly into micelles is induced. This confines the growing chain ends in the cores of the particles and promotes monomer migration to solvate the insoluble hydrophobic chains.<sup>3</sup> Due to differences in solubility of the 4CPA block copolymer compared to the BA homopolymer, the critical DP at which micellization occurs could be influenced, which would explain the prolonged induction phase.

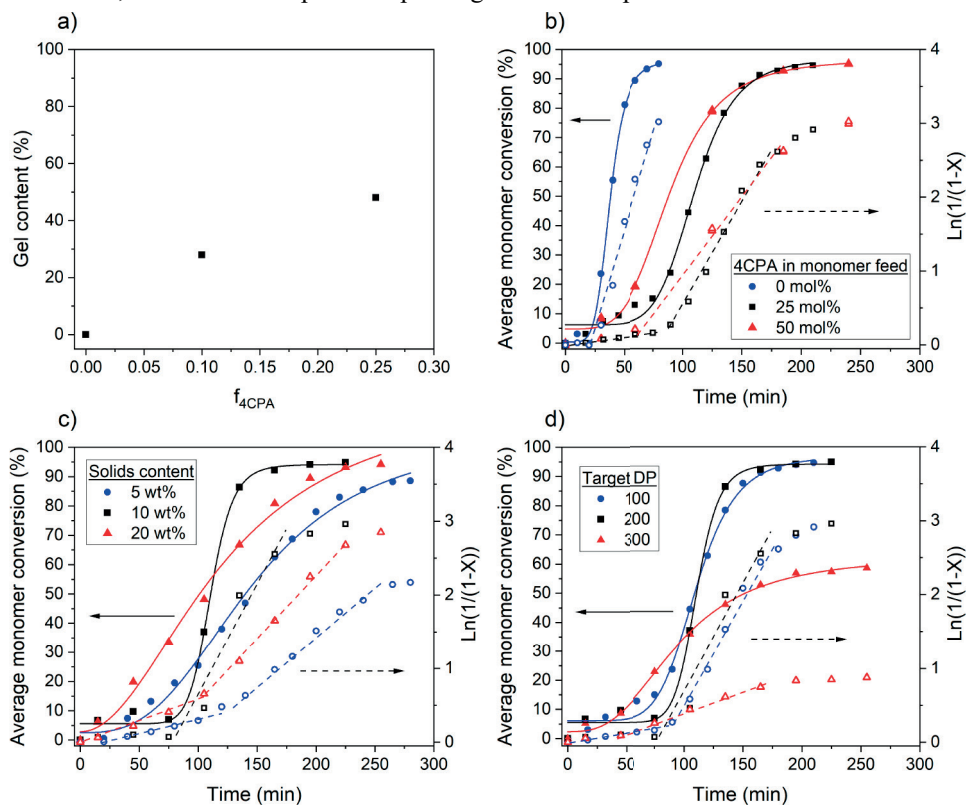


Figure 4.5. a) Gel content of the latex as a function of the fraction of 4CPA in the monomer feed (Table 4.1, entry 1 and Table 4.2, entry 4 and 5). Average monomer conversion and first order plots of the RAFT PISA of 4CPA and BA investigating the effect of b) 4CPA fraction in monomer feed, c) solid content, d) targeted DP.

A strong effect on the reaction kinetics is observed when the solid content is changed between 5 and 20 wt%. In Figure 4.5c, the conversion and 1<sup>st</sup> order plots are shown for a solid content of 5, 10 and 20 wt%. Curiously, the most pronounced S-curve is observed for a solid content of 10 wt%, while at a higher and lower solid content the curve is flattened and almost follows a linear trend. The 1<sup>st</sup> order plots show the same trend where the highest reaction rate was observed for the polymerization carried out at 10 wt% solids. Possibly, dilute conditions

promote the formation of well-defined and separated micellar particles, while operating at higher solids could produce a more continuous phase resulting in a kinetic behavior similar to a solution polymerization. Under the selected conditions, all attempts to improve the solid content to 20 wt% or higher resulted in either larger particle sizes or unstable latexes.

While working at a low solid content of 10 wt%, the targeted DP was varied between 100 and 300. While a target DP of 100 and 200 did not result in a large difference in kinetics, a target DP of 300 resulted only in an overall monomer conversion of about 55% (Figure 4.5d). Also the particle size was strongly affected by the target DP, which increased from 132 to 237 and 598 nm for target DP of 100, 200, and 300, respectively (Table 4.2, entries 4, 7, and 9). To maintain a high hydrophobic-to-hydrophilic block ratio, and aim for high molecular weights as possible, a target DP of 200 was maintained for the remaining experiments.

In an effort to facilitate the particle formation process during polymerization and improve the stability and particle size of high solid latexes, the addition of a non-ionic surfactant Tween-80 at the beginning of the polymerization was evaluated (Table 4.2, entries 10-14). This was in some cases combined with a sonication step prior to polymerization to aid an initial particle formation. The addition of Tween-80 did result in a slight decrease in the particle size. In the reactions with 0, 0.17, and 0.51 wt% Tween-80 relative to solids, the final particle sizes were 234, 201, and 188 nm, respectively. A sonication step at the beginning of the polymerization does not appreciably benefit the particle size or monomer conversion. Again, attempts to increase the solid content to above 20 wt% resulted in coagulation of the heterogeneous mixture.

### Low temperature RAFT PISA of 4CPA and comonomers

In the previous section, the understanding of the role of 4CPA in RAFT PISA polymerizations was developed. However, optimizations in the solid content and particle size to industrially relevant levels were desired to obtain a suitable latex for further development. Therefore, the initiation system was changed specifically to perform the polymerization at a lower temperature. This was theorized to benefit the self-assembly process involving the POEGA macro-RAFT agent. Despite the high LCST temperature of POEGA<sub>9</sub> of 92 °C<sup>25</sup> we found that performing the RAFT PISA at 50 °C or lower in contrast to 65 °C, allowed for polymerization under higher solid content values while in the meantime small particle sizes were obtained. A screening of three different initiation systems was performed to select and optimize the most suitable one (Figure 4.6). The first system was a redox initiation using potassium persulfate (KPS) and tetramethylethylenediamine (TMEDA) at 30 °C. The second initiator system is azo initiator VA-044 at 50 °C. The third system is a Fenton initiation using Mohr's salt and hydrogen peroxide at room temperature. The results are listed in table C1.

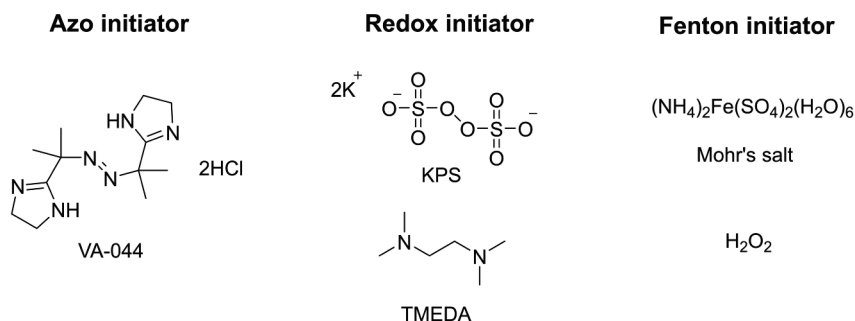


Figure 4.6 Chemical structures of the used initiators in the screening of low temperature polymerization.

All initiator systems resulted in a rapid and complete monomer conversion. The redox and azo initiators were employed in a copolymerization of 4CPA with BA and IBOA and resulted in latexes with a small particle size between 55 and 76 nm. These sizes are significantly smaller than what was generally obtained using ACVA at 65 °C as the initiator, which yielded particles between 102 and 957 nm of size. In the case of the redox initiator, a significant amount of coagulation was obtained even at 10 wt% solids. The Fenton initiator was only tested on the homopolymerization of BA, which resulted in relatively large particles and a broad size distribution. Therefore, it was not attempted on the 4CPA copolymerization. The polymerization using VA-044 at 50 °C as the initiator was selected as subject for further investigation. The added advantage is the simplicity of the one component azo initiator compared to the redox and Fenton initiators. VA-044 can simply be added together with the other reagents or in one shot, and does not require a metered addition approach. The polymerization executed at 50 °C with VA-044 (Table 4.4, entry 1) was compared to the 65 °C polymerization from Table 4.2, entry 4. At 50 °C, near complete monomer conversions are obtained after 90 minutes instead of 210 minutes, and the particle size was reduced from 132 to 78 nm.

Table 4.4. RAFT PISA at low temperature in comparison with experiment in Table 4.2, entry 4.

Entry	Molar ratio I:RAFT:M	Molar feed ratio		Time (min)	Conversion			PDI
		4CPA	BA		4CPA (%)	BA (%)	Size (nm)	
1	1:1:100	0.25	0.75	90	96	98	78	0.189

Under the selected temperature of 50 °C and using VA-044 as the initiator, several polymerizations containing BA, THFA, and IBOA in the feed served to test if controlled polymerization conditions are maintained using the POEGA macro-RAFT agent. IBOA was included in the monomer feed in order to enable manipulation of the  $T_g$  of the copolymer without altering the 4CPA feed fraction. The  $T_g$  of the final copolymer is an important consideration when coating and film applications are targeted. The results of the copolymerizations without 4CPA are listed in table C2. All reactions resulted in high

monomer conversion of >96%. The molecular weight increased linearly with the average monomer conversion indicating controlled polymerization conditions (Figure C2). The five trials resulted in polymers with a  $M_n$  of between 16.8 and 39.9 kg/mol, and a dispersity of between 1.14 and 1.81. The emulsions were stable and particle sizes of between 45 and 194 nm were obtained. Furthermore, the polymerizations could be carried out at a solid content of 30 wt%, while maintaining small particle sizes.

The next step was to introduce 4CPA to the polymerization. We continued with the same monomer feed ratios as applied in table C1, entry 2. The results are summarized in Table 4.5.

Table 4.5. Optimization of the small-scale emulsion polymerization conditions containing 4CPA, BA, and IBOA in a monomer feed ratio of 0.25:0.40:0.35.

Entry	I:RAFT:M	Time (min)	Solids <sup>a</sup> (wt%)	Conversion			Size (nm)	PDI	Gel content (%)
				4CPA (%)	BA (%)	IBOA (%)			
1	1:1:200	180	20	99	99	98	81	0.067	94
2	0.5:1:200	180	20	94	95	93	83	0.03	80
3	0.25:1:200	300	20	18	7	0	N/A	N/A	N/A
4	0.5:1:200	210	10	88	96	96	78	0.033	89
5	0.5:1:200	190	30	90	95	93	89	0.032	86
6	0.5:1:200	150	40	90	87	85	96	0.033	86

<sup>a</sup> In the calculation of the solid content is considered the amount of monomers in water.

Similar to the polymerizations executed at 65 °C and in the presence of ACVA, the polymerizations performed at 50 °C required a relative high amount of initiator in order to reach complete monomer conversion (Table 4.5). Most importantly, the solid content could be improved to 40 wt%, without drastically influencing the particle size. Although the particle size increases from 78 nm at 10 wt% to 96 nm at 40 wt% solids, the sizes observed at a polymerization temperature of 50 °C are still significantly smaller than those observed at 65 °C. Furthermore, the latexes were colloiddally stable and without coagulation.

To improve the biobased content of the polymer, tetrahydrofurfuryl acrylate (THFA) was investigated as a comonomer to replace BA, which is a conventional fossil based ‘soft monomer’ in emulsion polymerization. The results are summarized in Table 4.6.

Table 4.6. Results of the RAFT PISA reactions replacing BA with THFA using an initiator-to-RAFT agent-to-monomer ratio of 1:1:200.

Entry	THFA:4CPA: IBOA:2OA	Time (min)	Solids <sup>b</sup> (wt%)	Conversion				Size (nm)	PDI	Gel (%)
				THFA (%)	4CPA (%)	IBOA (%)	2OA (%)			
Latex0 <sup>a</sup>	75:25:0:0	240	10	82	89	-	-	399	0.421	89
Latex10	65:25:10:0	150	30	88	93	87	-	406	0.254	76
Latex25_30wt%	50:25:25:0	205	30	93	96	94	-	122	0.560	86
Latex50_30wt%	25:25:50:0	180	30	96	98	93	-	92	0.072	86
Latex25	50:25:25:0	205	40	94	97	93	-	138	0.030	87
Latex50	25:25:50:0	240	40	97	99	93	-	98	0.028	85
Latex2OA	0:25:10:65	190	40	-	99	97	98	100	0.107	93

<sup>a</sup> This experiment was also performed at 30 wt% solids but the mixture gelled. <sup>b</sup> In the calculation of the solid content is considered the amount of monomers in water.

Complete substitution of BA and IBOA with THFA resulted in a latex with large particle size of 399 nm and low solid content of 10 wt% (Latex0). With the introduction of 10 wt% of the more hydrophobic and rigid IBOA, a solid content of 30 wt% was reached while maintaining the particle size of 406 nm. The latex was named Latex10 (Figure 4.7). Further incorporation of IBOA to 25 and 50 mol% resulted in latexes with smaller particle size and higher solid content, named Latex 25 and Latex50, respectively (Table 4.6, Figure 4.7). The same latex polymers, but synthesized at a lower solid content of 30 wt% instead of 40 wt%, resulted in a slightly lower particle size (Figure 4.7). In an additional experiment and under the same conditions, THFA was replaced with 2-octyl acrylate (2OA), another promising biobased monomer for acrylate dispersions (Latex2OA, Table 4.6).

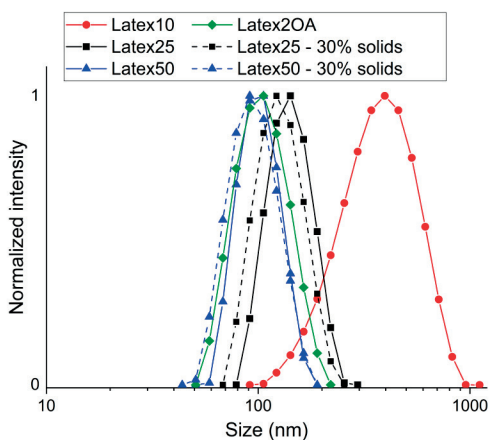


Figure 4.7. Overlay of the normalized DLS graphs of the synthesized latexes presented in Table 4.6.

In general, high monomer conversions were achieved in the polymerizations with THFA and 2OA. In Figure 4.8a, the typical s-curve of monomer conversion is observed more

pronounced in the polymerizations containing the hydrophobic monomers 2OA and IBOA, which experience a longer induction phase. The monomer conversion graph of Latex2OA in Figure 4.8b shows that the more polar 4CPA tends to polymerize in the beginning of the polymerization soon followed by a rapid increase in the monomer conversion of IBOA and 2OA.

Despite the relatively high gel content of the synthesized latexes,  $^1\text{H}$  NMR spectroscopy of the dried Latex2OA revealed the resonances belonging to all the monomers in the feed (Figure 4.8d). The resonances at 8.51, 6.29, 5.77, and 2.73 ppm suggest the presence of intact cyclopentenone double bonds, which is required for post-polymerization UV induced dimerization to obtain cross-linked films. As mentioned before, quantification of the double bonds via NMR spectroscopy is not possible due to the partial cross-linking of the latex, visualizing only the soluble fraction of the latex polymer in the  $^1\text{H}$  NMR spectrum.

Subsequently, we explored the reactivity of 4CPA with comonomers in solution by determining the reactivity ratios via the method described by Jaacks<sup>24</sup> (Figure C3). Previous research has shown that 4CPA shows a slightly higher reactivity in the RAFT controlled copolymerization with several acrylate comonomers.<sup>22</sup> This is the case for IBOA, THFA, and 2OA, where the reactivity ratio of 4CPA is  $>1$  and the comonomer reactivity ratio is  $<1$  in all monomer pairs (Figure 4.8c). Nevertheless,  $r_1r_2$  is close to 1 in all cases suggesting a near statistical copolymerization. This suggests that the observed differences in monomer reactivity reside in different transport rates through water in the heterogeneous systems. This is especially true in the early stages of the emulsion polymerization of Latex2OA (Figure 4.8b), where 4CPA shows reactivity but the comonomers do not.

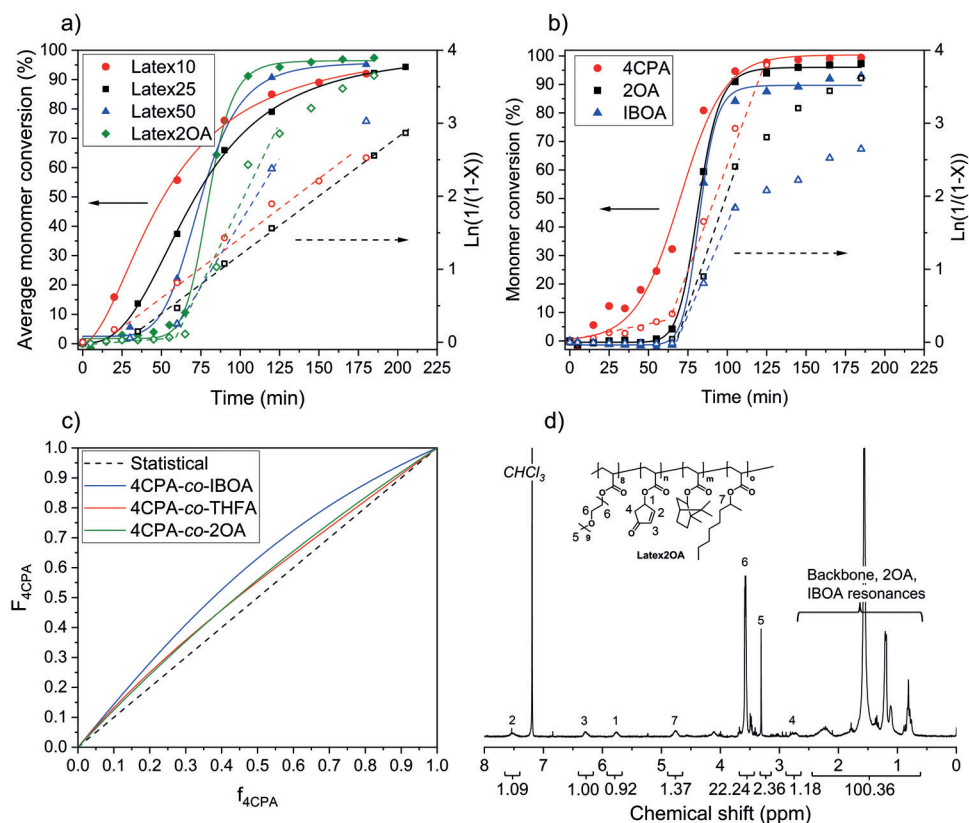


Figure 4.8. Copolymerization of 4CPA a) average monomer conversion as a function time and first order plots of latexes 10, 25, 50, and 20A. b) Individual monomer conversion and first order plots in the emulsion polymerization of Latex20A, c) Copolymerization graph of 4CPA with comonomers IBOA, THFA, and 2OA. d)  $^1\text{H}$  NMR spectrum of dried Latex20A.



## Conclusions

In this work, the RAFT PISA of biobased acrylic monomers with the use of a POEGA macro-RAFT agent for the production of high solid content latexes was developed. The biobased 4CPA was successfully incorporated in the polymer structure with a molar feed ratio of 25%. Using  $^1\text{H}$  NMR spectroscopy, intact 4CPA units were detected in the final latexes indicating the possibility for post-polymerization photocyclodimerization reactions. Furthermore, as the continuous phase, water was used without co-solvent, which makes the resulting latexes suitable for low VOC, UV curable coating and film applications.

Emulsion polymerization of commercially available monomers such as butyl acrylate occurred under RAFT control and resulted in polymers with narrow dispersity using the selected POEGA macro-RAFT agent. However, the introduction of the biobased 4CPA as functional monomer in the feed always resulted in partially cross-linked latexes. To limit the extend of cross-linking, the amount of 4CPA in the monomer feed was limited to 25 mol%. In this way, stable latexes with a solid content of 10 wt% were successfully synthesized.

The solid content was drastically improved by switching from ACVA to VA-044 as the initiator, and performing the polymerization at 50 °C instead of 65 °C. Stable latexes were obtained with a solid content up to 40 wt% and the resulting particle sizes were sub 100 nm. Again, polymerization occurred under controlled conditions for BA, THFA, and IBOA. A series of latexes containing 4CPA and the biobased comonomers THFA, IBOA and 2OA were produced at 40 wt% solid content and with a particle size between 98 and 406 nm. Determination of the copolymerization parameters in solution between 4CPA and THFA, IBOA, and 2OA revealed only a slight preference of 4CPA propagation relative to the comonomer. Therefore, the copolymerizations proceeded close to a statistical copolymerization. This suggest that strong differences in monomer conversion in the heterogeneous system might be explained by differences in transport rates through water.

The results described here offer the foundation to further development on biobased latex products based on 4CPA. RAFT PISA proved to be a suitable technique for the production of functional biobased latexes. The functionality of 4CPA in biobased latexes is further exploited for the production of UV cured (freestanding) films in chapter 5.

## References

1. Bibaut-Renaud, C.; Burget, D.; Fouassier, J.; Varelas, C.; Thomatos, J.; Tsagaropoulos, G.; Ryrfors, L.; Karlsson, O., Use of  $\alpha$ -diketones as visible photoinitiators for the photocrosslinking of waterborne latex paints. *Journal of Polymer Science Part A: Polymer Chemistry* **2002**, *40* (18), 3171-3181.
2. Ferguson, C. J.; Hughes, R. J.; Nguyen, D.; Pham, B. T.; Gilbert, R. G.; Serelis, A. K.; Such, C. H.; Hawket, B. S., Ab initio emulsion polymerization by RAFT-controlled self-assembly. *Macromolecules* **2005**, *38* (6), 2191-2204.
3. Canning, S. L.; Smith, G. N.; Armes, S. P., A critical appraisal of RAFT-mediated polymerization-induced self-assembly. *Macromolecules* **2016**, *49* (6), 1985-2001.
4. d'Agosto, F.; Rieger, J.; Lansalot, M., RAFT-Mediated Polymerization-Induced Self-Assembly. *Angewandte Chemie International Edition* **2020**, *59* (22), 8368-8392.
5. Le, D.; Keller, D.; Delaittre, G., Reactive and Functional Nanoobjects by Polymerization-Induced Self-Assembly. *Macromolecular Rapid Communications* **2019**, *40* (2), 1800551.
6. Chiefari, J.; Chong, Y.; Ercole, F.; Krstina, J.; Jeffery, J.; Le, T. P.; Mayadunne, R. T.; Meijs, G. F.; Moad, C. L.; Moad, G., Living free-radical polymerization by reversible addition-fragmentation chain transfer: the RAFT process. *Macromolecules* **1998**, *31* (16), 5559-5562.
7. St Thomas, C.; Guerrero-Santos, R.; d'Agosto, F., Alkoxyamine-functionalized latex nanoparticles through RAFT polymerization-induced self-assembly in water. *Polymer Chemistry* **2015**, *6* (30), 5405-5413.
8. Boussiron, C.; Le Behec, M.; Sabalot, J.; Lacombe, S.; Save, M., Photoactive rose bengal-based latex via RAFT emulsion polymerization-induced self-assembly. *Polymer Chemistry* **2021**, *12* (1), 134-147.
9. Guimarães, T. R.; Bong, Y. L.; Thompson, S. W.; Moad, G.; Perrier, S.; Zetterlund, P. B., Polymerization-induced self-assembly via RAFT in emulsion: Effect of Z-group on the nucleation step. *Polymer Chemistry* **2021**, *12* (1), 122-133.
10. Martín-Fabiani, I.; Makepeace, D. K.; Richardson, P. G.; Lesage de la Haye, J.; Venero, D. A.; Rogers, S. E.; D'agosto, F.; Lansalot, M.; Keddie, J. L., In situ monitoring of latex film formation by small-angle neutron scattering: evolving distributions of hydrophilic stabilizers in drying colloidal films. *Langmuir* **2019**, *35* (10), 3822-3831.
11. Such, C. H.; Rizzardo, E.; Serelis, A. K.; Hawket, B. K.; Gilbert, R. G.; Ferguson, C. J.; Hughes, R. J.; Olejnik, E. Aqueous dispersions of polymer particles. WO03055919A1, 2002.
12. Nguyen, D.; Huynh, V.; Lam, M.; Serelis, A.; Davey, T.; Paravagna, O.; Such, C.; Hawket, B., Encapsulation by Directed PISA: RAFT-Based Polymer-Vesiculated Pigment for Opacity Enhancement in Paint Films. *Macromolecular Rapid Communications* **2021**, *42* (10), 2100008.
13. Albigès, R.; Klein, P.; Roi, S.; Stoffelbach, F.; Creton, C.; Bouteiller, L.; Rieger, J., Water-based acrylic coatings reinforced by PISA-derived fibers. *Polymer Chemistry* **2017**, *8* (34), 4992-4995.
14. Lesage de la Haye, J.; Martín-Fabiani, I.; Schulz, M.; Keddie, J. L.; D'agosto, F.; Lansalot, M., Hydrophilic MacroRAFT-mediated emulsion polymerization: Synthesis of latexes for cross-linked and surfactant-free films. *Macromolecules* **2017**, *50* (23), 9315-9328.
15. Martín-Fabiani, I.; Lesage de la Haye, J.; Schulz, M.; Liu, Y.; Lee, M.; Duffy, B.; D'Agosto, F.; Lansalot, M.; Keddie, J. L., Enhanced Water Barrier Properties of Surfactant-Free Polymer Films Obtained by MacroRAFT-Mediated Emulsion Polymerization. *ACS Applied Materials & Interfaces* **2018**, *10* (13), 11221-11232.

16. Dehan, V.; Bourgeat-Lami, E.; d'Agosto, F.; Duffy, B.; Fortini, A.; Hilton, S.; Krassa, K.; Keddie, J. L.; Koh, M. L.; Lansalot, M., High-performance water-based barrier coatings for the corrosion protection of structural steel. *Steel Construction* **2017**, *10* (3), 254-259.
17. Chenal, M.; Rieger, J.; Véchambre, C.; Chenal, J. M.; Chazeau, L.; Creton, C.; Bouteiller, L., Soft Nanostructured Films with an Ultra-Low Volume Fraction of Percolating Hard Phase. *Macromolecular Rapid Communications* **2013**, *34* (19), 1524-1529.
18. Nguyen, D.; Huynh, V. T.; Serelis, A. K.; Davey, T.; Paravagna, O.; Such, C. H.; Hawckett, B. S., Janus particles by simplified RAFT-based emulsion polymerization process for polymer coating. *Colloid and Polymer Science* **2022**, 1-9.
19. Alexakis, A. E.; Engström, J.; Stamm, A.; Riazanova, A. V.; Brett, C. J.; Roth, S. V.; Syrén, P.-O.; Fogelström, L.; Reid, M. S.; Malmström, E., Modification of cellulose through physisorption of cationic bio-based nanolatexes—comparing emulsion polymerization and RAFT-mediated polymerization-induced self-assembly. *Green Chemistry* **2021**, *23* (5), 2113-2122.
20. Do Amaral, M.; Van Es, S.; Asua, J. M., Effect of the particle size distribution on the low shear viscosity of high-solid-content latexes. *Journal of Polymer Science Part A: Polymer Chemistry* **2004**, *42* (16), 3936-3946.
21. Kan, C. S., Role of particle size on latex deformation during film formation. *Journal of Coatings Technology* **1999**, *71* (896), 89-97.
22. Stouten, J.; Vanpoucke, D. E.; Van Assche, G.; Bernaerts, K. V., UV-Curable Biobased Polyacrylates Based on a Multifunctional Monomer Derived from Furfural. *Macromolecules* **2020**, *53* (4), 1388-1404.
23. Gupta, J.; Keddie, D. J.; Wan, C.; Haddleton, D. M.; McNally, T., Functionalisation of MWCNTs with poly (lauryl acrylate) polymerised by Cu (0)-mediated and RAFT methods. *Polymer Chemistry* **2016**, *7* (23), 3884-3896.
24. Jaacks, V., A novel method of determination of reactivity ratios in binary and ternary copolymerizations. *Die Makromolekulare Chemie: Macromolecular Chemistry and Physics* **1972**, *161* (1), 161-172.
25. Vancoillie, G.; Frank, D.; Hoogenboom, R., Thermoresponsive poly (oligo ethylene glycol acrylates). *Progress in Polymer Science* **2014**, *39* (6), 1074-1095.

## Appendix C

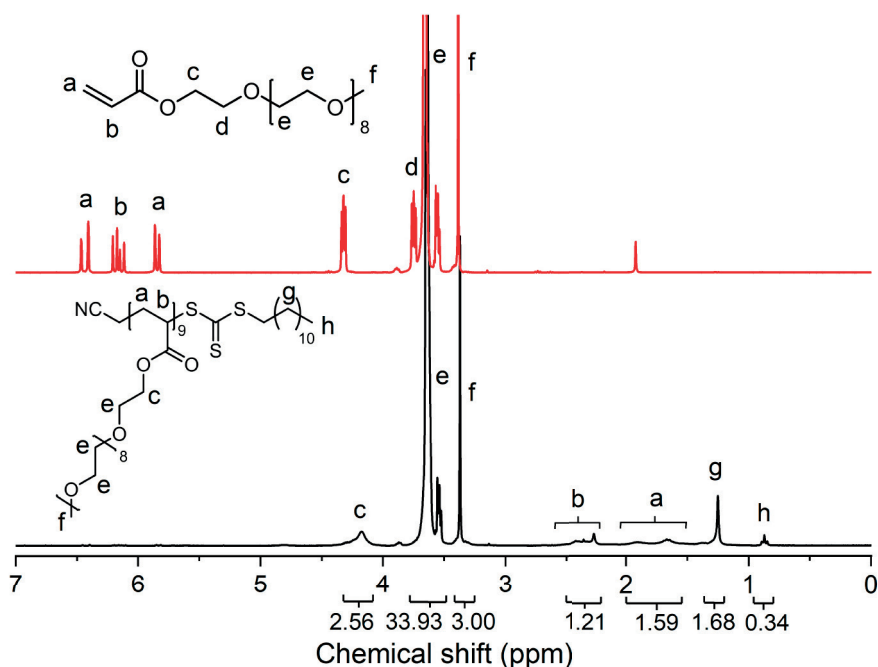


Figure C1. Overlay of the  $^1\text{H}$  NMR spectra in  $\text{CDCl}_3$  of OEGA monomer (red) and POEGA<sub>9</sub> macro-RAFT agent (black).

Table C1. RAFT PISA of 4CPA and comonomers using different initiator systems and at 10 wt% solids.

Entry	Initiator	Molar ratio I:RAFT: M	Molar feed ratio 4CPA : BA : IBOA	Time (min)	Temp. (°C)	Conversion				Size (nm)	PDI
						4CPA (%)	BA (%)	IBOA (%)			
1	KPS/TMEDA	0.5:1:200	0.25 : 0.4 : 0.35	330	30	97	99	97	55	0.041	
2	VA-044	1:1:200	0.25 : 0.4 : 0.35	165	50	92	97	95	76	0.036	
3 <sup>a</sup>	$\text{Fe}^{2+}/\text{H}_2\text{O}_2$	2.1:1:200	0 : 1 : 0	120	25	-	99	-	265	0.405	

<sup>a</sup> Metered addition of  $\text{Fe}^{2+}$  (Mohr's salt) at 0.008 mL/min, 1 mL solution of 15 mg/mL.

Table C2. Results of the small-scale emulsion polymerization without 4CPA using VA-044 as the initiator at 50 °C and performed at 30 wt% solids unless stated otherwise.

Entry	Molar ratio I:RAFT:M	Monomer feed ratio THFA : BA : IBOA	Conversion								
			Time (min)	THFA (%)	BA (%)	IBOA (%)	Size (nm)	PDI	$M_{n,th}^a$ (kg/mol)	$M_{n,GPC}$ (kg/mol)	$\bar{D}$
1	0.5:1:200	0 : 0.5 : 0.5	120	-	99	99	92	0.065	37.5	38.7	1.14
2 <sup>b</sup>	0.5:1:200	1 : 0 : 0	180	98	-	-	194	0.095	34.8	30.4	1.81
3	0.1:1:150	0.5 : 0 : 0.5	150	99	-	96	72	0.205	30.8	22.8	1.33
4	0.2:1:300	0.5 : 0 : 0.5	150	98	-	98	133	0.051	57.7	39.9	1.62
5 <sup>b</sup>	1:1:100	0 : 1 : 0	45	-	99	-	45	0.030	16.8	16.7	1.33

<sup>a</sup> Calculated as follows: target  $DP_{THFA} \times conversion_{THFA} \times 156.18 + target DP_{BA} \times conversion_{BA} \times 128.17 + target DP_{IBOA} \times conversion_{IBOA} \times 208.30 + 4157$ . <sup>b</sup> Performed at 10 wt% solids. In the calculation of the solid content is considered the amount of monomers in water.

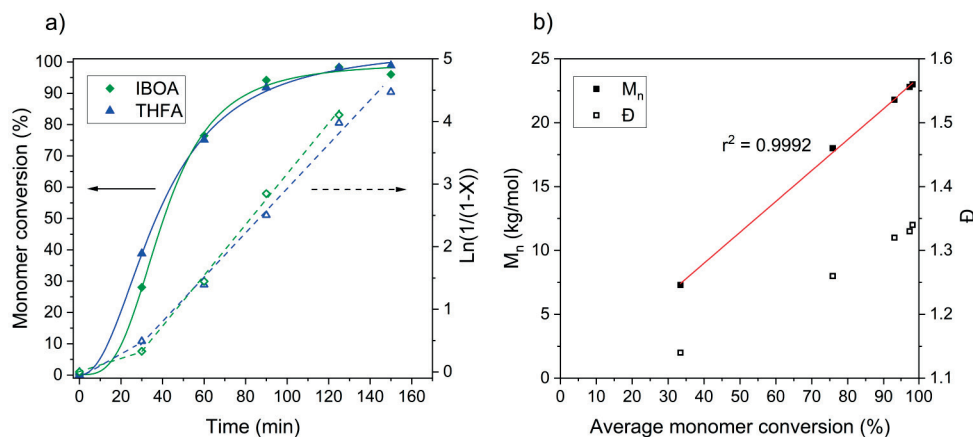


Figure C2. Results of small-scale emulsion polymerization experiment from Table C2, entry 3. a) Monomer conversion as a function of time. b)  $M_n$  and  $\bar{D}$  as a function of the average monomer conversion.

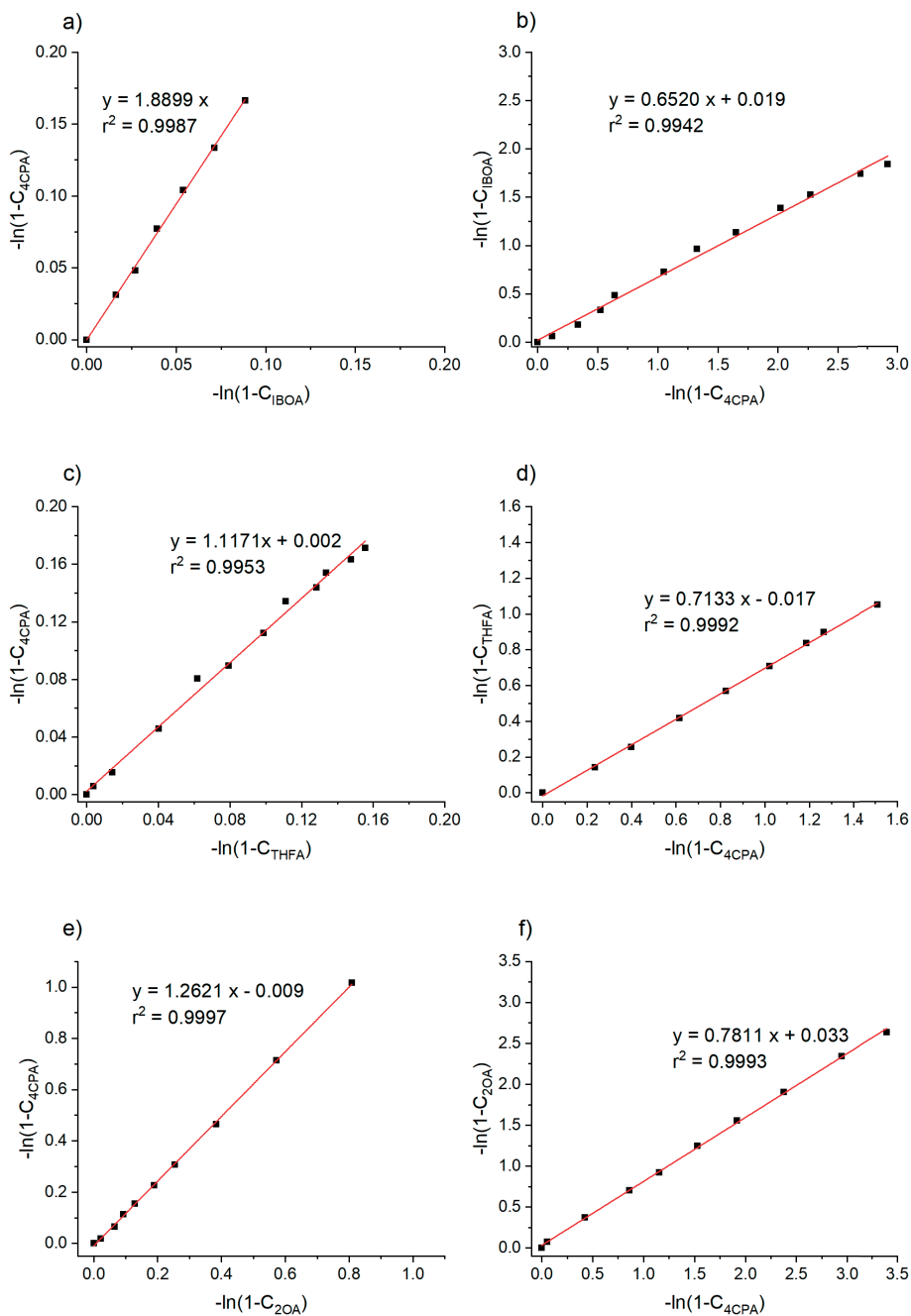
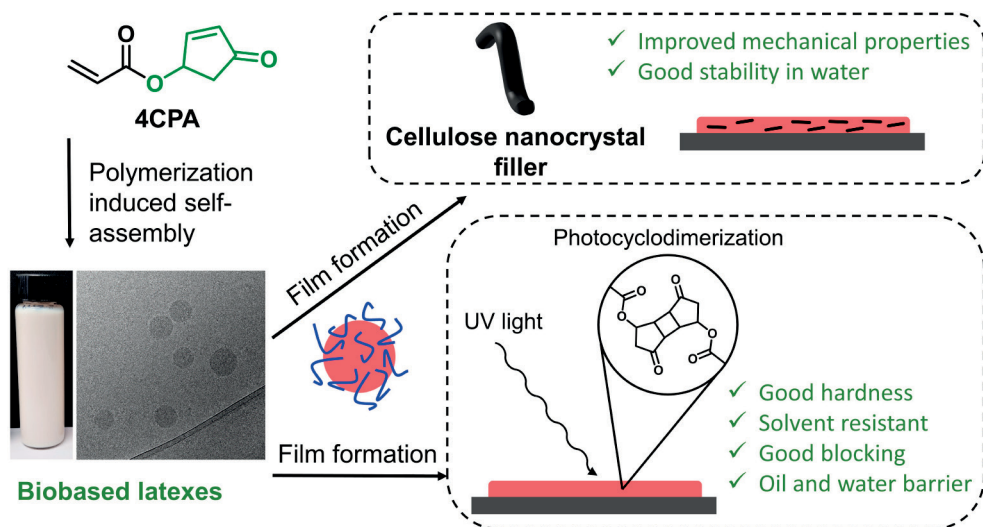


Figure C3. Jaacks plots of the copolymerization of 4CPA with comonomers IBOA, THFA, and 2OA. a) Excess 4CPA relative to IBOA. b) Excess IBOA. c) Excess 4CPA relative to THFA. d) Excess THFA. e) Excess 4CPA relative to 2OA. f) Excess 2OA.



# 5





---

## Chapter 5 Biobased and Functional Latexes Synthesized by Polymerization Induced Self- Assembly for UV Curable Films

---

### **Abstract**

Next to the development of polymer coatings and films based on renewable resources, there remains a challenge of combining the advantages of water-borne acrylic latexes, which are usually not cross-linked, with the excellent physical properties of cross-linked solvent borne coatings. To achieve this, functional groups built in the polymer chains can be employed in the cross-linking after film formation by means of external stimuli. It has been shown previously that after polymerization, the biobased 4-oxocyclopentenyl acrylate is capable of undergoing photocyclodimerization under UV light yielding a cross-linked polyacrylate. In this work, we investigate the polymerization induced self-assembly of 4CPA with several biobased acrylic monomers in the presence of a macro-RAFT agent. The produced latexes had advantageous, commercially relevant properties such as high solid content, small particles size, good colloidal stability, and low viscosity. After film formation and UV curing, flexible to rigid films can be obtained, depending on the monomer composition. By controlling the UV irradiation time, the cross-linking degree of the films can be tuned, and therefore their mechanical properties. Furthermore, the cross-linked films show promise as oil and water barriers in paper coating applications. Further drastic improvement of the mechanical properties was obtained after mixing the latex with cellulose nanocrystals. Due to the affinity of the CNC's with the latex polymer, the sensitivity to water of the film was greatly reduced, even at a CNC content of 80 wt%. This work outlines the development and application of biobased and functional cross-linkable latexes synthesized by PISA.

### Introduction

Waterborne acrylic coatings play an important role in the modern world. They contribute to the durability, performance, and beautification of material surfaces in for example, construction and carpentry. The drive to reduce hazardous Volatile Organic Compound (VOC) levels in coating formulations led to the development and increased use of waterborne acrylic latex binders.<sup>1</sup> These latex formulations require much less VOC to achieve film formation but suffer from certain downsides compared to solvent based coatings such as reduced barrier and mechanical properties, gloss, blocking and chemical resistance.<sup>2</sup> These downsides are linked to the latex particle coalescence mechanism and the absence of a cross-linked network.<sup>3</sup> Another problem is that the acrylate esters used for latex binder synthesis are derived from finite fossil resources, the global production of which exceeds 5.2 million metric tons per year.<sup>4</sup> Therefore, with the increasing global trend to reduce fossil resource consumption, it is evident that renewable alternatives need to be investigated to continue materials production.

Currently, biobased polymers are attracting increased attention, however, the polymerization of biobased acrylic monomers in industrially relevant aqueous emulsion processes remains considerably underexplored.<sup>5</sup> This situation is partially due to the stricter conditions under which water-borne polymerizations are executed, in contrast to solvent borne polymerizations, reducing the range of suitable monomers. Next to that, the availability of biobased monomers containing radical polymerizable groups is limited. Therefore, the introduction of novel structures in polymer systems by functionalization of biobased building blocks with polymerizable acrylic groups is an important topic, moving towards the reduction of fossil components in latex systems.

The invention of controlled radical polymerization techniques has widened the scope of radical polymerization research; however, the translation of controlled radical polymerization performed in solution to an aqueous dispersed system is not straightforward. This complication has been alleviated by the development of a Polymerization-Induced Self-Assembly (PISA) procedure under Reversible Addition-Fragmentation chain-Transfer (RAFT) control.<sup>6</sup> PISA requires the synthesis of a hydrophilic prepolymer, functionalized with a RAFT agent end-group, a macro-RAFT agent. Upon propagation from the macro-RAFT agent with hydrophobic monomers in the aqueous phase, spontaneous self-assembly into micelles with a core-shell structure takes place.<sup>7</sup> The resulting particles are stabilized by the covalently bonded macro-RAFT agent, and thus the use of free surfactant can be avoided. The RAFT mediated PISA technique has also been employed to produce high solid content latexes but its use for coatings has been reported only sparsely.<sup>8-15</sup> Other benefits of producing polymers under RAFT control is that the molecular weight can be controlled, and backbiting reactions are suppressed, reducing the amount of branching.<sup>16-17</sup> These characteristics allow for the incorporation of biobased monomers with a more complex structure that add functionality to the polymer backbone, without extensive cross-linking or side reactions.

In contrast to fossil derived molecules, which consist mainly of aliphatic and aromatic hydrocarbons, biobased platform molecules typically contain a higher functional group density. This attribute requires not only a change in approach towards monomer and polymer synthesis, but it also affects the resulting polymer properties. Through various chemical conversions, it is possible to mimic conventional plastics by synthesizing biobased replacements for fossil derived monomers that are chemically the same but consist of renewable carbon, for example bio-PE. Alternatively, novel building blocks can be engineered to bring unique polymer properties, or in such a way that they match the performance of conventional plastics. In this work, we utilize the high functional group density of a novel biobased acrylic monomer for the use in UV curable water-borne coatings. 4-hydroxycyclopentenone (4HCP), which is obtained via the Piancatelli rearrangement of furfuryl alcohol<sup>18</sup> is modified with an acrylate group by esterification of the hydroxyl group. This reaction yields the radically polymerizable monomer 4-oxocyclopentenyl acrylate (4CPA). Polymerization of 4CPA via RAFT polymerization in solution was previously reported in chapter 2.<sup>17</sup> The pendent cyclopentenone units on the resulting polymer can engage in a [2 + 2] photocyclodimerization under UV light to obtain polymeric networks.

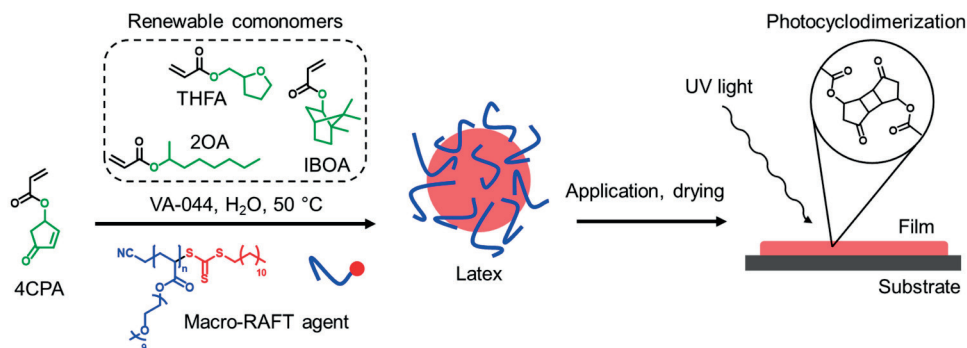


Figure 5.1. Schematic overview of the production of the latexes, and their implementation as UV cross-linked films.

Here, the post-polymerization modification is utilized in emulsion polymerization with biobased comonomers to produce UV curable latexes. UV post-curing overcomes some of the aforementioned downsides related to thermoplastic films and coatings, and results in good hardness, mechanical rigidity, chemical resistance, and blocking resistance. Previous reports on biobased UV curable polyacrylate latexes required the addition of a cross-linker, or lacked high solid content and tailoring towards applicable coating applications.<sup>19-20</sup> In this work, we propose the use of a poly oligoethylene glycol (POEGA) macro-RAFT agent for the RAFT mediated PISA of biobased monomers 4CPA, tetrahydrofurfuryl acrylate (THFA), 2-octyl acrylate (2OA), and isobornyl acrylate (IBOA) (Figure 5.1). By modifying the comonomer composition, while maintaining the 4CPA feed, the polymer  $T_g$  and coating properties can be altered. Similarly, the UV curing time can be adjusted in order to tune the degree of cross-linking, hence affecting the final film properties. The hydrophilic POEGA shell of the latex

particles also improves the interaction and compatibility of the polymer with hydrophilic composite materials. In this way, we investigate the reinforcement with cellulose nanocrystals (CNC) to improve the mechanical properties of the resulting films.

## Experimental section

### Materials

Azobisisobutyronitrile (AIBN, Sigma-Aldrich) was recrystallized from methanol prior to use. Isobornyl acrylate (IBOA, technical, Sigma-Aldrich), tetrahydrofurfuryl acrylate (THFA, 98%, abcr), 2-octyl acrylate (2OA, >98%, abcr), and oligo(ethylene glycol) methyl ether acrylate (OEGA, average  $M_n$  of 480 g/mol, Sigma-Aldrich) were passed over an alumina column and stored at -20 °C. 4-Oxocyclopent-2-ene-1-yl acrylate (4CPA) was synthesized according to the procedure mentioned in chapter 2 and stored at -20 °C.<sup>17</sup> Cyanomethyl dodecyl trithiocarbonate (CDT) was synthesized according to a procedure mentioned in the literature.<sup>21</sup> 1,3,5-Trioxane ( $\geq 99\%$ , Sigma-Aldrich), castor oil (Sigma-Aldrich), cellulose nanocrystals (CNC, length: 300-900 nm, width: 10-20 nm, Nanografi), naphthalene (>99%, Alfa-Aesar), 2,2'-Azobis[2-(2-imidazolin-2-yl)propane]dihydrochloride (VA-044, >98.0%, TCI), and  $CDCl_3$  (99.8%, Cambridge Isotope Laboratories) were used as received. All other solvents were obtained from Biosolve and were used as received.

### Synthesis of Poly(oligo(ethylene glycol) methyl ether acrylate) (POEGA) macro-RAFT agent

The procedure of the macro-RAFT agent synthesis was the same as described in chapter 4, except the quantities were increased. A 250 mL 3-neck flask equipped with magnetic stirrer was charged with AIBN (91 mg, 0.56 mmol, 1 eq.), CDT (2646 mg, 8.33 mmol, 15 eq.), OEGA (average  $M_n = 480$  g/mol) (40.00 g, 83.33 mmol, 150 eq.), toluene (184 mL), and trioxane (400 mg, as internal standard). The mixture was homogenized by stirring and degassed by bubbling nitrogen through the liquid for 30 minutes. After degassing an aliquot for NMR analysis was taken and the flask was placed in a 70 °C oil bath. During the reaction, several aliquots for NMR analysis were taken to observe the plateauing of the monomer conversion. The integrals of the acrylate resonances were compared to the trioxane resonance. After 360 minutes, the flask was taken out of the oil bath and cooled to room temperature. The polymer was precipitated three times in hexane and dried overnight in a vacuum oven at 40 °C. A yellow, transparent, and viscous liquid was obtained. The results of the POEGA macro-RAFT agent are summarized in Table 5.1.

Table 5.1. Results of the POEGA macro-RAFT agent.

Polymer	Molar ratio I:RAFT:OEGA	OEGA conversion (%)	$M_{n, th}$ (kg/mol)	$M_{n, GPC}$ (kg/mol)	$\bar{D}$	Yield (g)
POEGA macro-RAFT	0.07:1:10	78	4.1	5.9	1.06	29.7 (70%)

## RAFT PISA

All the emulsion polymerization reactions were performed in a similar fashion. In this example, the synthesis of Latex25 is described. The emulsion polymerization was performed in a 500 mL double-walled cylindrical glass reactor equipped with mechanical paddle stirrer with 3 holes. To the reactor were added 4CPA (16.63 g, 109.40 mmol, 50 eq.), THFA (34.19 g, 218.90 mmol, 100 eq.), IBOA (22.79 g, 109.40 mmol, 50 eq.), POEGA macro-RAFT agent (10.15 g, 2.189 mmol, 1 eq.), and distilled water (110 mL). The mixture was degassed by bubbling nitrogen through the liquid for 30 minutes. Then, the purging was stopped and a low nitrogen flow was applied on the overhead space of the reactor. While stirring at 250 rpm, oil regulated by a thermostat at 53 °C, was pumped through the double wall of the reactor to bring inside temperature to 50 °C. After the temperature was stable, VA-044 (708 mg, 2.189 mmol, 1 eq.) was added at once to the reaction mixture, marking the start of the polymerization. After 220 minutes, the reaction was stopped by cooling the reactor to room temperature. The latex was filtered over a 190 micron nylon filter and an off-white, turbid, and viscous latex was obtained. The latex was stored at 4 °C. Yield: 173.67 g (89.1%).

For the synthesis of the other scaled up latex syntheses, the following reagent quantities were used.

### Latex10:

4CPA (16.39 g, 107.82 mmol, 50 eq.), THFA (43.78 g, 280.32 mmol, 130 eq.), IBOA (8.98 g, 43.13 mmol, 20 eq.), POEGA macro-RAFT agent (10.00 g, 2.16 mmol, 1 eq.), distilled water (161 mL), and VA-044 (697 mg, 2.16 mmol, 1 eq.). Yield: 229.12 g (95.0%).

### Latex50:

4CPA (16.39 g, 107.81 mmol, 50 eq.), THFA (16.84 g, 107.81 mmol, 50 eq.), IBOA (44.92 g, 215.63 mmol, 100 eq.), POEGA macro-RAFT agent (10.00 g, 2.16 mmol, 1 eq.), distilled water (117 mL), and VA-044 (697 mg, 2.16 mmol, 1 eq.). Yield: 179.49 g (87.1%).

### Latex20A:

4CPA (16.63 g, 109.45 mmol, 50 eq.), 20A (52.44 g, 284.57 mmol, 130 eq.), IBOA (9.12 g, 43.78 mmol, 20 eq.), POEGA macro-RAFT agent (10.15 g, 2.19 mmol, 1 eq.), distilled water (117 mL), and VA-044 (708 mg, 2.19 mmol, 1 eq.). Yield: 144.48 g (70.3%). Some coagulant was retrieved after filtration (15.65 g, 17.6 wt% based on solids), and material loss on the reactor walls.

## Freestanding film preparation

3 mL of latex was diluted to 12 mL with distilled water and casted in a circular PTFE evaporation dish with a diameter of 75 mm. The films were dried for 2 days to the air. The dish was then transferred to a nitrogen-filled Dymax 2000 ECE UV chamber equipped with a 400 W metal halide UVA lamp. After 20 minutes of irradiation, the film was flipped upside

down and irradiated for another 20 minutes to achieve a homogenous curing. The distance from the sample to the lamp was 18 cm. The final dry film thickness was about 0.2 mm.

The CNC reinforced composite films were prepared as follows: First, a 3 wt% CNC dispersion was prepared by manual stirring the CNC powder in water until a homogenous viscous mixture was obtained. This step was followed by 30 minutes of sonication in a Branson 3800 sonication bath at room temperature, resulting in a mixture with considerably lower viscosity. An accurate amount of CNC dispersion was thoroughly mixed with 3 mL of diluted latex to a total amount 12 mL. The mixture was casted in a PTFE evaporation dish with a diameter of 75 mm. The mixing ratio of CNC dispersion and latex was determined based on a targeted solids ratio in the final dried film. After drying at room temperature for three days, the films were irradiated in the UV chamber as described above. Final dry film thickness was about 0.2 mm.

### **Film preparation**

The latexes were directly applied on Leneta cards, and cold-rolled R-46 steel Q-panels (obtained from Benelux Scientific BV) using a manual bar coater with a 120  $\mu\text{m}$  gap. Films on bleached printer paper with an average weight of  $78 \pm 1 \text{ g/m}^2$  were applied using the manual bar coater at specified wet layer thicknesses. The films were dried at room temperature for one day. Films from Latex50 were dried in an 80 °C oven for 30 minutes because of the high minimum film formation temperature. After drying, the films were transferred to a Dymax ECE 2000 UV chamber under nitrogen flow and irradiated using a 400 W metal halide, UVA lamp. The distance of the sample from the lamp was 18 cm. The films were irradiated for a specified amount of time.

### **Characterization**

#### *Gel permeation chromatography (GPC)*

Gel permeation chromatography (GPC) was performed at 30 °C using a Waters GPC equipped with a Waters 2414 refractive index detector. Tetrahydrofuran (THF) was used as the eluent at a flow rate of 1 mL/min. Three linear columns (Styragel HR1, Styragel HR4, and Styragel HR5) including a Styragel Guard column were used. Molecular masses are given relative to polystyrene standards. The polymers were dissolved in THF with a concentration of 3 mg/mL and filtered over a 0.2  $\mu\text{m}$  PTFE syringe filter.

#### *Nuclear magnetic resonance (NMR) spectroscopy*

$^1\text{H}$  NMR (300 MHz) spectra were recorded on a Bruker Avance III HD Nanobay 300 MHz apparatus at 298K in  $\text{CDCl}_3$  using 16 scans. NMR spectroscopy was used for polymer structural confirmation and for the determination of monomer conversion in the macro-RAFT agent synthesis. The disappearance of the vinyl resonances relative to the trioxane (internal standard) resonance were followed over time.

*Gas chromatography with flame ionization detector (GC-FID)*

Individual monomer conversions during emulsion polymerization were determined using gas chromatography with flame ionization detection (GC-FID). Aliquots taken from reaction mixtures were dissolved in THF prior to measurement. The disappearance of the monomer peaks relative to naphthalene (internal standard) were followed. Measurements were performed on a Shimadzu GC-2010 equipped with a Supelco SPB-1 capillary column (30 m × 0.25 mm × 0.25 μm film thickness). The temperature program was as follows: an initial temperature of 80 °C was maintained for 3 min and then increased to 140 °C with a heating rate of 10 °C/min. This temperature was maintained for 1 min and further increased to 300 °C with a heating rate of 20 °C/min and was maintained at 300 °C for 5 min (the total run time of 23 min).

*Differential scanning calorimetry (DSC)*

The glass transition temperature ( $T_g$ ) of polymer samples were determined using a Netzsch DSC 214 Polyma instrument. Prior to measurement, the samples were dried at 40 °C in a vacuum oven. The samples were heated in 2 cycles from -40 °C to 100 °C or from -60 °C to 100 °C with a rate of 10 °C/min under nitrogen atmosphere. The second cycle was used for determination of the phase transition points. The inflection point was used for reporting of the  $T_g$ .

*Thermogravimetric analysis (TGA)*

TGA on dried polymer films was performed on a TA Instruments TGA Q500 under nitrogen atmosphere. The samples were heated from 25 °C to 700 °C with a rate of 10 °C/min.

*Dynamic light scattering (DLS)*

The particle size distribution of the 4CPA latexes was determined using DLS. The aqueous emulsions were diluted with distilled water until they became visually slightly turbid. The samples were measured on a Malvern Instruments Zetasizer Nano ZS DLS instrument at 25 °C and a fixed angle of 173°. Zeta potential measurements were performed with the same instrument, using folded capillary cells.

*Wide angle x-ray diffraction (WAXD)*

The presence and orientation of CNC in the polymer was assessed with 2D wide-angle X-ray diffraction. 2D WAXD patterns were recorded on a SAXSLAB Ganesha instrument using Cu  $K\alpha$  radiation ( $\lambda = 0.154$  nm). The beam center and  $\theta$ -range were calibrated using the diffraction pattern of silver behenate. The conversion of 2D into 1D data was performed using the SaxsGui v2.13.01 software.

*Cryogenic transmission electron microscopy (Cryo-TEM)*

The 4CPA latexes were visualized by the Cryo-TEM method. The latex was firstly diluted to 1 wt% with distilled water. A thin aqueous film was formed by applying a 5 μl droplet of the

suspension to a bare specimen grid. Glow-discharged holey carbon grids were used. After the application of the suspension, the grid was blotted against filter paper, leaving thin sample film spanning the grid holes. These films were vitrified by plunging the grid into ethane, which was kept at its melting point by liquid nitrogen, using a Vitrobot (Thermo Fisher Scientific Company, Eindhoven, Netherlands) and keeping the sample before freezing at 95% humidity. The vitreous sample films were transferred to a Tecnai Arctica cryo-electron microscope (Thermo Fisher Scientific, Eindhoven, Netherlands). Images were taken at 200 kV with a field emission gun using a Falcon III direct electron detector.

### *Scanning electron microscopy (SEM)*

SEM was performed on a Jeol JSM-IT200 scanning electron microscope operated at 10 kV. Sample preparation was performed by freezing the sample in liquid nitrogen before fracturing the specimen in half. The sample was mounted with the fracture surface facing upward. The samples were sputtered with gold under argon atmosphere.

### *Gel content determination*

Of every latex, several droplets were deposited on a piece of accurately weighed cellulose filtration paper ( $W_1$ ). The filter paper was dried overnight and weighed ( $W_2$ ). Subsequently, the sample was extracted with THF in a Soxhlet extractor for 24 hours. Afterwards, the sample was dried and weighed ( $W_3$ ). The gel content was calculated as follows:

$$\text{Gel content (\%)} = \frac{(W_3 - W_1)}{(W_2 - W_1)} \times 100$$

Weighing of the sample and filtration paper was performed on a drying balance, which heated the sample to 105 °C until a steady weight was obtained.

The gel content of cross-linked films was performed by extracting an accurately weighed piece of film ( $W_1$ ) with THF or water in a Soxhlet extractor for 24 hours. After extraction, the films were dried in a 40 °C vacuum oven overnight and weighed again ( $W_2$ ). The gel content was calculated as follows:

$$\text{Gel content (\%)} = \frac{W_2}{W_1} \times 100$$

### *Solid content*

The solid content of the latexes was measured by accurately weighing an amount of latex in an aluminum dish ( $W_1$ ). The latex was dried in a 60 °C vacuum oven for 24 hours after which the solids were weighed ( $W_2$ ). The solid content was calculated as follows:

$$\text{Solid content (\%)} = \frac{W_2}{W_1} \times 100$$



### *Latex stability*

The stability of the latexes was evaluated by the freeze-thaw method and by the addition of salt solution and solvent (ethanol). For the freeze-thaw evaluation, 1 mL of latex sample was frozen for 24h at -20 °C and then thawed at room temperature. For the evaluation of addition of salt solution and solvent 1 equivalent of salt solution or solvent was added to 1 mL of latex sample. The latex was visually inspected for phase separation prior and after each latex stability method. Also, a DLS measurement was performed to evaluate the effect on the particle size.

### *Solvent swelling ratio*

The swelling ratio of cross-linked polymer films was determined by placing an accurately weighed piece of film ( $W_1$ ) (about 100 – 200 mg) in a flask containing 10 mL THF for 24 hours. The film was taken out of the flask and excess solvent on the surface was removed before weighing ( $W_2$ ). The swelling ratio was calculated as follows:

$$\text{Swell ratio} = \frac{(W_2 - W_1)}{W_1}$$

### *Water uptake*

The water uptake of the cross-linked polymer films was determined by placing an accurately weighed piece of film ( $W_1$ ) (about 100-200 mg) in a flask containing 10 mL distilled water for 48 hours. The film was taken out of the flask and excess solvent on the surface was removed before weighing ( $W_2$ ). The water uptake was calculated as follows:

$$\text{Water uptake (\%)} = \frac{(W_2 - W_1)}{W_1} \times 100$$

The water uptake tests were performed three times on each sample. The reported values are the average and the reported errors are standard deviations between three tests.

### *Minimum film formation temperature (MFFT)*

The MFFT was measured on a Rhopoint MFFT Bar 90 instrument according to ASTM D 2354.

### *Tensile test*

The mechanical performance of the freestanding polymer films was assessed by tensile testing. Tensile tests were performed on a Linkam micro tensile stage equipped with a 200N or 20N load cell. Freestanding films with a thickness of about 0.2 mm were cut into dog bone shaped specimens with dimensions of  $31 \times 2$  mm (length  $\times$  width), the broad part of the dog bone specimen had a width of 4 mm. The tensile tests were performed with a deformation rate of 33.3  $\mu\text{m/s}$ . All measurements were performed at room temperature. The Young's modulus of each measurement was determined between 0.2 and 0.6% strain. The values

reported are the average of five tensile measurements and errors reported are the standard deviations.

### *Rheology*

Rheological measurements were performed on a TA Instruments DHR rheometer equipped with a 40 mm parallel plate and Peltier element. Pure latexes and mixtures with CNC dispersion were deposited on the Peltier element controlled at 25 °C and the gap was set at 1000 μm. Frequency sweep experiments were performed at 2% deformation. Steady shear and oscillatory experiments were carried out to investigate the effect of shear rate on viscosity and viscoelastic properties. The hysteresis loop (performed with step times between 30 s and 600 s) test and the three interval thixotropy test (3ITT) (alternating between low shear 1 s<sup>-1</sup> for 90 s, and high shear 100 s<sup>-1</sup> for 120 s) were carried out to investigate the thixotropic behavior. Flow sweep measurements were carried out with a shear rate from 0.01 to 1000 s<sup>-1</sup>.

### *Raman spectroscopy*

Raman spectra were recorded on a Bruker RFS 100/S Raman spectrophotometer between 400 and 3500 cm<sup>-1</sup>, using a resolution of 4 cm<sup>-1</sup> and 700 scans. The sample was ground into a powder prior to measurement.

### *UV-Vis spectroscopy*

The opacity of CNC loaded films was measured using UV-Vis spectroscopy. Measurements were performed on a Shimadzu UV-3600 UV-Vis-NIR spectrophotometer. The spectra were recorded from 700 to 200 nm with a slit width of 32 nm. The transmittance at 600 nm of each film was recorded and the opacity was calculated according to the following equation.

$$\text{Opacity} = -\log(T600)/x$$

Where T600 is the fractional transmittance at a wavelength of 600 nm, and x is the film thickness. A lower transmittance results in a higher opacity value.

### *Fourier transform infrared (FTIR) spectroscopy*

Attenuated Total Reflection FTIR spectroscopy (ATR-FTIR) was performed on a PerkinElmer Spotlight 400 equipped with a PIKE GladiATR. Accumulations of 64 spectra were collected in the range of 4000–400 cm<sup>-1</sup> with a spectral resolution of 2 cm<sup>-1</sup>.

## **Film characterization techniques**

### *Blocking resistance*

The blocking resistance of polymer films was determined according to the following procedure. Films on Leneta cards were cut in strips of 5 cm × 3 cm and stacked face to face. The strips were loaded with a pressure of 1 Kg for 4 hours at 50 °C. The visual evaluation of the films was performed according to standard method ASTM D 2793-99. Grades were

appointed to each film evaluating the degree of blocking and the surface damage according to the following criteria. Grades were appointed to each coating evaluating the degree of blocking (from A = free fall separation to F = tool required to separate) and the surface damage (from 0 = none to 5 = >50% damage).

#### *Contact angle*

Contact angle measurements were performed on an Attension Theta optical tensiometer. Using the equipment sample stage, a drop of distilled water (5  $\mu\text{L}$ ) was deposited on the film surface in front of a camera. After 10 seconds equilibration time, the angle between the film surface and tangent line of the water droplet was measured using the OneAttension analysis software. The reported values are the average of five measurements. The reported errors are the standard deviations.

#### *Surface tension*

The surface tension was determined by the pendant drop method using an Attension Theta optical tensiometer. Block copolymer solutions with known concentration were prepared in milli-Q water. The surface tension was calculated by the OneAttension analysis software from the shape of the drop (5  $\mu\text{L}$ ) using the Young-Laplace equation. The concentration range that was evaluated was between  $5 \times 10^{-5}$  and  $2.1 \times 10^{-2}$  mM. The critical aggregation concentration (CAC) was calculated at the intersection of the tangent lines of the linear region and the plateau.

#### *Water and methyl ethyl ketone (MEK) double rub*

The water and solvent resistance was evaluated by the double rub method. Films on steel plates were gently rubbed with a cotton swab that was previously immersed in distilled water or MEK. The amount of double rubs (one time back and forth) were counted for each test until visual damage on the surface appeared. The double rub tests were performed three times on each sample. The reported values are the average and the reported errors are standard deviations.

#### *Gloss*

Gloss measurements were performed on films applied on steel substrates using a BYK micro-TRI-gloss instrument at 20°, 60°, and 85°. The average of three measurements at different spots was taken as the final value.

#### *Cross-cut adhesion*

Adhesion of the films applied on steel substrates was evaluated using an Elcometer 1542 cross-cut adhesion tester. The adhesion test and evaluation was performed according to ASTM D 3359-B. After the test, the tested area was classified into grades between 5B for no surface damage, and 0B for 65% to complete flaking (Figure 5.2).

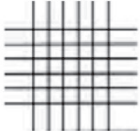





<p><b>ISO Class: 0/ASTM Class: 5B</b> The edges of the cuts are completely smooth; none of the squares of the lattice is detached.</p>	
<p><b>ISO Class: 1/ASTM Class: 4B</b> Detachment of small flakes of the coating at the intersections of the cuts. A cross-cut area not significantly greater than 5% is affected.</p>	
<p><b>ISO Class: 2/ASTM Class: 3B</b> The coating has flaked along the edges and/or at the intersections of the cuts. A cross-cut area significantly greater than 5%, but not significantly greater than 15%, is affected.</p>	
<p><b>ISO Class: 3/ASTM Class: 2B</b> The coating has flaked along the edges of the cuts partly or wholly in large ribbons, and/or it has flaked partly or wholly on different parts of the squares. A cross-cut area significantly greater than 15%, but not significantly greater than 35%, is affected.</p>	
<p><b>ISO Class:4/ASTM Class: 1B</b> The coating has flaked along the edges of the cuts in large ribbons, and/or some squares have detached partly or wholly. A cross-cut area significantly greater than 35%, but not significantly greater than 65%, is affected.</p>	
<p><b>ISO Class: 5/ASTM Class: 0B</b> Any degree of flaking that cannot even be classified by classification 4.</p>	

Figure 5.2. Classification of cross-cut adhesion according to ASTM D 3359-B.

*Pencil hardness*

The hardness of coated films applied on steel substrates was evaluated using an Elcometer 3086 motorized pencil hardness tester according to ASTM D 3363. The hardness was evaluated using a range of leads between 6H and 6B. A weight of 7.5 N on the lead was used (Figure 5.3). The hardest lead, which did not leave a scratch on the film surface, was selected as the hardness value.

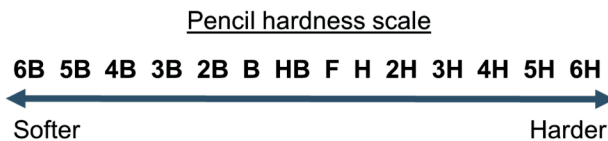


Figure 5.3. The pencil hardness scale.

*KIT grease resistance test*

The KIT grease resistance test was performed in accordance with the standard Tappi 559 pm-96. The mixtures of castor oil, toluene and n-heptane were prepared according to Table 5.2. A drop of the test liquid was deposited on the film and wiped after 15 seconds. The darkening as result of wetting of the oil on the underlying substrate was visually examined. If darkening occurred, the test failed and a lower KIT no. was tested. The highest number that does not cause darkening is reported. A higher KIT value indicates better oil barrier properties. The test was repeated three times on three different coatings. The values were averaged to the nearest 0.5.

Table 5.2. Composition of the mixtures used in the KIT grease resistance test.

KIT no.	Castor oil (mL)	Toluene (mL)	n-Heptane (mL)
1	100	0	0
2	90	5	5
3	80	10	10
4	70	15	15
5	60	20	20
6	50	25	25
7	40	30	30
8	30	35	35
9	20	40	40
10	10	45	45
11	0	50	50
12	0	45	55

The films that were evaluated were prepared by applying a layer of latex with a wet film thickness of 30, 90, or 120  $\mu\text{m}$  using a manual bar coater on bleached uncoated paper with an average weight of  $78 \pm 1 \text{ g/m}^2$ . The film was dried for several hours before UV curing for 40 minutes in a nitrogen-filled Dymax UV chamber equipped with a 400 W metal halide UVA lamp.

*Cobb-Unger oil and water absorbency*

The Cobb-Unger oil and water absorbency test was based on Scan-P 37:77 procedure. The absorbency value in g/m<sup>2</sup> was calculated according to the following equation.

$$\text{Absorbency} = \frac{(W_2 - W_1)}{A}$$

Where  $W_1$  is the weight of the sample before exposure to liquid, and  $W_2$  is the weight after exposure to the liquid.  $A$  indicates the area of the test specimen, which was 0.001452 m<sup>2</sup>. The evaluated liquids were castor oil and water. The test specimens were exposed to castor oil for 10 minutes and water for 60 seconds. In short, the test was executed by filling a cup with the test liquid followed by placing the test specimen on the cup. When the cup was turned upside down, a timer was started. Five seconds before the end of the exposure, the cup was turned and excess liquid was blotted using paper tissue. The average absorbency value was taken over three measurements.

## Results and discussion

### Synthesis and characterization of 4CPA latexes

As determined in chapter 4, an optimum of 25 mol% 4CPA in the monomer feed was found, yielding stable, high solids latexes. In this chapter, we proceeded with upscaling the most promising polymerizations, latexes 10, 25, 50, and 2OA. The reactions were performed on a scale of about 200 mL, to produce enough material for the evaluation of applied films on substrates and freestanding film properties. For one, we sought out to evaluate the effect on the amount of IBOA in the monomer feed, and thus the effect of polymer  $T_g$  on the film properties. To further reduce the  $T_g$  to below room temperature, THFA was replaced by 2OA, a proposed biobased alternative to the fossil based 2-ethyl hexyl acrylate. The results of the latex characterization are summarized in Table 5.3. The appearance of the latexes was opaque and the color ranged from off-white to pale yellow (Figure 5.4a). In general, high solid contents between 34.6 and 47.1 wt% were obtained, which is in the range of commercial latex binder products.<sup>22</sup>

Table 5.3. Properties of the scaled up latexes with 25 mol% 4CPA in the feed.

Code	THFA feed (mol%)	IBOA feed (mol%)	2-OA feed (mol%)	$T_g$ (°C)	MFFT (°C)	Gel content (%)	Size <sub>DLS</sub> (nm)	PDI	Size <sub>Cryo-TEM</sub> (nm)	$\zeta$ (mV)	Solids (%)
Latex10	65	10	0	8	< 0	93	549	0.264	350 ± 111	-13.2	34.6
Latex25	50	25	0	19	13.7	90	187	0.010	177 ± 28	-14.6	47.1
Latex50	50	50	0	56	46	92	115	0.090	94 ± 10	-7.5	45.1
Latex2OA	0	10	65	-21	< 0	95	136	0.142	82 ± 19	-7.4	42.6

MFFT = Minimum Film Formation Temperature.

From the results summarized in Table 5.3, it is clear that the amount of IBOA and 2OA in the monomer feed drastically influences the  $T_g$  of the latex polymer. The  $T_g$  increases from 8 to 56 °C with an IBOA feed of 10 and 50 mol%, respectively. Since the minimum film

formation temperature (MFFT) is mainly dictated by the  $T_g$ , this also increases with increasing amount of IBOA in the monomer feed. Samples Latex10, Latex25, and Latex2OA have an MFFT below 15 °C and are expected to form a homogenous layer at room temperature. Latex50 however, has an MFFT of 46 °C and thus elevated temperatures are required during drying to achieve coalescence of the latex particles.

As it was also observed in the small-scale screening reactions in chapter 3, the IBOA feed fraction did also clearly affect the particle size distribution. According to dynamic light scattering (DLS), relatively large particles of 549 nm and a broad  $\text{D}$  were obtained at low IBOA feed of 10 mol% in Latex10. At higher feeds of 25 and 50 mol% IBOA, the particle size dropped drastically to 187 and 115 nm, respectively. A similar small particle was observed for Latex2OA. It is possible that the relatively hydrophobic IBOA and 2OA influence the self-assembly during the PISA process in a different way than the more hydrophilic THFA.<sup>23</sup> The cryo-TEM images in Figure 5.4c clearly show the difference in morphology of the different latex particles. Large and coarse particles were obtained in the Latex10 sample, possible consisting of a coagulation of multiple smaller particles. Core-shell type particles are observed in Latex25, whereas in Latex50 homogenous spherical particles were obtained. In Latex2OA, small, spherical, and partially coagulated particles were obtained, which is also represented in the overview of the DLS distributions (Figure 5.4b), where Latex2OA shows a rather broad distribution. In general, the sizes observed in cryo-TEM correspond well with those measured by DLS (Table 5.3).

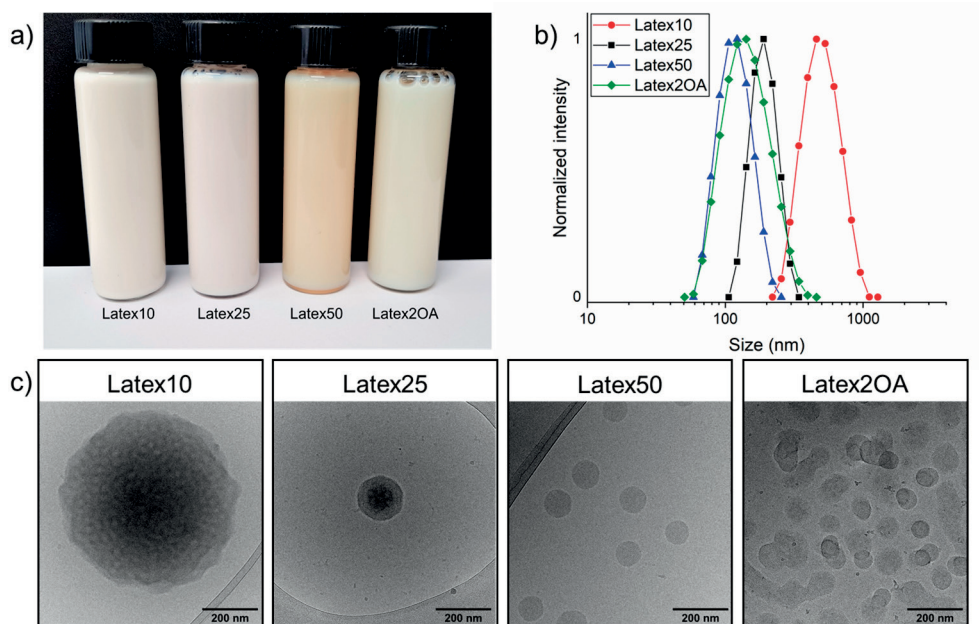


Figure 5.4. a) Photograph depicting the appearance of the synthesized latexes, b) Overlay of the DLS particle size distributions, c) Representative cryo-TEM images of the synthesized latexes as presented in Table 5.3.

The main mode of particle stabilization is by steric repulsions of the nonionic POEGA macro-RAFT shell. This is evident from the measured  $\zeta$ -potential values, which are close to zero (Table 5.3). In contrast to linear macro RAFT agent stabilizers, the brush-type POEGA is known to exhibit strong steric repulsion due to the densely populated side chains that are covalently bonded to the particles.<sup>24</sup> Indeed, the emulsions were stable over several months of storage. No visual sedimentation or coagulation was observed and the particle size remained the same after 11 months storage at 4 °C according to DLS (Table D1). The latexes were subjected to several stabilization tests to evaluate the resistance against freeze-thaw, addition of one equivalent of salt solution (1 M NaCl and 0.1 M MgSO<sub>4</sub>), and solvent (ethanol). The latexes were evaluated visually for any macroscopic phase separation. None of the latexes showed any phase-separation after the addition of salt solution or solvent (Table D2). High resistance towards the addition of ions is characteristic of sterically stabilized latexes.<sup>25</sup> Latexes 10, 25, and 50 were macroscopically stable after the freeze-thaw step, whereas Latex20A coagulated and showed phase separation. DLS measurement before and after freeze-thawing showed that only Latex50 was completely resistant, while the other latexes showed an increased particle size and broader distribution (Table D1). A higher increase in the particle size was observed for the latexes with low  $T_g$ , suggesting that coagulation of the soft particle cores is the cause of the increase in particle size during the freeze-thaw step.

The amount of unreacted macro-RAFT agent remaining in the latexes was determined gravimetrically from the solids that remained from the supernatant after centrifugation for 2.5 hours at 15000 rpm (Table D3). <sup>1</sup>H NMR spectroscopy suggests that the majority of said residue consists of POEGA macro-RAFT agent, together with a small amount of unidentified impurities. The amount of free surfactant in the synthesized latexes was calculated to be between 35 and 46%. Formation of a small amount of dead chains are expected during RAFT polymerization of OEGA, which partially contribute to the amount of free surfactant. Incomplete chain transfer efficiency would explain the remaining free surfactant. Free polymeric surfactant can also be beneficial during formulation and application of the latex since it lowers the surface tension and aid with leveling and wetting on the desired surface.<sup>26</sup> The surface tension of the latexes ranged between 44.8 and 49.3 mN/m, which is significantly lowered compared to that of pure water at 72.5 mN/m (Table D3).

Rheological measurements confirmed the low viscosity of the latexes of below 100 Pa.s, with shear thinning behavior (Figure D2). The viscosity of a latex is governed by many factors including particle size, morphology and solid content.<sup>27</sup> Since multiple factors differ between the latexes in this work, no conclusions can be drawn regarding the influence on the rheological properties.

### **Film formation, UV curing, and tensile properties of the freestanding films**

Freestanding films of the latexes presented in Table 5.3 were prepared by casting of the latex in PTFE dishes and drying, followed by irradiation in a UV chamber for 40 minutes. This yielded optically clear and homogeneous cross-linked films. Since cross-linking occurs by



photocyclodimerization of the pendent cyclopentenone double bonds, no addition of cross-linker or photoinitiator was required.<sup>17</sup> The extent of cross-linking was followed by the disappearance of the cyclopentenone double bond using Raman spectroscopy. First, the unmodified films of Latex10 was analyzed. In Figure 5.5a, the overlay of the Raman spectra belonging to 4CPA, 4HCP acetate and Latex10 are shown. By comparing the spectra, it can be determined that the peaks at 1726, 1633, and 1595  $\text{cm}^{-1}$  belong to the carbonyl, acrylate double bond, and cyclopentenone double bond, respectively. As a result of the UV irradiation, the C=C double bond corresponding to the cyclopentenone group disappears relative to the signal at 2939  $\text{cm}^{-1}$  (C-H stretching). By measuring the integral of the C=C double bond signal and assuming that at 0 minutes UV irradiation 100% of the bonds are intact, the conversion can be calculated (Figure 5.5c). After 10 minutes of UV irradiation, conversions between 21 and 51% are obtained. After 40 minutes the conversion is increased to between 69 and 89%. During the UV curing, the temperature of the films reached to about 90 °C, which is above the  $T_g$  of all the cross-linked freestanding films (Figure 5.5d).

The  $T_g$  was visible in the DSC traces but appeared as very broad transitions. A general trend of gradual  $T_g$  increase during UV curing was observed, and reached a plateau after about 40 minutes. The effect of the UV irradiation time on the freestanding film swelling ratio also indicated cross-linking. The swelling ratio steadily decreases as a result of the UV irradiation time, also plateauing after about 40 minutes for every latex film.

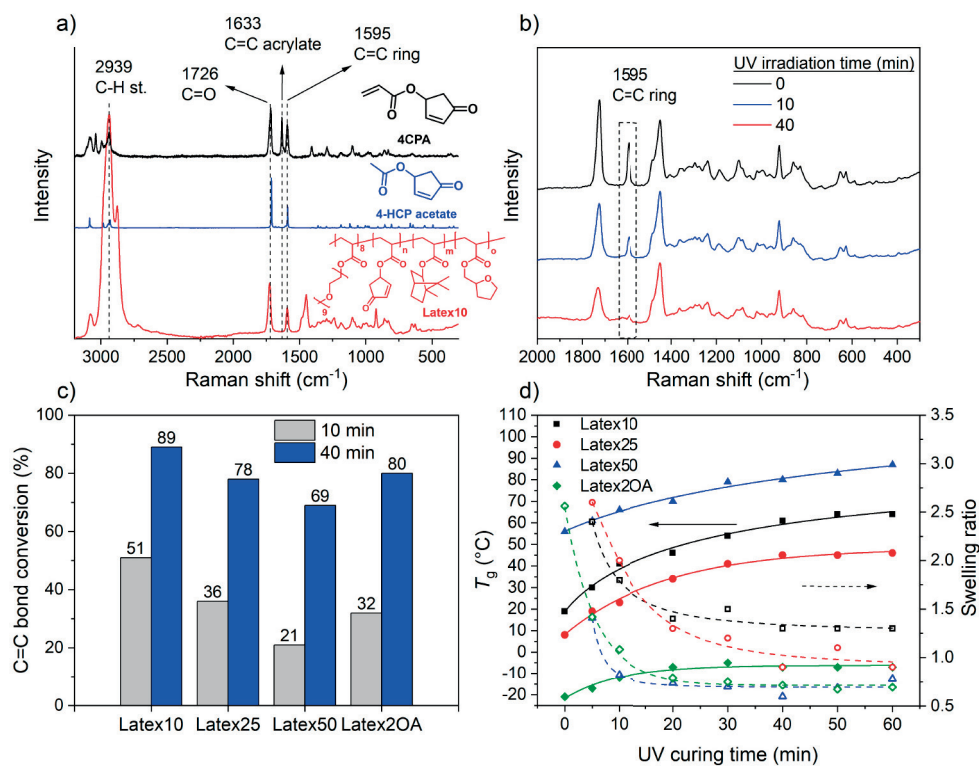


Figure 5.5. Characterization of the extent of cross-linking of the latex freestanding films. a) Overlay of the Raman spectra of 4CPA, 4HCP acetate, and Latex10 between 300 and 3300 cm<sup>-1</sup>. b) Overlay of the Raman spectra of Latex10 between 300 and 2000 cm<sup>-1</sup> after 0, 10, and 40 minutes in the UV chamber. The spectra were normalized against the band at 2939 cm<sup>-1</sup> (C-H stretch). c) The C=C double bond conversion from the cyclopentenone group for each latex. d) The influence of UV curing time on the  $T_g$  (closed symbols) and swelling ratio (open symbols) in THF for each latex.

Despite the relatively large gel content of the latexes (Table 5.3) homogenous dried films with good mechanical performance were obtained after UV curing. This suggests that sufficient coagulation and migration of non-cross-linked or dangling hydrophobic chains between the particles took place to achieve interparticle cross-links and a macroscopically robust film. The results of the tensile tests are reported in Table D4. The monomer composition had a significant influence on the Young's modulus and ultimate tensile strength. Latex10, 25 and 50 had a Young's modulus of 749, 1052, and 1248 MPa, respectively. The Young's modulus was drastically decreased to 63 MPa by using the soft monomer 20A to obtain films with higher flexibility. The strain at break for all freestanding films was relatively low between 5.4 and 13.0%, which can be expected for extensively cross-linked polymers. Indeed films with a lower degree of cross-linking yielded a lower Young's modulus, but a much higher strain at break. The extent of cross-linking was controlled by limiting the UV irradiation time. In Figure 5.6, the stress-strain curves of freestanding films

from Latex10 with different UV irradiation times are presented. The numerical data is summarized in Table D5. The unmodified films were soft and ductile, with a strain at break of 80%. Increasing the UV irradiation time results in an increase in Young's modulus and ultimate tensile strength, while the strain at break decreases. In this way, the properties of the freestanding films can be facily tuned by controlling the UV irradiation time. For example, high stiffness films might be desired in applications where scratch resistance is required, whereas a higher ductility is generally desired for wood coating applications.<sup>28</sup>

Additional evidence of the relationship between tensile properties and UV irradiation time was provided by a comparison latex containing 10 mol% 4CPA instead of 25 mol%. The details of this latex are summarized in Table D6. Freestanding films that were irradiated for 40 minutes had similar tensile properties as the films from Latex10 that were irradiated for 5 minutes (Figure D3). In order to see if prolonged UV irradiation times would result in improved tensile properties one freestanding film prepared from Latex25 was irradiated for a total of 60 minutes (30 minutes on each side) (Table D5). This resulted in similar tensile properties as 40 minutes UV irradiation time (Table D4). Similarly, a film with three times the thickness (0.61 mm) was prepared and irradiated for a total of 40 minutes. The Young's modulus and ultimate tensile strength were significantly reduced, while the strain at break was improved (Table D5). This indicates incomplete conversion of the 4CPA bond due to the limited penetration depth of the UV light resulting in a less dense network.

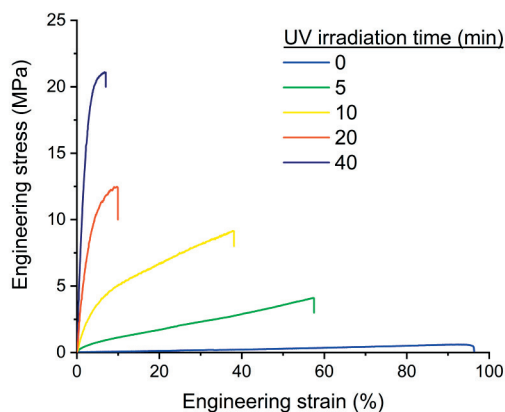


Figure 5.6. Tensile curves of the freestanding films from Latex10 cured at different times in the UV chamber.

The thermal stability of the unmodified and cross-linked films was investigated by TGA. The temperature at 5 wt% weight loss was between 225 and 259 °C, and the residue at 700 °C was between 5.3 and 8.7% for all films (Table D7). No significant influence of the UV curing on the thermal stability was observed (Figure D4).

## Films

To investigate the application of the polymer latexes as potential binders in coating formulations, latex films were applied on steel plates and Leneta cards to evaluate the unformulated film properties. The latexes were applied with a wet film thickness of 120  $\mu\text{m}$ , then dried, and cured in the UV chamber. The contact angle, gloss, solvent and water resistance, hardness, and blocking resistance were evaluated on the cured films with a dry thickness of between 24 and 46  $\mu\text{m}$  (Table 5.4).

Table 5.4. Evaluation of the film properties.

Code	Curing time (min)	Thickness ( $\mu\text{m}$ )	Contact angle ( $^\circ$ )	Gloss 60 $^\circ$ (GU)	MEK double rub	H <sub>2</sub> O double rub	Pencil <sup>a</sup> hardness	Blocking resistance <sup>b</sup>	Cross-cut adhesion
Latex10	0	30 $\pm$ 5	11.6 $\pm$ 1.0	34.7 $\pm$ 0.1	5 $\pm$ 2	>200	3B	C1	5B
	5	24 $\pm$ 5	54.8 $\pm$ 0.7	N/A	38 $\pm$ 11	>200	H	B0	3B
	10	26 $\pm$ 5	59.5 $\pm$ 0.7	N/A	140 $\pm$ 59	>200	H	B0	3B
	40	30 $\pm$ 1	64.3 $\pm$ 0.5	31.4 $\pm$ 0.9	>200	>200	2H	A0	5B
Latex25	0	35 $\pm$ 2	17.3 $\pm$ 1.7	49.9 $\pm$ 0.3	5 $\pm$ 0	>200	3B	A0	5B
	40	46 $\pm$ 2	67.6 $\pm$ 0.5	35.5 $\pm$ 0.4	>200	>200	4H	A0	5B
Latex50	0	34 $\pm$ 3	36.3 $\pm$ 1.4	79.5 $\pm$ 0.8	6 $\pm$ 0	>200	HB	A0	4B
	40	40 $\pm$ 2	76.8 $\pm$ 0.5	92.0 $\pm$ 1.6	>200	>200	5H	A0	5B
Latex20A	0	31 $\pm$ 2	60.0 $\pm$ 0.7	75.8 $\pm$ 0.9	12 $\pm$ 5	93 $\pm$ 8	<6B	D5	5B
	40	28 $\pm$ 6	96.3 $\pm$ 0.3	84.9 $\pm$ 0.5	>200	>200	H	C0	5B

All characterizations were performed on the coatings using steel substrates, except the blocking resistance, which was performed on Leneta cards. <sup>a</sup> Ranging between 6B (soft) to 6H (hard). <sup>b</sup> Ranging between A0 (excellent blocking) to F5 (poorest blocking properties).

The film properties were evaluated before and after UV irradiation. The results in Table 5.4 show that UV irradiation improves all the evaluated properties. Firstly, the solvent resistance represented by the amount of double rubs with methyl ethyl ketone (MEK) is drastically increased. All unmodified films showed surface damage after only a few rubs with MEK, while all fully cross-linked films remained intact after at least 200 MEK double rubs. Secondly, the pencil hardness improved after UV irradiation. The cured films had a pencil hardness of between 2H and 5H, with a pronounced effect of the  $T_g$  of the initial latex polymer. A higher  $T_g$  resulted in a higher pencil hardness. In the development of waterborne coatings, it remains a challenge to achieve both good blocking resistance and film formation at ambient temperature. The low  $T_g$  of the binder required for particle coalescence also impairs the blocking resistance of the resulting film.<sup>29</sup> After extensive cross-linking however, the  $T_g$  of the polymer is increased and chain diffusion is restricted by the covalent bonds. Therefore, the cross-linked films studied in this research had good blocking resistance properties as indicated in Table 5.4. The blocking resistance was poor for the unmodified films from Latex10 and 20A, but complete separation of the films without surface damage was achieved after the UV irradiation step. The UV irradiation also improved the gloss of most films resulting in medium to high gloss values. Overall, the films showed good adhesion to steel substrates.

Finally, the contact angle with water was determined. As expected, increasing the amount of the hydrophilic THFA monomer and decreasing the amount of hydrophobic monomer IBOA and 2OA results in a decrease in the contact angle. Furthermore, the films after UV irradiation had a significantly higher contact angle than before (Figure 5.7). In the case of films from Latex10 the Contact angle increased from  $11.6^\circ$  before UV curing to  $64.3^\circ$  after UV curing. Change of the contact angle as a result of the UV curing can be explained by morphological changes as a result of the photocyclodimerization reaction. Possibly, rearrangement of the POEGA hydrophilic shell, and hydrophobic cores during UV-curing could explain the increase in surface hydrophobicity.

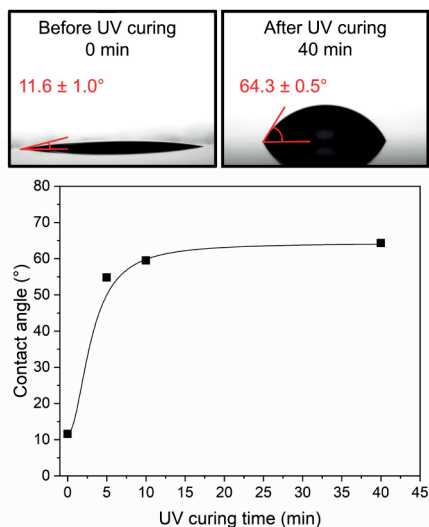


Figure 5.7. The effect of the UV curing time on the surface contact angle with water.

### Barrier layers for paper applications

Layers of latex2OA were applied on paper substrates and UV cured to investigate the potential application as oil and water barrier layers for paper applications. Since the UV curing of the applied films leads to a cross-linked network with high solvent resistance (>200 MEK double rubs) and high contact angle with water ( $96.3^\circ$ ) (Table 5.4), the ability to block oil and moisture is promising. Furthermore, this latex exhibits a low  $T_g$ , facilitating film formation at room temperature and maintaining the flexibility on flexible substrates after UV curing. Latex2OA was applied on bleached uncoated paper with various wet layer thicknesses resulting in a weight of between  $3.3 \text{ g/m}^2$  and  $27.6 \text{ g/m}^2$  of the dried and UV cured film. The results are summarized in Table 5.5. Oil barrier properties were assessed using the KIT oil and grease resistance test. All the applied layers showed the highest KIT test number of 12, except from the two lowest weight layers corresponding to the single layers with a dry coating weight of  $3.3 \text{ g/m}^2$  and  $6.2 \text{ g/m}^2$ . Nonetheless, these films still resulted in high KIT test numbers of 8.5 and 9.5, respectively.

Table 5.5. Results of the paper substrates coated with Latex2OA with various wet layer thicknesses and a single and double layer.

Entry	Wet layer thickness ( $\mu\text{m}$ )	Single or double layer	Dry coating weight ( $\text{g}/\text{m}^2$ )	KIT-test no.
1	30	Single	$3.3 \pm 1.0$	$8.5 \pm 0.5$
2	30	Double	$6.8 \pm 0.7$	$12 \pm 0$
4	90	Single	$6.2 \pm 1.7$	$9.5 \pm 0.5$
5	90	Double	$18.6 \pm 2.7$	$12 \pm 0$
7	120	Single	$10.3 \pm 2.0$	$12 \pm 0$
8	120	Double	$27.6 \pm 5.6$	$12 \pm 0$

Further oil and water barrier properties were characterized using the Cobb-Unger test method (Figure 5.8). The paper substrate was compared to the two films with the lowest and highest dry coating weight of Latex2OA. In both cases, a drastic decrease in the oil and water absorbency was observed for the coated substrates. An absorbency of below  $1 \text{ g}/\text{m}^2$  is typically desirable, and the values obtained for the coating with a weight of  $3.3 \text{ g}/\text{m}^2$  are  $1.1 \text{ g}/\text{m}^2$  for castor oil, and  $1.6 \text{ g}/\text{m}^2$  for water. There was only a slight improvement in the oil and water absorbency of the coating with a weight of  $27.6 \text{ g}/\text{m}^2$  resulting in absorbency values of  $0.9 \text{ g}/\text{m}^2$  and  $0.3 \text{ g}/\text{m}^2$ , respectively. This small difference indicates that an application of  $3.3 \text{ g}/\text{m}^2$  already results in drastically improved properties at the evaluated conditions. From a commercial perspective, low coating weights are desired, while maintaining good barrier properties.

The gloss of the final surfaces was also improved after coating with Latex2OA. The single wet layer of  $30 \mu\text{m}$  gave only a slight increase in the gloss at  $60^\circ$  from 3.7 GU for the paper substrate to 7.3 GU for the coated substrate. The most glossy films were obtained with also the thickest wet layer of  $120 \mu\text{m}$  (double layer) resulting in a gloss at  $60^\circ$  of 31.9 GU (Figure 5.8).

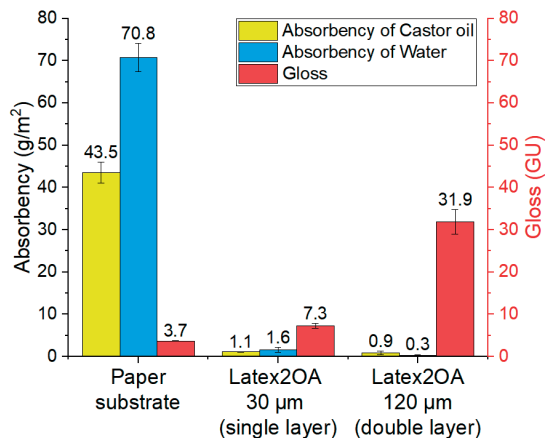


Figure 5.8. Cobb-Unger test results after exposure to castor oil (10 minutes) and water (60 seconds), for the paper substrate and the coated substrates. Gloss values of the paper substrate and the coated substrates. Layer thicknesses are given of wet films.

### Properties of cellulose nanocrystal (CNC) reinforced latexes and freestanding films

The covalently bonded PEG hydrophilic stabilizer is potentially compatible with fillers that are able to form hydrogen bonds to produce composite materials. Cellulose nanocrystals (CNC) are of high interest due to their biocompatibility, low toxicity, applicability in food applications<sup>30</sup>, and high aspect ratio in order to mechanically reinforce polymer materials.<sup>31</sup> PEG is able to form hydrogen bonds with the free hydroxyl groups that are present on the surface of CNC's.<sup>32</sup> Therefore, the same affect is expected for the POEGA macro-RAFT agent. Latex polymer functionalized with carboxylic acid groups have been shown to be succesfully reinforced with CNC due to the interactions between the carboxylic acid and hydroxyl groups.<sup>33</sup> In here, the latexes were simply mixed with a 3 wt% CNC dispersion in water in various amounts. After casting, drying and UV curing, CNC reinforced freestanding films were obtained with various ratio's of polymer and CNC.

The first indication of the presence of an interaction between the CNC and latex was observed during mixing of the latex and CNC dispersion. A mixture was obtained with a drastically increased viscosity relative to those of the original components. This indicates towards a bridging interaction between the CNC's and the PEG hydrophilic stabilizer shells through hydrogen bonding. Using rheological measurements, it was confirmed that the latex CNC mixtures had strong shear thinning properties (Figure D5). Two experiments were performed to confirm thixotropic behavior, the hysteresis loop and the three interval thixotropy test (3ITT). The rheology curves are presented in Figure 5.9. In the 3ITT the material is subjected to periods of low ( $1 \text{ s}^{-1}$ ) and high ( $100 \text{ s}^{-1}$ ) shear rates. As a result of the sudden change in shear rate, the hydrogen bonded network is disturbed and a drastic drop on the viscosity is observed (Figure 5.9a). The decrease in viscosity is so strong, that almost the same low viscosity of the pure latex is reached at  $100 \text{ s}^{-1}$ . A sudden decrease in the shear rate resulted

in a delayed increase of the viscosity, caused by the build up of the hydrogen bonded network. The 3ITT curves corresponding to Latex2OA, 10 and 25 containing various amounts of 3 wt% CNC dispersion are presented in Figure D6. The difference in viscosity  $\Delta\eta_e$  between  $\eta_e(1\text{ s}^{-1})$  and  $\eta_e(100\text{ s}^{-1})$  depends on the mixing ratio of latex and CNC dispersion. The  $\Delta\eta_e$  is especially high for the latexes containing 9 and 18 wt% CNC relative to the solids (Table D8). In most cases, the original viscosity was regained after decreasing the shear rate to  $1\text{ s}^{-1}$  within 90 seconds. The exceptions are the mixtures containing 18 and 28 wt%, which showed a recovery in the viscosity of 78 and 76%, respectively. The thixotropic behavior was also visualized by the hysteresis loop, which is formed after linearly increasing and decreasing the shear rate within a certain timeframe.<sup>34</sup> Firstly, the step time was varied from 30 to 600 seconds, which resulted in a larger hysteresis effect with decreasing step time for Latex2OA containing 9 wt% CNC (Figure D7). The hysteresis loop curves of the other latex-CNC mixtures were measured with a step time of 60 seconds. In Figure 5.9b, the hysteresis loop curve of the Latex2OA containing 18 wt% CNC is shown. The changes in viscosity as a result of shear rate and step time are considerable larger than for the pure latex. Similar behaviour was observed for Latex10, 25, and 20A containing different amounts of CNC relative to the solids (Figure D8). The rheological interactions observed here are in fact similar to the interaction between some surfactants and associative thickeners as described previously.<sup>35</sup>

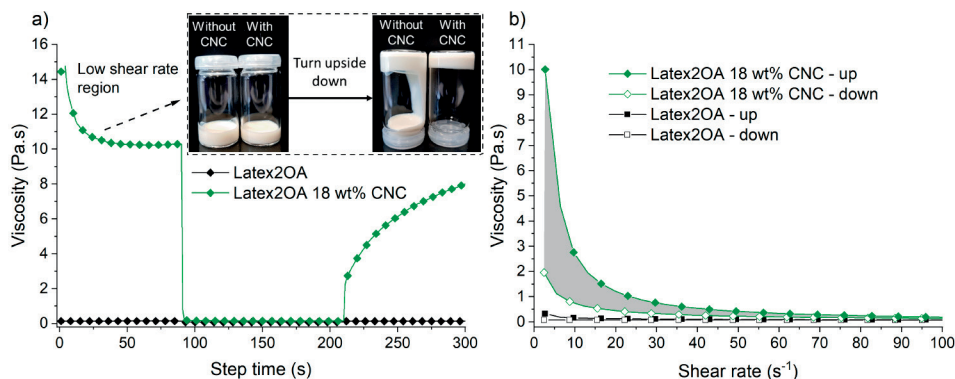


Figure 5.9. a) 3ITT curves of Latex2OA and the 18 wt% CNC mixture alternating between a shear rate of  $1\text{ s}^{-1}$  for 90 s and  $100\text{ s}^{-1}$  for 120 s. b) Hysteresis loop curves of Latex2OA and the 18 wt% CNC mixture with a step time of 60 seconds.

The latexes mixed with CNC dispersion were casted and dried at room temperature to obtain freestanding films. After 40 minutes of UV irradiation, clear and homogeneous films were obtained. From the freestanding films, dog bone shaped bars were stamped and the tensile properties were measured. In addition, to develop an understanding on the interaction with water as a result of the hydrophilic CNC filler, water uptake, contact angle, and gel content measurements were performed. The numerical data is summarized in Table D4.

Indication of the reinforcing effect of CNC in the polymer latex films was the mechanical performance observed in tensile testing. Due to the rod-like structure of CNC, improvements



in the stiffness are expected. The results in Table D4 display significant improvements in the Young's modulus for Latex10, 25, and 20A containing 9 wt% CNC or more. In the case of Latex20A, drastic increase in the Young's modulus was observed up to 28 wt% CNC while the strain at break remained largely unaffected Figure 5.10. The largest strain at break of 16% was observed for samples containing 18 wt% CNC. Further increase of the CNC content up to 80 wt% still resulted in transparent and homogenous films, but reduced the strain at break. Instead, the Young's modulus showed an exponential increase as a function of the amount of CNC in the composite. Composite films from Latex20A had a Young's modulus of 63 MPa at 0 wt% CNC and 8330 MPa at 80 wt% (Figure 5.11c).

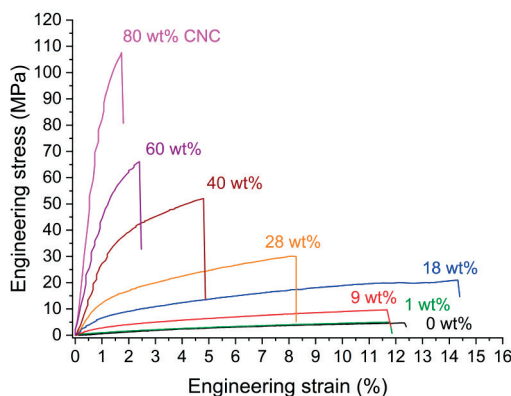


Figure 5.10. Overlay of representative tensile curves obtained from the UV cured films of Latex20A containing various amounts of CNC as a reinforcing filler.

The presence of CNC in the composite was confirmed with FTIR spectroscopy (Figure D9) and WAXD (Figure D10). With increasing amount of CNC in the composite, the characteristic signals belonging to CNC in the 1D WAXD signals became more prevalent.<sup>36</sup> 2D WAXD characterization of the CNC loaded films was performed from two directions on the sample. The X-ray beam was directed on the front of the sample and from the side, which distinguishes in-plane and through-plane orientation of the CNC's that can occur as a result of the casting and drying process. The 2D WAXD patterns measured from the front show an isotropic signal (Figure 5.11a). The samples measured from the side clearly show orientation judging from the localized signal distribution perpendicular to the sample orientation, which was vertical (Figure 5.11a), suggesting a layered in-plane oriented structure. The full width at half maximum (FWHM) of the azimuthal signal from the 2D WAXD patterns gives an indication of the relative degree of CNC orientation (Figure 5.11b). The FWHM decreases with an increasing amount of CNC in the composite suggesting an increase in orientation. Both increase in the amount of reinforcing filler as well as increased orientation thereof supports the observed exponential relationship between the mechanical properties and amount of CNC in the films (Figure 5.11c). Further evidence of orientation of the CNC in the film was supplied by SEM imaging of the fracture surfaces (Figure 5.11d). Clear

transitions were observed from a smooth surface for the 0 and 1 wt% CNC loaded films to a more coarse and speckled surface for the 9, 18, and 28 wt% CNC loaded films. No evidence of microscale agglomeration of CNC was observed in the SEM for these samples, suggesting good distribution of the filler in the matrix. With CNC loadings of 40, 60, and 80 wt%, a transition to a layered and oriented structure is observed. The layers are in-plane oriented (the sample orientation in the images is horizontal) and therefore correlate well with the observations made with WAXD. The layered morphology resembles a nacre-like structure, which is known for contributing to high stiffness materials and is suggesting the promise in barrier applications.<sup>37-38</sup>

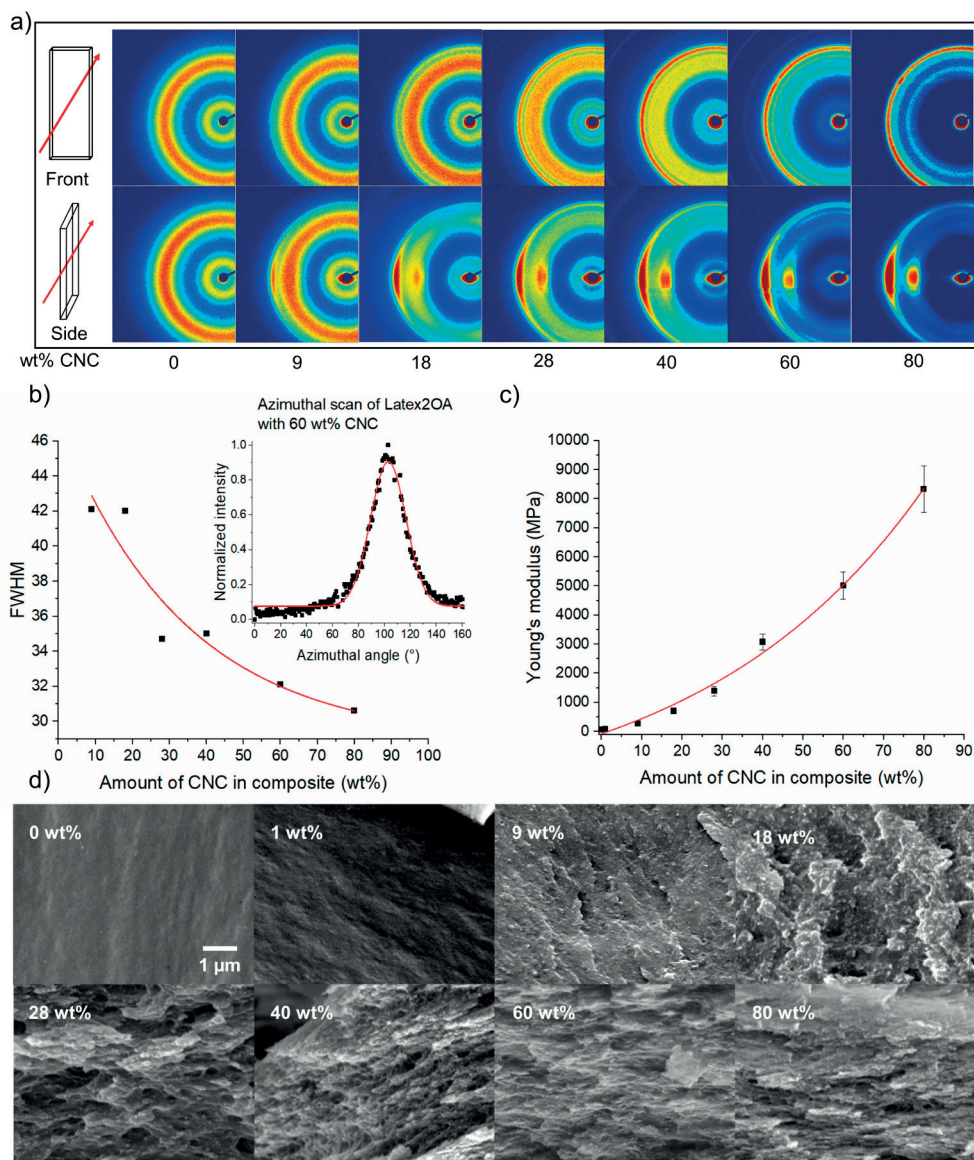


Figure 5.11. a) 2D WAXD patterns of the CNC loaded films from Latex2OA measured from the front and from the side of the film. The orientation of the film in the sample holder was vertical. b) Full width at half maximum (FWHM) of the signal from the azimuthal angle of the 2D WAXD patterns as a function of the amount of CNC in the composite. c) The Young's modulus of the films as a function of the amount of CNC in the composite. d) SEM images of the fraction surfaces of the CNC loaded films with a magnification of 16000 $\times$ . The orientation of the sample is horizontal.

The opacity of the films was measured using UV-Vis, and remained largely unaffected up to 28 wt% CNC (Figure 5.12a). While all films were optically transparent and homogenous, further increase in the CNC content of 40, 60 and 80 wt% resulted in a significant increase in opacity (Figure 5.12a). These results correlate with the observations made in SEM (Figure 5.11d) also indicating a clear morphological transition between 28 and 40 wt% CNC in the composite.

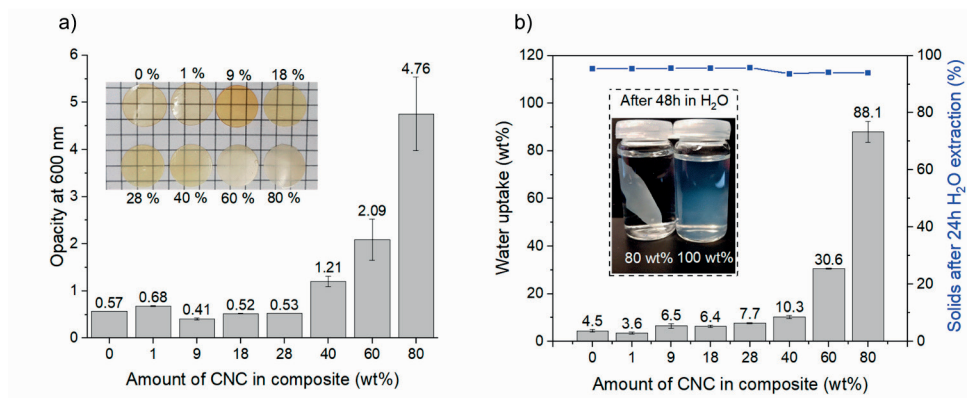


Figure 5.12. a) Opacity of the CNC loaded films measured by UV-Vis at a wavelength of 600 nm. b) Water uptake and solid content after extraction with H<sub>2</sub>O of the CNC loaded films.

The water uptake of the films was influenced by the amount of CNC in the composite film (Figure 5.12b). One of the major drawbacks of films composed of CNC, is the high water sensitivity due to the disruption of hydrogen bonding at the interface between the cellulose crystals.<sup>39-40</sup> However, in the case of the present materials, swelling in water was largely negated. After submersion into water for 48 hours, all films remained intact and similar in appearance. Even the films containing 80 wt% retained its structure, whereas a film based on pure CNC rapidly disintegrated after introduction to water (Figure 5.12b). Only slight increases in the water uptake were observed for films containing up to 40 wt% CNC. The films containing 60 and 80 wt% CNC showed a more significant water uptake of 30.6 and 88.1 wt%, respectively. We hypothesize that a good distribution of the UV cross-linked hydrophobic latex effectively diminishes the destabilizing effect of water on the CNC's. All the films retained more than 94% of their mass after 24h Soxhlet extraction with both THF and water, while pure CNC leaves no residues after extraction with water. Furthermore, the surface contact angle with water was not decreased as a result in CNC incorporation (Table D4).

## Conclusions

In this work, we have successfully developed the synthesis of biobased latexes based on polymerization induced self-assembly using a macro-RAFT agent. The key innovation is the use of a novel functional monomer 4CPA that can undergo post polymerization UV curing without the addition of external cross-linker, sensitizer, or initiator. This allowed overcoming one of the major contradictions in waterborne latexes, which desire both facile film formation at ambient temperature while avoiding the use of solvents, and combining this with good hardness, blocking resistance and scratch resistance.

The latex film formation was investigated in a series of selected latexes with a high solid content of between 34.6 and 47.1 wt%, small particle size, good colloidal stability, and low viscosity. Film formation followed by UV curing by photocyclodimerization of the cyclopentenone side groups lead to mechanically rigid films. Since the extent of dimerization, and thus cross-linking is dependent of the UV exposure time, the properties of the film could be tuned from soft and flexible, to rigid. Application of the latex on a substrate leads to films with high hardness, good solvent resistance and blocking resistance as a result of the UV curing process. Depending on the monomer composition of the latex, the surface contact angle with water is between 64.3° and 96.3°, indicating that the choice of monomer type and ratios yields different surface interactions with water. The UV curing step also drastically increased the contact angle of all evaluated films, suggesting a change of chemical or morphological nature on the surface.

As a proof of concept, films with various amount of application on a paper substrate were prepared in order to evaluate the oil and water barrier properties. A low coating weight of 3.3 g/m<sup>2</sup> drastically reduced the amount of oil and water absorption by the substrate compared to uncoated paper, and forms an effective oil barrier according to the KIT test results. At the same time, the absorbency and gloss of the paper could be further improved by applying thicker layers.

The morphology of the latex particles containing POEGA chains that are covalently attached allow for interaction with hydrophilic fillers that are able to undergo hydrogen bonding. Therefore, cellulose nanocrystals (CNC) were investigated as a potential filler showing effective improvement of the mechanical properties of the freestanding films. By increasing the amount of CNC from 0 to 80 wt% the Young's modulus showed an exponential increase. XRD measurements and SEM imaging confirmed in-plane layered orientation of the CNC crystals in the polymer film matrix that became more oriented with increasing amount of CNC. The contribution of the rigidity of the CNC filler and the alignment might explain the exponential relationship between filler amount and Young's modulus. Further characterization of the freestanding films showed that the water absorption remains low, retaining the structural integrity after submersion in water. Furthermore, all the films were transparent. Water absorption and opacity however, increased with increasing amount of CNC. The simple mixing of CNC dispersion with the emulsions is a facile and effective strategy to introduce CNC in a hydrophobic matrix and to alleviate many of the problems

that are associated with CNC films mainly related to the high water sensitivity. Further research could recognize the implementation of these latex CNC composites as gas, oil, and water barrier films.

## References

1. Winnik, M. A.; Feng, J., Latex blends: an approach to zero VOC coatings. *Journal of Coatings Technology* **1996**, *68*, 39-50.
2. Koukiotis, C.; Sideridou, I. D., Synthesis and characterization of latexes based on copolymers BA\MMA\DAAM and BA\MMA\VEOVA-10\DAAM and the corresponding 1K crosslinkable binder using the adipic acid dihydrazide as crosslinking agent. *Progress in Organic Coatings* **2010**, *69* (4), 504-509.
3. Ho, J.; Mudraboyina, B.; Spence-Elder, C.; Resendes, R.; Cunningham, M. F.; Jessop, P. G., Water-borne coatings that share the mechanism of action of oil-based coatings. *Green Chemistry* **2018**, *20* (8), 1899-1905.
4. Fouilloux, H.; Thomas, C. M., Production and Polymerization of Biobased Acrylates and Analogs. *Macromolecular Rapid Communications* **2021**, *42* (3), 2000530.
5. Molina-Gutiérrez, S.; Ladmiral, V.; Bongiovanni, R.; Caillol, S.; Lacroix-Desmazes, P., Radical polymerization of biobased monomers in aqueous dispersed media. *Green Chemistry* **2019**, *21* (1), 36-53.
6. Ferguson, C. J.; Hughes, R. J.; Nguyen, D.; Pham, B. T.; Gilbert, R. G.; Serelis, A. K.; Such, C. H.; Hawket, B. S., Ab initio emulsion polymerization by RAFT-controlled self-assembly. *Macromolecules* **2005**, *38* (6), 2191-2204.
7. Perrier, S., 50th Anniversary Perspective: RAFT Polymerization, A User Guide. *Macromolecules* **2017**, *50* (19), 7433-7447.
8. Alexakis, A. E.; Engström, J.; Stamm, A.; Riazanova, A. V.; Brett, C. J.; Roth, S. V.; Syrén, P.-O.; Fogelström, L.; Reid, M. S.; Malmström, E., Modification of cellulose through physisorption of cationic bio-based nanolatexes—comparing emulsion polymerization and RAFT-mediated polymerization-induced self-assembly. *Green Chemistry* **2021**, *23* (5), 2113-2122.
9. Nguyen, D.; Huynh, V.; Lam, M.; Serelis, A.; Davey, T.; Paravagna, O.; Such, C.; Hawket, B., Encapsulation by Directed PISA: RAFT-Based Polymer-Vesiculated Pigment for Opacity Enhancement in Paint Films. *Macromolecular Rapid Communications* **2021**, *42* (10), 2100008.
10. Albigès, R.; Klein, P.; Roi, S.; Stoffelbach, F.; Creton, C.; Bouteiller, L.; Rieger, J., Water-based acrylic coatings reinforced by PISA-derived fibers. *Polymer Chemistry* **2017**, *8* (34), 4992-4995.
11. Lesage de la Haye, J.; Martin-Fabiani, I.; Schulz, M.; Keddie, J. L.; D'agosto, F.; Lansalot, M., Hydrophilic MacroRAFT-mediated emulsion polymerization: Synthesis of latexes for cross-linked and surfactant-free films. *Macromolecules* **2017**, *50* (23), 9315-9328.
12. Martín-Fabiani, I.; Lesage de la Haye, J.; Schulz, M.; Liu, Y.; Lee, M.; Duffy, B.; D'Agosto, F.; Lansalot, M.; Keddie, J. L., Enhanced Water Barrier Properties of Surfactant-Free Polymer Films Obtained by MacroRAFT-Mediated Emulsion Polymerization. *ACS Applied Materials & Interfaces* **2018**, *10* (13), 11221-11232.
13. Dehan, V.; Bourgeat-Lami, E.; d'Agosto, F.; Duffy, B.; Fortini, A.; Hilton, S.; Krassa, K.; Keddie, J. L.; Koh, M. L.; Lansalot, M., High-performance water-based barrier coatings for the corrosion protection of structural steel. *Steel Construction* **2017**, *10* (3), 254-259.
14. Chenal, M.; Rieger, J.; Véchambre, C.; Chenal, J. M.; Chazeau, L.; Creton, C.; Bouteiller, L., Soft Nanostructured Films with an Ultra-Low Volume Fraction of Percolating Hard Phase. *Macromolecular Rapid Communications* **2013**, *34* (19), 1524-1529.
15. Nguyen, D.; Huynh, V. T.; Serelis, A. K.; Davey, T.; Paravagna, O.; Such, C. H.; Hawket, B. S., Janus particles by simplified RAFT-based emulsion polymerization process for polymer coating. *Colloid and Polymer Science* **2022**, 1-9.

16. Ballard, N.; Rusconi, S.; Akhmatskaya, E.; Sokolovski, D.; de la Cal, J. C.; Asua, J. M., Impact of competitive processes on controlled radical polymerization. *Macromolecules* **2014**, *47* (19), 6580-6590.
17. Stouten, J.; Vanpoucke, D. E.; Van Assche, G.; Bernaerts, K. V., UV-Curable Biobased Polyacrylates Based on a Multifunctional Monomer Derived from Furfural. *Macromolecules* **2020**, *53* (4), 1388-1404.
18. Piancatelli, G.; Scettri, A.; Barbadoro, S., A useful preparation of 4-substituted 5-hydroxy-3-oxocyclopentene. *Tetrahedron Letters* **1976**, *17* (39), 3555-3558.
19. Ladmiral, V.; Jeannin, R.; Lizarazu, K. F.; Lai-Kee-Him, J.; Bron, P.; Lacroix-Desmazes, P.; Caillol, S., Aromatic biobased polymer latex from cardanol. *European Polymer Journal* **2017**, *93*, 785-794.
20. Yan, Y.; Wu, J.; Wang, Y.; Fang, X.; Wang, Z.; Yang, G.; Hua, Z., Strong and UV-Responsive Plant Oil-Based Ethanol Aqueous Adhesives Fabricated Via Surfactant-free RAFT-Mediated Emulsion Polymerization. *ACS Sustainable Chemistry & Engineering* **2021**, *9* (40), 13695-13702.
21. Gupta, J.; Keddie, D. J.; Wan, C.; Haddleton, D. M.; McNally, T., Functionalisation of MWCNTs with poly (lauryl acrylate) polymerised by Cu (0)-mediated and RAFT methods. *Polymer Chemistry* **2016**, *7* (23), 3884-3896.
22. Bilgin, S.; Bahraçian, S.; Liew, M. L.; Tomovska, R.; Asua, J. M., Surfactant-free latexes as binders in paint applications. *Progress in Organic Coatings* **2022**, *162*, 106591.
23. Figg, C. A.; Carmean, R. N.; Bentz, K. C.; Mukherjee, S.; Savin, D. A.; Sumerlin, B. S., Tuning hydrophobicity to program block copolymer assemblies from the inside out. *Macromolecules* **2017**, *50* (3), 935-943.
24. Zhou, J.; Yao, H.; Ma, J., Recent advances in RAFT-mediated surfactant-free emulsion polymerization. *Polymer Chemistry* **2018**, *9* (19), 2532-2561.
25. Lazaridis, N.; Alexopoulos, A.; Chatzi, E.; Kiparissides, C., Steric stabilization in emulsion polymerization using oligomeric nonionic surfactants. *Chemical Engineering Science* **1999**, *54* (15-16), 3251-3261.
26. Tan, B.; Grijpma, D. W.; Nabuurs, T.; Feijen, J., Crosslinkable surfactants based on linoleic acid-functionalized block copolymers of ethylene oxide and  $\epsilon$ -caprolactone for the preparation of stable PMMA latices. *Polymer* **2005**, *46* (4), 1347-1357.
27. Guyot, A.; Chu, F.; Schneider, M.; Graillat, C.; McKenna, T., High solid content latexes. *Progress in Polymer Science* **2002**, *27* (8), 1573-1615.
28. Nejad, M.; Cooper, P., Exterior wood coatings. Part-2: modeling correlation between coating properties and their weathering performance. *Journal of Coatings Technology and Research* **2011**, *8* (4), 459-467.
29. Picchio, M. L.; Passeggi Jr, M. C.; Barandiaran, M. J.; Gugliotta, L. M.; Minari, R. J., Waterborne acrylic-casein latexes as eco-friendly binders for coatings. *Progress in Organic Coatings* **2015**, *88*, 8-16.
30. Mu, R.; Hong, X.; Ni, Y.; Li, Y.; Pang, J.; Wang, Q.; Xiao, J.; Zheng, Y., Recent trends and applications of cellulose nanocrystals in food industry. *Trends in Food Science & Technology* **2019**, *93*, 136-144.
31. Ferreira, F.; Pinheiro, I.; Gouveia, R.; Thim, G.; Lona, L., Functionalized cellulose nanocrystals as reinforcement in biodegradable polymer nanocomposites. *Polymer Composites* **2018**, *39*, E9-E29.



32. Gu, M.; Jiang, C.; Liu, D.; Prempeh, N.; Smalyukh, I. I., Cellulose nanocrystal/poly (ethylene glycol) composite as an iridescent coating on polymer substrates: Structure-color and interface adhesion. *ACS Applied Materials & Interfaces* **2016**, *8* (47), 32565-32573.
33. Dogan-Guner, E. M.; Brownell, S.; Schueneman, G. T.; Shofner, M. L.; Meredith, J. C., Enabling zero added-coalescent waterborne acrylic coatings with cellulose nanocrystals. *Progress in Organic Coatings* **2021**, *150*, 105969.
34. Lu, M.; Song, C.; Wan, B., Influence of prepolymer molecular weight on the rheology and kinetics of HEUR-thickened Latex Suspensions. *Progress in Organic Coatings* **2021**, *156*, 106223.
35. Olesen, K. R.; Bassett, D. R.; Wilkerson, C. L., Surfactant co-thickening in model associative polymers. *Progress in Organic Coatings* **1999**, *35* (1-4), 161-170.
36. Wan Ishak, W. H.; Ahmad, I.; Ramli, S.; Mohd Amin, M. C. I., Gamma irradiation-assisted synthesis of cellulose nanocrystal-reinforced gelatin hydrogels. *Nanomaterials* **2018**, *8* (10), 749.
37. Podsiadlo, P.; Kaushik, A. K.; Arruda, E. M.; Waas, A. M.; Shim, B. S.; Xu, J.; Nandivada, H.; Pumplun, B. G.; Lahann, J.; Ramamoorthy, A., Ultrastrong and stiff layered polymer nanocomposites. *Science* **2007**, *318* (5847), 80-83.
38. Visanko, M.; Liimatainen, H.; Sirviö, J. A.; Mikkonen, K. S.; Tenkanen, M.; Sliz, R.; Hormi, O.; Niinimäki, J., Butylamino-functionalized cellulose nanocrystal films: Barrier properties and mechanical strength. *RSC Advances* **2015**, *5* (20), 15140-15146.
39. Lossada, F.; Guo, J.; Jiao, D.; Groeer, S.; Bourgeat-Lami, E.; Montarnal, D.; Walther, A., Vitrimer chemistry meets cellulose nanofibrils: bioinspired nanopapers with high water resistance and strong adhesion. *Biomacromolecules* **2018**, *20* (2), 1045-1055.
40. Shrestha, S.; Diaz, J. A.; Ghanbari, S.; Youngblood, J. P., Hygroscopic swelling determination of cellulose nanocrystal (CNC) films by polarized light microscopy digital image correlation. *Biomacromolecules* **2017**, *18* (5), 1482-1490.

## Appendix D

Table D1. DLS data of latexes directly after synthesis and after 11 months of storage at 4 °C.

Latex	Size	PDI	Size	PDI	$\Delta$ Size	Size	PDI	$\Delta$ Size
	initial (nm)	initial	aged (nm)	aged	aged (nm)	freeze-thaw (nm)	freeze-thaw	freeze-thaw (nm)
Latex10	549	0.264	557	0.292	+8	664	0.403	+115
Latex25	187	0.010	182	0.061	-5	230	0.206	+43
Latex50	115	0.090	114	0.031	-1	109	0.021	-6
Latex2OA	136	0.142	132 <sup>a</sup>	0.117 <sup>a</sup>	-4	385	0.469	+249

<sup>a</sup> DLS spectrum was measured after 4 months of storage at 4 °C.

Table D2. Latex stability evaluation by freeze-thaw test, addition of 1 equivalent of salt solution and ethanol.

Latex	Freeze-thaw test	1.0 M NaCl	0.1 M MgSO <sub>4</sub>	Ethanol
Latex10	+	+	+	+
Latex25	+	+	+	+
Latex50	+	+	+	+
Latex2OA	-	+	+	+

+ Macroscopically stable, no phase separation

- Macroscopically unstable, phase separation

Table D3. Surface properties of the synthesized latexes.

Latex	Weight fraction POEGA in feed <sup>a</sup> (%)	Unreacted surfactant (in supernatant) (%)	Surface tension (mN/m)
Latex10	12.5	35.0	46.6
Latex25	12.0	38.2	44.8
Latex50	11.3	39.5	49.3
Latex2OA	11.4	45.5	49.1

<sup>a</sup> Relative to monomers.

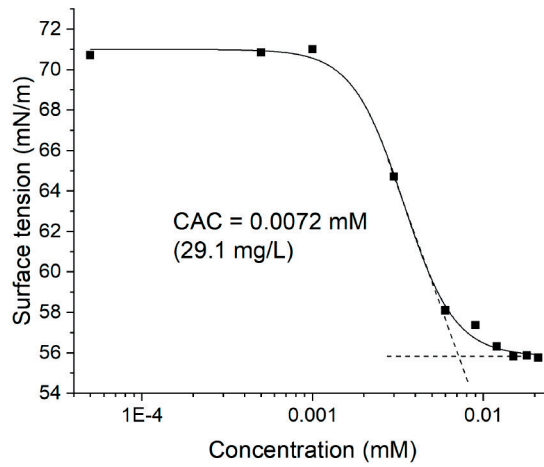


Figure D1. Surface tension as a function of the concentration for the POEGA macro-RAFT agent stabilizer.

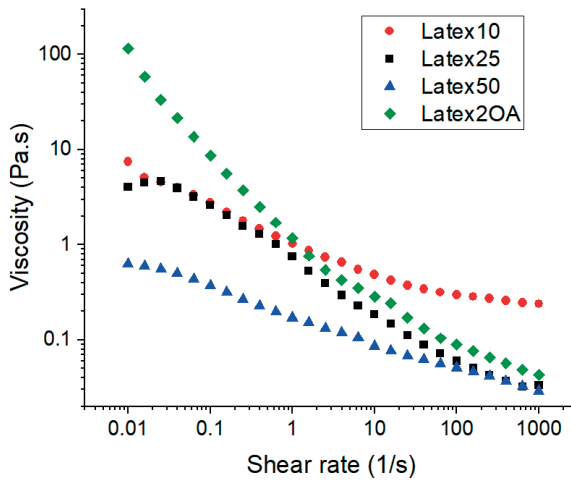


Figure D2. Rheology of the latexes in this work. Flow sweep measurement.

Table D4. Results of the freestanding films after 40 minutes UV irradiation from the synthesized latexes with various amount of CNC loading.

Code	CNC (wt%)	E (MPa)	$\sigma_{\max}$ (MPa)	$\epsilon$ (%)	Water uptake <sup>a</sup> (%)	Contact angle (°)	Gel content THF <sup>b</sup> (%)	Gel content H <sub>2</sub> O <sup>b</sup> (%)
Latex10	0	749 ± 85	22.2 ± 1.6	12.4 ± 2.2	7.1 ± 0.9	71.3 ± 1.1	99.2	95.2
	1	641 ± 96	18.8 ± 1.6	9.5 ± 3.4	7.4 ± 0.5	60.3 ± 4.2	97.0	95.1
	9	1435 ± 62	23.7 ± 0.9	4.9 ± 0.9	9.5 ± 0.5	43.9 ± 3.1	97.8	94.9
Latex25	0	1052 ± 47	27.2 ± 2.1	5.8 ± 1.0	5.8 ± 0.2	83.7 ± 2.0	98.2	94.9
	1	833 ± 101	27.6 ± 3.5	10.4 ± 2.2	5.8 ± 0.2	86.3 ± 1.6	97.1	95.4
	9	1339 ± 220	31.6 ± 1.0	8.2 ± 1.4	7.5 ± 0.3	86.7 ± 3.8	98.4	95.0
Latex50	0	1248 ± 117	32.4 ± 2.0	5.4 ± 1.0	4.1 ± 1.2	94.2 ± 2.8	99.7	95.6
Latex-20A	0	63 ± 16	4.5 ± 0.5	13.0 ± 1.8	4.5 ± 0.5	94.7 ± 0.8	99.8	95.4
	1	86 ± 13	5.3 ± 0.3	12.3 ± 0.9	3.6 ± 0.4	99.1 ± 1.8	97.1	95.4
	9	277 ± 16	9.6 ± 1.1	13.1 ± 2.6	6.5 ± 1.0	91.6 ± 2.4	97.7	95.5
	18	702 ± 42	20.5 ± 1.5	16.0 ± 3.2	6.4 ± 0.4	104.6 ± 1.5	97.7	95.5
	28	1386 ± 170	28.0 ± 2.9	8.0 ± 1.6	7.7 ± 0.3	104.1 ± 1.4	98.1	95.7
	40	3075 ± 272	50.8 ± 3.9	5.4 ± 1.2	10.3 ± 0.7	95.0 ± 4.5	99.0	93.6
	60	5018 ± 469	66.9 ± 0.8	2.5 ± 0.1	30.6 ± 0.2	77.4 ± 2.9	99.8	94.1
	80	8330 ± 798	79.4 ± 19.6	1.3 ± 0.4	88.1 ± 4.4	91.4 ± 5.0	99.8	93.9

<sup>a</sup> After immersion in H<sub>2</sub>O for 48h. <sup>b</sup> After 24 hours Soxhlet extraction. The errors reported are the standard deviation between repeated measurements.

Table D5. Tensile properties of freestanding films.

Code	Curing time (min)	E (MPa)	$\sigma_{\max}$ (MPa)	$\epsilon$ (%)
Latex10	20	370 ± 49	12.5 ± 0.7	11.0 ± 1.6
	10	136 ± 8.0	9.0 ± 1.1	34.7 ± 4.4
	5	24 ± 7.7	4.2 ± 1.1	60.3 ± 7.6
	0	1.8 ± 0.7	0.6 ± 0.1	80 ± 32.3
Latex25	60	965 ± 65	25.6 ± 1.5	5.7 ± 0.9
	<sup>a</sup> 40	721 ± 39	21.4 ± 0.9	11.3 ± 3.5

<sup>a</sup> Conditions were the same as Latex25 native film but the film thickness was about three times thicker (0.61 ± 0.06 mm).

Table D6. Properties of the reference latex containing 10 mol% 4CPA.

Latex	Molar feed ratio			Time (min)	Monomer conversion (%)			$T_g$ (°C)	Gel (%)	Size (nm)	PDI	Solids <sup>a</sup> (%)
	4CPA	THFA	IBOA		4CPA	THFA	IBOA					
RefLatex	10	80	10	120	99	97	99	-8.8	84	184	0.108	30

<sup>a</sup> Theoretical amount.

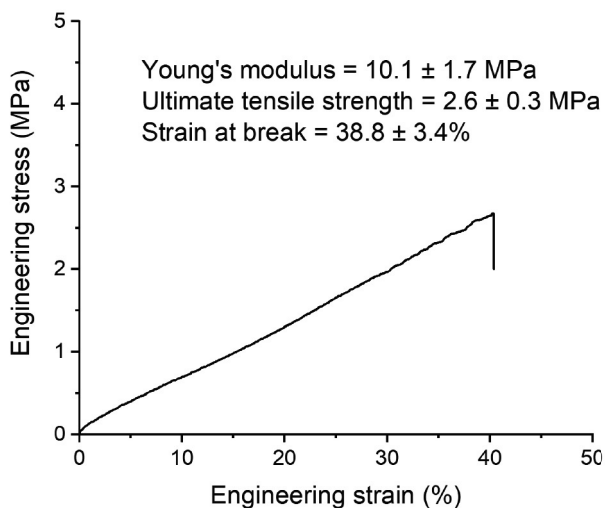


Figure D3. Tensile graph of the reference latex containing 10 mol% 4CPA.

Table D7. Overview of the TGA data of the unmodified and cross-linked freestanding films.

Latex	UV curing time (min)	T <sub>5%</sub> (°C)	Residue (%)
Latex10	0	256	5.3
	40	248	8.7
Latex25	0	251	6.2
	40	239	7.8
Latex50	0	258	6.0
	40	240	7.9
Latex2OA	0	259	6.5
	40	225	8.2

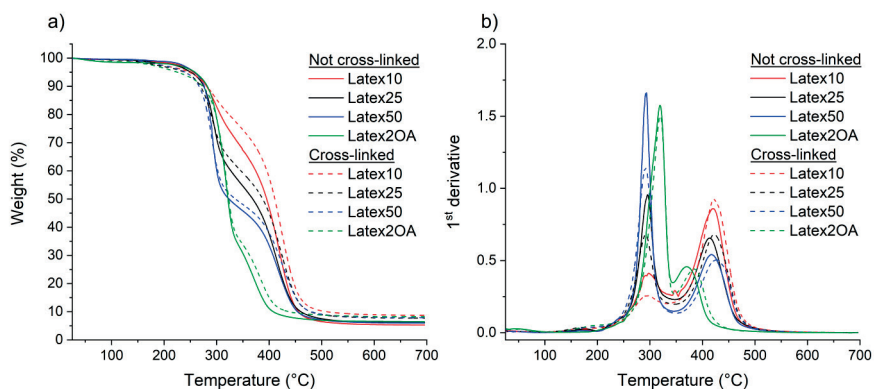


Figure D4. TGA results of unmodified and cross-linked freestanding films. a) Weight loss graph. b) 1<sup>st</sup> derivative as a function of the temperature.

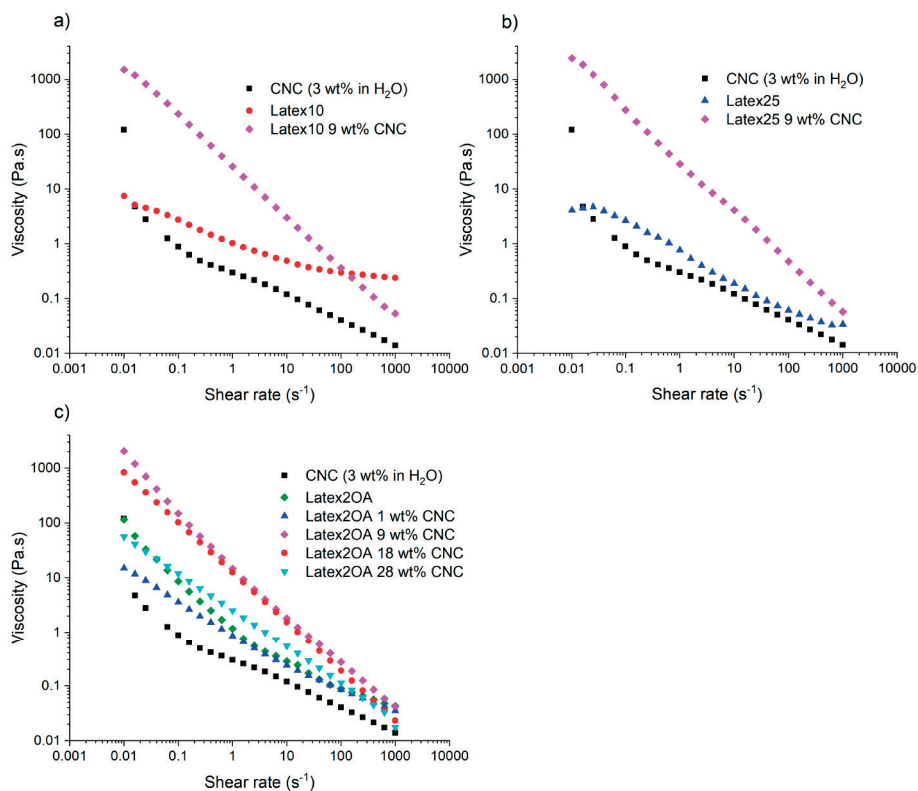


Figure D5. Flow sweep measurements of latex mixtures with 3 wt% CNC dispersion. a) Latex10. b) Latex25. c) Latex2OA.

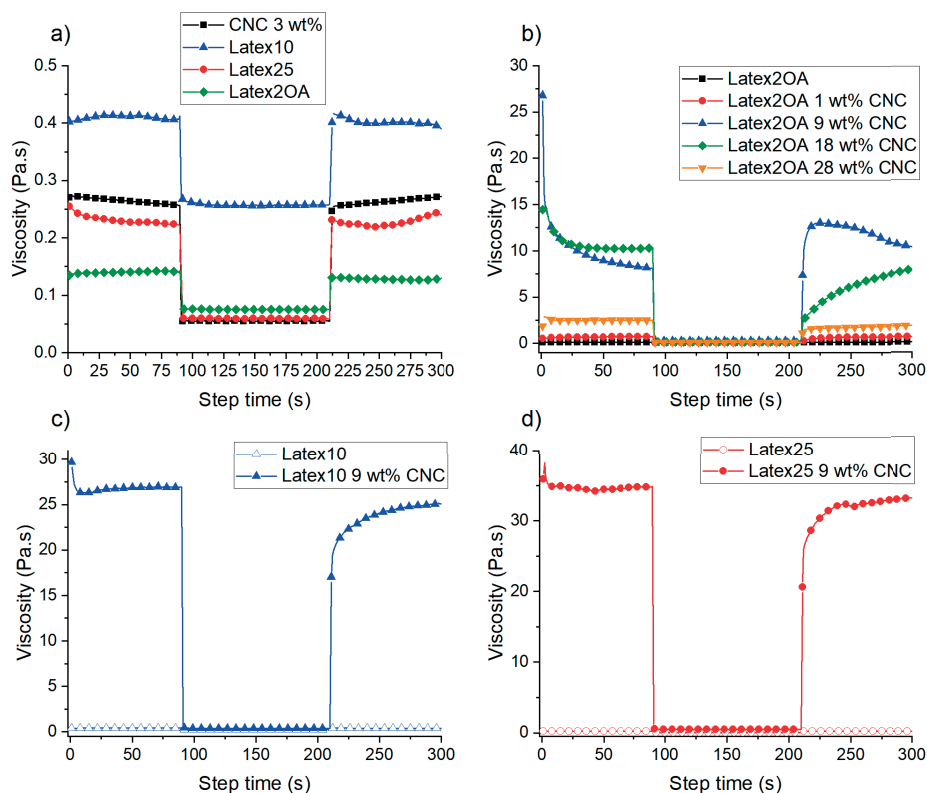


Figure D6. 3ITT curves alternating between low shear rate of 1 s<sup>-1</sup> for 90 s, and a high shear rate of 100 s<sup>-1</sup> for 120 s. a) The latexes and 3 wt% CNC dispersion. b) Latex2OA containing various amounts of CNC relative to solids. c) Latex10 containing 0 and 9 wt% CNC relative to solids. d) Latex25 containing 0 and 9 wt% CNC relative to solids.

Table D8. Viscosity recovery data from the 3ITT of latex mixtures with 3 wt% CNC dispersion.

Latex	CNC (wt%)	$\eta_e$ (Pa.s) at		$\Delta\eta_e$ (Pa.s)	$\eta$ (Pa.s) recovery after			$\eta_{(90-10)s}$ (Pa.s)
		1 s <sup>-1</sup>	100 s <sup>-1</sup>		1 s	10 s	90 s	
Latex10	9	26.9	0.4	26.5	17.0 (63%)	21.7 (81%)	25.1 (93%)	3.4
Latex25	9	34.8	0.5	34.3	20.6 (59%)	29.2 (84%)	33.2 (95%)	4.0
Latex2OA	1	0.7	0.1	0.6	0.3 (43%)	0.5 (71%)	0.7 (100%)	0.2
	9	8.2	0.3	7.9	7.4 (90%)	12.9 (157%)	10.4 (127%)	-2.5
	18	10.3	0.2	10.1	2.2 (21%)	3.7 (36%)	8.0 (78%)	4.3
	28	2.5	0.1	2.4	1.1 (44%)	1.6 (64%)	1.9 (76%)	0.3

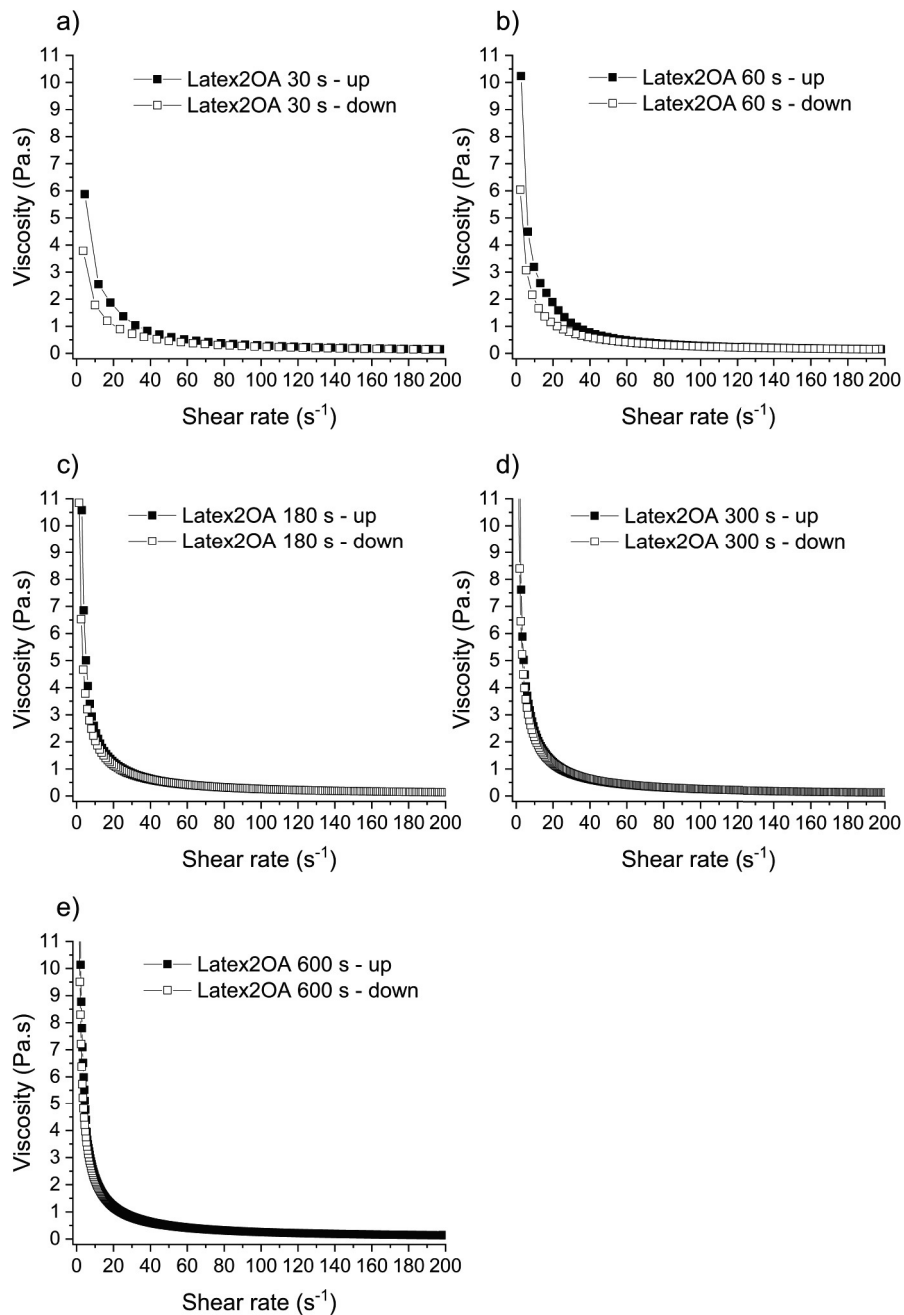


Figure D7. Rheology hysteresis curves of Latex2OA containing 9 wt% CNC, investigating the influence of the step time. a) 30s. b) 60 s. c) 180s. d) 300 s. e) 600 s.



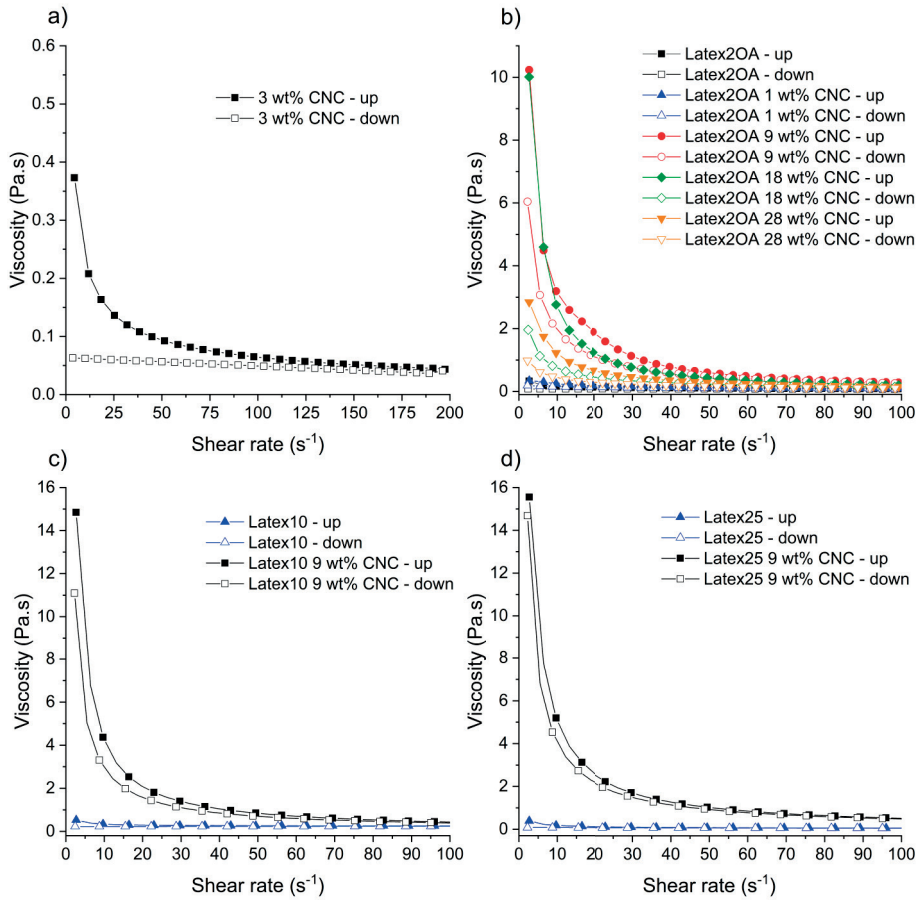


Figure D8. Rheology hysteresis loop curves with a step time of 60 s of a) 3 wt% CNC dispersion. b) Latex20A mixed with various amount of CNC dispersion. c) Latex10 mixed with 9 wt% CNC dispersion. d) Latex25 mixed with 9 wt% CNC dispersion.

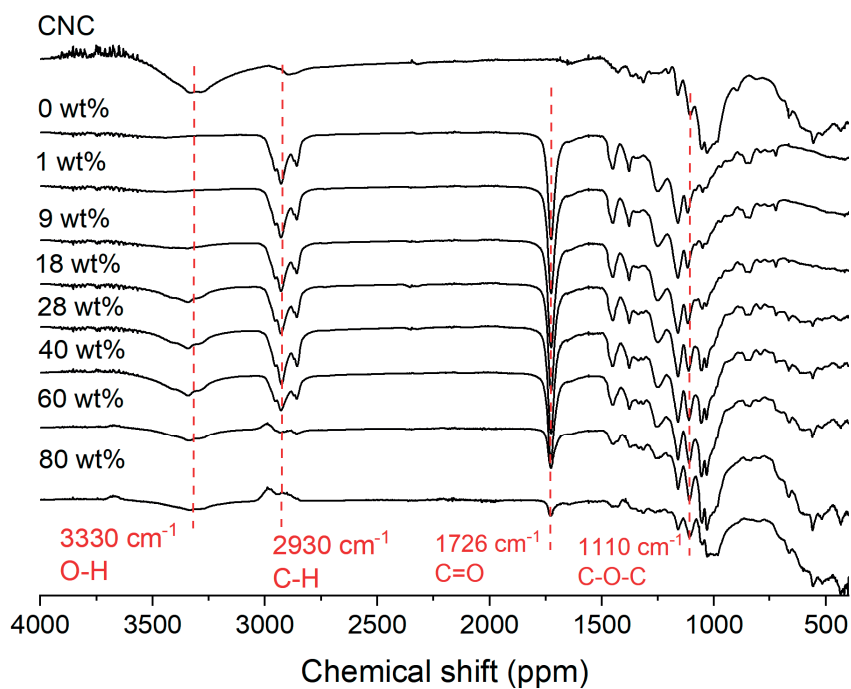


Figure D9. Overlay of FTIR spectra of the CNC loaded films.

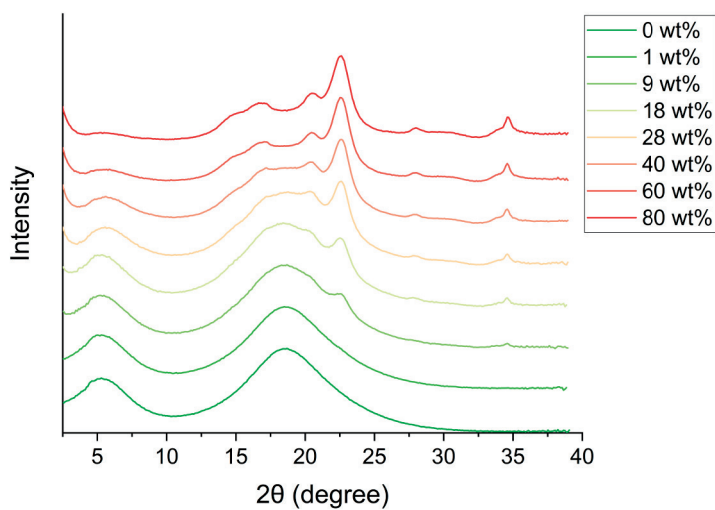
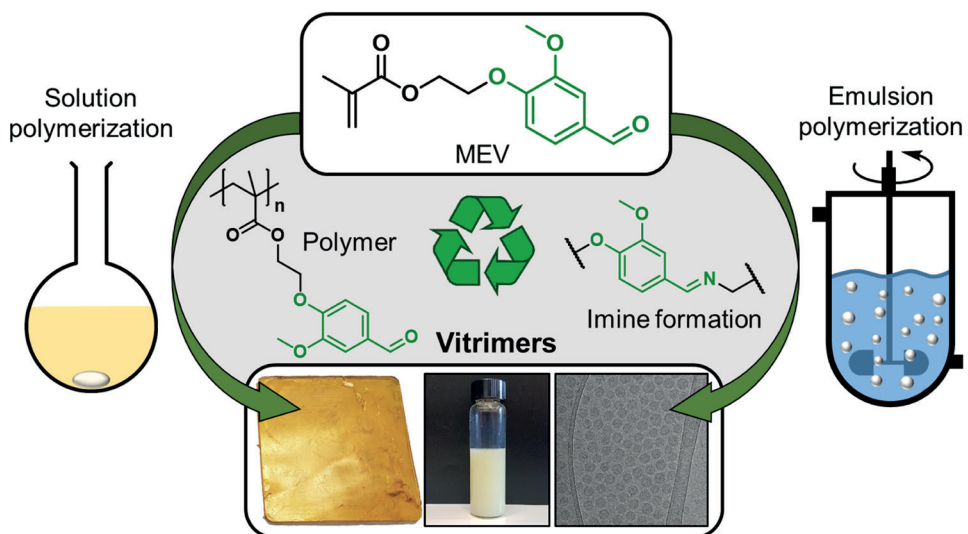


Figure D10. Overlay of 1D WAXD curves of the CNC loaded films.



# 6



---

## Chapter 6 Synthesis and Characterization of Water-borne Vanillin Polymethacrylates Containing Dynamic Imine Cross-links

---

This chapter is based on the following publication:

Stouten, J., de Roy, M. K., & Bernaerts, K. V. (2023). Synthesis and Characterization of Water-borne Vanillin Derived Copolymers Containing Dynamic Imine Cross-links. *Materials Today Sustainability*, 100396. DOI: 10.1016/j.mtsust.2023.100396

### Abstract

In the effort towards the production of circular plastics, the use of lignin derived aromatic building blocks such as vanillin is interesting due to their high amount of functional groups. Nonetheless, the water-borne polymerization of acrylic monomers derived from vanillin is still lacking. Vanillin can be readily functionalized with a methacrylate group for the radical polymerization to yield polymers containing functional aldehyde side groups. The functionality can be exploited via imine formation to produce vitrimers, a class of recyclable cross-linked polymers. Besides recycling, synthesis via a water-borne emulsion polymerization is desired to reduce the negative contribution of solvents on the environment and health. In the present work, polymethacrylates based on 2-(methacryloyloxy)ethyl vanillin and 2-octyl acrylate were synthesized via a polymerization induced self-assembly approach to produce a water-borne latex. A latex with a small particle size (49 nm) and solid content of 31 wt% was obtained. For comparative purposes, a similar polymer was synthesized via solution polymerization. Both polymers were cross-linked using a multifunctional amine to produce recyclable imine vitrimers. This research investigates the unique combination of water-borne synthesis and vitrimer polymers, and therefore contributes to future development of vitrimer latex products such as coatings and films.

## Introduction

In the effort to improve the global waste management of plastics, the research towards the production of circular polymer materials has become increasingly relevant. Therefore, thermosetting polymers are of special interest due to their non-recyclability, resulting in single use products. Recently, a new class of cross-linked polymers was invented, called vitrimers.<sup>1</sup> Vitrimers are a class of covalent adaptable networks (CAN's) and contain covalent dynamic cross-links that can exchange under the influence of external stimuli such as heat, and light, enabling recycling under such conditions.<sup>2</sup> To achieve this, many different dynamic covalent bonds such as imines,<sup>3</sup> esters,<sup>4</sup> and vinylogous urethanes<sup>5</sup> have recently been implemented as cross-links in polymers. Especially imine vitrimers are of interest due to their facile synthesis, unique interaction with moisture, and rapid bond exchange.<sup>2-3</sup>

Besides end-of-life issues of conventional polymer systems, the use of biobased feedstock is also relevant for the production of circular plastics. Especially the resourcing of biobased aromatic monomers for plastics is challenging, and is mainly based on lignin depolymerisation. The most prevalent building block originating from lignin is vanillin.<sup>6</sup> The aldehyde functionality of vanillin has previously been employed in the production of vitrimers based on systems including polyimines,<sup>7</sup> curable vinyl resins,<sup>8</sup> polyurethanes,<sup>9</sup> and epoxy resins.<sup>10-11</sup> However, the water-borne emulsion polymerization of vanillin (meth)acrylate esters has not been properly investigated. In one recent case, the miniemulsion copolymerization of vanillin methacrylate was described, but the vanillin groups were not employed for further modification.<sup>12</sup> In general, the research on water-borne synthesis of biobased aromatic vinyl monomers is lacking.<sup>13</sup>

In order to yield polymethacrylates of vanillin, esterification of the phenol group with methacrylic acid is performed, followed by radical polymerization. This has been demonstrated in solution.<sup>14</sup> However, the transfer from solution to a water-borne synthesis is not always straightforward. During synthesis and storage of the latex, the monomers need to be hydrolytically stable. In addition, when keeping the application of latexes as films and coatings in mind, film formation at ambient temperature is generally desired. Therefore, in this work, we investigate the water-borne polymerization of 2-(methacryloyloxy)ethyl vanillin (MEV) containing an ethylene oxide segment (Figure 6.1a). Aliphatic esters typically display better hydrolytic stability compared to phenolic esters.<sup>15</sup> Furthermore, the ethylene oxide segment is introduced to reduce the glass transition temperature ( $T_g$ ) of the resulting polymer.

The combination of the aforementioned water-borne synthesis together with the use of biobased monomers for the production of recyclable vitrimers is required to produce circular materials. In this work, the emulsion polymerization was carried out via a polymerization induced self-assembly (PISA) process using a macro-RAFT agent based on poly(oligo(ethylene glycol) methyl ether methacrylate) (POEGMA) (Figure 6.1a).<sup>16</sup> In order to further tune and reduce the  $T_g$ , copolymerization with the biobased 2-octyl acrylate (2OA) (castor oil derived) was investigated. Analogous to latex synthesis, a comparable

polymer was synthesized in solution. Both polymers obtained from each synthesis method will be cross-linked using the trifunctional tris(2-aminoethyl) amine (TREN) by imine formation (Figure 6.1b). Imine bonds show thermal induced dynamic exchange via metathesis reactions. In the case of the presence of an excess of amine, also amine exchange reactions are possible. Imine bonds can also be hydrolyzed with water. The mechanical, thermal, and rheological properties of the imine vitrimers synthesized in this chapter were investigated. The vitrimers can be mechanically recycled through grinding and pressing at elevated temperature.

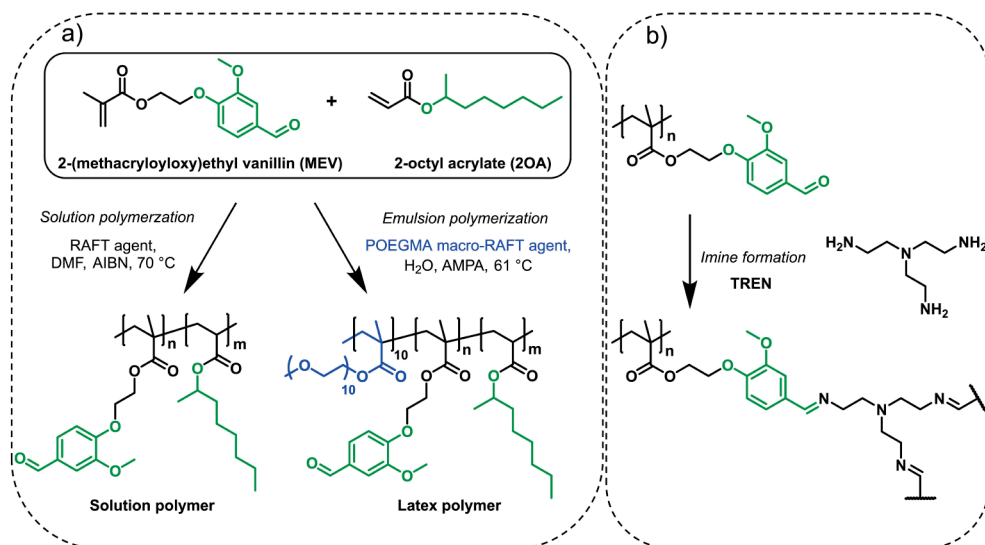


Figure 6.1. a) Reaction scheme for the synthesis of poly(MEV-co-2OA) via solution polymerization and via polymerization induced self-assembly. b) Reaction scheme for the production of vitrimers via cross-linking with TREN to obtain reversible imine bonds.

## Experimental section

### Materials

Azobisisobutyronitrile (AIBN, Sigma-Aldrich) was recrystallized from methanol prior to use. 2-octyl acrylate (2OA, >98%, abcr), and oligo(ethylene glycol) methyl ether methacrylate (OEGMA<sub>500</sub>, average  $M_n = 500$  g/mol, >95%, Sigma-Aldrich) were passed over a basic alumina column to remove the inhibitor prior to use. Tris(2-aminoethyl) amine (TREN, 96% Acros), naphthalene (>99%, Alfa Aesar), 1,3,5-trioxane (>99%, Sigma-Aldrich), 2,2'-azobis[2-(2-imidazolin-2-yl)propane] dihydrochloride (VA-044, TCI, >98.0%), 2,2'-azobis[2-methylpropionamide] dihydrochloride (AMPA, >97%, Sigma-Aldrich), 4-cyano-4-[(dodecylsulfanylthiocarbonyl)sulfanyl]pentanoic acid (>97.0%, TCI), 4-cyano-4-(phenylcarbonothioylthio)pentanoic acid (>95%, TCI), vanillin (99%, Sigma-Aldrich), ethylene carbonate (98%, Sigma-Aldrich), methacrylic anhydride (94%, Sigma-Aldrich), triethylamine (reagent grade, Fischer), 4-methoxyphenol (MEHQ, 99%, Sigma-

Aldrich), and chloroform-D ( $\text{CDCl}_3$ , 99.8%, Cambridge Isotope Laboratories) were used as received. All solvents were obtained from Biosolve and were used as received.

### **Synthesis of 2-(methacryloyloxy)ethyl vanillin (MEV)**

#### *Preparation of 4-(2-hydroxy)ethyl vanillin*

A mixture of vanillin (400.0 g, 2.63 mol),  $\text{K}_2\text{CO}_3$  (363.4 g, 2.63 mol) and ethylene carbonate (252.3 g, 2.87 mol) in dry DMF (3.9 l) was stirred for 24 h at 110 °C under nitrogen atmosphere. The reaction mixture was cooled to room temperature and drained from the reactor. A portion of the reaction mixture (1.5 L) was diluted with  $\text{H}_2\text{O}$  (0.9 L), and the resulting solution was extracted with DCM ( $3 \times 0.7$  L). The combined organic layers were washed with brine ( $2 \times 0.7$  L) and concentrated under reduced pressure (5 mbar, 50 °C). The rest of the reaction mixture (~3 L) was split in two equal portions, and each portion was processed as described for the first part. After extractive work-up, an off-white to yellow solid (643.61 g) was obtained.

This protocol was repeated once to have sufficient starting material for the preparation of 500 g MEV. The amount of 4-(2-hydroxy)ethyl vanillin obtained in the second reaction was 609.71 g.

The crude 4-(2-hydroxy)ethyl vanillin from both reactions was combined (1253.32 g). Diethyl ether (2.5 L) was added and the solids were crushed, and stirred mechanically for 2 h. The solids were recovered by filtration, washed with a small volume of diethyl ether and dried overnight in a vacuum oven (6 mbar, 40 °C). Yield: 768.17 g (3.92 mol; 74.6%).

#### *Preparation of 2-(methacryloyloxy)ethyl vanillin (MEV)*

Under nitrogen atmosphere, methacrylic anhydride (273.3 mL, 1.83 mol) was added dropwise to a stirred solution of 4-(2-hydroxy)ethyl vanillin (300.0 g, 1.53 mol), DMAP (0.93 g, 7.65 mmol) and triethylamine (302.6 mL, 2.17 mol) in dry DCM (2.5 L) at room temperature. The reaction mixture was stirred 18 h, after which it was washed subsequently with 2M HCl (1.5 L), saturated  $\text{NaHCO}_3$  (1.5 L) and brine (1.5 L). The organic phase was dried over  $\text{Na}_2\text{SO}_4$ . The drying agent was filtered, MEHQ (44 mg) was added to the filtrate to act as a stabilizer during storage, and the solvent was removed under reduced pressure (400 mbar, 30 °C). The residue was dried under high vacuum, protected from light. Yield: 423.7 g (1.60 mol; 104.9%); ~105 ppm MEHQ.

This protocol was repeated. The total amount of 2-(methacryloyloxy)ethyl vanillin obtained was 807.33 g (3.05 mol; 100%). Because this material still contained traces of methacrylic anhydride and minor traces of other impurities, it was further purified by trituration in diethyl ether.

The combined solids of both batches were crushed and trituated in diethyl ether (800 mL), and stirred mechanically for 1 h. The solids were filtered off, washed with a small volume of diethyl ether and dried under high vacuum, protected from light.



Yield: 652.67 g (2.47 mol; 80.8%). Melting point: 75.4 °C. LC-MS: theoretical mass = 264 g/mol, Mass found:  $[M+H]^+$  = 265 g/mol. The proton and carbon NMR spectra are shown in Figures E1 and E2.

### Homopolymerization of MEV

To a 25 mL Schlenk flask equipped with magnetic stir bar was added, MEV (1500 mg, 5.68 mmol, 100 eq.), AIBN (1 mg, 0.006 mmol, 0.1 eq.), 4-cyano-4-[(phenylcarbonothioyl)thio]pentanoic acid (16.8 mg, 0.06 mmol, 1 eq.), and DMF (3.635 mL). The mixture was homogenized and degassed by three consecutive freeze-pump-thaw cycles. The flask was sealed with a nitrogen-filled balloon and placed in a 70 °C oil bath whilst stirring. After 16 hours, the flask was cooled to room temperature and the polymer was precipitated three times in a 20-fold excess of diethyl ether. The polymer was dried overnight in a 50 °C vacuum oven and a pale pink glassy material was obtained. Yield: 930.8 mg (62%).

### Determination of the reactivity ratios

The monomer reactivity ratios between MEV and 2OA were determined using the Jaacks method.<sup>17</sup> Two polymerizations were carried out, each with an excess (95:5) of one of the monomers, MEV or 2OA. In an exemplary synthesis, a 10 mL Schlenk flask equipped with magnetic stirrer was filled with MEV (396 mg, 1.5 mmol, 500 eq.), 2OA (13.8 mg, 0.075 mmol, 25 eq.), 4-cyano-4-[(dodecylsulfanylthiocarbonyl)sulfanyl]pentanoic acid (12.1 mg, 0.03 mmol, 10 eq.), AIBN (2.5 mg, 0.015 mmol, 5 eq.), DMF (1.725 mL), and naphthalene (10 mg, as internal standard). The mixture was degassed by sparging with nitrogen for at least 30 minutes. The flask was sealed with a nitrogen-filled balloon and the polymerization was started by placing the flask in a 70 °C oil bath. The monomer conversion was followed by GC-FID, by observing the disappearance of the monomer peaks relative to the internal standard peak. The reactivity ratios were determined from the resulting Jaacks plots.

### Solution polymer: copolymerization of MEV with 2OA in solution

To a 250 mL Schlenk flask equipped with magnetic stir bar was added, MEV (12.0 g, 45.4 mmol, 40 eq.), 2OA (15.6 mL, 72 mmol, 60 eq.), AIBN (100 mg, 0.6 mmol, 0.5 eq.), 4-cyano-4-[(dodecylsulfanylthiocarbonyl)sulfanyl]pentanoic acid (484 mg, 1.2 mmol, 1 eq.), and DMF (92 mL). The mixture was homogenized and degassed by sparging with nitrogen for about 30 minutes. The flask was sealed with a nitrogen-filled balloon and placed in a 70 °C oil bath. A sample was taken for GC-FID analysis. During the reaction, samples were taken at several time intervals. When the monomer conversion plateaued, the reaction was stopped. After 390 minutes, the mixture was cooled to room temperature and the polymer was precipitated three times in a 10-fold excess of methanol. The polymer was dried overnight in a 40 °C vacuum oven and a pale yellow sticky solid was obtained. Yield: 19.92 g (76.2%).

### Synthesis of Poly(oligo(ethylene glycol) methyl ether methacrylate) (POEGMA) macro-RAFT agent

To a 250 mL Schlenk flask equipped with magnetic stir bar was added, OEGMA<sub>500</sub> (33.0 mL, 60 mmol, 10 eq.), VA-044 (200 mg, 0.6 mmol, 0.1 eq.), 4-cyano-4-[(dodecylsulfanylthiocarbonyl)sulfanyl]pentanoic acid (2460 mg, 6.0 mmol, 1 eq.), water (48 mL), and 1,4-dioxane (72 mL). The mixture was homogenized and degassed by sparging with nitrogen for about 30 minutes. The flask was sealed with a nitrogen-filled balloon and placed in a 46 °C oil bath. After 24 hours the mixture was cooled to room temperature and the polymer was precipitated twice in hexane and recovered by centrifugation. The polymer was dried overnight in a 40 °C vacuum oven and a pale yellow viscous liquid was obtained. <sup>1</sup>H NMR monomer conversion = 100%,  $M_{n, \text{theo}} = 5.4 \text{ kg/mol}$ ,  $M_{n, \text{GPC}} = 5.4 \text{ kg/mol}$ ,  $\bar{D} = 1.12$ .

### Latex polymer: copolymerization of MEV with 2OA via RAFT PISA

To a 500 mL 3-necked round-bottom flask was added, MEV (39.326 g, 148.8 mmol, 23.3 eq.), 2OA (54.0 mL, 256.5 mmol, 40.2 eq.), POEGMA macro-RAFT agent (34.462 g, 6.4 mmol, 1 eq.), and distilled water (270 mL). The flask was placed in a sonication bath (Branson 3800) and sonicated for 90 minutes. Afterwards, a mechanical, anchor shaped stirrer was attached and the mixture was stirred at 400 rpm while sparging with nitrogen for about 45 minutes. Meanwhile the initiator AMPA (818 mg, 3.0 mmol, 0.5 eq.) was dissolved in 10 mL water and also sparged with nitrogen. The flask containing the emulsified monomer mixture was equipped with a nitrogen inlet flow, maintaining an inert environment in the overhead space of the reactor. The flask was placed in a 61 °C oil bath and after 10 minutes, the initiator solution was injected in one shot to mark the start of the polymerization. After 3 hours, the mixture was cooled to room temperature and the latex was filtered over a 190 micron nylon filter and stored at 4 °C. The result was a pale yellow opaque latex.

### Cross-linking and film formation

#### *Solution polymer*

2 g of the solution polymer (containing 4 mmol aldehyde groups calculated from the monomer ratio in the final copolymer according to <sup>1</sup>H NMR) was dissolved in 10 mL THF and to the solution 200 μL TREN (containing a theoretical amount of 4 mmol amine groups) was added. The mixture was quickly homogenized and within one minute, the mixture turned into a hard gel. The gel was dried overnight in a 60 °C vacuum oven.

#### *Latex*

The latex (5.0 mL, 2.92 mmol aldehyde groups calculated from the monomer ratio in the final copolymer according to <sup>1</sup>H NMR) was diluted with 5 mL water. To the diluted latex was added 95 μL TREN (containing a theoretical amount of 1.90 mmol amine groups), and the mixture was homogenized. The mixture was poured into a circular PTFE evaporation dish with a diameter of 65 mm and dried for 18 days at room temperature. The evaporation

dish was covered to reduce the rate of evaporation. Afterwards, the film was dried overnight in a 40 °C oven and subsequently at 120 °C for 8 hours.

### Vitrimer recycling

The cross-linked polymers obtained from the solution or latex process were granulated into particles of several millimeters, and about 3 g was placed in a square steel mold with a dimension of 55 mm × 55 mm. The granules were pressed at 150 °C and 50 bar for 15 minutes for the solution polymer and the latex polymer for 50 minutes. The recycling was performed by granulating the square plate into particles of several millimeters and subsequent molding under the same conditions. After each cycle, a longer residence time in the press was required to achieve a homogenous film.

### Characterization

#### *Nuclear magnetic resonance (NMR) spectroscopy*

Structural characterization of the final copolymers and OEGMA monomer conversion determination was performed using <sup>1</sup>H NMR and <sup>13</sup>C NMR spectroscopy. <sup>1</sup>H NMR (300 MHz) and <sup>13</sup>C NMR (75 MHz) spectra were recorded on a Bruker Avance III HD Nanobay 300 MHz apparatus at 298K and with 16 scans. OEGMA conversion was determined by following the disappearance of OEGMA methacrylate group resonances relative to trioxane as the internal standard, which was added at the beginning of the polymerization. The latex polymer was dried in a 40 °C vacuum oven for 24 hours, prior to dissolution in CDCl<sub>3</sub>.

#### *Gas chromatography with flame ionization detection (GC-FID)*

GC-FID measurements were performed on a Shimadzu GC-2010 equipped with a Supelco SPB-1 capillary column (30 m × 0.25 mm × 0.25 μm film thickness). GC-FID was used to follow the disappearance of the individual monomers in the copolymerizations relative to naphthalene as the internal standard, which was added at the beginning of the polymerization. Reaction aliquots (3-4 drops) were dissolved in 1.5 mL THF. The temperature program was as follows: an initial temperature of 80 °C was maintained for 3 min and then increased to 140 °C with a heating rate of 10 °C/min. This temperature was maintained for 1 min and further increased to 300 °C with a heating rate of 20 °C/min and was maintained at 300 °C for 5 min (the total run time of 23 min). Prior to measurement, samples from both solvent and emulsion polymerization were diluted in THF. Several drops of the reaction mixture were dissolved in 1.5 mL THF.

#### *Liquid chromatography-mass spectrometry (LC-MS)*

LC-MS analysis was performed on a Shimadzu system equipped with a Shimadzu Nexera HPLC solvent delivery system (LC-30AD) with photo-diode array detector (PDA/SPD-M20A), evaporative light scattering detector (ELSD-LTII) and a single quadrupole mass spectrometer (LCMS 2020). The MS was attributed with a dual ionization source consisting of both electron spray ionization (ESI) and atmospheric pressure chemical ionization (APCI).

The separation was performed on Vision HT Classic C18 columns with 1.5  $\mu\text{m}$  pore size (3.5  $\mu\text{m}$ , 3 mm  $\times$  75 mm) at flow rate of 1 mL/min, an oven temperature of 30  $^{\circ}\text{C}$  and an injection volume of 10  $\mu\text{L}$ . A solvent gradient was applied starting from 95:5 water : acetonitrile for 2 minutes. Then, the composition was linearly changed over the course of 6 minutes to a 5:95 water : acetonitrile mixture, total run time: 11 minutes.

### *Gel permeation chromatography (GPC)*

GPC was used to determine the molar mass and the dispersity of the polymers. Approximately 5 mg of polymer was dissolved in 1.5 mL THF. The solution was filtered over a 0.2  $\mu\text{m}$  PTFE syringe filter. The molar masses were then measured on a Waters GPC equipped with a Waters 2414 refractive index detector. THF was used as the eluent at a flow rate of 1 mL/min. Three linear columns were used (Styragel HR1, Styragel HR4 and Styragel HR5) including a Styragel Guard column. Molecular masses are given relative to polystyrene standards.

### *Differential scanning calorimetry (DSC)*

The glass transition point of the polymers was measured on a Netzsch DSC 214 Polyma instrument. Prior to measurement, the samples were dried at 40  $^{\circ}\text{C}$  in a vacuum oven. The samples were heated in 2 cycles under nitrogen atmosphere from -70  $^{\circ}\text{C}$  to 200  $^{\circ}\text{C}$  with a rate of 10  $^{\circ}\text{C}/\text{min}$ . The second cycle was used for determination of the phase transition points. The inflection point was used for reporting of the  $T_g$ .

### *Thermogravimetric analysis (TGA)*

The thermal stability of the polymers was analyzed with TGA on a TA instruments Qseries, TGA Q500 with autosampler using a temperature ramp of 10  $^{\circ}\text{C}/\text{min}$  under nitrogen flow.

### *Dynamic light scattering (DLS)*

The particle size distribution of the latex was determined using DLS. The samples were measured on a Malvern Instruments Zetasizer Nano ZS DLS instrument at 25  $^{\circ}\text{C}$  and a fixed angle of 173 $^{\circ}$ . Prior to measurement, the latex was diluted with distilled water until a slightly opaque mixture was obtained.

### *Cryogenic electron microscopy (Cryo-TEM)*

The latex particles were visualized by Cryo-TEM. The latex was diluted with water to a concentration of 5 mg/mL. A thin aqueous film was formed by applying a 5  $\mu\text{L}$  droplet of the latex to a bare specimen grid. Glow-discharged holey carbon grids were used. After the application of the suspension, the grid was blotted against filter paper, leaving thin sample film spanning the grid holes. These films were vitrified by plunging the grid into ethane, which was kept at its melting point by liquid nitrogen, using a Vitrobot (Thermo Fisher Scientific Company, Eindhoven, Netherlands) and keeping the sample before freezing at 95% humidity. The vitreous sample films were transferred to a Tecnai Arctica cryo-electron

microscope (Thermo Fisher Scientific, Eindhoven, Netherlands). Images were taken at 200 kV with a field emission gun using a Falcon III direct electron detector.

### *Rheology*

Rheological stress relaxation experiments were performed on a MCR 702 TwinDrive rheometer (Anton Paar) equipped with an oven surrounding a parallel plate geometry (diameter of 12 mm, and an axial force of 2-10 N). Stress relaxation experiments were carried out at various temperatures by applying an initial angular strain of 1% to 3%, while recording the relaxation modulus over time. The characteristic relaxation time  $\tau^*$  (when  $G/G_0$  reached  $1/e$ ,  $\sim 0.37$  according to the Maxwell model for stress relaxation) was determined at several temperatures. The results were plotted in an Arrhenius equation from which the activation energy of each vitrimer was derived.

### *Gel content*

Gel content measurements were performed on the cross-linked polymers. A sample of dry polymer was accurately weighed ( $W_1$ ) and was then extracted in a Soxhlet setup using THF for 24 hours. Afterwards, the polymer was dried overnight in a 40 °C vacuum oven and weighed again ( $W_2$ ). The gel content was calculated as follows:

$$\text{Gel content} = \frac{W_2}{W_1} \times 100\%$$

### *Tensile test*

The mechanical performance of the cross-linked polymers was assessed by tensile testing. Tensile tests were performed on a Linkam micro tensile stage equipped with a 200N load cell. Casted films and pressed plates with a thickness of between 0.3 and 0.8 mm were cut into dog bone shaped specimens with dimensions of  $31 \times 2$  mm (length  $\times$  width), the broad part of the dog bone specimen had a width of 4 mm. The tensile tests were performed with a deformation rate of 33.3  $\mu\text{m/s}$ . All measurements were performed at room temperature. The Young's modulus of each measurement was determined between 0.2 and 0.6% strain. The values reported are the average of five tensile measurements and errors reported are the standard deviations.

### *Fourier-transform infrared (FTIR) spectroscopy*

FTIR spectra were recorded on a Shimadzu (MIRacle 10) spectrometer. Samples were measured by applying a sample on the ATR crystal and the spectra were recorded between 400  $\text{cm}^{-1}$  and 4000  $\text{cm}^{-1}$ , with a resolution of 4  $\text{cm}^{-1}$  and with 64 accumulations per spectrum.

### *Dynamic mechanical analysis (DMA)*

The  $T_a$  of the cross-linked films was obtained by recording a temperature ramp from 25 to 250 °C using a heating rate of 3 °C/min. The temperature ramp was performed in the tension mode on a DMA 1 STAR system (Mettler Toledo) with a frequency of 1.0 Hz, and an

amplitude of 1.0%. Creep recovery experiments were performed at an alternating stress of 0.28 MPa for 5 minutes and 0 MPa for 10 minutes. The cycle was repeated at 30 °C, 70 °C, and 100 °C.

## **Results and discussion**

### **Polymer synthesis in solution**

Homopolymerization of the target monomer MEV was initially performed under RAFT conditions. The reaction served to elucidate the thermal and structural properties of the final homopolymer of MEV. According to GPC, a polymer with a molecular weight of 24.3 kg/mol and a dispersity of 1.37 relative to polystyrene standards was obtained. The NMR spectrum of the purified polymer corresponded well with the proposed structure; with the intact aldehyde groups present (Figure E3). According to DSC, the  $T_g$  of the polymer was 76 °C (Figure E4), which is substantially lower than previously reported poly(vanillin methacrylate) polymer, which has a  $T_g$  of 110 °C.<sup>14</sup> The decrease in  $T_g$  is a result from the increased conformational freedom originating from the ethylene oxide segment between the methacrylate and vanillin group. Typical for poly(meth)acrylates, longer and more flexible side groups have a suppressing effect on the  $T_g$ .<sup>18</sup>

Typically, a low  $T_g$  is required in latex polymers in order to facilitate film formation during drying. Conventionally, a decrease in  $T_g$  is achieved by copolymerization with so called ‘soft monomers’ such as 2-ethylhexyl acrylate. Since we want to investigate biobased alternatives to these fossil based monomers, 2-octyl acrylate (2OA) was investigated as comonomer to further decrease the  $T_g$  of the resulting copolymer.<sup>19</sup> Because 2OA contains an acrylate group and MEV a methacrylate group, the reactivity during radical polymerization can differ significantly resulting in tapered polymers and subsequently vitrimers with unevenly distributed cross-links. Therefore, the reactivity ratios were determined (Figure 6.2b, Figure E5). In the copolymerization of MEV with 2OA reactivity ratios of 1.32 and 0.58 were obtained. With reactivity ratios of  $r_1 > 1$  and  $r_2 < 1$ , a copolymerization is obtained where MEV is being built into the chain faster than 2OA. The obtained values are in the range of what can be expected for an acrylate, methacrylate copolymerization.<sup>20</sup>

The copolymerization of MEV and 2OA was performed in solution and in water as a heterogeneous system. A molar feed ratio of MEV:2OA of 40:60 was selected to achieve a significant reduction in  $T_g$ , while maintaining enough functionality for cross-linking with a multifunctional amine. In both cases MEV shows a slightly faster reactivity (Figure 6.2a), as expected from the copolymerization parameters. In the solution polymerization, monomer conversions of 93% and 80% were obtained for MEV and 2OA, respectively. In the latex synthesis, (near) complete monomer conversions were obtained, which is essential since the latex serves as the final product and does not undergo any purification step, as is the case for the solution polymer.

The molecular weight of the purified polymer prepared via solution polymerization corresponds well with the theoretical molecular weight (Table 6.1), although a direct

comparison is unfair since GPC gives relative molecular weights. In case of the latex polymerization, GPC confirmed the chain extension of the macro-RAFT agent, showing a polymer peak shifted to lower elution volumes, containing a small shoulder resulting from unreacted macro-RAFT agent (Figure E6). The final molecular weight in GPC of the dried latex polymer was 9.9 kg/mol, which is slightly lower than the theoretical molecular weight, presumably caused by the presence of unreacted macro-RAFT agent in the GPC trace.

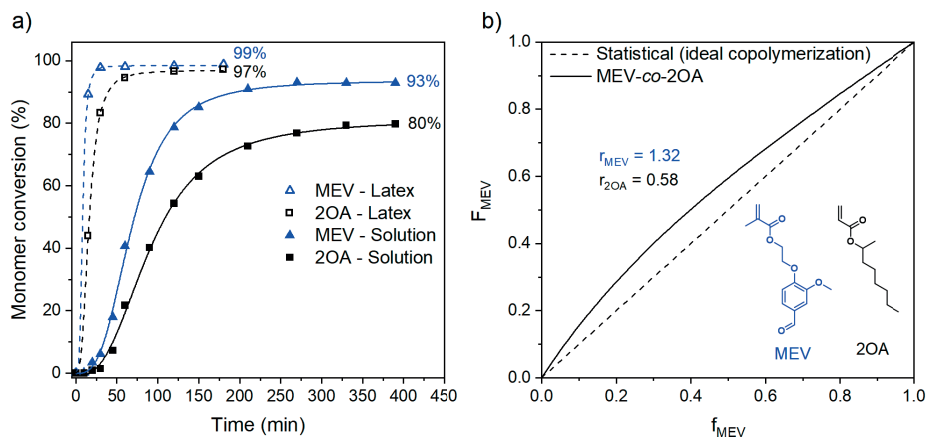


Figure 6.2. a) Plot showing the monomer conversion of MEV and 2OA in the latex and solution polymerization. b) Copolymerization plot of MEV and 2OA.

The copolymerization of MEV and 2OA proceeded well judging from the decrease in  $T_g$  observed relative to poly(MEV) (Table 6.1). The solution polymer had a  $T_g$  of 13 °C and the latex polymer a  $T_g$  of -16 °C according to DSC. The lower  $T_g$  observed in the latter can be related to the presence of a large fraction of POEGMA macro-RAFT agent (28 wt%), which is covalently attached to the polymer and can act as a plasticizer for the MEV-2OA copolymer. Another confirmation of the successful copolymerization of MEV with 2OA was provided by analysis of the  $^1H$  NMR spectra of the purified polymers. They showed a molar ratio between MEV and 2OA that corresponded well with the feed ratio of 40:60 mol% MEV:2OA (Table 6.1). In Figure 6.3a, The  $^1H$  NMR spectra of the copolymers originating from the solvent and water-borne process are shown. Similar to the homopolymer from MEV, the spectra match the proposed structures well, and the characteristic aldehyde resonance at 9.80 ppm matches the expected integral. In the case of the latex polymer, the resonances corresponding to the POEGMA macro-RAFT agent are also visible at 3.65 and 3.38 ppm.

Table 6.1. Characterization of the solution and latex polymer.

Polymer	Feed Eq. MEV:2OA:I (macro-)RAFT	$M_{n,theo}^a$ (kg/mol)	$M_{n,GPC}$ (kg/mol)	$\bar{D}$	$T_g$ (°C)	Molar ratio POEGMA:MEV: 2OA in copolymer <sup>b</sup>	Size cryo- TEM (nm)	Size DLS (nm)	Solids (wt%)
<i>Solution<sup>c</sup></i>									
poly(MEV <sub>37-co</sub> - 2OA <sub>48</sub> )	40:60:0.5:1	19.1	20.6	1.40	13	0:40:60	N/A	N/A	N/A
<i>Latex<sup>c</sup></i>									
Poly(POEGMA <sub>8-b-</sub> (MEV <sub>23-co</sub> -2OA <sub>39</sub> ))	23:40:0.5:1	18.8	9.9	1.31	-16	15:31:54	49 ± 5	71	31.2

<sup>a</sup> The theoretical molecular weight was calculated as follows:  $M_{n,theo} = \text{target DP}_{MEV} \times 264.28 \times \text{conversion}_{MEV} + \text{target DP}_{2OA} \times 184.28 \times \text{conversion}_{2OA} + MW_{(\text{macro-})RAFT}$ . <sup>b</sup> Calculated from the <sup>1</sup>H NMR spectra shown in Figure 6.3. The resonances at 9.80 ppm (MEV), 4.82 ppm (2OA), and 3.38 ppm (OEGMA) were taken for the calculation of the monomer ratio in the final copolymer. <sup>c</sup> Subscripts are DP calculated from  $DP_{th} \times \text{conversion}_{monomer}$

Further characterization of the off-white latex shown in Figure 6.3b, was performed by cryo-TEM and DLS. DLS analysis shows a distribution of small particles with an average size of 71 nm (Figure 6.3c). Since DLS measures the hydrodynamic radius of the latex particles, the actual size is typically smaller. This is visualized in cryo-TEM imaging (Figure 6.3d). The image shows the latex particles with spherical morphology and uniform in size. The average diameter measured was 49 ± 5 nm. The latex was colloiddally stable, showing no signs of phase separation, after 10 months of storage at 4 °C. According to DLS measurements, the size of the latex particles remained the same after 10 months, but the dispersity increased slightly (Figure 6.3c).



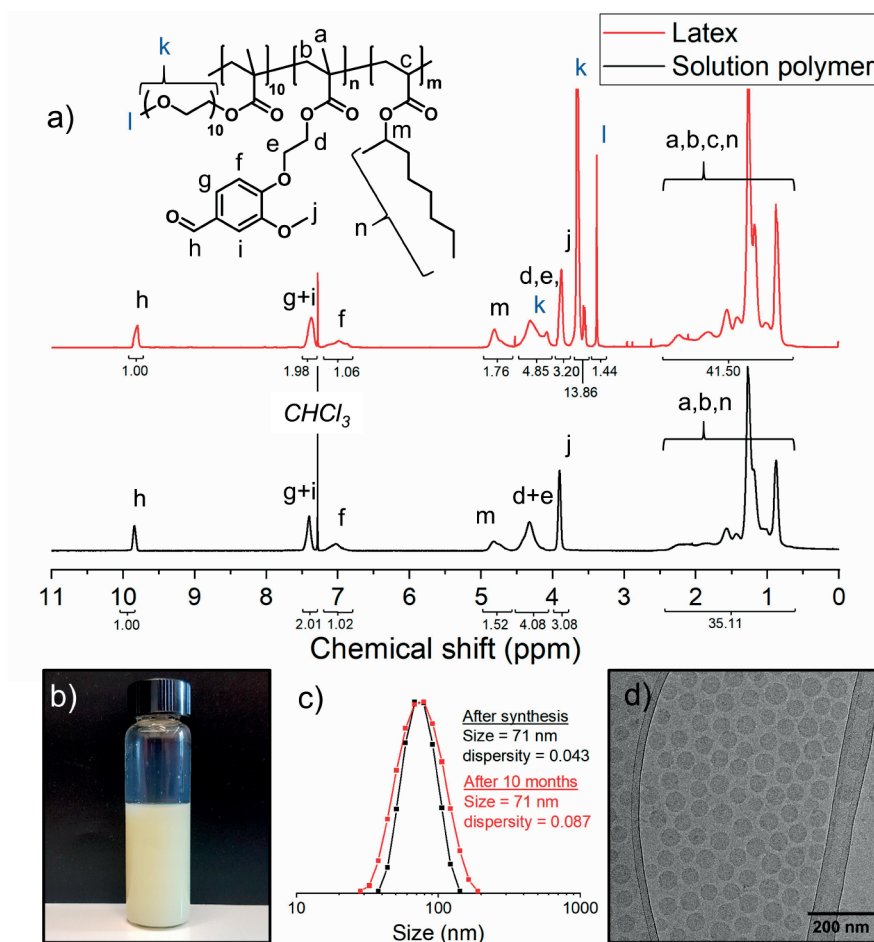


Figure 6.3. a) Overlay of the  $^1\text{H}$  NMR spectra of the solvent polymer after precipitation (containing no POEGMA macro-RAFT agent in the structure) and the latex polymer after drying (containing POEGMA macro-RAFT agent in the structure). b) Photograph of the latex. c) DLS spectrum of the latex. d) Cryo-TEM image of the latex.

### Cross-linking and film formation

Cross-linking of the aldehyde side groups of the solution and latex polymer was achieved by addition of the multifunctional amine tris(2-aminoethyl) amine (TREN). Cross-linking of the purified solution polymer was performed in THF solution, while the latex polymer was cross-linked in the absence of volatile organic compounds by dissolving the TREN in the latex followed by casting and drying. In principle, the ratio between amine-to-aldehyde groups was maintained at 1, in order to achieve complete cross-linking of the functional groups and facilitate metathesis reactions during recycling. However, film formation after casting of the latex containing an equivalent amount of TREN yielded inhomogeneous and brittle films.

Therefore, the amount of TREN added to the latex was decreased to yield an amine-to-aldehyde ratio of 0.67. The cross-linking, accompanied by the formation of imine groups and disappearance of aldehyde groups was followed by FTIR (Figure 6.4a). As a result of the cross-linking with TREN, the aldehyde vibration signal at  $1674\text{ cm}^{-1}$  disappears and an imine vibration appears at  $1643\text{ cm}^{-1}$  in the solvent polymer. In the case of the latex polymer, a small aldehyde peak remains visible as a result of the discrepancy in the amount of amine and aldehyde groups.

Following the cross-linking step, films were prepared for further characterization. The latex was casted and dried at room temperature, followed by drying at elevated temperature. The solution polymer was granulated and pressed into a film at  $150\text{ }^{\circ}\text{C}$  and 50 bar for 15 minutes. Samples were prepared for rheological characterization to determine the activation energy via stress relaxation experiments. On the samples, an angular strain was applied and the relaxation modulus ( $G$ ) was followed over time. The relaxation curves were obtained after normalization of the relaxation modulus ( $G/G_0$ ). The results are shown in Figure 6.4c-e. The relaxation time ( $\tau$ ) was determined at the point where  $G/G_0$  reached  $1/e$  ( $\sim 0.37$ ). Both vitrimers show rapid relaxation between  $110\text{ }^{\circ}\text{C}$  and  $150\text{ }^{\circ}\text{C}$ .

The calculated activation energies were  $57\text{ kJ/mol}$  for the cross-linked solution polymer and  $64\text{ kJ/mol}$  for the latex. These values correspond well with previously found activation energies for imine exchange vitrimers.<sup>21-22</sup> Interestingly, the stress relaxation curves show complete relaxation after 1000 s for the solution polymer, but to a small extent incomplete relaxation for the latex polymer. Incomplete relaxation can indicate the presence of permanent cross-links (Figure 6.4c and e). While some amount of permanent cross-links can improve properties such as creep resistance in vitrimers, too many, can result in poor reprocessability.<sup>23</sup> It is not known what exactly is the cause of those permanent cross-links, but it could be due to side reactions happening due to the excess aldehyde (Aldol condensation, Cannizzaro, oxidation to carboxylic acid and further reaction with amine to amide) or unknown crosslinking side reactions at the OEGMA chains upon processing at high temperature in the hot-press.

One of the major downsides of vitrimer materials is their low resistance to creep.<sup>24</sup> In Figure 6.4b, the creep recovery curves of the solution ( $T_{\alpha} = 68\text{ }^{\circ}\text{C}$ ) and latex vitrimer ( $T_{\alpha} = 73\text{ }^{\circ}\text{C}$ ) are shown. The materials were subjected to a constant stress of  $0.28\text{ MPa}$  for 300 s, followed by a recovery time of 600 s at several temperatures. At  $30\text{ }^{\circ}\text{C}$ , very little deformation is observed for both vitrimers. At a temperature of  $70\text{ }^{\circ}\text{C}$  and  $100\text{ }^{\circ}\text{C}$ , significantly higher deformations are observed. In all cases, the materials are able to recover the majority of the applied strain after 700 s, even at elevated temperatures above the  $T_g$  and in the region of imine bond exchange. Any loss in recovery might result from imperfections in the cross-linked network that are not inherently elastic, or from bond exchange within the vitrimer network. Furthermore, the strain recovery above the  $T_g$  is retarded, while below the  $T_g$  it is immediate.

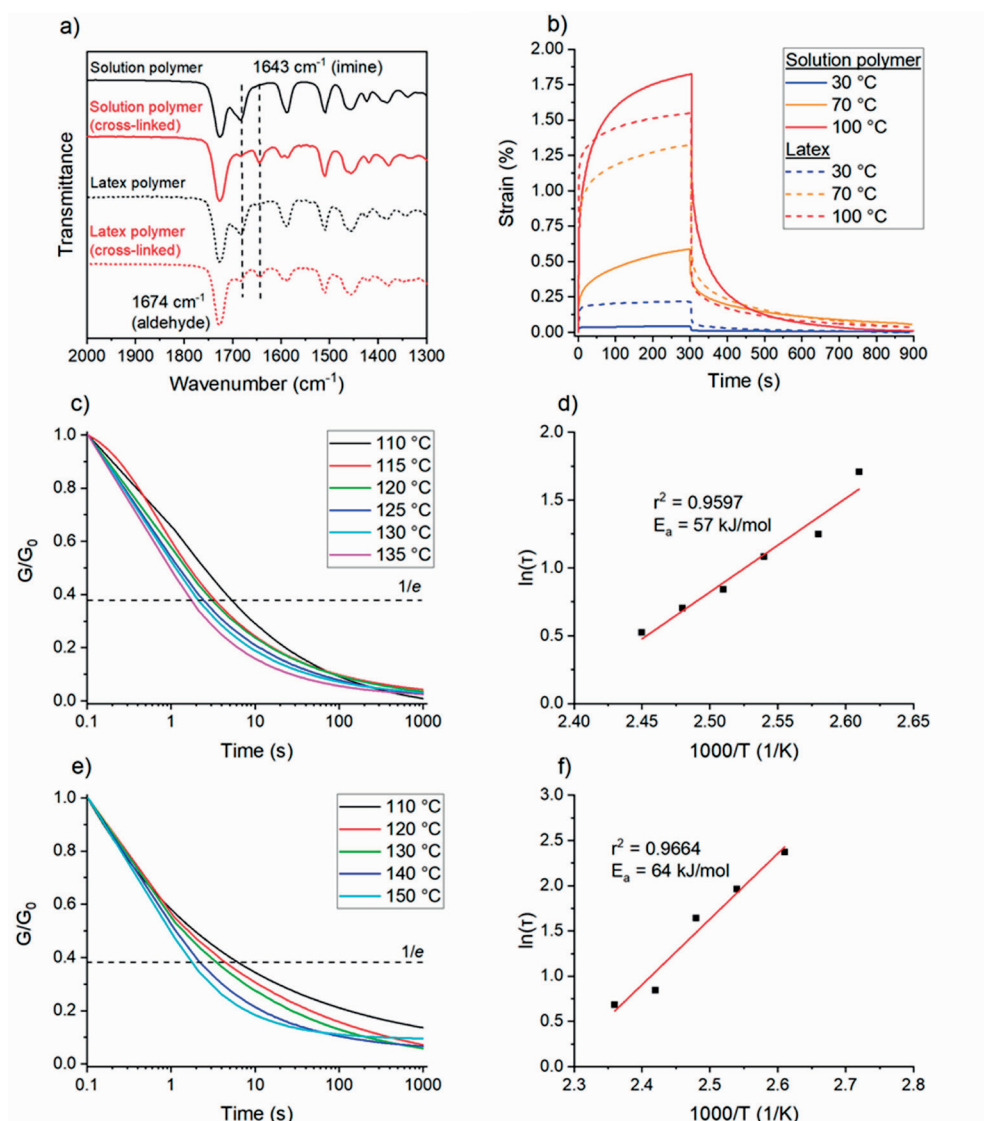


Figure 6.4. a) Overlay of the FTIR spectra of solution polymer (amine-to-aldehyde ratio of 1), latex polymer (amine-to-aldehyde ratio of 0.67), and the cross-linked equivalents. b) Overlay of the creep recovery curves performed at various temperatures. Rheological stress relaxation experiment of the solution polymer using an amine-to-aldehyde ratio of 1 with c) normalized relaxation modulus at various temperatures and d) Arrhenius plot. Rheological stress relaxation experiment of the latex polymer using an amine-to-aldehyde ratio of 0.67 with e) normalized relaxation modulus at various temperatures and f) Arrhenius plot.

The effect of amine-to-aldehyde ratio was further investigated by rheological stress relaxation experiments. In Table 6.2, the activation energies are reported of the vitrimers with

an amine-to-aldehyde group ratio of 0.67, 1, and 1.1. Clearly, the functional group ratio strongly influences the  $E_a$ . At an equimolar functional group ratio, dynamic exchange occurs via methathesis reactions. When the amount of amine groups is increased, another mode of dynamic exchange is additionally enabled, the amine exchange reactions. This caused the  $E_a$  to decrease from 57 kJ/mol, to 32 kJ/mol (Figure E7). A drastic increase in the  $E_a$  to 120 kJ/mol was observed when the amine-to-aldehyde ratio was lowered to 0.67 (Figure E8). The increase in  $E_a$ , is related to decrease in network density, leading to a lower probability that two imine bonds meet for metathesis exchange due to dilution of the cross-linking points.<sup>25-26</sup> In case of the latex vitrimer, a similar effect of the functional group ratio was not found (Table 6.2, entry 4 and 5) (Figure E9). Possibly, the more complex nature of the latex vitrimer plays a role in the relaxation modes, considering the block copolymer structure.

Table 6.2. Measured activation energies corresponding to vitrimers obtained from the solution and latex polymer with various amine-to-aldehyde group ratios.

Entry	Synthesis method	Amine-to-aldehyde group molar ratio	$E_a$ (kJ/mol)
1	Solution	0.67	120
2		1	57
3		1.1	32
4	Latex	0.67	64
5		1	63

An amine-to-aldehyde group ratio of 1 was maintained for thermal and mechanical characterization of the vitrimer synthesized in solution. For the latex vitrimer, an amine-to-aldehyde ratio of 0.67 was used to facilitate the film formation after casting. In Table 6.3, characterization of the solution and latex vitrimer are summarized. Both vitrimers, exhibited a high gel fraction of 99 wt% after Soxhlet extraction with THF. The  $T_a$  of the solution vitrimer lies at 68 °C according to the peak of the  $\tan \delta$  in the DMA spectrum (Figure 6.5a). In the case of the latex vitrimer, several thermal transitions were observed (Figure 6.5b). At -59 °C and -3 °C two minor transitions are observed, which coincides with the  $T_g$  (-64 °C) and melting temperature ( $T_m$ ) (-3 °C) of the POEGMA macro-RAFT agent, respectively (Figure E10). Then, a major transition is observed at 73 °C, which like the solution polymer corresponds to the relaxation of the cross-linked poly(MEV-co-2OA) segment. The presence of a separate thermal transition might suggest the formation of a phase-separated network. A phase-separated network originating from block copolymer vitrimers has been shown to show a strongly reduced macroscopic flow at elevated times and deformations.<sup>27</sup>

Partially as a result of the presence of the POEGMA macro-RAFT agent in the latex polymer, the mechanical properties of the solution and latex vitrimer differed significantly. The solution vitrimer was stiff, whereas the latex vitrimer was much more flexible. This difference is reflected in the values for the Young's modulus and ultimate tensile strength,

which were significantly higher for the solution vitrimer (Table 6.3). The strain at break was between 13.5 and 15.3% for both vitrimers, showing brittle behavior.

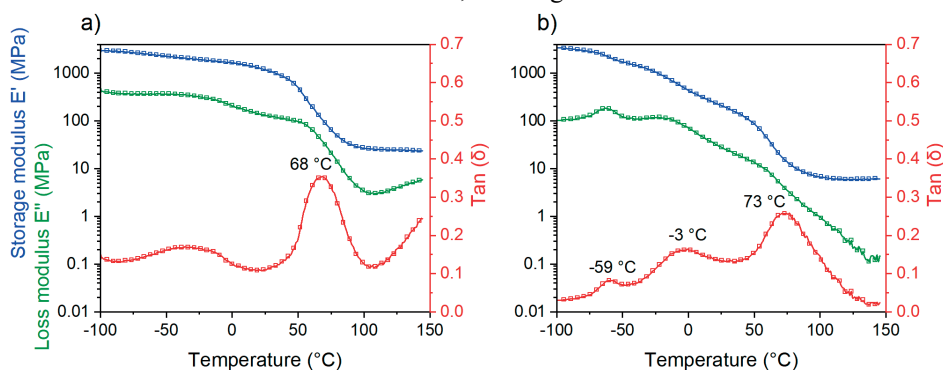


Figure 6.5. DMA temperature ramp of a) the solution vitrimer and b) the latex vitrimer.

Table 6.3. Characterization of the solution and latex vitrimers.

Polymer	Amine-to-aldehyde group ratio	Gel content (%)	Young's modulus (MPa)	Ultimate tensile strength (MPa)	Strain at break (%)
Solution	1	99	717 ± 49	20.1 ± 0.8	15.3 ± 8.3
Latex	0.67	99	154 ± 3	7.5 ± 0.3	13.5 ± 1.7

## Recycling

Both vitrimers were subjected to multiple recycling cycles (Figure 6.6d) and the tensile properties were evaluated after each cycle. In case of the solution polymer, homogenous films were obtained after each cycle, but longer residence times in the press were required after each cycle. The pristine film was pressed, and after 15 minutes was homogenous. The 3<sup>rd</sup> cycle required 1 hour in the press before a homogenous sample was obtained. Nonetheless, in Figure 6.6a, judging from the tensile curves, the solvent vitrimer retains its mechanical properties after several recycles. A slight decrease in the strain at break is observed after several recycling steps, which could be the result of backbone chain scission. However, the values are still within the margin of the standard deviation.

The latex vitrimer shows significantly lower tensile properties than the solution polymer. This can be related to the difference in amine-to-aldehyde ratio that was used and the lower molecular weight that was obtained for the latex polymer. After one recycle, the ultimate tensile strength is slightly decreased while the strain at break is retained. After the second recycling step, a drastic decrease in properties is observed. Incomplete fusion of the granules during recycling was observed even after a residence time of 6 hours in the press. Incomplete particle fusion leads to premature breaking of the tensile bar during tensile testing and thus a decreased ultimate tensile strength and strain at break. The resistance against reprocessing could be the result of the formation of permanent cross-links. The two main differences with

the solution polymer is the presence of OEGMA, and the excess of aldehyde groups, which could have caused cross-linking side reactions. Alternatively, unreacted thermal initiator that remained after latex synthesis caused the formation of permanent cross-links during recycling through hydrogen abstraction of the polymer backbone. Indication of the presence of permanent cross-links was also provided previously in the stress relaxation results, which showed, to a slight degree, incomplete relaxation of the network (Figure 6.4c). The presence of a previously mentioned phase-separated network might restrict the recycling as well.

Interestingly, the Young's modulus is maintained for both vitrimers after each recycling step (Figure 6.6c). Another favorable result is the sustaining of the thermal stability of the vitrimers through the recycling steps, suggesting no significant thermal degradation during recycling at the evaluated conditions (150 °C, 50 bar). Both the solution and latex vitrimer exhibit similar thermal degradation profile in the TGA measurement (Figure 6.6b). Furthermore, the gel content remains high (>98%), suggesting no major decross-linking has occurred during recycling. In the FTIR spectra taken after each sample, some decrease in the imine peak is observed for the latex vitrimer, suggesting the decreased recycling potential. In case of the solution polymer a minute amount of unreacted aldehyde groups was present in the pristine film (Figure E11). The corresponding signal at 1674  $\text{cm}^{-1}$  in the FTIR spectrum disappeared after the following recycling steps. In the latex polymer, containing excess of aldehyde, the aldehyde signal remains visible upon recycling (Figure E12).

The appearance of the vitrimers changes mildly as an influence of the recycling steps (Figure 6.6d). Due to the presence of RAFT agent during polymer synthesis, all films appear yellow and transparent. After each recycling step, a slight darkening occurred in each sample, the effect was more prevalent in the latex vitrimer.

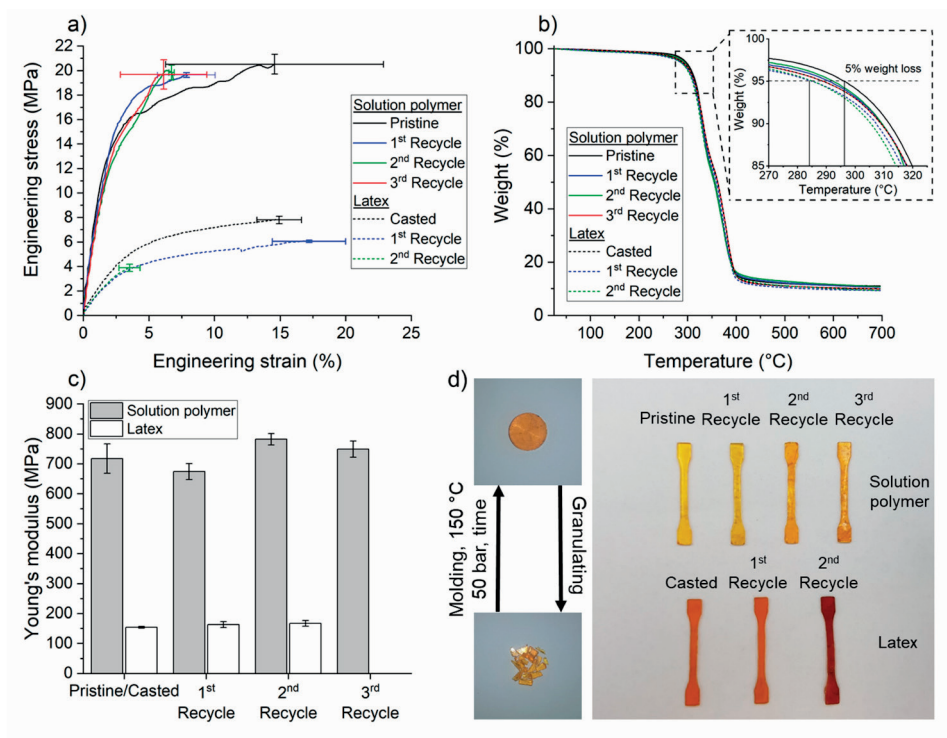


Figure 6.6. Characterization of the recycled solution and latex vitrimers. a) Overlay of the tensile graphs. b) Overlay of the TGA curves. c) Bar graph indicating the evolution of the Young's modulus through the recycling steps. d) Photograph of the recycled tensile bars and a scheme representing the recycling process.

### Conclusions

In this work, the polymerization of a novel monomer MEV was successfully executed via RAFT controlled radical polymerization. Structural characterization via NMR spectroscopy and GPC showed that linear polymers with low dispersity were obtained containing aldehyde side group functionality along the backbone. Copolymerization with the biobased 2-octyl acrylate was investigated in solution and by determining the reactivity ratios, showing slightly higher reactivity for MEV compared to 2OA. The transfer from solvent to a water-borne synthesis process was performed through polymerization induced self-assembly using a water-soluble macro-RAFT agent. Via this way, a colloiddally stable surfactant free latex was obtained with a high solid content of 31 wt%, and consisting of small spherical particles with a size of 49 nm.

The pendent aldehyde groups of both the solvent and latex polymer was reacted with the multifunctional amine TREN to form imine bonds and obtain vitrimers. The dynamic exchange of the cross-links was characterized with rheological stress relaxation experiments and an activation energy of 57 and 63 kJ/mol was found for the solvent and latex polymer, respectively. Further characterization of the functional group ratio showed a strong effect on the activation energy, resulting from changes in the dynamic exchange chemistry and network density. Both polymers were successfully reprocessed through various cycles, generally maintaining mechanical and thermal stability properties. In case of the latex vitrimer, loss in the ultimate tensile strength and strain at break after recycling was observed, presumable related to the difference in polymer structure and synthesis method compared to the solvent polymer.

This research shows the unique combination of water-borne synthesis of biobased and functional latexes, and the implementation as vitrimers. While further fine-tuning of the latex synthesis and film formation is required to improve upon the recyclability of the latex vitrimers compared to the solvent borne polymer, the results indicate potential for future recyclable and self-healing latex binders in materials such as coatings.

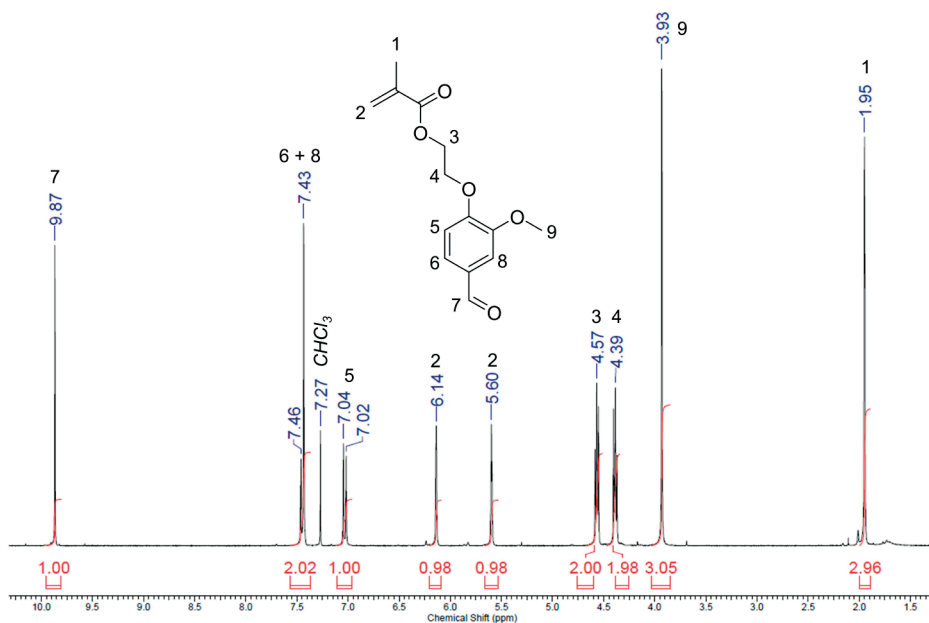
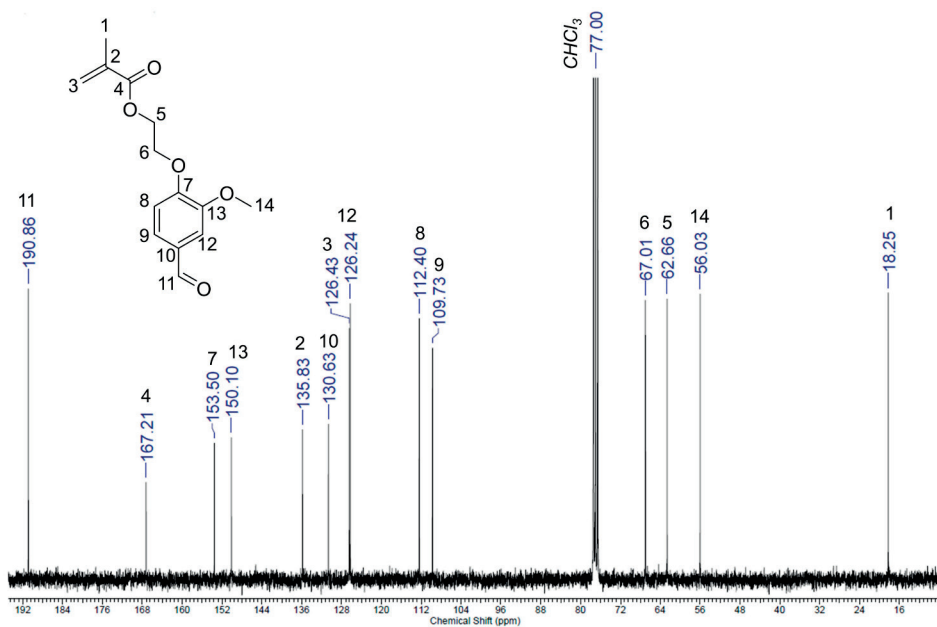


## References

1. Montarnal, D.; Capelot, M.; Tournilhac, F.; Leibler, L., Silica-like malleable materials from permanent organic networks. *Science* **2011**, *334* (6058), 965-968.
2. Denissen, W.; Winne, J. M.; Du Prez, F. E., Vitrimers: permanent organic networks with glass-like fluidity. *Chemical Science* **2016**, *7* (1), 30-38.
3. Taynton, P.; Yu, K.; Shoemaker, R. K.; Jin, Y.; Qi, H. J.; Zhang, W., Heat-or water-driven malleability in a highly recyclable covalent network polymer. *Advanced Materials* **2014**, *26* (23), 3938-3942.
4. Capelot, M.; Montarnal, D.; Tournilhac, F.; Leibler, L., Metal-catalyzed transesterification for healing and assembling of thermosets. *Journal of the American Chemical Society* **2012**, *134* (18), 7664-7667.
5. Denissen, W.; Rivero, G.; Nicolaÿ, R.; Leibler, L.; Winne, J. M.; Du Prez, F. E., Vinylogous urethane vitrimers. *Advanced Functional Materials* **2015**, *25* (16), 2451-2457.
6. Fache, M.; Boutevin, B.; Caillol, S., Vanillin production from lignin and its use as a renewable chemical. *ACS Sustainable Chemistry & Engineering* **2016**, *4* (1), 35-46.
7. Zhou, Z.; Su, X.; Liu, J.; Liu, R., Synthesis of Vanillin-Based Polyimine Vitrimers with Excellent Reprocessability, Fast Chemical Degradability, and Adhesion. *ACS Applied Polymer Materials* **2020**, *2* (12), 5716-5725.
8. Xu, Y.; Odelius, K.; Hakkarainen, M., Photocurable, thermally reprocessable, and chemically recyclable vanillin-based imine thermosets. *ACS Sustainable Chemistry & Engineering* **2020**, *8* (46), 17272-17279.
9. Sun, Y.; Sheng, D.; Wu, H.; Tian, X.; Xie, H.; Shi, B.; Liu, X.; Yang, Y., Bio-based vitrimer-like polyurethane based on dynamic imine bond with high-strength, reprocessability, rapid-degradability and antibacterial ability. *Polymer* **2021**, *233*, 124208.
10. Liu, X.; Liang, L.; Lu, M.; Song, X.; Liu, H.; Chen, G., Water-resistant bio-based vitrimers based on dynamic imine bonds: Self-healability, remodelability and ecofriendly recyclability. *Polymer* **2020**, *210*, 123030.
11. Memon, H.; Liu, H.; Rashid, M. A.; Chen, L.; Jiang, Q.; Zhang, L.; Wei, Y.; Liu, W.; Qiu, Y., Vanillin-based epoxy vitrimer with high performance and closed-loop recyclability. *Macromolecules* **2020**, *53* (2), 621-630.
12. Zhang, L.; Ma, J.; Lyu, B.; Zhang, Y.; Thakur, V. K.; Liu, C., A sustainable waterborne vanillin–eugenol–acrylate miniemulsion with suitable antibacterial properties as a substitute for the styrene–acrylate emulsion. *Green Chemistry* **2021**, *23* (19), 7576-7588.
13. Molina-Gutiérrez, S.; Ladmiral, V.; Bongiovanni, R.; Caillol, S.; Lacroix-Desmazes, P., Radical polymerization of biobased monomers in aqueous dispersed media. *Green Chemistry* **2019**, *21* (1), 36-53.
14. Zhou, J.; Zhang, H.; Deng, J.; Wu, Y., High Glass-Transition Temperature Acrylate Polymers Derived from Biomasses, Syringaldehyde, and Vanillin. *Macromolecular Chemistry and Physics* **2016**, *217* (21), 2402-2408.
15. Molina-Gutiérrez, S.; Ladmiral, V.; Bongiovanni, R.; Caillol, S.; Lacroix-Desmazes, P., Emulsion polymerization of dihydroeugenol-, eugenol-, and isoeugenol-derived methacrylates. *Industrial & Engineering Chemistry Research* **2019**, *58* (46), 21155-21164.
16. d'Agosto, F.; Rieger, J.; Lansalot, M., RAFT-Mediated Polymerization-Induced Self-Assembly. *Angewandte Chemie International Edition* **2020**, *59* (22), 8368-8392.

17. Jaacks, V., A novel method of determination of reactivity ratios in binary and ternary copolymerizations. *Die Makromolekulare Chemie: Macromolecular Chemistry and Physics* **1972**, *161* (1), 161-172.
18. Li, T.; Li, H.; Wang, H.; Lu, W.; Osa, M.; Wang, Y.; Mays, J.; Hong, K., Chain flexibility and glass transition temperatures of poly (n-alkyl (meth) acrylate) s: Implications of tacticity and chain dynamics. *Polymer* **2021**, *213*, 123207.
19. Badía, A. n.; Movellan, J.; Barandiaran, M. a. J. s.; Leiza, J. R., High biobased content latexes for development of sustainable pressure sensitive adhesives. *Industrial & Engineering Chemistry Research* **2018**, *57* (43), 14509-14516.
20. Brandrup, J.; Immergut, E. H.; Grulke, E. A.; Abe, A.; Bloch, D. R., *Polymer handbook*. Wiley New York: 1999; Vol. 89.
21. He, Z.; Niu, H.; Liu, L.; Xie, S.; Hua, Z.; Li, Y., Elastomeric polyolefin vitrimer: Dynamic imine bond cross-linked ethylene/propylene copolymer. *Polymer* **2021**, *229*, 124015.
22. Dhers, S.; Vantomme, G.; Avérous, L., A fully bio-based polyimine vitrimer derived from fructose. *Green Chemistry* **2019**, *21* (7), 1596-1601.
23. Li, L.; Chen, X.; Jin, K.; Torkelson, J. M., Vitrimers designed both to strongly suppress creep and to recover original cross-link density after reprocessing: Quantitative theory and experiments. *Macromolecules* **2018**, *51* (15), 5537-5546.
24. Van Zee, N. J.; Nicolaÿ, R., Vitrimers: Permanently crosslinked polymers with dynamic network topology. *Progress in Polymer Science* **2020**, *104*, 101233.
25. Liu, Y.; Tang, Z.; Chen, J.; Xiong, J.; Wang, D.; Wang, S.; Wu, S.; Guo, B., Tuning the mechanical and dynamic properties of imine bond crosslinked elastomeric vitrimers by manipulating the crosslinking degree. *Polymer Chemistry* **2020**, *11* (7), 1348-1355.
26. Guerre, M.; Taplan, C.; Winne, J. M.; Du Prez, F. E., Vitrimers: directing chemical reactivity to control material properties. *Chemical Science* **2020**, *11* (19), 4855-4870.
27. Lessard, J. J.; Scheutz, G. M.; Sung, S. H.; Lantz, K. A.; Epps III, T. H.; Sumerlin, B. S., Block copolymer vitrimers. *Journal of the American Chemical Society* **2019**, *142* (1), 283-289.

## Appendix E

Figure E1. Assigned  $^1\text{H}$  NMR spectrum of MEV in  $\text{CDCl}_3$ .Figure E2. Assigned  $^{13}\text{C}$  NMR spectrum of MEV in  $\text{CDCl}_3$ .

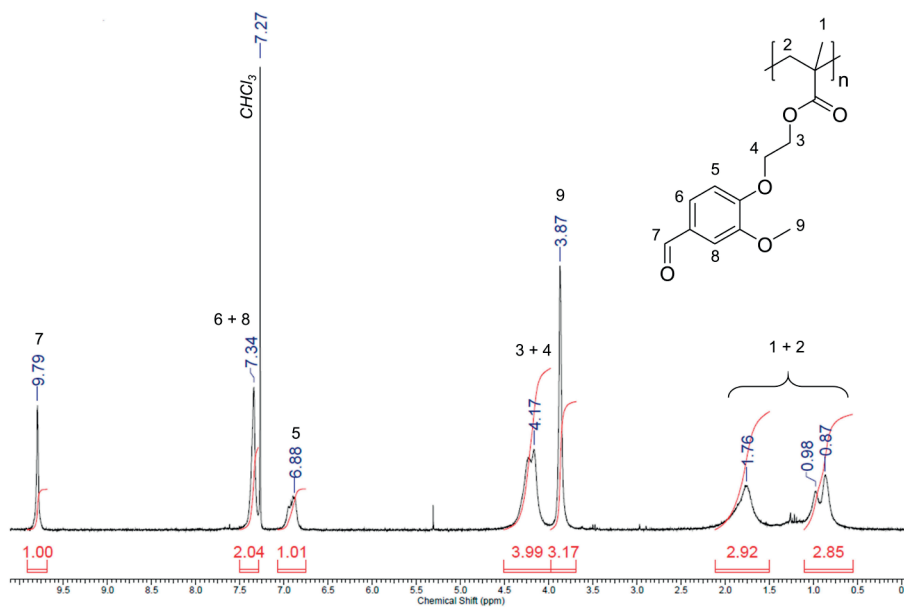
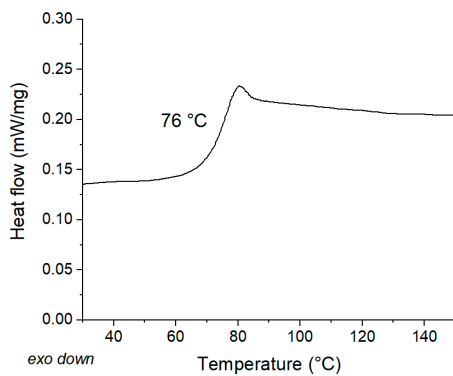
Figure E3. Assigned  $^1\text{H}$  NMR spectrum of poly(MEV) in  $\text{CDCl}_3$ .

Figure E4. DSC thermogram of poly(MEV).

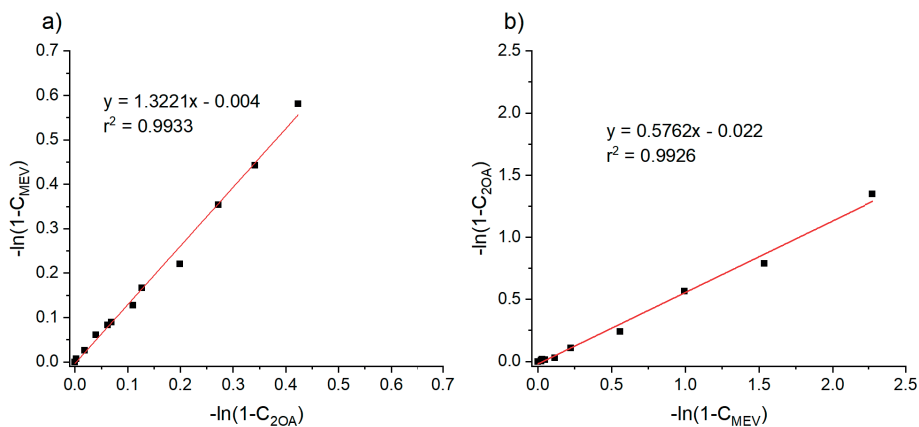


Figure E5. Jaacks plots for the copolymerization with a) excess MEV and b) excess 2OA.

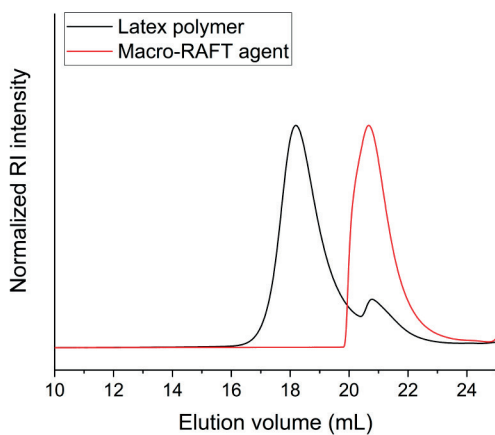


Figure E6. GPC overlay of the POEGMA macro-RAFT agent and the latex polymer.

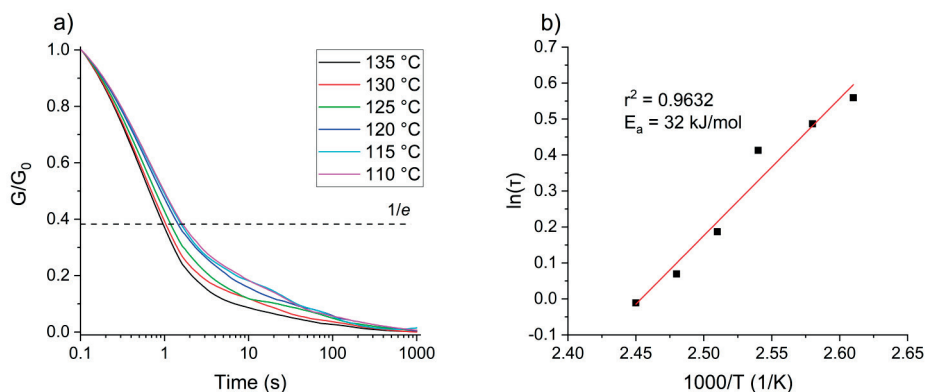


Figure E7. Rheological stress relaxation for the solution vitrimer containing an amine-to-aldehyde group ratio of 1.1, with a) normalized relaxation modulus at various temperatures and b) Arrhenius plot.

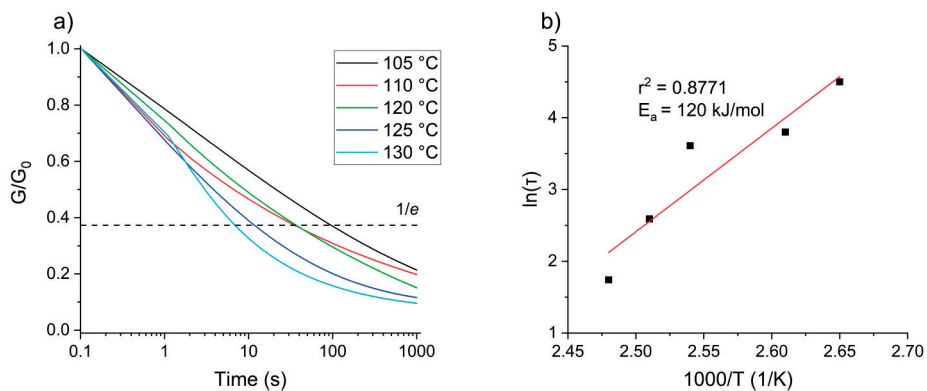


Figure E8. Rheological stress relaxation for the solution vitrimer containing an amine-to-aldehyde group ratio of 0.67, with a) normalized relaxation modulus at various temperatures and b) Arrhenius plot.

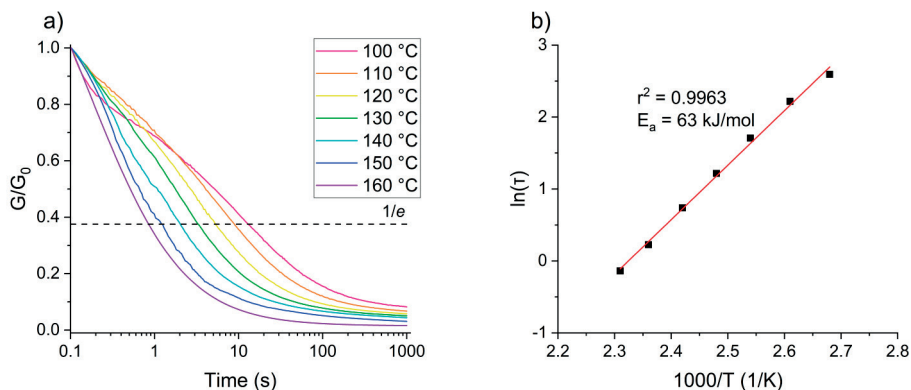


Figure E9. Rheological stress relaxation for the latex vitrimer containing an amine-to-aldehyde group ratio of 1, with a) normalized relaxation modulus at various temperatures and b) Arrhenius plot.

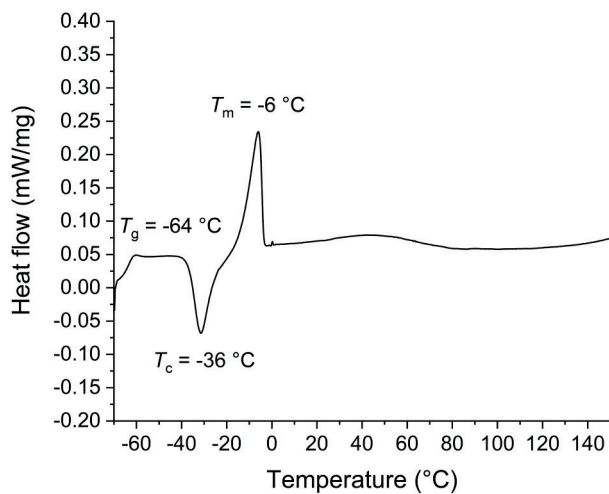


Figure E10. DSC thermogram of the POEGMA macro-RAFT agent.

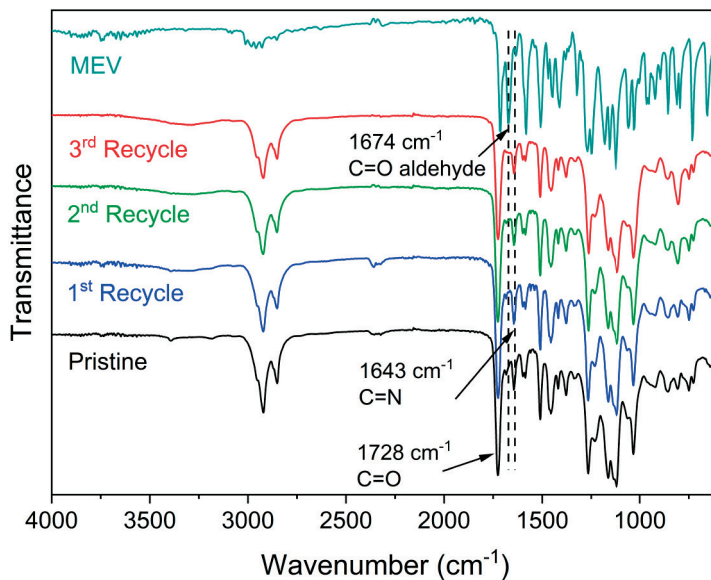


Figure E11. Overlay of the normalized FTIR spectra of MEV and the pristine and recycled solution vitrimers.

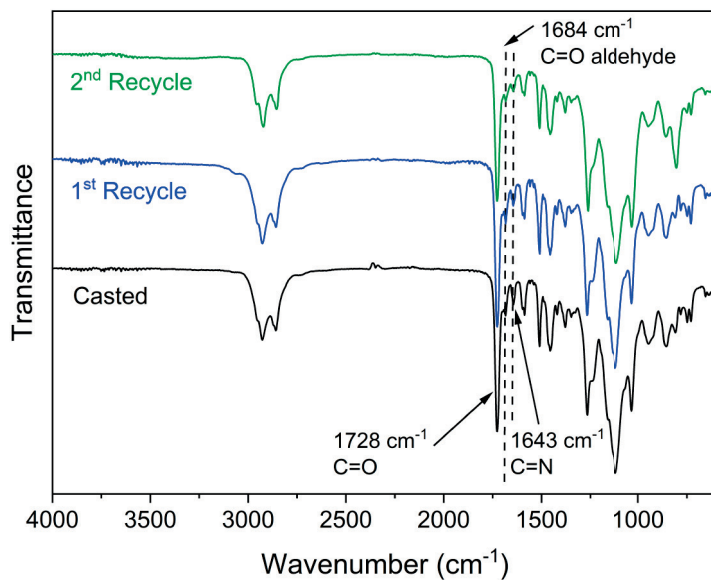


Figure E12. Overlay of the normalized FTIR spectra of the pristine and recycled latex vitrimers.



## Thesis conclusions

The main goal of this thesis was to investigate novel and functional biobased monomers in order to develop acrylic latexes based on biobased monomers for cross-linked film and coating applications. Two main modes of cross-linking were investigated, each requiring the incorporation of a functional side group in the polymer backbone. The first monomer was 4-oxocyclopentenyl acrylate (4CPA), which is able to dimerize under UV light. The second monomer is 2-(methacryloyloxy)ethyl vanillin (MEV), which can undergo imine formation in the presence of an amino functional cross-linker. The aim of the cross-linking step was firstly to improve the physical properties of the resulting film, but also to introduce value-added properties in the resulting applications, supporting the concepts of circularity and reducing environmental pollution.

The first part of this work focused on the exploration of the Reversible Addition-Fragmentation chain-Transfer (RAFT) controlled solution homo- and copolymerization of 4CPA (**Chapter 2**). In the homopolymerization of 4CPA, only low molecular weight polymers were obtained without cross-linking. Model studies showed that cross-linking likely occurs due to the participation of the cyclopentenone group in the RAFT controlled radical polymerization. Nonetheless, the selectivity between the acrylate and cyclopentenone group during RAFT polymerization was high enough to yield polymers containing intact cyclopentenone side groups according to  $^1\text{H}$  NMR spectroscopy. In the copolymerization of 4CPA with comonomers such as methyl acrylate (MA), isobornyl acrylate (IBOA), and lauryl acrylate (LA), higher monomer conversions and molecular weights were reached. In this case, copolymerization is a straightforward strategy to tune the thermal properties of the polymer, and reduce the degree of functionality along the polymer backbone. The cyclopentenone side groups belonging to the 4CPA were successfully dimerized under UV light to yield cross-linked freestanding films. The results were supported by a  $[2 + 2]$  photocyclodimerization reaction of the model molecule, 4-oxocyclopentenyl acetate, yielding the head-to-head and head-to-tail dimers. The cross-linked films showed a high gel fraction and increase in the glass transition temperature ( $T_g$ ) as a result of the UV irradiation.

The development of copolymers based on 4CPA and LA in chapter 2 was exploited in the synthesis of amphiphilic block copolymers in **Chapter 3**. The block copolymers consisting of poly(oligo(ethylene glycol) methyl ether acrylate) (POEGA) as the water-soluble block and a copolymer of 4CPA and LA as the hydrophobic block self-assembled after introduction in water. The micelles could serve as nano-sized drug vehicles. A series of nine block copolymers was synthesized consisting of different hydrophilic and hydrophobic block lengths. The 4CPA block copolymers could self-assemble in water either after direct dissolution, or by a solvent exchange method resulting in different morphologies and sizes. The micellar cores could be cross-linked after irradiation of UV light resulting in core-cross-linked micelles. The therapeutic drug doxorubicin (DOX) was successfully loaded in the micelles and cell viability essays indicated a high cytotoxicity towards breast adenocarcinoma cells as a result of the DOX loading. On the other hand, non-loaded micelles were not toxic to healthy cells at the evaluated concentrations in the cancer cell essay.

Furthermore, 4CPA could serve as a UV cross-linkable monomer for the production of core-cross-linked drug delivery vehicles.

4CPA latexes were developed in **Chapter 4**. A RAFT controlled Polymerization Induced Self-Assembly (PISA) process was developed for the production of 4CPA latexes containing several biobased monomers. The investigated comonomers were butyl acrylate (BA), tetrahydrofurfuryl acrylate (THFA), IBOA, and 2-octyl acrylate (2OA). Using a POEGA macro-RAFT agent in a low temperature polymerization of 50 °C, stable and high solid content latexes containing a small particle size were successfully developed, and high monomer conversion was demonstrated. These properties are desirable in an industrial setting, which targets high space-time efficiency, and applicability since the latex functions as a final product. Four selected latexes consisting of various monomer compositions were subjected to further investigation in **Chapter 5**. The latexes were colloidally stable after 11 months of storage at 4 °C according to visual assessment and DLS measurement. After film formation and UV curing, stiff freestanding films were obtained. The tensile properties could be modified by controlling the UV irradiation time. Furthermore, the latex containing 2OA showed promise as an oil and water barrier film for paper applications. In general, cross-linking resulted in drastic increases in solvent resistance, hardness, and blocking resistance of the films applied on a substrate. For some films containing more hydrophobic monomers, water droplets applied on the film showed a high contact angle. These results support the promise as potential water or oil barrier films. Composites of the latex with cellulose nanocrystals (CNC) were also investigated. The resulting films exhibited drastically increased tensile properties and the formation of a layered cellulose structure was observed in SEM. At the same time, water resistance of the composite was greatly improved compared to pure CNC. The composites could serve as potential gas barrier films in food packaging or electronics.

Using the latex synthesis procedure developed in chapter 4, the polymerization of the vanillin derived MEV was investigated in **Chapter 6**. Latexes containing aldehyde side group functionality were successfully produced. After addition of tris(2-aminoethyl)amine (TREN) as the cross-linker, the latex was casted and dried, resulting in cross-linked films. The latex films were compared to a similar polymer produced via solution polymerization, and cross-linked using the same cross-linker. Since cross-linking proceeds via imine formation, the resulting polymers are cross-linked with thermally reversible covalent bonds and thus can be characterized as vitrimers. Both vitrimers showed rapid stress relaxation at temperatures between 110 and 150 °C with corresponding activation energies of 57 and 64 kJ/mol for the solution and latex vitrimer, respectively. Furthermore, a strong influence of the amount of TREN in the solution vitrimer on the activation energy was observed. This is related to the amount of imine cross-links. A lower concentration of imine groups reduces the likelihood of bond exchange and thus increased the activation energy. The creep recovery of the vitrimers was evaluated, and both showed near complete recovery (though with a retardation) after being subjected to a stress of 0.28 MPa for 5 minutes. Both vitrimers could be recycled. However, the solution polymer showed no significant decrease in tensile properties after 3

cycles, whereas the latex vitrimer could not retain the same mechanical performance after more than one cycle. This could possibly be related to the formation of permanent cross-links and the presence of a phase separated network as a result of the block copolymer structure in the latex vitrimer.

In this thesis, the use of functional and biobased monomers for the production of water-borne acrylic latexes was thoroughly explored. Stable latexes with a good solid content can be obtained by the RAFT PISA method that are suitable for application as films or coatings. Further in-depth research on their behavior as barrier films, composites, or in formulations holds potential according to the results described in this thesis.



## Impact

With the European green deal<sup>1</sup> and the Paris climate agreement<sup>2</sup>, there is an increasing pressure in the reduction of greenhouse gas emissions and transition to a circular economy. This, in combination with other factors such as the slow depletion of fossil fuels, and global unrest resulting in strong fossil energy price fluctuations, the transition away from fossil resources is becoming a subject of discussion. More specifically, in the production of acrylic coatings, the industry relies heavily on the use of fossil derived monomers. Therefore, the exploration of novel biobased monomers is of interest in order to safeguard the production of plastic materials that are of importance in the modern world. By widening the scope of available monomer structures, the transition from fossil to biobased monomers while maintaining tailored polymer properties could be facilitated. Besides renewability, solvent emissions to the environment and waste production related to the production and use of acrylic coatings is undesirable. Therefore, attention has to be paid to polluting factors that are associated with the use of these materials. This can be done by transitioning towards safer and more environmental friendly water-borne systems instead of solvent-based systems, and by improving the recyclability of the final products.

The main objective of this thesis was the development of water-borne acrylic latexes based on biobased and functional monomers for coating and film applications. The polymerization of novel monomer structures can be challenging, especially when the monomers bring added functionality in the form of functional groups. Functional groups can be involved in all kinds of side reactions resulting either in loss of functionality or premature cross-linking of the polymers. Therefore, the polymerization of such novel and functional monomers was systematically investigated and therefore understood. The polymerization conditions that were investigated in a solution type polymerization, were successfully transferred to a water-borne procedure. The resulting polymers retained their functionality to serve as anchor points for further cross-linking reactions.

The functionality of the monomers served additional purpose within the acrylic water-borne polymer. Firstly, cross-linking of the functional polymer latexes improves the physical and thermal properties of the final materials. Secondly, there is a contribution within the scope of reduction in environmental pollution and the circular economy. Using a UV sensitive monomer derived from sugars, we have developed a UV cross-linkable polymer latex, without the use of any Volatile Organic Compounds (VOC's). VOC's are linked to environmental and health related issues.<sup>3</sup>

Conventional thermosets are cross-linked polymers that cannot be recycled and are disposed after use. Therefore, we have developed a biobased water-borne polyacrylate based on a monomer derived from lignin that is cross-linked using dynamic covalent bonds. The covalent bonds that are formed from an aldehyde and an amine are called imines, which can exchange at elevated temperatures. This results in a material that behaves similar to a conventional thermoset at ambient temperature, but can show macroscopic flow at elevated temperature, enabling the recyclability of these materials. The development of vitrimers is

currently receiving a lot of attention in academia, and is finding ways into industry as well.<sup>4</sup>  
<sup>5</sup> To date, not many vitrimers that are based on biobased and water-borne systems have been investigated. Therefore, this research promotes the application of innovative technologies like vitrimers into a wider application scope consisting of circular products from water-borne polyacrylates.

In this thesis, we have briefly investigated the addition of cellulose nanocrystals (CNC) to the UV curable latex to prepare composite films. The result obtained, indicates towards an affinity between the CNC and latex possibly due to the presence of hydrogen bonding interactions. The composites lead to films consisting of a layered structure at high CNC fractions. Because of this, a drastic increase in mechanical properties of the film are obtained, while only a limited increase in sensitivity to water is achieved. The results show promise for further research towards the barrier performance of such layered composite materials. For example, films and coatings for food packaging and electronics require excellent gas and moisture barrier properties. The use of cellulose in such films is promising due to its properties and abundance of this renewable material. However, the moisture sensitivity is one of the main drawbacks. This research proposes a promising and straightforward solution for the reduction in moisture sensitivity of CNC based films. Despite cellulose, other fillers capable of hydrogen bonding such as chitosan and nanoclays can be investigated in the future for composites with improved physical and barrier properties.

One application of the UV curable latex was investigated as a proof of concept for paper barrier films. The UV cross-linked films show excellent reduction in absorption of oil and water of the paper substrate after exposure compared to uncoated paper. This result highlights a potential industrial application as barrier for paper and cardboard food packaging materials. Nonetheless, the long-term stability, safety, and biocompatibility of the polymers and materials need to be evaluated when food contact or biomedical applications are targeted.

In general, this thesis contributes to the trend of the development of renewable and water-borne systems in the coating industry. Manufacturers of latexes and coating formulations might use the renewable character of their products to promote it to the public with an increasing awareness of circularity. Otherwise, increasing legislative restrictions, or incentives could promote the reduction of fossil materials in the future. The research herein is also published in peer-reviewed scientific journals, which increases its exposure to the industry and scientific community.

---

## References

1. A European green deal. [https://ec.europa.eu/info/strategy/priorities-2019-2024/european-green-deal\\_en](https://ec.europa.eu/info/strategy/priorities-2019-2024/european-green-deal_en) (accessed 27-05-2022).
2. UN Shifting to a Circular Economy Essential to Achieving Paris Agreement Goals. <https://unfccc.int/news/shifting-to-a-circular-economy-essential-to-achieving-paris-agreement-goals> (accessed 27-05-2022).
3. Winnik, M. A.; Feng, J., Latex blends: an approach to zero VOC coatings. *Journal of Coatings Technology* **1996**, *68*, 39-50.
4. Alabiso, W.; Schlögl, S., The impact of vitrimers on the industry of the future: Chemistry, properties and sustainable forward-looking applications. *Polymers* **2020**, *12* (8), 1660.
5. Vitrimat. <https://www.vitrimat.eu/> (accessed 27-05-2022).





## Samenvatting

Het concept van zelforganisatie van kleine moleculen om vet en olie te dispergeren in water is zeer oud. Rond het jaar 2800 voor Christus beschreven de Sumeriërs de chemische synthese van zeep. Tot op de dag van vandaag gebruiken we een gelijksoortig recept. Hoewel we in het alledaagse leven zeep gebruiken voor het schoonmaken van oppervlaktes van vet resten, worden zeepen ook grootschalig gebruikt in de industrie. Bijvoorbeeld voor het maken van water gedragen plastics voor lakken. Plastics die normaal niet wateroplosbaar zijn, worden als kleine deeltjes met een grootte van enkele tientallen tot honderden nanometer gestabiliseerd door de zeep moleculen. Op deze manier worden onder andere polyacrylaat latices geproduceerd. Met behulp van een latex kan een onoplosbaar polymeer toch gemakkelijk op een substraat aangebracht worden zonder dat het gebruik maakt van schadelijke oplosmiddelen of Vluchtige Organische Stof (VOS). In de afgelopen tientallen jaren is er veel vooruitgang geboekt in het terugdringen van het gebruik van VOS in lakken. Het gebruik en verdamping van VOS in lakken wordt geassocieerd met schadelijke effecten op de atmosfeer en de gezondheid. Vandaar dat steeds meer water gedragen lakken in gebruik worden genomen. Zelfs water gedragen lakken maken soms gebruik van kleine hoeveelheden VOS om laagvorming te bevorderen. Het gebruik van VOS is grotendeels gerelateerd aan de filmvorming van de binder in de lak. De polymeer binder (latex) zorgt voor de fysieke eigenschappen in de lak. Na aanbrenging en verdamping van het water zullen de deeltjes moeten samensmelten om een homogene laag te verkrijgen. Of dit proces plaatsvindt bij kamertemperatuur hangt grotendeels af van de glastransitie temperatuur ( $T_g$ ) van het polymeer. Om een goede laagvorming te krijgen in combinatie met goede fysieke eigenschappen onder de  $T_g$ , worden VOS toegevoegd om het polymeer te ‘verzachten’ tijdens de laagvorming. Doordat versmelting van de deeltjes nodig is voor de laagvorming, zijn latex lakken over het algemeen niet chemisch verknoot, zoals oplosmiddel gedragen lakken dat vaak wel zijn. Verknoping zorgt onder andere voor betere mechanische en barrière eigenschappen, en resistentie tegen oplosmiddelen. Daarom kunnen de eigenschappen tussen water gedragen en oplosmiddel gedragen lakken sterk verschillen. Een grote uitdaging is nog steeds om dezelfde goede eigenschappen te verkrijgen met de water gedragen latices, die normaal met oplosmiddel gedragen lakken verkregen worden.

Een ander probleem met de huidige polyacrylaat latices is het gebruik van monomeren die verkregen worden uit fossiele bronnen. Met de huidige ontwikkelingen rondom de regulering van broeikasgassen, uitputting en prijsfluctuaties van fossiele bronnen als olie en gas, wordt het voor academici en industrie steeds interessanter om hernieuwbare alternatieven te onderzoeken. Moleculen die gewonnen worden uit hernieuwbare bronnen bevatten over het algemeen meer heteroatomen dan fossiele monomeren. Dit heeft als gevolg dat de hoeveelheid functionele groepen beschikbaar voor chemische reacties ook groter is. Dit levert veel potentie maar ook uitdagingen voor de productie van functionele monomeren die een speciale rol kunnen vervullen in het uiteindelijke polymeer.

In deze thesis stellen we twee nieuwe hernieuwbare en functionele monomeren voor die, na polymerisatie in water, verknoping reacties kunnen ondergaan. Hierdoor kunnen de

resulterende water gedragen polymeren toch zorgen voor verbetering van bepaalde eigenschappen door het verknopen van de functionele groepen na de laag vorming. Het eerste monomeer is 4-oxocyclopentenyl acrylaat (4CPA) wat verkregen wordt uit furfuryl alcohol, een hernieuwbaar platform molecuul gewonnen uit suikers. Het tweede molecuul is 2-(methacryloyloxy)ethyl vanilline (MEV) wat verkregen wordt uit lignine.

In **Hoofdstuk 2** wordt de oplossingspolymerisatie van 4CPA onder Reversibele Additie-Fragmentatie keten-Transfer (RAFT) controle onderzocht. In de homopolymerisatie van 4CPA, konden alleen laag molecuulgewicht polymeren verkregen worden zonder dat premature verkoping plaatsvond tijdens de reactie. Modelstudies toonden aan dat tijdens de radicaalpolymerisatie zijreacties plaats kunnen vinden aan de cyclopentenon zijgroep. Dit zorgt voor verknoping bij hoge monomeer conversies en molgewichten. Desondanks konden lineaire polymeren verkregen worden met intacte cyclopentenon zijgroepen. Door de hoeveelheid cyclopentenon groepen te verdunnen met een comonomeer, kunnen hoge monomeerconversies en dus hogere molgewichten verkregen worden. Door het gebruik van een comonomeer wordt niet alleen de hoeveelheid verknoppingen gereduceerd in het uiteindelijke verknoopte polymeer, maar kan ook de  $T_g$  en andere polymeer eigenschappen gestuurd worden. De copolymeren werden met succes verknoopt onder UV licht doormiddel van [2 + 2] photocyclodimerisatie tussen de cyclopentenon zijgroepen. De UV dimerisatie werd andermaal met het model molecuul 4-oxocyclopentenyl acetaat aangetoond. Onder UV-bestraling werden de twee kop-kop en kop-staart dimeren gevormd. De verknoopte films vertoonden een hoge gel fractie en verhoging van de  $T_g$  als het gevolg van de UV bestraling.

De ontwikkeling van de 4CPA polymeren gesynthetiseerd via RAFT polymerisatie werd gebruikt in de productie van amfifiele blok copolymeren in **Hoofdstuk 3**. Blok copolymeren bestaande uit poly(oligo(ethyleen glycol) methyl ether acrylaat) (POEGA) als het hydrofiele blok en een copolymeer van 4CPA en lauryl acrylaat als het hydrofobe blok organiseerden zichzelf in micellen na introductie in water. De micellen dienden als potentiële dragers voor medicijnen in biomedische toepassingen. In totaal werden negen verschillende blok copolymeren gesynthetiseerd, allen met een verschillende grootte en verhouding van hydrofiele en hydrofobe blok. De blok copolymeren zelf-organiseerden in water na oplossing of door middel van een oplosmiddel vervanging methode, hetgeen resulteerde in verschillende micellaire vormen en groottes van enkele tientallen nanometer. De hydrofobe kernen die 4CPA bevatten konden worden verknoopt met UV licht. Verknoopte micel structuren bevatten een verhoogde stabiliteit in verdunde omgeving. Het hydrofobe medicijn doxorubicine (DOX) was in de micellen geïncorporeerd en toonden een hoge toxiciteit jegens borst adenocarcinoma cellen. Dit werk toont aan dat 4CPA polyacrylaten potentie hebben als water gedragen plastics aangezien de blok copolymeren gemakkelijk zelf-organiseren. Bovendien kunnen de blok copolymeer micellen met 4CPA in de hydrofobe kern dienen als medicijn dragers.

De conversie van oplossingspolymerisatie naar water gedragen polymerisatie van 4CPA was bereikt met een Polymerisatie Induced Self-Assembly (PISA) methode (**Hoofdstuk 4**). Het macro-RAFT middel gebaseerd op POEGA werd gebruikt om de polymeer deeltjes te

stabiliseren in de water gedragen latex. Verscheidene hernieuwbare comonomeren werden onderzocht. Dit waren butyl acrylaat (BA), tetrahydrofurfuryl acrylaat (THFA), isobornyl acrylaat (IBOA), en 2-octyl acrylaat (2OA). De beste resultaten werden verkregen met een polymerisatie die uitgevoerd werd op een lage temperatuur van 50 °C. Dit resulteerde in stabiele latices met een hoge vaste stofgehalte van rond de 40 gewichtsprocent, hoge monomeer conversie, en kleine deeltjesgrootte. Aangezien latices als eindproduct gebruikt worden, zijn de genoemde eigenschappen interessant vanuit een industrieel perspectief. Vier geselecteerde latices werden opgeschaald naar 200 gram materiaal en verder onderzocht in **Hoofdstuk 5**. De latices waren stabiel na 11 maanden in opslag bij 4 °C. Rigide en verknoopte vrijstaande films waren verkregen na filmvorming en UV-bestraling. Door de hoeveelheid UV-bestraling te controleren, kon de verknoping worden verminderd en werden meer flexibelere films verkregen. De latex films bestaande uit 2OA toonden veelbelovende olie en water barrière eigenschappen voor papier substraten. Over het algemeen resulteerde de UV-verknoping van latex films in een drastische verbetering in de oplosmiddelresistentie, hardheid, blokkeerresistentie, en contacthoek met water. Deze resultaten tonen nogmaals de potentie als barrière lagen aan. Composieten van de latices werden gemaakt door ze te mengen met cellulose nanokristallen (CNC). De resulterende films toonden een drastische verhoging in de mechanische eigenschappen door de vorming van een georiënteerde gelaagde structuur, hetgeen geobserveerd was in elektronenmicroscopie en röntgendiffractie metingen. Tegelijkertijd, was de resistentie tegen de absorptie van water flink verhoogd vergeleken met films gebaseerd op pure CNC. De composieten bleven volledig intact bij een CNC lading van 90 gewichtsprocent, terwijl de film gebaseerd op pure CNC direct uit elkaar valt in water. De composieten kunnen mogelijk dienen als gas barrière lagen in voedselverpakkingen of elektronica.

Gebruik makende van de latex synthese procedure beschreven in **Hoofdstuk 4**, hebben we de polymerisatie van MEV onderzocht in **Hoofdstuk 6**. Latices met aldehyde functionaliteit waren succesvol gesynthetiseerd. Na toevoeging van de tris(2-aminoethyl) amine (TREN) als het verknopingsmiddel, werd de latex gedroogd en daarna uitgehard bij verhoogde temperatuur. De resulterende film met imine bindingen als de verknopingspunten wordt een vitrimeer genoemd en kan gerecycled worden bij verhoogde temperatuur. Het latex vitrimeer werd vergeleken met een gelijksoortig vitrimeer gesynthetiseerd in oplossing. Beide vitrimeren toonden in rheologiemetingen een snelle relaxatie tussen 110 en 150 °C met een activatie energie van 57 en 64 kJ/mol voor de oplossing en latex vitrimeer, respectievelijk. Een sterk effect van de hoeveelheid TREN in de vitrimeer samenstelling op de activatie energie was gevonden. Dit is gerelateerd aan de hoeveelheid verknopingen, die veranderd met de TREN : polyacrylaat ratio. Minder TREN zorgt voor minder verknopingen en dus een lagere kans op uitwisseling tussen de imine bindingen, met een verhoogde activatie energie tot gevolg. Beide vitrimeren konden met succes worden gerecycled, echter het latex vitrimeer verloor mechanische eigenschappen na de 1<sup>ste</sup> en 2<sup>de</sup> cyclus. Dit kan mogelijk gerelateerd zijn aan de vorming van permanente verknopingspunten, of de aanwezigheid van een fase gescheiden netwerk door de blok copolymeer structuur van het vitrimeer.



## Acknowledgments

This diverse research on the topic of polymer chemistry was not the work of a single person. I have many people to thank and acknowledge for their contribution directly and indirectly. First of all, I would like to thank my promotor Dr. Katrien Bernaerts for giving me the opportunity to promote at Maastricht University. My interest for polymer chemistry was truly sparked when we first worked together during my Bachelor thesis, and this is reflected by the path I have followed afterwards. I am grateful for your trusting supervision over the past years and for believing in my capabilities. In addition, I would like to thank my promotor Prof. Dr. Andrij Pich for his supervision. I have always highly appreciated the discussions during our scientific meetings, which helped improving and expanding my work to a higher level. Therefore, your contributions are also extensively present in this thesis.

This being said, I would also like to thank my assessment committee Prof. Dr. Romano Orrù (chair), Prof. Dr. Maarten Honing, Prof. Dr. Guillaume Delaittre, and Dr. Bart Noordover for assessing my thesis and to take place as opponents during my defense.

A big thank you to my Paranympths Monika and Enzo. Thank you for being great coworkers and all the laughs we shared on the lab. I cherish our friendship and am happy to share this special moment with you by my side.

Large contributions to this thesis were also made by Bachelor and Master students of whom I had the pleasure to supervise. Therefore, I would like to thank Nick Sijstermans, Davy Vedder, and Maria de Roy for performing their internship or graduation research projects with me and in the group. I have enjoyed each moment working with you, and your work is reflected directly or indirectly in this thesis.

One of the main factors that influences the course of the PhD research are the colleagues with whom we are working with. With this, I was very lucky. As PhD candidates and post-doctoral researchers, we are all working on our own topics. However, we do the research in the same lab. Being in this situation together creates a special bond. Therefore, a big thank you to Monika, Ola, Marie, Christian, Vahid, Anne, Danny, Tinashe, Nick, Milo, Naveen, Enzo, Sofiya, Marcin, Ramiro, Rocio, Thomas, Martien, Yawen, Huixing, Jian, Zhou, Nattiya, Florine, Antoine, Amol, and Hongjuan. At the same time, I would like to thank the UM colleagues Joeri, Hay, Peter, and Hans, whose technical support enabled the scientific research of the university, and with whom I have shared a pleasurable time during my PhD.

Special thanks goes out to my former bachelor thesis supervisor, colleague, and friend Joeri Noordijk. Who inspired and motivated me throughout my academic career and with whom I have the pleasure to regularly visit scientific lectures on topics such as physics and astronomy.

Milo, bedankt voor al je hulp met onderwerpen waar ik minder bedreven in was dan jij; calculus, FT-IR spectroscopie, en XRD om maar enkele te noemen. Ik merkte dat tijdens onze master en PhD we samen altijd het beste in elkaar naar boven haalden en elkaar konden

## Acknowledgments

---

aanvullen. Dit heeft me ontzettend geholpen om te komen waar ik nu ben. We zaten tijdens ons promotieonderzoek in een ander gebouw, maar iedere keer als ik bij jouw labs langs was geweest en terug de trap naar beneden liep, spiekte ik even door de glazen deur of ik je achter je bureau zag zitten. Dan konden we even nieuwtjes uitwisselen, vraagstukken op tafel leggen, en weer door aan de slag op het lab.

Kiril, Luc, Joey, ik ben blij dat we altijd in contact zijn gebleven sinds we samen in 2011 aan onze bachelor chemie begonnen in Heerlen. Onze vriendschap heeft me er met momenten echt door de Bachelor gesleept. De regelmatige ‘last minute’ studietoetsen, milkshakes, en rondjes MediaMarkt maakte het studeren in Heerlen nog wat grappiger. Luc, bedankt voor je geduldige hulp met het organiseren van de regelmatige DLS metingen in jouw lab. Naast dat ik het altijd erg leuk vond om naar jouw gebouw te lopen en even bij te praten, waren de DLS metingen ook van vitaal belang voor mijn thesis. Had ik dit niet kunnen doen, dan had de thesis er erg anders uit gezien. Dankjewel hiervoor.

Graag wil ik ook mijn ouders Loek en Daphne, mijn jongere broer Abel, en mijn jongere zussen Coco en Holly bedanken voor al hun onvoorwaardelijke liefde en steun. Jullie hebben mij de kans gegeven om te gaan studeren wat uiteindelijk geleid heeft tot deze thesis. Zonder jullie was het dus nooit gelukt. Jullie hebben altijd interesse getoond en met veel geduld geluisterd naar mijn verhalen over de voortgang van het promotieonderzoek. Zo’n publiek kan een wetenschapper, zoon, en broer alleen maar van houden.

My dear,

Thank you for your wonderful support and love all this time. The fact that we experienced our PhD journey at the same time bonded us in a special way. I am grateful that we could share every concern, setback, breakthrough and joyous moment during the whole journey. Not only did we fully understand each other, we could also help with each other’s research conceptually, and by checking manuscripts, presentations etc. which makes this thesis just as much your accomplishment as it is mine. The special memories that we have made during this period, I will forever cherish. Finalizing our PhD marks the start of a new phase in our lives, which I cannot wait to experience with you. Much love, kocham cię.

Jules

## Curriculum Vitae



Jules Stouten was born on the 12<sup>th</sup> of August 1994 in 's-Gravenhage, The Netherlands. After receiving his HAVO diploma from 'het Bonnefanten College' in Maastricht in 2011, he started a bachelor of Applied Science in the direction of chemistry at the Hogeschool Zuyd in Heerlen. During his Bachelor, he did an industrial internship at Lawter in Maastricht, and started working on the Brightlands Chemelot campus in Geleen for a minor research and Bachelor thesis. In 2016, he obtained his BSc diploma with a thesis on the synthesis of (semi-)aromatic polyamides via polycondensation

methods under the supervision of Jurrie Noordijk and Dr. Katrien Bernaerts. In the same year, he started the Biobased Materials master program at Maastricht University (UM). He graduated Summa Cum Laude with a thesis on the ring opening polymerization of low ceiling temperature lactones. In the same group, he started his PhD on water-borne polyacrylate synthesis under the supervision of Dr. Katrien Bernaerts and Prof. Dr. Andrij Pich. The work performed during this PhD is described in this thesis to obtain the degree of Doctor. In June 2022, he joined Stahl in Waalwijk as a compounding chemist.

### List of publications

Publications that are part of this thesis:

**Stouten, J.**, Pich, A., & Bernaerts, K. V., (2023). Biobased and Functional Latexes Synthesized by Polymerization Induced Self-Assembly for UV Curable Films. *In preparation*.

**Stouten, J.**, de Roy, M. K., & Bernaerts, K. V. (2023). Synthesis and Characterization of Water-borne Vanillin Derived Copolymers Containing Dynamic Imine Cross-links. *Materials Today Sustainability*, 100396. DOI: 10.1016/j.mtsust.2023.100396

**Stouten, J.**, Sijstermans, N., Babilotte, J., Pich, A., Moroni, L., & Bernaerts, K. V. (2022). Micellar drug delivery vehicles formed from amphiphilic block copolymers bearing photo-cross-linkable cyclopentenone side groups. *Polymer Chemistry*, 13(33), 4832-4847.

**Stouten, J.**, Vanpoucke, D. E., Van Assche, G., & Bernaerts, K. V. (2020). UV-Curable Biobased Polyacrylates Based on a Multifunctional Monomer Derived from Furfural. *Macromolecules*, 53(4), 1388-1404.

Other publications by the author:

**Stouten, J.**, Schnelting G.H.M., Hul, J., Sijstermans, N., Janssen, K., Darikwa, T., Ye, C., Loos, K., Voet, V.S.D., & Bernaerts K.V. (2022) Biobased Photopolymer Resin for 3D Printing Containing Dynamic Imine Bonds for fast Reprocessability. *Under review*.

**Stouten, J.**, & Bernaerts, K. V. (2022). Condensation Polyesters. In Dusselier, M., & Lange, J. P. (Eds.). *Biodegradable Polymers in the Circular Plastics Economy* (pp. 113-144). John Wiley & Sons.21

Vanpoucke, D. E., Delgove, M. A., **Stouten, J.**, Noordijk, J., De Vos, N., Matthysen, K., Deroover, G. G. P., Mehrkanoon, S., & Bernaerts, K. V. (2022). A machine learning approach for the design of hyperbranched polymeric dispersing agents based on aliphatic polyesters for radiation-curable inks. *Polymer International*. DOI: 10.1002/pi.6378

**Stouten, J.**, Wróblewska, A. A., Grit, G., Noordijk, J., Gebben, B., Meeusen-Wierds, M. H., & Bernaerts, K. V. (2021). Polyamides containing a biorenewable aromatic monomer based on coumalate esters: From synthesis to evaluation of the thermal and mechanical properties. *Polymer Chemistry*, 12(16), 2379-2388.

Delgove, M. A., Wróblewska, A. A., **Stouten, J.**, van Slagmaat, C. A., Noordijk, J., De Wildeman, S. M., & Bernaerts, K. V. (2020). Organocatalyzed ring opening polymerization of regio-isomeric lactones: Reactivity and thermodynamics considerations. *Polymer Chemistry*, 11(21), 3573-3584.

Van Slagmaat, C. A., Delgove, M. A., **Stouten, J.**, Morick, L., Van Der Meer, Y., Bernaerts, K. V., & De Wildeman, S. M. (2020). Solvent-free hydrogenation of levulinic acid to  $\gamma$ -valerolactone using a Shvo catalyst precursor: optimization, thermodynamic insights, and life cycle assessment. *Green Chemistry*, 22(8), 2443-2458.





